Site-specific Bioorthogonal Modification of Antibodies and T cell Receptor Ligands for Use in Cancer Therapy and Research

Dissertation der Fakultät für Biologie
der Ludwig-Maximilians-Universität München

Andreas Stengl

München, 2019

Diese Dissertation wurde angefertigt
unter der Leitung von Herrn Prof. Dr. Heinrich Leonhardt
im Bereich von Humanbiologie und BioImaging
an der Ludwig-Maximilians-Universität München

Erstgutachter/in: Prof. Dr. Heinrich Leonhardt
Zweitgutachter/in: Prof. Dr. Dirk Eick

Tag der Abgabe: **01.07.2019**

Tag der mündlichen Prüfung: **11.12.2019**

ERKLÄRUNG

Ich versichere hier mit an Eidesstatt, dass meine Dissertation selbständig und ohne unerlaubte Hilfsmittel angefertigt worden ist.
Die vorliegende Dissertation wurde weder ganz, noch teilweise bei einer anderen Prüfungskommission vorgelegt.
Ich habe noch zu keinem früheren Zeitpunkt versucht, eine Dissertation einzureichen oder an einer Doktorprüfung teilzunehmen.

München, den **01.07.2019**

Andreas Stengl

Parts of this thesis have been published or submitted for publication elsewhere:

Kasper MA, **Stengl A,** Ochtrop P, Gerlach M, Stoschek T, Schumacher D, Helma J, Penkert M, Krause E, Leonhardt H and Hackenberger CPR. Synthesis of stable phosphonamidate-linked Antibody-Drug-Conjugates with increased linker hydrophilicity, accepted manuscript in *Angew Chem Int Ed Engl*

Kasper MA, Glanz M, **Stengl A**, Penkert M, Klenk S, Sauer T, Schumacher D, Helma J, Krause E, Cardoso MC, Leonhardt H and Hackenberger CPR (**2019**). Cysteine-selective phosphonamidate electrophiles for modular protein bioconjugations. *Angew Chem Int Ed Engl*

Stengl A, Gerlach M, Kasper MA, Hackenberger CPR, Leonhardt H, Helma J and Schumacher D (**2019**). TuPPL: Tub-tag mediated C-terminal Protein-Protein-Ligation Using Complementary Click-Chemistry Handles. *Org Biomol Chem*

Effenberger M[1], **Stengl A**[1], Schober K[1], Gerget M, Kampick M, Müller RT, Schumacher D, Helma J, Leonhardt H & Busch DH (**2019**) FLEXamers: A double-tag for universal generation of versatile pMHC multimers. *J Immunology*

Stengl A, Hörl D, Leonhardt H, Helma J (**2016**) A Simple and Sensitive High-Content Assay for the Characterization of Antiproliferative Therapeutic Antibodies. *J Biomol Screen*

[1] contributed equally

1 SUMMARY

Cancer is a tremendously heterogeneous and dynamic disease and for that reason challenging to treat. Classical, broad-spectrum therapies like surgery, radiation, chemotherapy and combinations thereof contributed greatly to increased life expectancy of cancer patients. The universality of these therapies makes them applicable for a broad range of cancer types and patients but comes along with the risk of severe side effects or diminished efficacy. The desire for cancer-type-specific drugs and patient-personalized therapies has spurred the development of novel therapeutic concepts. Two very prominent targeted concepts, both inspired by the immune system, are antibody based drugs and immune cell therapy. Antibodies form the structural basis for multiple therapeutic molecules. Three salient formats are addressed in this thesis, namely antiproliferative monoclonal antibodies, bispecific antibodies and antibody-drug conjugates (ADCs). First, a high content assay for parallel investigation of antiproliferative potency and mode of action combining base-analog incorporation and DNA content quantification is described. Second, Tub-tag mediated C-terminal protein-protein-ligation (TuPPL) using complementary click-chemistry handles is demonstrated as a convenient method for bispecific antibody generation. Especially screening of bispecific antibody pairs could be streamlined by combinatorial linkage of individual candidates after protein production. Modification of proteins after expression is currently promoted by the advance of bioorthogonal conjugation strategies. Modification of endogenous amino acids, incorporation of unnatural amino acids and enzymatic modification are widely used for the introduction of universal bioorthogonal handles or direct attachment of functional groups. Along this line, a novel cysteine selective modular bioconjugation method using phosphonamidate electrophiles to generate stable cysteine conjugates is described here. The method was further applied to stably attach cytotoxic drug molecules to antibodies. The resulting ADCs show promising *in vitro* as well as *in vivo* efficacy and increased serum stability compared to standard maleimide conjugation. Although antibody based drugs indeed open the therapeutic window by lowering off-target effects as well as increasing tumor specific toxicity they still face limitations. Degradation and systemic clearance of the biomolecule require administration in regular intervals and tissue penetrance is limited by passive diffusion. In contrast, the use of cells as “living drugs” is a revolutionary new concept bypassing some limitations of “dead drugs”. The use of tumor specific immune cells, especially T cells, for cancer therapy shows promising results, however, the “living” nature of these drugs requires thorough characterization of the cell product. Along this line a novel T cell characterization agent, called FLEXamer, is described in this thesis that allows isolation and characterization of antigen specific T cells and associated T cell receptors. FLEXamers retain the high precision of conventional multimer reagents but unite the individual multimers in a single versatile reagent that can be functionalized on demand for the specific need. Taken together this work presents site-specific conjugation methods and novel sensitive tools for production and comprehensive characterization of sensitive and patient-specific next-generation cancer therapeutics.

2 ZUSAMMENFASSUNG

Die Behandlung von Krebs stellt Wissenschaftler vor eine große Herausforderung, da es sich um eine sehr heterogene und dynamische Erkrankung handelt. Mit klassischen Methoden wie operativen Eingriffen, Bestrahlung, Chemotherapie und deren Kombination konnte die Lebenserwartung von Krebspatienten deutlich verlängert werden. Diese Therapieoptionen sind zwar über ein weites Spektrum an Krebserkrankungen einsetzbar, jedoch birgt die geringe Spezifität ein hohes Risiko für Nebenwirkungen oder verminderte Wirksamkeit. Der Wunsch nach Therapeutika, die eine höhere Spezifität für die unterschiedlichen Krebsarten aufweisen und gleichzeitig eine personalisierte Behandlung des einzelnen Patienten erlauben, hat die Entwicklung von neuen therapeutischen Konzepten vorangetrieben. Zwei aktuelle Konzepte, die beide Komponenten des Immunsystems als Grundlage nutzen, sind antikörperbasierte Wirkstoffe und Immunzelltherapie. Antikörper bilden den strukturellen Kern bei einer Vielzahl von therapeutischen Molekülen. Wachstumshemmende monoklonale Antikörper, bispezifische Antikörper und Antikörper-Wirkstoff-Konjugate stellen hierbei die drei Hauptformate dar und werden in dieser Arbeit adressiert. Zuerst wird ein high-content Verfahren beschrieben, welches den Einbau von DNA-Basenanaloga und anschließende Quantifizierung des DNA-Gehalts nutzt, um das Potential eines wachstumshemmenden Antikörpers zu bestimmen. Zusätzlich ermöglicht es Einblicke in dessen Wirkmechanismus zu gewinnen. Ferner wird der Einbau komplementärer Klick-Gruppen mittels Tub-tag Konjugation zur C-terminalen Verknüpfung von Proteinen beschrieben und dessen Eignung zur Herstellung von bispezifischen Antikörpern demonstriert. Vor allem bei der Selektion von geeigneten Antikörperpaaren bietet eine solch modulare Ligationsmethode die Möglichkeit viele Kandidaten kombinatorisch zu verknüpfen nachdem sie individuell exprimiert wurden, um so komfortabel eine Bibliothek von bispezifischen Molekülen zu generieren. Im Allgemeinen wird durch die Entwicklung und Optimierung einer Vielzahl von bioorthogonaler Konjugationsmethoden die Modifikation von Proteinen aktuell stark vorangetrieben. Weit verbreitet ist die Modifikation von endogenen natürlichen Aminosäuren, der Einbau von unnatürlichen Aminosäuren und die enzymatische Modifikation, um entweder direkt eine funktionelle Einheit anzuheften oder um universelle bioorthogonale Gruppen einzubringen. In diesem Zusammenhang wird in dieser Arbeit eine neue cystein-selektive, modulare Biokonjugationsmethode beschrieben, die elektrophile Phosphonamidate verwendet, um stabile Cysteinkonjugate herzustellen. Ferner wird diese Methode zur stabilen Verknüpfung von cytotoxischen Molekülen und Antikörpern verwendet. Die daraus resultierenden Antikörper-Wirkstoff-Konjugate sind sowohl *in vitro* als auch *in vivo* aktiv und zeigen darüber hinaus eine erhöhte Plasmastabilität im Verglichen zur standardmäßigen Maleimidkonjugation. Antikörperbasierte Wirkstoffe erweitern zwar wie erwartet das therapeutische Fenster indem sie off-target Effekte reduzieren und zugleich tumor-spezifische Toxizität erhöhen, stoßen jedoch auch auf Limitationen. Biomoleküle werden aktiv abgebaut und aus dem Körper entfernt und erfordern somit eine wiederholte Verabreichung des Therapeutikums in regelmäßigen Zeitabständen. Außerdem ist die Verteilung im Körper hauptsächlich durch passive Effekte bestimmt,

wodurch die Penetration in das Gewebe erschwert wird. Im Gegensatz hierzu steht der revolutionär neue Ansatz “lebendige Medikamente” zu verwenden, die aktiv im Körper proliferieren, und somit Limitationen von “leblosen Medikamenten” umgehen. Vielversprechend zeigt sich hier der Einsatz von Immunzellen, allen voran von T Zellen für die Krebstherapie. Die “lebendige” Natur dieser zellbasierten Medikamente erfordert jedoch eine umfassende Charakterisierung bevor sie dem Patienten verabreicht werden. In diesem Zusammenhang wird in dieser Arbeit ein neues Multimerreagenz, namens FLEXamer, zur Isolierung und Charakterisierung von T Zellen und deren T Zellrezeptoren beschrieben. FLEXamere erhalten die hohe Präzision von konventionellen Multimerreagenzien, vereinen jedoch die unterschiedlichen Multimere in einem einzigen vielseitigen Reagenz, das bedarfsgerecht, individuell funktionalisiert werden kann. Zusammenfassend beschäftigt sich diese Arbeit mit ortsgerichteten Biokonjugationsmethoden und neuen sensitiven Werkzeugen zur Herstellung und umfassenden Charakterisierung von sensitiven und patientenspezifischen Krebstherapeutika der nächsten Generation.

3 INTRODUCTION

3.1 NEXT-GENERATION CANCER THERAPEUTICS

Cancer is one of the leading causes of death in developed countries and with 22 % of total the second most cause in the United States in 2016 just behind chronic heart diseases (Heron, 2018). Even more alarming are the numbers for the world wide projections with an expected increase in cancer cases and deaths of approximately 50 % until 2035 (Ferlay et al., 2019; Ferlay J, 2018). Heart diseases on the contrary are on the decline due to effective prevention and treatment (Mensah et al., 2017). For cancer the situation is very different since up till now we lack effective tools to cure the disease. One striking reason for this is the substantial diversity of cancer resulting from the evolutionary character of its pathogenesis. Basically every organ or tissue in the body can be affected, some more susceptible than others. Furthermore, cancer arises from a body's own cells and therefore will be different in each and every patient even if the same organ is affected. This observation already hints to a major problem in cancer treatment which is heterogeneity (Alizadeh et al., 2015). Nevertheless, cells need to acquire some common traits that allow them to form a malignant tumor (Hanahan & Weinberg, 2011). Most of these so called "hallmarks of cancer" are related to uncontrolled proliferation such as resisting cell death and sustaining proliferative signaling. However, which underlying molecular mechanism is altered to gain those traits can be very different and adds further to the complexity of cancer. In addition, cancer cells evolve over time and therefore diversify over the course of disease and treatment (Falzone, Salomone, & Libra, 2018; Mel Greaves & Carlo C. Maley, 2012; Janiszewska & Polyak, 2015; McGranahan & Swanton, 2017). All those facts make "the cancer" a tremendously heterogeneous disease which is extremely challenging to diagnose, treat or even cure.

Consequently, the treatment of cancer has undergone constant development (Arruebo et al., 2011; DeVita & Rosenberg, 2012). A straightforward approach for solid tumors is to physically remove the malignant tissue by surgery. However, it is likely that not all cancer cells are removed, thus increasing the chance for relapse. On that account, additional treatment options such as radiation, chemotherapy and hormone treatment have been developed in the last century and considerably advanced cancer therapy. Chemotherapy is administered systemically but preferentially kills fast dividing cells, thereby suppresses the growth of cancer cells (Chabner & Roberts Jr, 2005). Although this strategy allows the treatment of inoperable tumors and leukemia, severe side effects occur by unspecific toxicity to healthy, strongly proliferating cells such as the hematopoietic system (Maxwell & Maher, 1992). This issue was addressed by targeted therapy approaches that aimed for specifically manipulating cancer cells but leaving healthy tissue unaffected. In recent years this novel therapeutic concept has been realized in many different ways but two approaches draw particular strong attention and have made their way to clinical application. Both approaches harness the immune system's outstanding capability of detecting and fighting foreign or degenerate objects. The first approach relies on the use of antibodies as targeting probes to manipulate the cancer cell directly, deliver a toxic payload or redirect the immune system to clear

marked cancer cells (Sawyers, 2004; Shuptrine, Surana, & Weiner, 2012). The second approach relies on the administration of immune cells as living drugs that autonomously identify and specifically eliminate cancer cells (June, Riddell, & Schumacher, 2015; Perica, Varela, Oelke, & Schneck, 2015). Although the two concepts are quite different, both aim for higher targeting precision which, on the one hand, increases treatment efficacy but, on the other hand, also allows for more personalized therapy.

3.1.1 THERAPEUTIC ANTIBODIES

For the most time pharmaceuticals have predominantly been small molecules, mainly produced by extraction from natural sources or chemical synthesis (Jones, 2011). When in 1922, at the University of Toronto, Banting and Best isolated insulin from cow pancreas and used it for diabetes therapy, a new era of drugs began (Banting & Best, 1990; Karamitsos, 2011; Lewis, 2002). For the first time a protein has been used as a therapeutic agent. With the development of recombinant protein techniques proteinaceous drugs could not only be produced in large scale by fermentation but also became editable (Tobin, Richards, Callender, & Wilson, 2014; Young, Britton, & Robinson, 2012). Structure and function of proteins could now be designed to fulfill specific needs of particular applications. Owing to this development antibodies have become available as a versatile scaffold for biological probes to target and manipulate disease related antigens (Chames, Van Regenmortel, Weiss, & Baty, 2009; Ecker, Jones, & Levine, 2014; Hudson & Souriau, 2003). Three important antibody formats that are used for therapeutic applications will be outlined in the following paragraphs.

3.1.1.1 MONOCLONAL ANTIBODIES

Antibodies are an essential part of the humoral, adoptive immune system. They are produced by B cells to label pathogens or pathogenic substances for clearance. Antibodies exist in two forms, either membrane bound to B cells, also referred to as the B cell receptor (BCR), or in a free soluble form in blood and extracellular space. The BCR serves to recognize specific antigens and activate the respective B cell to i) differentiate into antibody secreting plasma B cells or memory B cells and ii) internalize, process and present antigens to other immune cells such as T cells. Antibodies share a common overall structure comprising of two heavy chains and two light chains (Figure 1). The chains arrange in a Y-shaped structure where each light chain pairs with one heavy chain and the two heavy chains with each other. The pairing is mediated by matching hydrophobic patches on pairing domains and further stabilized through interchain disulfide bonds. The overall structure can be divided into three functional units. The two identical Fab fragments responsible for antigen binding and the glycosylated Fc fragment responsible for mediating immune effector functions. Whereas only constant domains of the heavy chain are part of the Fc fragment and determine the isotype of the antibody the variable domains of heavy and light chains comprise hypervariable regions that form the epitope binding site (also called paratope). Consequently, the binding specificity of an antibody to its antigen is determined and mediated by the Fab-arms, whereas the isotype specific Fc-arm determines which components of the immune system recognize the antibody and thereby defines the immunological response. Human

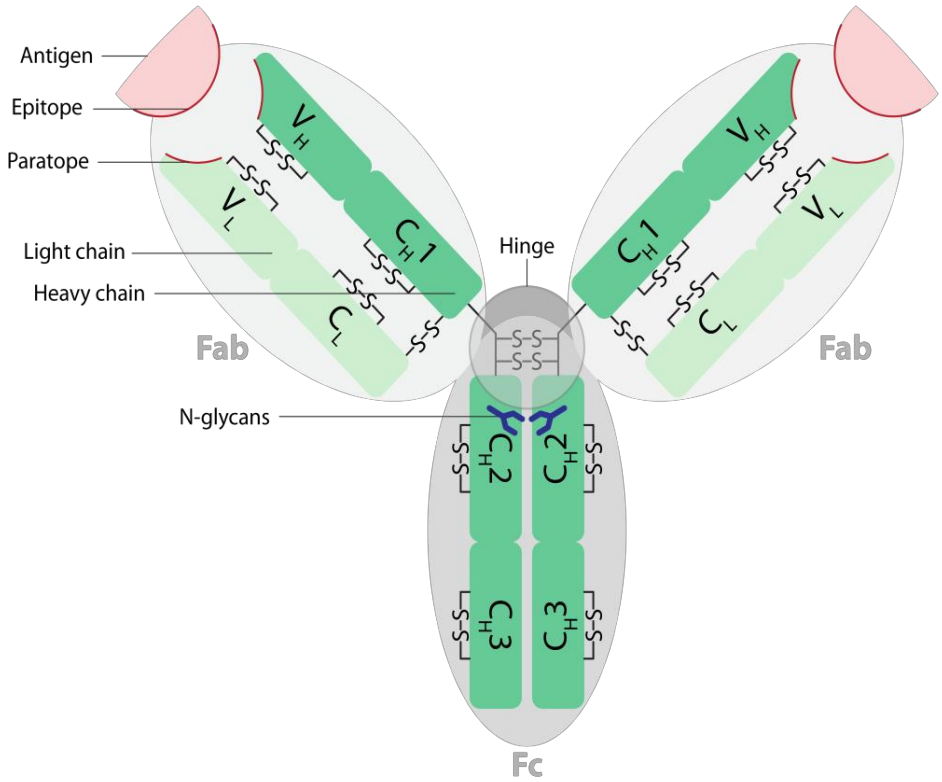

Figure 1 Y-shaped structure of an IgG antibody. Two heavy chains and two light chains associate into a Y-shaped tertiary structure. Association is mediated by surface patch interaction and interchain disulfide bridges (S-S). The heavy chain (HC) is built from three constant domains (CH_1, CH_2 and CH_3) and one variable domain (VH). The light chain comprises one constant domain (CL) and one variable domain (VL). Each individual domain is stabilized by an intramolecular disulfide bridge. The two paired variable domains (VL+VH) form the antigen binding sites (paratope). The flexible hinge region is susceptible to proteolytic digest by papain, yielding two antigen binding fragments (Fab) and one crystallizable fragment (Fc). The CH_2 domain is post translationally glycosylated with branched N-glycan chains.

Igs can be assigned to five different isotypes (IgA, IgD, IgG, IgE, IgM) (Schroeder & Cavacini, 2010). IgG is the most abundant isotype in blood serum and is involved in pathogen clearance. IgG does so through multiple mechanisms. For example, the binding to an extracellular structure of the pathogen can directly manipulate the target's function, such as binding to transmembrane receptors can block their signaling and render the pathogen benign. Another mechanism called complement dependent cytotoxicity (CDC) includes the decoration of pathogens with IgGs (opsonization), subsequent complement activation and phagocytosis by phagocytes. In a similar process, antibody-dependent cellular cytotoxicity (ADCC), the antibody recruits immune cells, predominantly natural killer cells, that promote lysis of pathogens or induce programmed cell death (apoptosis) in pathogen infected cells (L. L. Lu, Suscovich, Fortune, & Alter, 2017).

All these modes of action have been used in one or another way for therapeutic purposes (Schürch, 2018). However, in cancer therapy two mechanisms are especially important (Redman, Hill, AlDeghaither, & Weiner, 2015; Scott, Wolchok, & Old, 2012). Firstly, monoclonal antibodies have been selected or designed to specifically interfere with the function of critical cell surface receptors on cancer cells. For example, certain cancer types acquire enhanced proliferation by overexpression of growth factor

receptors (e.g. epidermal growth factor receptor, EGFR or human epidermal growth factor receptor 2, HER2)(Masuda et al., 2012) or immune checkpoint receptors (e.g. programmed cell death protein 1 ligand1, PD-L1) (X. Wang, Teng, Kong, & Yu, 2016). On the one hand, overexpressed receptors can serve as markers that make cancer cells distinguishable from normal body cells, yet, specifically targetable. On the other hand, enhanced proliferation or immune cell evasion can be dependent on the signaling of these receptors (Browne, O'Brien, Duffy, Crown, & O'Donovan, 2009), thus providing a weak point for therapeutic agents to interfere. Along this line several therapeutic antibodies have been developed that inhibit receptors e.g. by i) blocking ligand binding sites, ii) blocking dimerization sites crucial for downstream signaling or iii) depleting receptors from the cell surface by crosslinking-induced internalization. However, only a subset of cell surface markers can be manipulated in a way that directly reduces cancer cell growth or leads to cell death. Therefore, the second very important mode of action of monoclonal antibodies in cancer therapy is tagging cells for ADCC. Virtually any cell surface structure, such as transmembrane proteins, glycosylation patterns or lipid composition, can be recognized by antibodies. If these structures are either exclusively, preferentially or differentially present on cancer cells these markers can be targeted by antibodies and tag those cells for clearance. Besides these two mechanisms therapeutic antibodies can act in many more ways and in most cases the anti-proliferative activity results from a combination of multiple modes of action (Hudis, 2007).
During development of therapeutic monoclonal antibodies it is important to evaluate the anti-proliferative potency of potential candidates early on *in vitro*. This can be done in the presence (Lallemand et al., 2017) or absence of immune cells and will give insight into the predominant mode of action. For the detection of proliferating cells several methods are available (Aysun, Yağmur, & Yusuf, 2016). These differ from each other, on the one hand, in the generated signal (e.g. colorimetric, fluorimetric or radioactive) but more importantly also in the detected feature (e.g. surviving cell count, metabolic activity or DNA replication) (X. Lu & Bergelson, 2014; Vega-Avila & Pugsley, 2011). Independent of the working principle a suitable assay has to be sensitive and adaptable to high throughput handling to allow accurate comparison of a large number of antibody candidates in parallel.

3.1.1.2 Bispecific Antibodies

Although very promising treatment results could be achieved with monoclonal antibodies, relapse of tumors after prolonged treatment has been observed in many cases (Iwamoto et al., 2009). Several reasons for this observation have been proposed in recent studies (Reslan, Dalle, & Dumontet, 2009). For one, a tumor is a heterogeneous mixture of cancer cells that forms its own microenvironment. Consequently, individual cancer cells can be quite different from each other depending on many factors such as stage of tumor development, exact localization in the tumor or proliferative state. Therefore already from the beginning of treatment some cells will be more susceptible to a specific antibody than others due to differences in marker expression, accessibility and proliferative activity. In addition, upon treatment a selective pressure is exerted on the tumor that can cause adaption of individual cells by actively downregulating the marker antigen or survival of the unsusceptible, inaccessible population of cancer cells

within the tumor. After prolonged treatment or termination these cells may outgrow again and cause disease relapse (Chatterjee & Bivona, 2019; Gillies, Verduzco, & Gatenby, 2012; M. Greaves & C. C. Maley, 2012; Sotillo, Schvartzman, Socci, & Benezra, 2010). Consequently, the efficacy of monoclonal antibodies is, among other factors, dependent on accessibility of target cells, constant expression of the antigen and the ability to initiate immune responses. Since those aspects are susceptible to evasion by cancer cells many attempts have been made to address the related treatment resistance and resulted in alternative treatment strategies such as combination therapies and the design of new therapeutic molecules. One example is a novel class of antibody therapeutics that combines the binding specificity of multiple antibodies into a single biomolecules, so called bispecific or multispecific antibodies. With advancing recombinant antibody production and protein engineering a whole zoo of such multispecific formats has been designed in the recent past (Brinkmann & Kontermann, 2017). Although these formats are quite diverse in their specific architecture they follow general principles. They combine two or more different antigen-binding units into a single molecule which can in addition be equipped with an Fc-arm or other effector domains. Whereas monoclonal antibodies bind only one antigen, bispecifics bind two different antigens. This can be two antigens of the same cell, e.g. two tumor markers, or two antigens on different cells, e.g. a tumor marker and an immune cell marker (Husain & Ellerman, 2018). A bispecific of the first type can increase binding specificity if the two individual binding sites alone

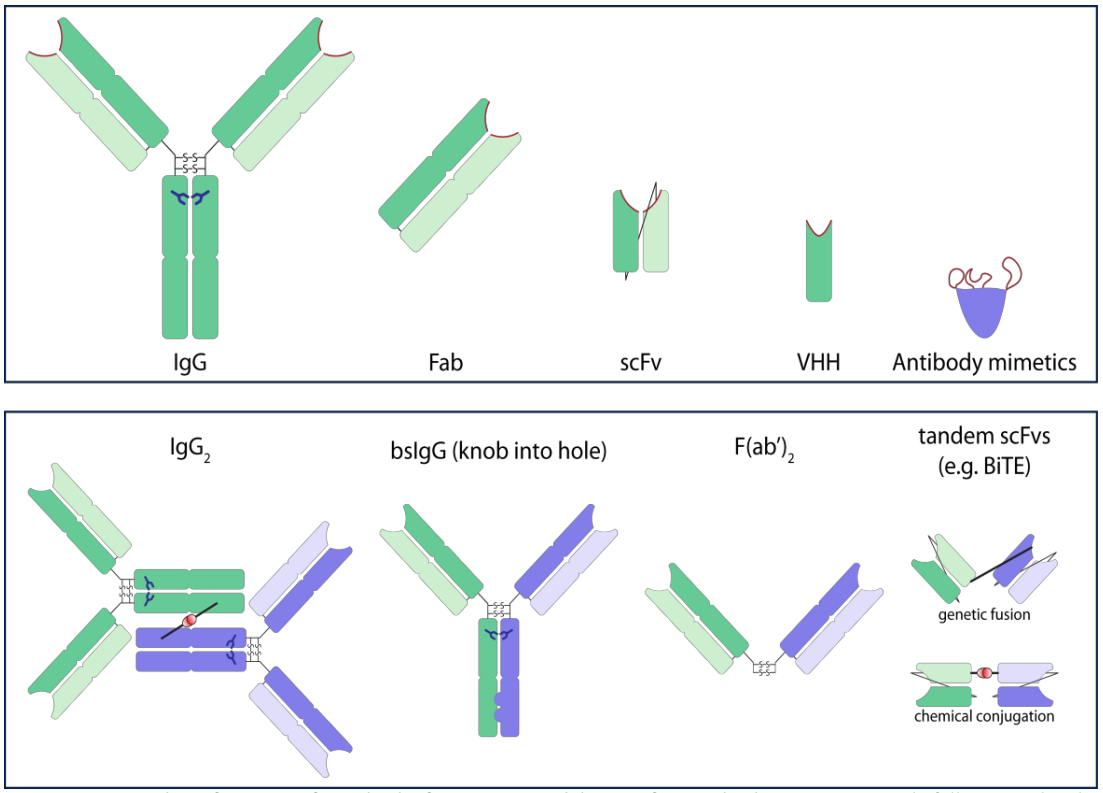

Figure 2 Exemplary formats of antibody fragments and bispecific antibodies. Upper panel: full IgG molecule; Fragment antigen binding (Fab); single chain Fragment variable (scFv) built by genetic fusion of VH and VL; Variable domain of heavy chain antibodies (VHH) e.g. nanobodies from camelid antibodies; alternative proteins with engineered binding sites (antibody mimetics) e.g. DARPins, anticalines and affimers. Lower panel: Chemically cross-linked bispecific antibody (IgG2); bispecific IgG (bsIgG) with knob into hole guided hetero-paired heavy chains; disulfide linked heterologous Fab fragments (F(ab')2); tandem scFvs formed by genetic or chemical fusion of two scFvs.

exhibit low binding affinity towards their respective antigen but in combination strong avidity towards cells presenting both antigens. This approach has been used to achieve tissue specific targeting of less differentially expressed tumor markers to reduce off-target toxicity (Gantke et al., 2017; N. K. Lee et al., 2018; McGaraughty et al., 2017). Furthermore, simultaneous targeting of two markers can reduce the chance for tumor evasion since two markers would need to be downregulated simultaneously. Besides increasing specificity bispecifics can also be used to crosslink (Brunker et al., 2016) or prevent cross linking (McDonagh et al., 2012) of two cell surface receptors in order to manipulate their signaling or enhance receptor internalization (Andreev et al., 2017; J. Y. Li et al., 2016). As opposed to this, bispecifics that target two antigens of two different cells follow a very different mechanistic concept. In this case, the antibody serves as a physical adaptor that brings and holds two cells in close proximity. Much like the Fc-arm of a monoclonal antibody recruits immune cells, the second binding site of a bispecific can also be designed to bind immune cell markers. However, by the choice of targeted markers one can i) control which type of immune cell is redirected to the tumor (Kellner, Peipp, & Valerius, 2011), ii) induce immune cell activation (Dreier et al., 2002; P. Hoffmann et al., 2005) or iii) override inhibitory immune checkpoint signaling (Knudson, Gameiro, Lo, & Schlom, 2017). Such bispecific formats are commonly designed omitting the Fc-arm since its immune effector function is expandable or undesirable. Yet, besides its effector function, the Fc-arm increases the overall size of the molecule, thus, reduces renal clearing of the molecule. Furthermore, it also promotes active recycling of antibodies via the FcRn receptor primarily in the liver. Both mechanisms significantly increase plasma half-life, and allow less frequent dosing of the drug which inspired the development of Fc-mutants lacking FcRn interaction. But, the larger molecular size also has disadvantages such as slow diffusion in the extravascular space and reduced tumor penetrance. Thus, besides the classical IgG format many more alternative architectures have been developed. These range from antibodies augmented with additional binding or effector domains, trimmed antibodies, antibody fragments such as Fab or scFv fragments over alternative antibodies such as cameloid single chain antibodies and fragments thereof (e.g. nanobodies) to non-antibody derived binding modules called antibody mimetics (e.g. affimers, anticalins and DARPins) (Brinkmann & Kontermann, 2017). Researchers have mixed and matched all those building blocks in manifold ways providing a variety of different bi- and multispecific molecules (Figure 2). However, some building blocks are used more frequently than others. For example Fab fragments originating from different antibodies can be combined to generate bispecific antibodies. Fab fragments are built from one light chain and one truncated heavy chain comprising the variable and first constant domain. Both chains are linked via a disulfide bridge. Since the two chains are not associated during expression it has to be ensured that the right chains pair. scFv (single chain Fragment variable) fragments on the other hand circumvent this issue by covalently linking the two variable domains. A scFv is a single polypeptide consisting of the two variable domains (VH and VL) joined by a flexible linker sequence. By covalently linking two scFvs either by genetic fusion or chemical conjugation a bispecific can be generated which comprises only antigen binding domains, therefore represents a very condensed bispecific format (Huehls, Coupet, & Sentman, 2015). This format has several advantages such as straightforward

recombinant production (Hornig & Farber-Schwarz, 2012), rapid diffusion and good tumor penetrance (Xenaki, Oliveira, & van Bergen En Henegouwen, 2017). scFvs are the structural basis for a therapeutic bispecific antibody format called Bispecific T cell Engagers (BiTE's). BiTE's combine a scFv specific for a tumor antigen with a scFv specific for a T cell antigen. For example, the first approved BiTE Blinatumomab (Przepiorka et al., 2015) binds CD19 on malignant B-cells and CD3, a subunit of the T cell receptor complex, on cytotoxic T cells (Loffler et al., 2000). By binding both antigens simultaneously the patient's own T cells are recruited to malignant cells. Subsequently, activated cytotoxic T cells induce apoptosis in the target cancer cell by the release of cytotoxins such as perforin and granzymes (Dreier et al., 2002). Based on i) the recent success of approved BiTEs in therapy, ii) evermore bispecifics in clinical trials showing promising results and iii) growing pharmaceutical research interest (Dahlén, Veitonmäki, & Norlén, 2018) more alternative bispecific formats are currently evaluated for their therapeutic applicability and will expand the set of therapeutic antibodies.

3.1.1.3 Antibody-Drug Conjugates

Targeted therapy with monoclonal or bispecific antibodies had a great impact on the treatment options for cancer patients. However, up till now these therapies are not used as standalone treatments but rather in combination with other antibodies or conventional radiation-/chemotherapy (Marrocco, Romaniello, & Yarden, 2019). A very recent development in this field was the combination of targeted- and chemotherapy in a single molecule called antibody-drug conjugate (ADC) (Diamantis & Banerji, 2016). ADCs physically link a very potent cytotoxic agent to a very specific probe - an antibody. This so called magic bullet allows specific accumulation of the toxin at the tumor site while sparing healthy tissue. Unlike fusion proteins such as bispecific antibodies the functional entities in ADCs are, usually, not two proteins but rather one large biomolecule - the antibody - and a small chemical compound - the toxin. Quite different from monoclonal or bispecific antibodies that are either cytotoxic by merely binding to the cancer cell or by recruiting cytotoxic immune cells, ADCs directly deliver the toxin to the cancer cell. Targeted delivery allows the use of very potent toxins that so far could not be used in classical chemotherapy. Different compounds such as auristatines, maytansinoids, calicheamicins, duocarmycin and doxorubicin derivatives have been successfully used as payloads. These compounds induce DNA damage, interfere with DNA replication or inhibit tubulin polymerization, thereby prohibiting cell division and causing cell death (Dan et al., 2018). A major requirement resulting from these modes of action is the delivery of the drug to the cytoplasm. Consequently, internalization is a crucial feature of antibodies used for ADCs and has been implemented in antibody production and selection strategies but is also addressed by antibody engineering approaches (R. M. Hoffmann et al., 2017). Furthermore, advances in antibody engineering put forth less immunogenic and more stable antibody scaffolds. For example immunogenicity of antibodies has been reduced by chimerization and humanization of animal-derived antibodies or the generation of fully human antibodies by *in vitro* selection strategies (Almagro, Daniels-Wells, Perez-Tapia, & Penichet, 2018).

Since antibody and toxin have rather opposing biophysical properties and require very different production strategies both components are usually produced separately and joined afterwards. The coupling of a small chemical entity to a large biomolecule is not trivial but several strategies have been developed since the idea of ADCs (Agarwal & Bertozzi, 2015b; Dominik Schumacher, Hackenberger, Leonhardt, & Helma, 2016). So besides the antibody and the cytotoxic payload an ADC has a third critical component - the linker (Figure 3). This adapter serves the main purpose of covalently linking antibody and payload (Tsuchikama & An, 2018). Although high stability of the linkage in circulation is a desirable feature for ADCs, most drugs need to be released from the antibody molecule to perform their cytotoxic action (Figure 3). Thus, the ideal linkage for such drugs is stable in the extracellular space but is labile intracellularly. Several cleavable linker designs have been described and used for ADCs. One strategy uses pH sensitive linkages cleaved under acidic conditions, thus, triggering drug release during endosomal and lysosomal processing of the internalized antibody. A second mechanism makes use of protease cleavable peptide sequences incorporated in the linker structure. For example a valine-citrulline (VC) motif recognized by the endosomal protease cathepsin B has been used for brentuximab vedotin. Furthermore, the composition and structure of the linker can also be designed to manipulate the ADC's overall properties. One such feature, tunable by linker composition, is the hydrophilicity of the assembled ADC. Surface exposed hydrophobic groups reduce the water solubility of the antibody and contribute to increased aggregation. Both are important parameters impacting stability and distribution of the ADC in the body. Commonly used cytotoxic agents are hydrophobic and destabilize the antibody when attached to its surface. On the one hand, this issue has been addressed by the design of hydrophilic linker sequences such as stretches of polyethylene glycol (PEG) that increase hydrophilicity of the attached moiety or the design of more hydrophilic toxins (Lyon et al., 2015). On the other hand,

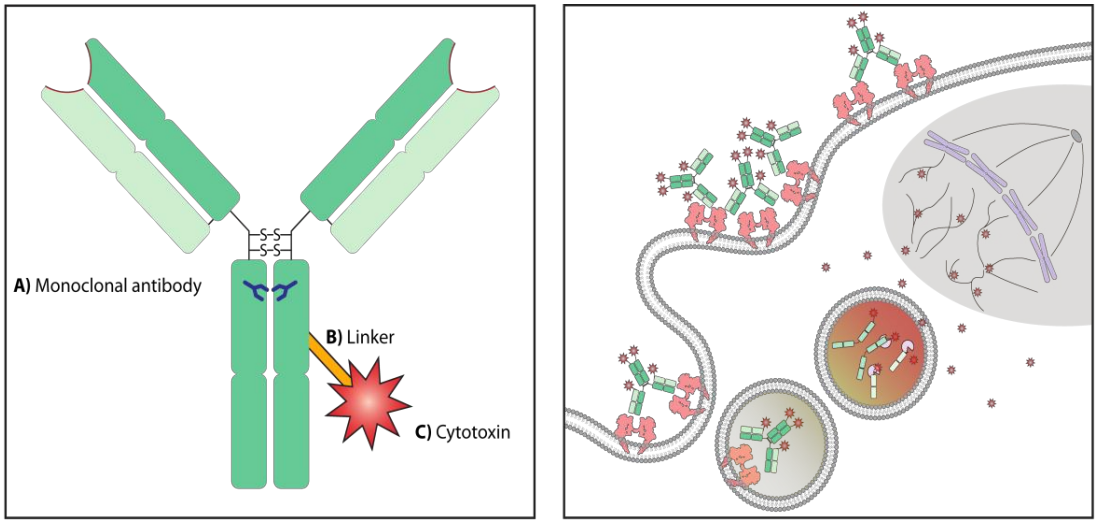

Figure 3 Structure of an antibody-drug conjugate (ADC) (left) and exemplary mechanism of action (right). Left panel: The three components of an ADC: A) the antigen targeting monoclonal antibody B) the linker connecting the drug to the antibody and, if applicable, facilitating triggered release C) the highly potent cytotoxic drug mediating cell killing. Right panel: The ADC binds to a cell surface antigen followed by internalization into endosomes and shuttling to lysosomes. Low pH and/or the presence of proteases in the lysosome triggeres release of the the cytotoxin. Toxins acting on microtubule organization hinder mitotic spindle formation, consequently, prohibiting cell division and inducing cell death.

hydrophobicity can be controlled by the number of drugs attached to the antibody molecule - the drug to antibody ratio (DAR) (Ross & Wolfe, 2016).
First and second generation ADCs like gemtuzumab ozogamicin (Hamann et al., 2002), trastuzumab emtansine (Lewis Phillips et al., 2008) and brentuximab vedotin (Senter & Sievers, 2012) were generated by conjugation via amine or thiol reactive groups, linking the drug to the antibodie's lysines or cysteines, respectively (Tsuchikama & An, 2018). The relative high abundance of surface exposed lysines leads to high heterogeneity in number and position of attached drugs (Figure 4) (L. Wang, Amphlett, Blattler, Lambert, & Zhang, 2005). ADCs generated by lysine-conjugation range from unconjugated, thus, unfunctional to highly conjugated, but unstable ADCs and encompass a large set of moderately conjugated ADC species modified at different positions. This heterogeneity has been shown to reduce functionality of the generated ADC (Lyon et al., 2015). Targeting less abundant side chains like interchain cysteines reduces heterogeneity and leads to a more defined product. For brentuximab vedotin, the first approved ADC generated by cysteine labeling, a maleimide was used to covalently link the drug to reduced interchain disulfides. However, the ADC suffered from poor in vivo stability due to premature drug release. Instability of the maleimide thioether bond allows attack of the linkage by other free thiol groups and thus the transfer of the drug by retro-Michael-addition to other reactive thiol-containing proteins such as serum albumin (Ponte et al., 2016; Shen et al., 2012). These insights have fostered the development of more stable cysteine-conjugation strategies (J. M. Chalker, G. J. Bernardes, Y. A. Lin, & B. G. Davis, 2009; Szijj, Bahou, & Chudasama, 2018b), however, a reduced IgG1 antibody presents a maximum of eight thiol groups, thus still

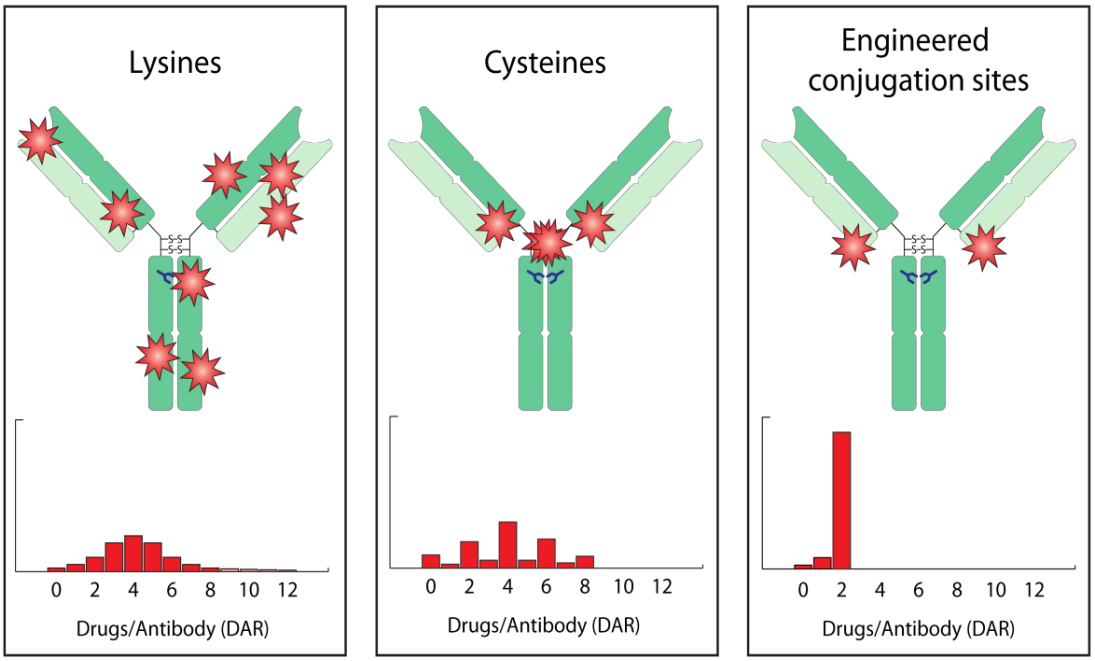

Figure 4 Conjugation methods for ADC generation. Left panel: Conjugation to amines of lysine residues leads to broad distribution of the drug to antibody ratio (DAR) and to high heterogeneity in the site of attachment. Although high DAR species are generated by lysine conjugation these are generally unstable in solution. Center panel: Conjugation to reduced interchain disulfides reduces the number of available conjugation sites, thus narrowing the DAR distribution. Right panel: The introduction of engineered conjugation sites allows the conjugation of a defined number of drugs at a desired site. Adapted from (Herrera & Molina, 2018)

leading to a considerable heterogeneous DAR distribution (Figure 4) (Sun et al., 2005). The quest for more stability, efficacy and homogeneity of ADCs has inspired the use of site-specific conjugation strategies for drug attachment (Agarwal & Bertozzi, 2015b). In contrast to endogenous lysine or cysteine conjugation these strategies are more specific since they either target less abundant reactive sites (e.g. glycan engineering (Qasba, 2015)) or rely on the introduction of a defined number of bioorthogonal handles at a specific position in the antibody sequence. A number of site-specific strategies such as engineered cysteines (Junutula et al., 2008), unnatural amino acid incorporation by amber suppression (Axup et al., 2012) or enzyme-mediated conjugation (Lotze, Reinhardt, Seitz, & Beck-Sickinger, 2016) in combination with bioorthogonal reactions such as oxime ligation, copper catalyzed (VanBrunt et al., 2015) or strain promoted alkyne-azide cycloaddition (Zimmerman et al., 2014) (CuAAC and SPAAC) and Inverse electron demand Diels–Alder reaction (Oller-Salvia, Kym, & Chin, 2018) have been used to generate site-specific conjugated ADCs with a defined DAR. The third generation of ADCs uses these techniques in combination with stability and specificity engineered antibodies and more potent toxins to further open up the therapeutic window implying reduced off-target and increased on-target toxicity (Dominik Schumacher et al., 2016).

3.1.2 ADOPTIVE T CELL THERAPY

Antibodies, whether monoclonal, bispecific or equipped with toxins have become an important pillar in current clinical cancer therapy. However, once administered these drugs disseminate in the body and are cleared or degraded over time by various mechanisms (Ryman & Meibohm, 2017). Although, characteristics such as molecular size, hydrophobicity, susceptibility to proteolytic digestion and recycling via FcRn can be modulated to increase dwell time of the drug in the body, it is necessary to re-administer the drug in certain time intervals to maintain an effective concentration (Haraya, Tachibana, & Igawa, 2019; Presta, 2008). A radically different concept has been developed in the last decades; the use of living drugs that proactively detect and kill cancer cells and ideally persist in the body long after administration for continuous protection (Kalos et al., 2011; Kochenderfer et al., 2010; S. A. Rosenberg, Spiess, & Lafreniere, 1986). Immune cells are known for their capability to detect foreign or degenerate cells and mediate their elimination. Thus, especially T lymphocytes are being explored for therapeutic use, summarized under the term adoptive cell therapy (ACT) (Steven A. Rosenberg, Restifo, Yang, Morgan, & Dudley, 2008).

Tumor infiltrating lymphocytes (TILs) are immune cells that accumulate in and around tumor tissue. These cells often have the capability of recognizing cancer cells but are frequently silenced or rendered nonfunctional by the tumor microenvironment. TIL therapy consists of the surgical removal of tumor tissue, outgrowth and *ex vivo* expansion of TILs by addition of stimulatory factors such as Il-2, αCD3-antibody and irradiated feeder cells and subsequent reintroduction into the patient (Riddell & Greenberg, 1990; Rohaan, van den Berg, Kvistborg, & Haanen, 2018). These procedures still result in a heterogeneous cell population, however, CD8+ T cells have been identified as the driving force of anti-tumoral activity in TILs (Radvanyi et al., 2012). To improve efficacy and increase response rates, several strategies have been developed. On the one hand, preconditioning of the patient for TIL therapy e.g. by high dose IL-2

treatment and lymphodepletion has been used (Andersen et al., 2016; Dudley et al., 2008). On the other hand, enrichment for tumor reactive T cells has also been investigated for TIL production. Several markers such as IFNγ secretion and CD137 expression upon coculture with tumor material, PD-1 expression and a high degree of T cells with T cell receptors specific for tumor antigen correlate positively with anti tumor activity and were used to generate more reactive TIL products (Inozume et al., 2010; Kelderman et al., 2016; S. A. Rosenberg et al., 2011; Ye et al., 2014). Despite promising results of this strategy in the treatment of melanoma, TIL therapy also has its limitations. TIL therapy is so far limited to few cancer types, it is a highly personalized concept, thus cost and time consuming and prone to heterogeneity in the product resulting in varying efficacy and safety (S. Lee & Margolin, 2012). Furthermore, this approach is limited by the selectivity, specificity and quality of the patient's T cell repertoire.

Much like protein engineering allowed the alteration and augmentation of antibodies to create recombinant monoclonal antibodies, bispecific antibodies and ADCs with enhanced or completely novel functions, genetic engineering has opened the door for alteration and augmentation of T cells. Genetically engineered T cells can be equipped with alternative TCRs or chimeric antigen receptors (CARs) to acquire desired new antigen specificity. Consequently, these techniques are not limited to quality and breadth of a patient's T cell repertoire. This approach has gained considerable momentum by the recent US Food and Drug Administration (FDA) approval of Tisagenlecleucel (KYMRIAH®) for the treatment of acute lymphocytic leukemia (ALL), the first gene edited autologous T cell therapy (O'Leary et al., 2019). CAR-T cell therapy includes the isolation and expansion of T cells from the patient, their transduction with a chimeric antigen receptor and subsequent reintroduction into the patient. In general, CARs are composed of intracellular T cell signaling domains, a transmembrane domain and an extracellular scFv fragment derived from a tumor antigen specific antibody (Dotti, Gottschalk, Savoldo, & Brenner, 2014). Tisagenlecleucel uses an antiCD19 CAR construct that redirects transduced T cells to detect and kill CD19 positive cells. CD19 is a B-cell lineage specific marker also expressed on ALL B-cells that have undergone neoplastic transformation (K. Wang, Wei, & Liu, 2012). AntiCD19 CAR-T cells have been used with great success for the treatment of ALL demonstrating remission in 81 % of patients treated with Tisagenlecleucel in a global, multicenter phase 2 trail (Maude et al., 2018). Despite the great efficacy in eliminating CD19+ B-cell lymphomas, current CAR-T cell therapy goes together with total B-cell ablation (Kochenderfer et al., 2010). Although, this is per se not a life threatening condition, the effects of long term B-cell ablation are not known and the absence of adoptive humoral immunity makes patients more susceptible to infections. Furthermore, this strong on-target/off-tumor activity might hamper the translation of CAR-T cell therapy to other malignancies with markers that are also expressed on vital tissues. Various strategies to overcome these limitations are currently explored in many research groups. Today's CARs use antibody derived scFv fragments as binding units which naturally have high binding affinities. Binding units with lower affinity might curb CAR T cell reactivity and allow fine tuning of the required antigen density for successful T cell activation (X. Liu et al., 2015). Also CAR T cells targeting two antigens in combination with logic gates that only allow activation when a

cell simultaneously binds both antigens could increase specificity (Davies & Maher, 2016). The concept of multiple low affinity interactions in close proximity resulting in avidity gain is also found in the natural interaction of T cells with target cells via TCR-MHC (major histocompatibility complex) interaction (Lanzavecchia, Iezzi, & Viola, 1999). The transduction of TCRs may allow physiological interaction and potentially more controlled activation of genetically engineered T cells. A major difference between CAR and TCR transgenic T cells results from the category of epitopes recognized by their binding units. CARs are based on antibodies that are selected to recognize a structure on a cell's surface but are excluded from accessing intracellular proteins, whereas, TCRs bind to MHC presented intracellular peptides. Depending on MHC class, these peptides originate from proteolytic digest of either cytosolic or internalized proteins. Thus, TCRs are very suitable for targeting intracellular disease markers. Furthermore, in comparison to TIL therapy, TCR transgenic T cells yield a more defined homogeneous cell product since their characteristics can be modulated by the choice of the transgenic TCR and comprehensively assessed before application. TCR transgenic T cells can be equipped with specificities that would not naturally occur in the patient. For example, self antigen reactive T cells are cleared from the body by negative selection in the thymus (L. Klein, Kyewski, Allen, & Hogquist, 2014). By genetic engineering specificity against self antigens can be introduced into T cells by transduction of selected or engineered TCRs exhibiting the desired specificity and affinity. However, complications from on-target/off-tumor toxicity linked with targeting self antigens are hard to predict, but can be avoided by targeting neoantigens that arise from tumor specific mutations (Yarchoan, Johnson, Lutz, Laheru, & Jaffee, 2017). However, the selection of suitable receptors proofs challenging due to factors such as low abundance of high avidity T cell clones and HLA diversity (Alanio, Lemaitre, Law, Hasan, & Albert, 2010; Schendel & Frankenberger, 2013; Zhang et al., 2016). These obstacles have fostered the recent development of sensitive tools and strategies for selection and characterization of T cell receptors with potential application in adoptive T cell therapy.

3.1.2.1 The T cell Receptor and its Ligand the Peptide Major Histocompatibility Complex

Effector T cells play a crucial role in executing and orchestrating cell-mediated immunity. Antigen specific activation of T cells is mediated by the T cell receptor (TCR) specific interaction with peptide antigens presented on major histocompatibility complexes (MHC) (Dustin, 2003). The TCR is a heterodimeric transmembrane protein consisting of α and β chain linked by a disulfide bond (Figure 5). The extracellular domain is structurally similar to the Fab arm of an antibody with one variable and one constant domain per chain. The hypervariable regions of the variable domains determine binding specificity and affinity (Garcia et al., 1996). The transmembrane domain facilitates interaction with CD3 and CD247 subunits of the TCR complex that is essential for intracellular downstream signaling (Wucherpfennig, Gagnon, Call, Huseby, & Call, 2010). This signaling is further modulated by TCR co-receptors CD4 and CD8. CD4 is expressed on T helper cells and regulatory T cells whereas CD8 is expressed on cytotoxic T cells. These co-receptors also define the MHC specificity of the TCR complex by binding to the constant domains of MHC class II or MHC class I molecules,

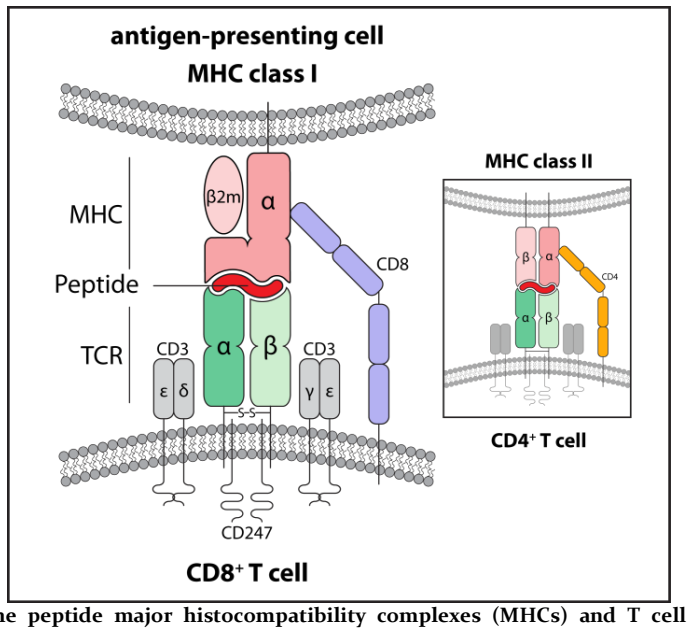

Figure 5 Structure of the peptide major histocompatibility complexes (MHCs) and T cell receptor (TCR) complex and their interaction. Peptide loaded class I MHCs present peptides of proteolytically digested intracellular proteins on the surface of nucleated cells. TCR presented on T cells binds pMHCs and by interaction with CD3 and CD247 co-receptors mediates intracellular signaling. T cell coreceptors CD8 and CD4 allow the discrimination between MHC class I or class II by interaction with the respective constant domains.

respectively (Rudolph, Stanfield, & Wilson, 2006). Thus, depending on the MHC context of a presented antigen either CD4+ or CD8+ T cells are recruited triggering distinct immunological cascades (Miceli & Parnes, 1991). MHC class II is predominantly found on professional antigen presenting cells (APCs) and presents peptide fragments of processed extracellular proteins (Holling, Schooten, & van Den Elsen, 2004). MHC class I is expressed on almost all nucleated cells and presents peptide fragments of proteolytically digested intracellular proteins (Hewitt, 2003).

Whereas MHC class II consists of two non-covalently associated, structurally similar transmembrane proteins (α and β chain) that both contribute to peptide binding, MHC class I proteins are made of a three-domain α chain, containing the peptide binding site and the noncovalently bound β_2 microglobulin (β2m) (Bjorkman et al., 1987). Only the association of all three components, 1) membrane anchored α chain, 2) soluble β2m and 3) antigenic peptide, forms a stable trimeric complex (T. N. M. Schumacher & Ploegh, 1994). The peptide binding groove formed by the α1 and α2 domain consists of six binding pockets that interact with side chains of the loaded peptide. Certain anchor residues and the overall biophysical properties of peptide and binding groove define the peptide-MHC affinity and therefore the stability of the peptide-MHC complex.

The rather unspecific, low affinity and generic peptide-MHC interaction and the large polymorphism of MHC α chain coding genes ensures the comprehensive display of intracellular peptides (J. Klein & Sato, 2000). Despite the large genetic polymorphism, MHCs - also referred to as human leukocyte antigens (HLAs) - can be grouped into classical MHCs (HLA-A, -B and -C) and less abundant non-classical MHCs (HLA-E, -F and G) (Halenius, Gerke, & Hengel, 2014). The TCR:pMHC contact surface is, on the one side, formed by the TCR's hypervariable region and, on the other side, by peptide loaded MHC α1 and α2 domains. Binding specificity of a TCR complex to its cognate peptide-MHC is consequently defined by i) the sequence of the loaded peptide ii) the HLA type

of the MHC and iii) the presence of complementary co-receptors such as CD4 or CD8 (Garcia et al., 1996). This interaction is typically rather weak compared to e.g. antibody-antigen interactions (Stone, Chervin, & Kranz, 2009). Multiple simultaneous TCR:pMHC binding events are necessary for strong interaction between T cell and APC and subsequent T cell activation. The total strength of this multipoint, multi-protein, multiple TCR:pMHC interaction is collectively described as binding avidity. Binding avidity is a critical factor for T cell activation and furthermore a modulator of T cell response (Corse, Gottschalk, & Allison, 2011). Avidity is a multifactorial component of T cell activation and is influenced by receptor binding affinities but also by copy number of the interaction partners (Labrecque et al., 2001). TCR avidity can be defined by the functional effects that are triggered upon antigen binding such as cytokine release, T cell proliferation/anergy or cytotoxic potential (functional avidity) or by the interaction strength of the TCR complex to a peptide MHC (structural avidity) (Viganò et al., 2012).

3.1.2.2 pMHC Multimer Reagents for T cell Characterisation

Several strategies to asses TCR binding affinity or structural avidity have been described in recent years (Ioannidou et al., 2017). These methods usually involve the recombinant expression of at least one interaction partner. Whereas recombinant TCR production proves difficult (Gunnarsen et al., 2018), soluble peptide-MHC complexes have been efficiently refolded from bacterially expressed proteins. Still, analysis by classical affinity measurement methods such as SPR, ITC or ELISA is challenging due to the weak affinity of monomeric pMHC molecules and the lack of co-receptor interactions. Multimerization of pMHC molecules on scaffolds allows analysis of weak and transient interactions and mimics the avidity gain of natural multivalent binding. For example, soluble pMHC monomers, biotinylated e.g. via an Avi-tag, can be multimerized on a dye-conjugated streptavidin backbone ('tetramer') and enable sensitive labeling of matching TCR complexes and isolation of antigen-specific T cells (Altman et al., 1996). The implementation of reversibly multimerizable pMHC reagents – such as 'Streptamers' – allow triggered release of pMHC reagents and traceless isolation of T cells (Knabel et al., 2002). Besides T cell identification and isolation, reversibly multimeriziable pMHC reagents are also used for the characterization of TCR:pMHC

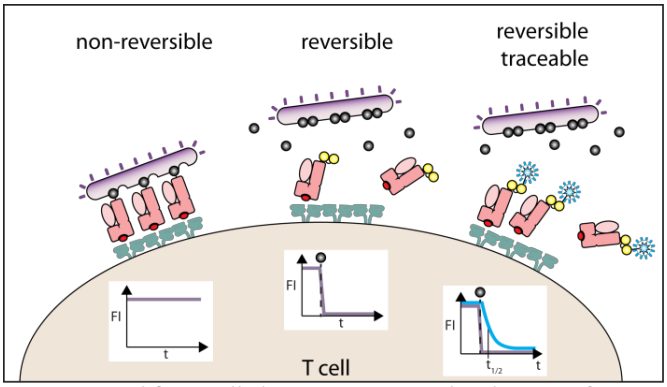

Figure 6 pMHC multimer reagents used for T cell characterization and isolation. Left: Non-reversible labeling of antigen specific TCRs with soluble pMHC molecules multimerized on a fluorescent backbone. Center: Reversibility of the multimerization allows triggered dissociation of the complex, thus removal of the label. Right: Fluorescently labeled pMHCs can be used to trace the dissociation of pMHC monomers after backbone dissociation. The dissociation kinetics (koff rates) can be used to describe a TCR's structural avidity.

interactions. When reversible pMHC monomers themselves are labeled with a fluorophore, their dissociation from TCRs on living T cells can be tracked over time and allows measurement of TCR k_{off}-rates, and thereby the assessment of TCR structural avidity in its endogenous T cell surface context (Figure 6) (Nauerth et al., 2013).
Although it is yet unclear what an optimal k_{off} rate is, it has been shown that TCR avidity is predictive for T cell functionality. It is agreed upon that interaction strength between T cell and antigen presenting cell has a strong influence on the subsequent immune response. On the one hand, too low avidity prevents sufficient T cell activation, on the other hand, too high avidity leads to overstimulation and T cell exhaustion. Consequently, avidity must be in a certain range to allow optimal activation of T cells. Furthermore, avidities leaning to the lower end of this spectrum might trigger different functional responses other than those leaning towards the higher end (Corse et al., 2011; Viganò et al., 2012). In a clinical setting the avidity and specificity of transgenic T cells can be crucial characteristics that significantly influence on-target efficacy but also off-target toxicity (Kunert, Obenaus, Lamers, Blankenstein, & Debets, 2017). Thus, pMHC multimer assisted selection of T cell receptors with beneficial properties might contribute to safer and more efficient transgenic T cells for therapeutic applications. Ideally, such reagents should, just like ADCs, be precise, well defined and stable. Thus, sensitive pMHCs also require gentle and robust modification strategies that yield homogeneous products with high efficacy.

3.2 Site-specific Modification and Bioorthogonal Conjugation of Recombinant Proteins

The thrive of ADCs was accompanied with growing interest in bioconjugation techniques. The fusion of biomolecule and toxin created the need for gentle conjugation strategies that are orthogonal to naturally occurring protein modification mechanisms. Historically bioorthogonal reactions also encompass specific modification of naturally occurring functional groups of biomolecules such as amines on lysine side chains or thiols on cysteine side chains, however, with orthogonal reaction mechanisms. More recently the understanding of bioorthogonality focuses on reactions involving reactive groups that are rare or absent in biological systems. The later demands the introduction of one of the reactive groups in the biomolecule to allow subsequent bioorthogonal modification. Initially, such techniques were developed for the labeling of endogenous biomolecules to investigate their function in the cellular context. Today bioorthogonal reactions are evermore used for site-specific functionalization of recombinant proteins (Bertozzi, 2011). Especially, the demanding requirements for therapeutic bioconjugates, such as ADCs, have promoted the latest interest in bioorthogonal site-specific bioconjugation techniques (Agarwal & Bertozzi, 2015a). Although antibodies conjugated to toxins are en vogue representatives of bioconjugates that attract attention owing to their clinical application, many more proteins are routinely modified with entities ranging from small reporter compounds (e.g. fluorophores, radioisotopes or biotin) over synthetic polymers (e.g. PEG), peptides, proteins or other macromolecules (e.g. DNA, sugars or lipids) all the way to even larger structures such as scaffolds (e.g. dextrans or dendrimers) or solid supports.

3.2.1 Modification of Proteinogenic Amino Acids

The 20 canonical amino acids can be grouped by the physico-chemical properties of their side chain residues. Non-polar aliphatic amino acids are mainly buried in the hydrophobic core of proteins and thus inaccessible for conjugation reactions. On the contrary, amino acids with polar or charged side chains are exposed to the polar solvent water, thus commonly found on the protein's surface. The side chains of serine, threonine, asparagine and glutamine carry polar hydroxyl or amide groups that can act as nucleophiles in conjugation reactions. These side chains are commonly modified by enzymes in the cellular context, however, their nucleophilic character is similar to that of water and thus hardly selectively addressable in aqueous environments. Polar, ionizable side chains are of particular interest for bioconjugation. In their unprotonated form the ionizable groups; thiol (cysteine), amine (lysine, arginine, histidine and N-terminus), carboxyl (aspartate, glutamate and C-terminus) and phenol (tyrosine) groups are strong nucleophiles listed with descending nucleophilicity (Figure 7). Although the reactivity of these nucleophiles is guided by their pK_a values, the very reactivity of each amino acid side chain is strongly dependent on the microenvironment surrounding the reactive group (e.g. active center of enzymes). In addition, carboxyls and amines, as opposed to thiols and phenols, are present in their charged form at neutral pH, thus frequently found on the solvent exposed protein surface and readily accessible for modification reactions. The relatively low pK_a of carboxyl groups leaves them in their

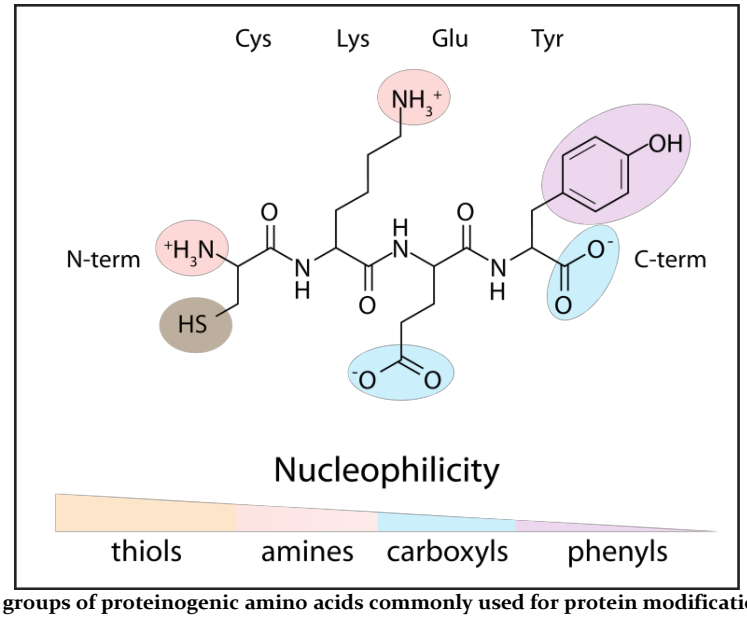

Figure 7 Reactive groups of proteinogenic amino acids commonly used for protein modification. Reactive groups are ordered by decreasing nucleophilicity. Adapted from (Hermanson, 2013a)

less reactive unprotonated form at physiological pH values, thus only reactive under harsh pH conditions or by applying intermediate activating reactions (Hermanson, 2013a).

3.2.1.1 Amine Modification

On the contrary, primary amines such as the N-terminal α-amines and lysines' ε-amines can be directly addressed by alkylation or acylation at neutral or slightly basic pH. Several amine reactive moieties have been described for protein modification or crosslinking. For example, isocyanates, acyl azides, aldehydes and phosphine derivatives are used, however, the most widely applied amine-acylating reagents are *N*-hydroxysuccinimide (NHS) esters. The NHS-activated carboxylates are attacked by nucleophilic amines to form a stable amide bond between protein and attached entity (Figure 8) (Hermanson, 2013b). Although amines of lysines and N-terminus are ubiquitous in proteins and peptides and thus allow the modification of virtually any protein (Gunnoo & Madder, 2016), their high abundance mostly impedes control over stoichiometry and site of conjugation. By minute optimization of reaction conditions, the average number of attached molecules per protein can be directed (Matos et al., 2018), however, individual proteins will still differ in extend and position of conjugation. For example, amine containing functional sites, such as antibody paratopes, can thus be compromised by conjugation (L. Wang et al., 2005).

3.2.1.2 Thiol Modification

The thiolat of cysteines is a less frequent nucleophile and allows for more homogeneous conjugation. Free cysteines are scarcely present on protein surfaces, however, predominantly exist in enzyme active site pockets or in the oxidized form as intermolecular or intramolecular disulfides. Disulfide bridges stabilize the three dimensional fold of proteins. Cysteine disulfides are relative hydrophobic, therefore mostly found in the hydrophobic core of proteins (intramolecular) or on the surface linking two individual peptide chains (intermolecular). Buried disulfides are relatively

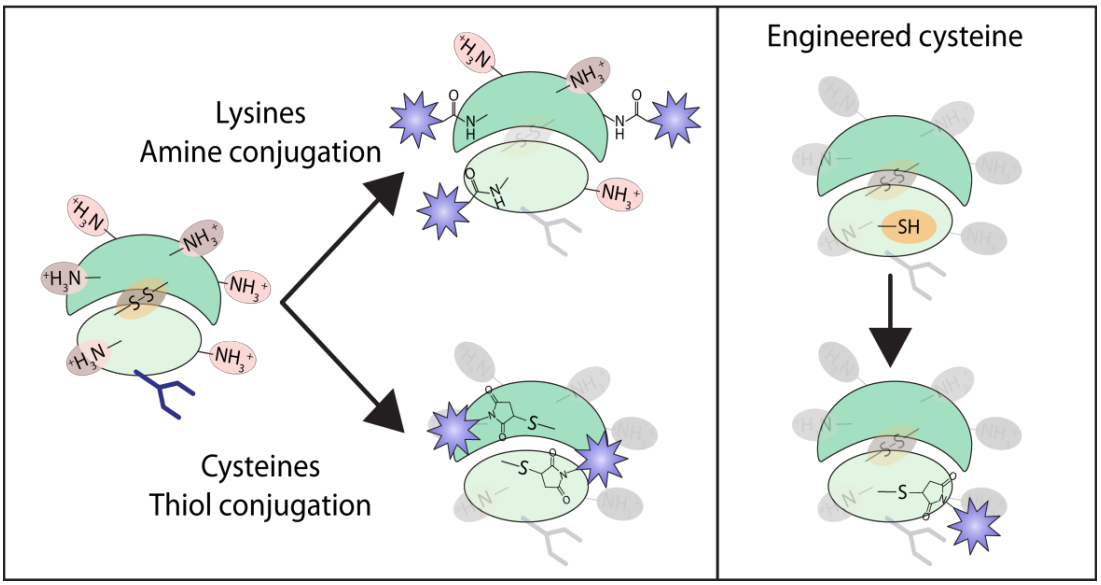

Figure 8 Modification of naturally occurring or engineered proteinogenic amino acids. Left panel: ε-amines of lysine side chains can be targeted by conjugation of N-hydroxysuccinimide (NHS) activated carboxylates. NHS is released as a leaving group and a stable amide bond is formed between the lysine and attached entity. Upon reduction, the thiol groups of disulfide cysteines are potent nucleophiles that can be addressed selectively, for example, with maleimide functionalized entities. Right panel: Proteinogenic amino acids, e.g. free unpaired cysteines can be introduced at solvent exposed positions by protein engineering and modified selectively with thiol reactive reagents.

inaccessible under aqueous buffer conditions. Intermolecular disulfides, such as the hinge-disulfide bridges of antibodies, are more readily accessible for reduction and subsequent conjugation reactions. Thiol reactive groups include, for example, haloacetyl or aryloyl derivatives, vinyl sulfones, thiol-exchange reagents and maleimides (J. M. Chalker, G. J. L. Bernardes, Y. A. Lin, & B. G. Davis, 2009). Maleimides are very commonly used for thiol modification. Their double bond is attacked by the nucleophilic thiol group to form a relatively stable thioether bond. At neutral pH, maleimides react specifically with thiols over amines (1000-fold faster) making it a convenient modification strategy for cysteine containing proteins (Ravasco, Faustino, Trindade, & Gois, 2019). However, reduction of disulfide bridges can affect protein stability and function, the thioether bond is prone to hydrolysis and thiol exchange (Shen et al., 2012) and eventually, a great number of proteins do not contain accessible cysteines. Yet, the recombinant production of proteins allows sequence manipulation and thus deletion, insertion or substitution of amino acids. For example, introduction of an engineered cysteine residue has been used for site-specific thiol-modification of antibodies (THIOMABs) (Bhakta, Raab, & Junutula, 2013). In this approach, a large set of positions has been screened for an exposed reactive cysteine residue that can be addressed selectively. The microenvironment dependent reactivity of the thiol group can be significantly different for the engineered cysteine than for the native disulfide cysteines. This allows specific modification of the engineered cysteine under optimized reduction/oxidation conditions (Figure 8) (Shen et al., 2012).

The installation of reactive groups with discriminative or orthogonal reactivity is a concept that underlies most site-specific bioconjugation methods. A large variety of engineering strategies has been developed for the introduction of bioorthogonal handles (Prescher & Bertozzi, 2005). For example, the substitution of amino acids has been

expanded from natural to unnatural, bioorthogonally reactive amino acids and site-specificity has been improved, for instance, by chemoenzymatic approaches. These two concepts will be described in more detail in the following paragraphs.

3.2.2 Incorporation and Modification of Unnatural Amino Acids

Besides the 20 canonical amino acids incorporated into proteins, many more amino acids have been isolated or generated by chemical synthesis (Wagner & Musso, 1983). However, these are not recognized by the natural protein biosynthesis machinery since they lack a matching anticodon and the necessary tRNA/tRNA-synthetase pair. Ribosomal incorporation of unnatural amino acids (UAAs) has been achieved by the selection of orthogonal tRNA/tRNA-synthetase pairs that i) recognize the unnatural amino acid and ii) covalently link it to a tRNA displaying an unused anti-codon (W. Liu, Brock, Chen, Chen, & Schultz, 2007; L. Wang, Brock, Herberich, & Schultz, 2001). Most approaches use an anti-codon matching the infrequent amber stop codon (TAG). This codon can be placed at any desired position in the protein sequence and, in expression hosts equipped with the matching orthogonal tRNA/tRNA synthetase pair, triggers the incorporation of the UAA (Chin, 2017; C. C. Liu & Schultz, 2010). By now, many different UAAs, carrying commonly used bioorthogonal handles, have been synthesized and incorporated by amber suppression (K. Lang & J. W. Chin, 2014). A great advantage of this technique is that UAAs can be placed at virtually any site in the protein and by introducing multiple orthogonal tRNA/tRNA synthetase pairs more than one bioorthogonal handle can be installed at different sites (Xiao et al., 2013). However, amber suppression is limited by the selection of a suitable pair for each new UAA and struggles with low protein expression yields compared to standard recombinant expression. Efficacy and fidelity of UAA incorporation during protein expression are crucial factors affecting expression yield.

3.2.3 Chemoenzymatic Approaches

Reduced expression yields can be addressed by incorporation of UAAs or other entities carrying bioorthogonal handles subsequent to recombinant expression. The great majority of these techniques rely on enzymatic incorporation of handles at either naturally occurring recognition sites (e.g. glycans) or at recombinantly introduced recognition sites (e.g. peptide tags). Glycosylation is a posttranslational modification of proteins and involves the assembly of oligosaccharides and their enzymatic linkage to the amide group of asparagine (N-linked) or the hydroxyl group of serine and threonine (O-linked) (Ohtsubo & Marth, 2006; Schachter, 2000). For example antibodies are N-glycosylated at asparagine 297 of the heavy chain (Abel, Spiegelberg, & Grey, 1968; Higel, Seidl, Sörgel, & Friess, 2016). These oligosaccharides have been used to site-specifically install bioorthogonal handles by enzymatic incorporation of modified sugar entities. For example, azido-sialic acid can be incorporated by α2,6-sialyltransferase whereas the azide can serve as a bioorthogonal handle for drug attachment by click chemistry (Du et al., 2009). Furthermore, mutant β1,4-galactosyltransferases, were developed that accept a variety of modified galactoses as substrates to modify degalactosylated antibodies (Figure 9) (Qasba, 2015). Although this approach does not require sequence manipulation it is limited to glycosylated proteins and the effects of glycan

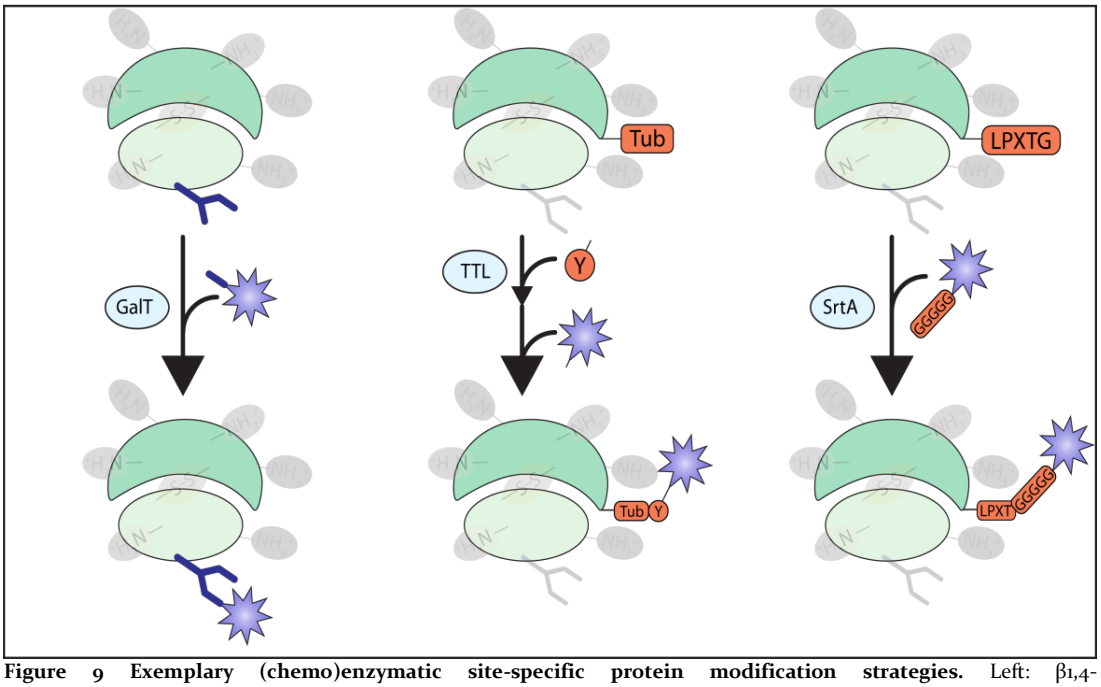

Figure 9 Exemplary (chemo)enzymatic site-specific protein modification strategies. Left: β1,4-galactosyltransferases (GalT) catalyzed introduction of modified galactoses in degalactosylated glycosylated proteins. Center: Tubulin-tyrosine ligase (TTL) catalyzed site-specific introduction of tyrosine derivatives in C-terminally Tub-tagged proteins and subsequent bioorthogonal conjugation of functional entities. Right: SortaseA (SrtA) catalyzes transpeptidation of poly-glycine- and LPXTG-recognition sequences. Terminal LPXTG serve as an acceptor sequence for the site-specific ligation of poly-glycine modified functional entities.

manipulation regarding stability, function or immunogenicity of the modified protein are to be fully evaluated (H. Li & d'Anjou, 2009).

An approach with a larger scope is the introduction of recognition sequences, such as peptide tags. One of the first peptide tags used for site specific protein modification is the 15 amino acid long AviTag. The AviTag is derived from the recognition sequence of the bacterial biotin ligase BirA. BirA catalyzes the conjugation of biotin to a lysine residue in the recognition sequence. The strong affinity of biotin to avidin allows immobilization of biotinylated proteins on surfaces or the assembly of multimeric complexes on avidin scaffolds (Beckett, Kovaleva, & Schatz, 1999; Fairhead & Howarth, 2015). Besides natural biotin, BirA also ligates biotin derivatives that have altered affinity to avidin or derivatives carrying bioorthogonal handles. The later has been used for site-specific attachment of functionalities such as fluorophores or toxins to AviTagged proteins (I. Chen, Howarth, Lin, & Ting, 2005; Slavoff, Chen, Choi, & Ting, 2008).

Following the same two-step principle, 1.) site-specific enzymatic incorporation or generation of a reactive handle and 2.) bioorthogonal conjugation of molecule of interest, several more tag-enzyme pairs have been developed such as Q-tag and transglutaminase (TGase) (Dennler et al., 2014; Jeger et al., 2010; Lin & Ting, 2006), Aldehyde-tag and formylglycine-generating enzyme (FGE) (I. S. Carrico, B. L. Carlson, & C. R. Bertozzi, 2007; Dierks et al., 2005; Drake et al., 2014), Sortag and Sortase A (SrtA) (Mao, Hart, Schink, & Pollok, 2004; Williamson, Fascione, Webb, & Turnbull, 2012) or Tub-tag and tubulin-tyrosine ligase (TTL) (D. Schumacher et al., 2015; D. Schumacher et al., 2017). SrtA is a streptococcal transpeptidase that recognizes the C-terminal sorting motif LPXTG and catalyzes the transfer of the LPXT motif to a pentaglycine acceptor peptide on the cell wall. SrtA cleaves the peptide bond between threonine and glycine

and forms a new peptide bond between the threonine and the N-terminal amine of the acceptor sequence (Spirig, Weiner, & Clubb, 2011). This reaction was first used by Mao et al (2004) to modify recombinant proteins. In general, the two components to be joined have to contain either a C-terminal LPXTG motif or a N-terminal $(Gly)_n$ motif. Consequently, N- or C-terminal modification of proteins can be realized by adding the respective motif. It should be noted that the product also contains an LPXTG motif and SrtA also catalyzes the reverse reaction removing the attached modification. However, sortagging has been developed further by many research groups resulting in optimized reaction conditions, engineered enzymes for faster reaction rates and a variety of applications (Antos, Truttmann, & Ploegh, 2016). Noteworthy, the transpeptidation reaction can also be used directly to assemble linear protein-protein fusions without an intermediate bioorthogonal reaction step (Levary, Parthasarathy, Boder, & Ackerman, 2011). However, the C-terminal installation of $(Gly)_n$ peptides carrying functional groups is a frequently used example that has also been applied for antibody modification and ADC generation (Figure 9) (Beerli, Hell, Merkel, & Grawunder, 2015; Stefan et al., 2017).
In contrast to SrtA, the tag-enzyme pair used in Tub-tag labeling is inspired by a eukaryotic system. In eukaryotes, α/β-tubulin heterodimers polymerize to form microtubules. Their assembly and disassembly is a highly dynamic process and is among others regulated by modification of the C-terminal tail of tubulins. α-tubulin is expressed with a C-terminal tyrosine which can be removed and added enzymatically after expression. Tyrosinated α-tubulin is found in more stable microtubules and serves as a signal for stabilization (Janke, 2014; Yu, Garnham, & Roll-Mecak, 2015). The enzyme responsible for retyrosination is tubulin-tyrosine ligase (TTL) an ATP-dependent peptide synthase that catalyzes peptide bond formation between the C-terminal glutamate and free L-tyrosine (Prota et al., 2013; Rudiger, Wehland, & Weber, 1994). Although TTL activity is influenced by binding to tubulin distinct from the tail region, recombinantly expressed TTL also catalyzes tyrosination of other proteins equipped with the 14 amino acid tail sequence (the Tub-tag) (D. Schumacher et al., 2015). Despite the high specificity for the tag sequence TTL is less specific regarding the amino acid to be attached. Besides incorporation of other natural amino acids like phenylalanine, more importantly, the TTL also tolerates a large set of tyrosine derivatives carrying diverse functionalities. Accordingly, Tub-tag labeling was used to C-terminally install bioorthogonal handles for subsequent site-specific attachment of a variety of small molecules (Figure 9) (D. Schumacher et al., 2017).

3.2.4 Bioorthogonal Conjugation Reactions

Bioorthogonal reactions were initially developed for modification of biomolecules in complex mixtures such as the cellular cytoplasm. Thus, they use reactive groups that are rare or not present in biomolecules and follow orthogonal reaction mechanisms to avoid unspecific modification. Many such reaction mechanisms are routinely applied in order to organic chemistry, yet the great majority of biomolecules do not tolerate the harsh reaction conditions applied in chemical synthesis such as high temperature or organic, non-polar solvents. Consequently, only a subset of those reactions can be carried out efficiently under mild conditions such as ambient temperature and use of aqueous solvents (Carell & Vrabel, 2016).

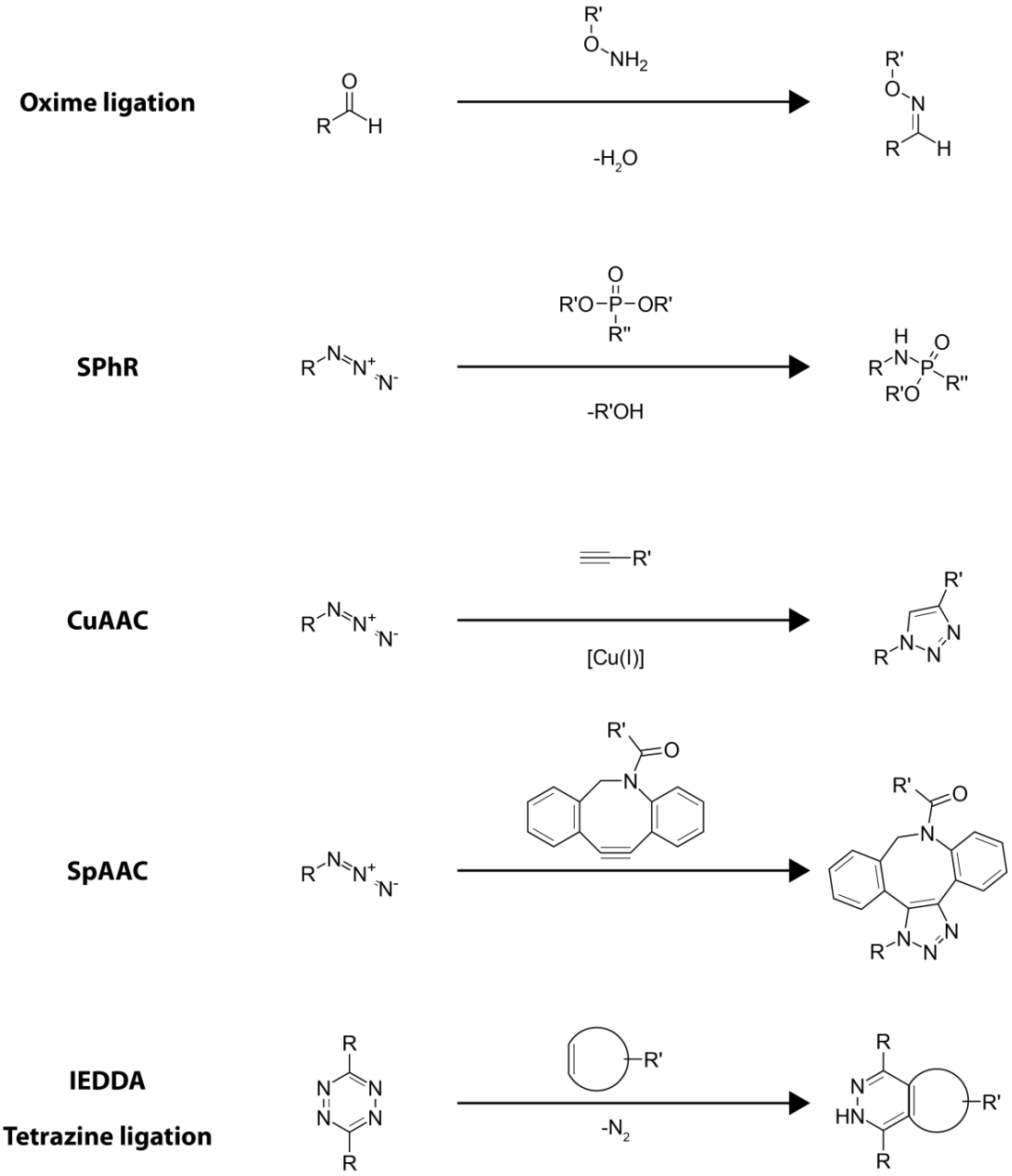

Figure 10 Exemplary bioorthogonal reactions. Oxime ligation of aldehydes and alkoxylamines. Staudinger-phosphonite reaction (SPhR) between azides and phosphonites. Click reactions: copper(I)-catalyzed alkyne-azide cycloaddition (CuAAC) and strain-promoted alkyne-azide cycloaddition (SpAAC) between azides and (strained) alkynes. Inverse electron-demand Diels-Alder reaction (IEDDA), also known as tetrazine ligation, between tetrazines and strained alkenes.

Although aldehydes and ketones are present in biomolecules such as saccharides, they are absent from proteins. Thus, aldehydes can serve as a bioorthogonal handle for site-specific modification of recombinant proteins (Isaac S. Carrico, Brian L. Carlson, & Carolyn R. Bertozzi, 2007). Alkoxylamines or hydrazines react with carbonyl groups under acidic conditions to form oximes or hydrazones, respectively. Oximes are more stable than hydrazones, hence, oxime ligation is generally preferred for bioconjugation. Carbonyls are small in size and may serve as a handle that minimally perturbates proteins. However, aldehydes can be attacked by many nucleophiles present in biological systems, the reaction is generally reversible and stability is strongly

dependent on pH and substituents in vicinity of the linkage (Foillard, Rasmussen, Razkin, Boturyn, & Dumy, 2008; Kölmel & Kool, 2017; Ulrich, Boturyn, Marra, Renaudet, & Dumy, 2014). Another very frequently used reaction mechanism is the Huisgen 1,3-dipolar cycloaddition between an azide and a terminal alkyne (Huisgen, 1963). Since both reactive groups are small and do not occur in natural systems, this reaction is very suitable for bioorthogonal conjugation, however, the reaction proceeds relatively slowly in biological systems. It was found that copper(I) can serve as a catalyst for the cycloaddition and drastically increases reaction rates (Rostovtsev, Green, Fokin, & Sharpless, 2002). Copper catalyzed azide alkyne cycloaddition (CuAAC) is a fast and specific reaction also known as "click chemistry". It's ease of use has initiated wide spread use of click chemistry and the development of many azide and alkyne handles that can be introduced in proteins by above mentioned techniques (Hein & Fokin, 2010; L. Li & Zhang, 2016). Yet, in living systems, the toxicity of copper(I) is problematic and reactive groups of proteins can be oxidized which can cause structural and functional damage (Kennedy et al., 2011). In this regard copper complexing ligands like Tris(3-hydroxypropyltriazolylmethyl)amine (THPTA), can be applied to reduce oxidation effects (Hein & Fokin, 2010; Hong, Presolski, Ma, & Finn, 2009). In addition, copper free alternatives such as strain promoted azide alkyne cycloaddition (SpAAC) have been developed (Agard, Prescher, & Bertozzi, 2004). Instead of metal-ion catalysis, SpAAC relies on activated alkynes which inherently exhibit higher reactivity towards azides. This is achieved by embedding the alkyne group in a strained ring system. The first strained alkyne used for SpAAC was cyclooctyne (OCT) followed by alkynes with higher reaction rates and/or increased water solubility like dibenzocyclooctyne (DBCO) and bicyclononyne (BCN) (Ramil & Lin, 2013). SpAAC circumvents the toxicity accompanied with copper catalysts, proceeds without the need of further additives and tolerates a range of biological buffer systems, pH values and temperatures. Thus, two entities carrying complementary SpAAC-handles can virtually be "clicked" together by simply mixing them. A variety of functional moieties such as fluorophores, affinity ligands, amino acids, nucleotides, crosslinkers, polymers or toxins are commercially available as azide or alkyne derivatives and have made click chemistry a standard tool for conjugation of biomolecules (Pickens, Johnson, Pressnall, Leon, & Berkland, 2018).

Azides also undergo bioorthogonal reactions with other reactive groups. For example, the reaction with trapped phosphines yields stable amide bonds and is termed Staudinger ligation (Staudinger & Meyer, 1919). Besides phosphines also phosphites and phosphonites react specifically with azides and have been used as an alternative to click chemistry for azide-directed site-specific bioconjugation of intracellular and recombinant biomolecules (Serwa et al., 2009; van Berkel, van Eldijk, & van Hest, 2011) (Vallée et al., 2011).

Another bioorthogonal pair that has become very prominent are 1,2,4,5-tetrazines and strained alkenes that react exceptionally fast in an inverse electron demand Diels–Alder cycloaddition (iEDDA) (Blackman, Royzen, & Fox, 2008; Devaraj, Weissleder, & Hilderbrand, 2008). The reaction releases gaseous N_2 which makes it practically irreversible in biological systems. Commonly used alkenes include trans-cyclooctene (TCO)(W. Chen, Wang, Dai, Hamelberg, & Wang, 2012), norbornene (Lang, Davis, Torres-Kolbus, et al., 2012) and cyclopropene (Patterson, Nazarova, Xie, Kamber, &

Prescher, 2012). Both alkene and tetrazine derivatives of amino acids have been incorporated in proteins (Lang, Davis, Wallace, et al., 2012; Mayer & Lang, 2017; Plass et al., 2012). The fast reaction kinetics allow efficient labeling of proteins even in living cells and *in vivo* which is why tetrazine ligation has found widespread application (Kathrin Lang & Jason W. Chin, 2014; Sečkutė & Devaraj, 2013).

Besides the mentioned popular mechanisms, many more bioorthogonal reactions have been described for bioconjugation in the recent past. Their application for site-specific protein modification presupposes the site-specific introduction or generation of the required bioorthogonal handle. Several pairs of incorporation techniques and bioorthogonal reactions have lately been used for a variety of applications ranging from *in vivo* labeling to precise modification of recombinant proteins. The later contributed to more sophisticated, more stable and better defined protein reagents used in research, diagnostic and therapy. Among the multitude of protein conjugate reagents this work focuses on antibody conjugates, bispecific antibodies and T cell characterization reagents.

4 Results

4.1 A Simple and Sensitive High-Content Assay for the Characterization of Antiproliferative Therapeutic Antibodies

Technical Note

A Simple and Sensitive High-Content Assay for the Characterization of Antiproliferative Therapeutic Antibodies

SLAS Discovery
2017, Vol. 22(3) 309–315

DOI: 10.1177/1087057116677821
journals.sagepub.com/home/jbx
SAGE

Andreas Stengl[1], David Hörl[1], Heinrich Leonhardt[1], and Jonas Helma[1]

Abstract

Monoclonal antibodies (mAbs) have become a central class of therapeutic agents in particular as antiproliferative compounds. Their often complex modes of action require sensitive assays during early, functional characterization. Current cell-based proliferation assays often detect metabolites that are indicative of metabolic activity but do not directly account for cell proliferation. Measuring DNA replication by incorporation of base analogues such as 5-bromo-2′-deoxyuridine (BrdU) fills this analytical gap but was previously restricted to bulk effect characterization in enzyme-linked immunosorbent assay formats. Here, we describe a cell-based assay format for the characterization of antiproliferative mAbs regarding potency and mode of action in a single experiment. The assay makes use of single cell–based high-content-analysis (HCA) for the reliable quantification of replicating cells and DNA content via 5-ethynyl-2′-deoxyuridine (EdU) and 4′,6-diamidino-2-phenylindole (DAPI), respectively, as sensitive measures of antiproliferative mAb activity. We used trastuzumab, an antiproliferative therapeutic antibody interfering with HER2 cell surface receptor-mediated growth signal transduction, and HER2-overexpressing cell lines BT474 and SKBR3 to demonstrate up to 10-fold signal-to-background (S/B) ratios for treated versus untreated cells and a shift in cell cycle profiles indicating antibody-induced cell cycle arrest. The assay is simple, cost-effective, and sensitive, providing a cell-based format for preclinical characterization of therapeutic mAbs.

Keywords

therapeutic antibodies, cell-based assays, high-content screening, EdU, proliferation

Introduction

Biological drugs such as therapeutic antibodies are in the process of replacing chemical compounds as the major class of future medicines. Therapeutic antibodies are often characterized by complex modes of action, such as inhibition of cell proliferation, induction of apoptosis, and targeted immune recruitment. Moreover, antibody drug conjugates (ADCs) that combine chemotherapeutic cytotoxicity with antibody-mediated tumor specificity even increase the diversity of potential modes of action.[1] Thus, the functional characterization during early drug development requires sensitive cell-based high-throughput assays that address this complexity and measure multiple cellular parameters.[2] One of the major modes of action of therapeutic antibodies is based on inhibition of target cell growth by, for example, blocking growth signaling pathways in cancer cells.[3] For assessing the antiproliferative potency of such candidates, several methods have been described.[4] A simple approach to quantify the number of cells that survive treatment consists of automated cell counting.[5] However, a significant proportion of remaining cells is likely to have entered apoptosis or cell cycle arrest, leading to an overestimation of the proliferating cell population. A more precise approximation of proliferation can be achieved by detecting metabolic activity in viable cells and thus excluding apoptotic cells. Compounds such as 3-(4,5-dimethylthiazol-2-yl)-2,5-diphenyltetrazolium bromide (MTT) are converted to a colored product by NAD(P)H-dependent cellular oxidoreductases, providing a quantifiable measure for metabolic activity.[6] An alternative approach to assess viability is the detection of intracellular adenosine triphosphate (ATP), which is maintained only at high levels in metabolically active cells and declines rapidly upon cell death or apoptosis. The release of intracellular ATP and its

[1]Department of Biology II, LMU Munich, Planegg-Martinsried, Germany

Received Aug 16, 2016, and in revised form Sep 27, 2016. Accepted for publication Oct 13, 2016.

Supplementary material for this article is available on the *Journal of Biomolecular Screening* Web site at http://jbx.sagepub.com/supplemental.

Corresponding Author:
[1]Department of Biology II, LMU Munich, Grosshadernerstrasse 2, 82152 Planegg-Martinsried, Germany.
Email: helma@biologie.uni-münchen.de

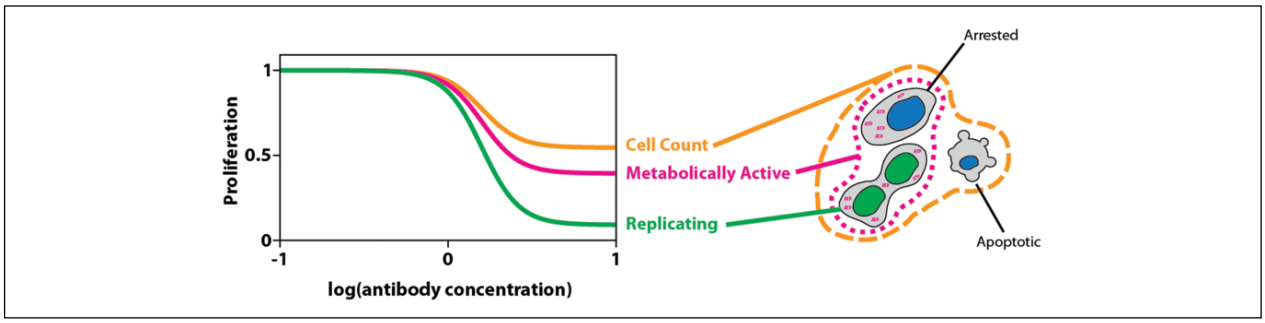

Figure 1. Addressing proliferation at different layers. Antiproliferative antibodies interfere with a cell's ability to replicate. Directly, detecting replicating cells (green) allows for the largest separation between maximal and minimal number of affected cells. Indirectly, restrained DNA replication also reduces the amount of metabolically active cells and the total number of cells remaining after treatment. However, the detection of metabolically active cells (magenta) includes arrested cells, resulting in an overestimation of proliferating cells. This effect is even more drastic when further generalizing the detection to all remaining cells (orange), which also includes apoptotic cells.

detection via ATP-dependent luciferase activity is widely used in proliferation assays.[7]

However, cells that have undergone cell cycle arrest are still metabolically active and consequently not distinguishable from proliferating cells by above-described assays. A major characteristic of proliferating cells is the replication of DNA during S phase. Thus, the incorporation of nucleotide analogues such as 5-bromo-2′-deoxyuridine (BrdU) into chromosomal DNA during replication allows for the distinction between proliferating and arrested cells. BrdU can be detected by antibodies and thus may be implemented with highly sensitive enzyme-linked immunosorbent assay (ELISA)–based multiwell assays.[8] It has been shown that a wider separation between signals from treated and untreated samples (signal-to-background [S/B] ratio) can be achieved with BrdU incorporation compared with assays detecting metabolic activity.[9] 5-Ethynyl-2′-deoxyuridine (EdU), an alternative nucleotide analogue, enables a simpler, milder, and more efficient detection via copper-catalyzed azide alkyne cycloaddition (CuAAC) of fluorescent dyes, such as 6-FAM–azide. The use of EdU coupled to fluorescent dyes simplifies the assay procedure and in addition improves compatibility with other nuclear stains such as 4′,6-diamidino-2-phenylindole (DAPI), thus representing the method of choice for sensitive microscopy-based detection of proliferation.

Accurate distinction between proliferating and nonproliferating cells improves the sensitivity of an antiproliferative potency assay (**Fig. 1**). Changing the mode of signal detection, on one hand, can further improve sensitivity but also provide additional information about the antiproliferative effect. Plate reader–based readouts are commonly used in screening experiments to validate lead candidates and produce statistically relevant data. Commonly used colorimetric multiwell proliferation assays are restricted to single-course parameters such as mean metabolic activity per well. To better understand the mode of action underlying an antiproliferative effect, cellular or subcellular information on signal localization and intensity may prove useful, which is usually not accessible with plate reader systems. Fluorescence microscopy is the method of choice to gain information about single cells with a variety of microscopic high-content screening (HCS) platforms developed in recent years that allow for automated image acquisition and analysis in a high-throughput manner.[10]

In the present study, we describe a simple and sensitive microscopic high-content assay for the quantification and characterization of the antiproliferative potency of therapeutic antibodies. The quantification of replicating cells, via EdU incorporation, as a measure for proliferation allows for most sensitive distinction between proliferating and nonproliferating cells. In addition to quantifying the antiproliferative potency of a monoclonal antibody (mAb), the mode of action can be investigated in the course of the same experiment. For example, potential induction of cell cycle arrest can be studied by cell cycle profiling based on nuclear DNA content quantification.

Materials and Methods

Cell Lines and Cell Culture

Antibodies were produced in FreeStyle HEK 293-F cells (Thermo Fisher Scientific, Waltham, MA, USA) cultured in FreeStyle 293 Expression Medium and maintained at cell densities from 3×10^5 to 3×10^6 cells/mL in a shaker flask at 37 °C, 5% CO_2, shaking at 120 rpm.

HER2 overexpression cell lines BT474 (ATCC HTB20) and SKBR3 (ATCC HTB30) and a control cell line with neglectable HER2 expression levels (1000-fold less than SKBR3), MDA-MB-468 (ATCC HTB-132), were cultured in Dulbecco's modified Eagle's medium (DMEM)/F12 + Gibco Glutamax-I (Thermo Fisher Scientific, Waltham,

MA, USA) supplemented with 10% fetal calf serum (FCS) at 37 °C, 5% CO_2.

Protein Expression and Purification

Trastuzumab was expressed in FreeStyle HEK 293-F cells as described previously from the pVITRO1-trastuzumab-IgG1/κ vector (Addgene plasmid 61883; Addgene, Cambridge, MA, USA).[11]

Antibody purification from cleared and sterile filtered cell culture supernatants was performed with an Äkta purifier system equipped with a 1-mL HiTrap Protein A HP column (GE Healthcare, Piscataway, NJ). The system was operated with a constant flow rate of 1 mL/min. After sample application, the column was washed with 10 column volumes (CVs) of wash buffer (20 mM phosphate buffer, 150 mM NaCl, pH 7.3). Bound antibody was eluted with a one-step pH decrease to 3.0 (10 mM Na-citrate buffer, pH 3.0). Eluted fractions of size 0.2 mL or 0.5 mL were collected followed by immediate neutralization of the pH with one-third volume 1 M Tris HCl, pH 8.0. Peak fractions were pooled and concentrated using an Amicon Ultra 4-mL Centrifugal Filter NMWL 10 kDa (Merck Millipore, Billerica, MA, USA) and stored at 4 °C or snap frozen in liquid nitrogen and transferred to −80 °C for long-term storage.

Antibody Treatment, EdU Incorporation, and Nuclear Staining

In total, 1×10^4 cells were seeded in each well of a 96-well optical cell culture plate supplemented with 100 µL culture media. To ensure proper attachment, cells were incubated for 4 h prior to addition of antibody. The 1:3 serial dilutions of trastuzumab in culture media were performed at threefold the desired final concentration, ranging from 50 nM to 0 nM. Then, 50 µL of each dilution was added in triplicates to individual wells. Cells were incubated with antibody for 4 days followed by the addition of EdU to a final concentration of 10 µM. To guarantee labeling of all proliferating cells, EdU treatment was done for 20 h followed by fixation of cells in phosphate-buffered saline (PBS) + 4% paraformaldehyde (PFA), permeabilization in PBS + 0.5% Triton X-100, and blocking of the well surface with PBT (PBS, 2% BSA, and 0.02% Tween 20). EdU was labeled via CuAAC by the addition of 30 µL of staining reagent (4 mM $CuSO_4$, 20 µM 6-FAM–azide, 50 µM Na-ascorbate in 100 mM Tris/HCl, pH 7.0) per well and incubated for 30 min at room temperature. Remaining unconjugated dye was removed by washing three times with 100 µL PBST (PBS + 0.02% Tween 20). Then, 100 ng/mL DAPI in PBST was added for 10 min at room temperature to counterstain nuclear DNA, followed by three washing steps with PBST and one additional wash with ddH_2O.

Image Acquisition and Data Analysis

Images were acquired with an Operetta High-Content Imaging system (PerkinElmer, Waltham, MA, USA) equipped with a 40× high NA objective. The 380/40-nm excitation and 410- to 480-nm emission filters were used to image DAPI, and the 475/30-nm excitation and 500- to 550-nm emission filters were used to image 6-FAM–EdU.

DAPI images were used to segment and count the total number of nuclei for each well, representing the total cell count. Each antibody concentration was tested in technical triplicates. Total cell counts of triplicates were averaged and normalized to the cell count of an untreated control (c(trastuzumab) = 0). Averaged and normalized cell counts were plotted against $\log_{10}$-transformed antibody concentrations. Fitting a nonlinear four-parametric model equation $y = \min + \frac{\max - \min}{1 + \left(\frac{IC_{50}}{x}\right)\text{Hill slope}}$ to the normalized cell counts y and antibody concentration x yielded inhibition curves with the descriptive parameters IC_{50} (concentration of half-maximal inhibition) and Hill slope.

Relative nucleic DNA quantities were obtained by calculating total DAPI intensities of segmented nuclei. Absolute DAPI intensities per nucleus were subgrouped by binning and plotted as a probability histogram to analyze probability distributions. A 10-parameter model function $p_x = P(x) = G_1(x) + G_2(x) + S(x)$, comprising the sum of two Gaussian terms $G_1(x) = a_{G1} * exp(-\frac{1}{2}\frac{(x-\mu_{G1})^2}{\sigma_{G1}^2})$ and $G_2(x) = a_{G2} * exp(-\frac{1}{2}\frac{(x-\mu_{G2})^2}{\sigma_{G2}^2})$ representing G1 and G2/M cell cycle phases, and a constant term with Gaussian fadeout,

$$S(x) = \begin{cases} h * exp(-\frac{1}{2}\frac{(x-x_{lower})^2}{\sigma_S^2}) & x < x_{lower} \\ h * exp(-\frac{1}{2}\frac{(x-x_{upper})^2}{\sigma_S^2}) & x > x_{upper} \\ h & else \end{cases},$$

modeling S phase, were fitted to the DAPI intensity probability densities p_x and histogram bin centers x to model the DNA content distribution throughout the cell cycle. The function was fitted by globally minimizing the squared error via simulated annealing using the GenSA package in R. By integrating over the respective term of the derived fit equation representing the G1, S, or G2/M phase, the relative proportion of each phase of the whole cell population was calculated—for example,

$$P(\mathrm{G1}) = \frac{\int_{-\infty}^{\infty} G_1(x)}{\int_{-\infty}^{\infty} P(x)}.$$

Based on 6-FAM–EdU signal, nuclei were classified as proliferating or nonproliferating. Data averaging, normalization, and curve fitting were done in a similar manner as described above for total cell counts.

All image processing was performed with the Harmony software (PerkinElmer); data analysis and curve fitting were done in MATLAB and R (2016, https://www.R-project.org). The R script used for the estimation of cell cycle distributions from DAPI intensity distributions is available at https://github.com/hoerldavid/CellCycleFit.

Results and Discussion

In the field of biologics, therapeutic antibodies have emerged as an especially promising drug format over the past years.[2] A role model for this class of drugs is trastuzumab, which binds the extracellular domain of the HER2 cell surface receptor. In a subset of breast cancers, the growth factor receptor HER2 is overexpressed and mediates increased proliferation.[12] Trastuzumab counteracts this accelerated growth by reducing HER2-mediated signaling and therefore acting as an antiproliferative drug on HER2-overexpressing cells.[13] To assess the antiproliferative potency of a therapeutic antibody, cells are subjected to a range of antibody concentrations. Higher antibody concentrations are expected to lead to lower numbers of viable cells and an even more pronounced decrease in proliferating cells (**Fig. 1**).

In the described assay, HER2-overexpressing cells (BT474 and SKBR3) and control cells (MDA-MB-468) were supplemented with EdU after 4 days of trastuzumab treatment. The proliferating fraction of the cell population incorporates EdU molecules into newly synthesized DNA during S phase. Surviving cells are stained with DAPI, whereas the incorporated EdU is labeled by CuAAC-mediated coupling of the fluorescent dye 6-FAM–azide. Imaging of stained cells on an Operetta system facilitates the detection and segmentation of nuclei, DNA content analysis using the DAPI signal, and definition of the proliferation status according to the EdU signal. Testing multiple antibodies over a range of concentrations is conveniently done in a multiwell tissue culture plate, which is compatible with the Operetta HCS imaging system. With this setup, an inhibition curve with 10 data points as technical triplicates can easily be generated for two individual antibodies in a 96-well format. Quantification of counted nuclei and detected proliferating cells can readily be done with the built-in software package of the Operetta system (Harmony), whereas statistical analysis and curve fitting are conveniently handled with respective MATLAB toolboxes. Besides the quantification of total cell counts and proliferating cells, the relative intensities of the DAPI and/or EdU signal per nucleus provide additional information with regard to cell cycle phase distributions.

Cell Survival and Cell Cycle Progression

Treatment of HER2-overexpressing cell lines with trastuzumab leads to a reduction in cell growth, but BT474 cells have been reported to be more susceptible than SKBR3 cells.[14] After 4 days of treatment, fluorescence microscopy of DAPI-stained nuclei indicates a clear reduction in cells with increasing concentrations of trastuzumab for BT474 (**Fig. 2A**) as well as SKBR3 cells. Next, we performed high-content image analysis by nuclei segmentation and subsequent quantification of surviving cells as a function of antibody concentration. By fitting a four-parametric nonlinear model to the obtained data points, we calculated inhibition curves. These fits revealed a decrease in total cell number with increasing antibody concentration and S/B ratios lower than 3 for BT474 (**Fig. 2B**) and SKBR3 (**Fig. 2C**). The maximal induction of cell death is 64% with a concentration of half maximal inhibition (IC_{50}) of 1.8 nM for BT474 cells and 65% with an IC_{50} value of 1.9 nM for SKBR3 cells. The low S/B values can be explained by the specific mode of action mediated by trastuzumab, decelerating cell proliferation rather than actively promoting cell death.[14] Therefore, cells that have already passed G1 phase will further progress in cell cycle. With BT474 and SKBR3 cells exhibiting long doubling times (2–3 days), S/B ratios greater than 4 (two doublings) are not to be expected in the time course of the assay, which holds also true for other assays merely detecting survival or viability.[9] Moreover, a very low Hill slope could be observed for SKBR3 cells compared with BT474, which is linked to the lower susceptibility of SKBR3 to trastuzumab.[9,14] Consistently, an unsusceptible cell line (MDA-MB-468) showed no difference in the number of viable cells between treated and untreated conditions (**Fig. 2B**,**C**). These results indicate that exclusively measuring cell survival is limiting the S/B ratio of proliferation assays, since arrested cells, which are still metabolically active, cannot be distinguished from proliferating cells.

High-content image analysis of DAPI-stained nuclei allows not only segmentation and quantification of nuclei but also the measurement of relative nuclear DNA contents. Since the amount of chromosomal DNA doubles through S phase from G1 to G2 phase, the absolute DAPI signal per nucleus can be used to analyze changes in cell cycle distributions. In this line, we generated frequency histograms of the absolute DAPI intensity per nucleus (**Fig. 3A** and **Suppl. Fig. S1**). Fitting a three-term model function to the data allowed us to determine the proportion of cells within each cell cycle phase (**Fig. 3B**). SKBR3 cells exhibited a clear change in cell cycle

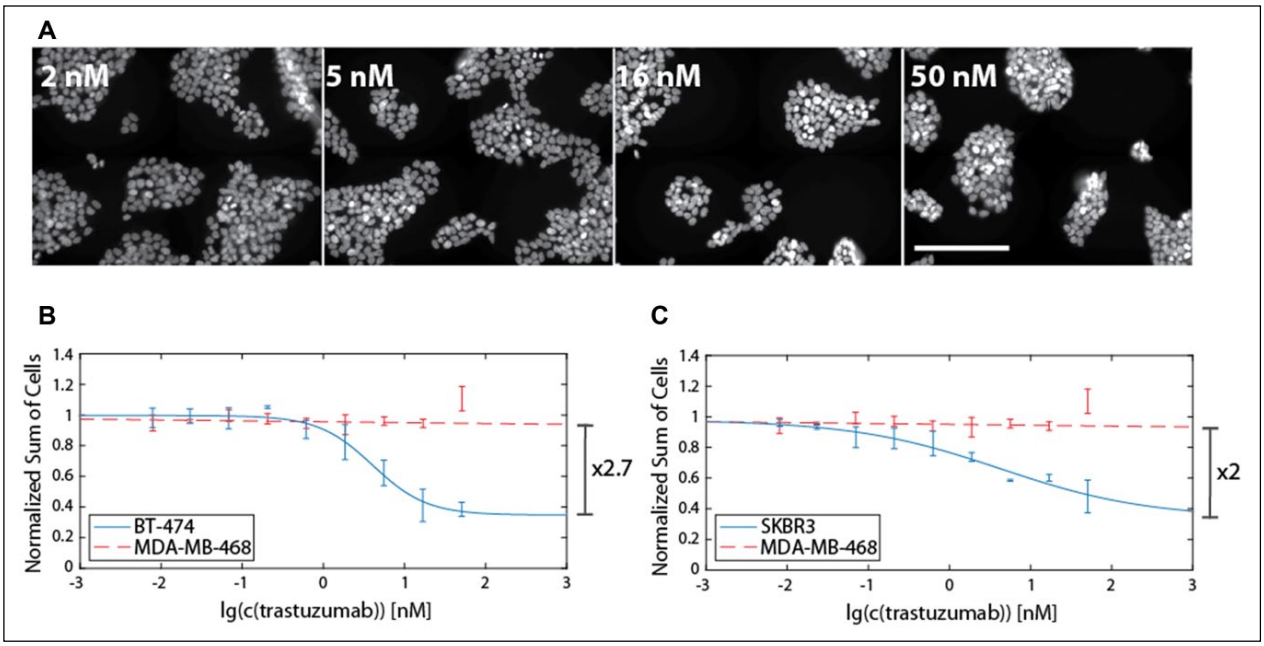

Figure 2. Quantification of antiproliferative potency by counting nuclei of surviving cells. 4′,6-Diamidino-2-phenylindole (DAPI)–stained nuclei were imaged with an Operetta high-content screening (HCS) system. Representative images of BT474 cells for four different antibody concentrations are shown in (**A**). Scale bar represents 100 µm. The observed decrease in surviving cells was quantified from technical triplicates for nine individual antibody concentrations (0.008–50 nM) and an untreated control. Averaged triplicates normalized to untreated control were plotted against $\log_{10}$-transformed trastuzumab concentrations for BT474 (**B**) and SKBR3 (**C**) and fitted to a four-parametric inhibition curve model equation (solid lines). Proliferation of a negative control cell line, MDA-MB-468, was unaffected by trastuzumab treatment (dashed line). The maximal difference in the number of surviving cells was 2.7-fold for BT474 as well as for SKBR3 cells.

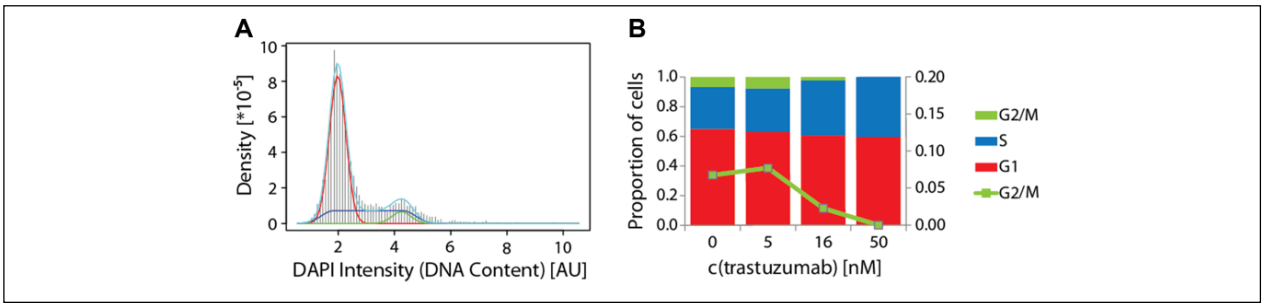

Figure 3. Shift in cell cycle distribution of trastuzumab-treated SKBR3 cells. Nuclear 4′,6-diamidino-2-phenylindole (DAPI) intensities were analyzed to categorize cells into cell cycle phases according to their relative DNA content. Probability density histograms of DAPI intensities were used to fit a model equation to the observed distribution. An exemplary histogram for c(trastuzumab) = 16 nM is given in (**A**) with the fitted curve in cyan and respective cell cycle phase terms in red (G1), blue (S), and green (G2/M). Integration over the individual terms yields the proportion of cells in each cell cycle phase treated with different trastuzumab concentrations (**B**). High concentrations of trastuzumab lead to a reduction in the G2/M phase proportion, indicating cell cycle arrest.

profiles upon trastuzumab treatment. The quantification of these data shows a decrease in the G2 phase population with increasing antibody concentration, which suggests an arrest in either G1 or S phase. This is consistent with the proposed G1 arrest induced by trastuzumab.[15]

Cell cycle profiles are an additional readout of the described assay and provide supplementary information about the mode of action of an antiproliferative antibody. Investigation of potency and mode of action in a single experiment was facilitated by increasing resolution to the single-cell level combined with high-throughput sample and data handling implemented in HCS systems. Cell cycle analysis of the less susceptible SKBR3 cell line showed that we are able to analyze an antibody's mode of action even if the overall

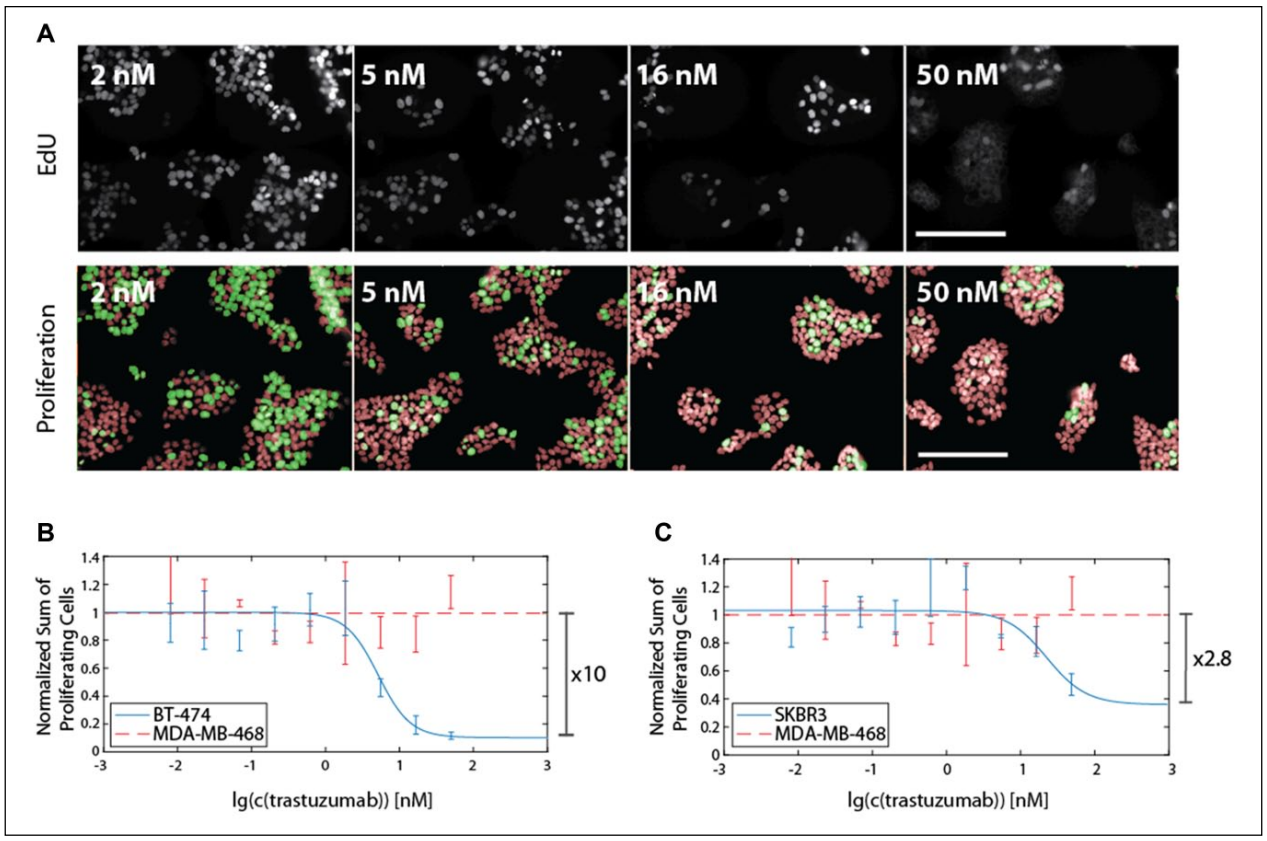

Figure 4. Improving assay sensitivity by detecting proliferating cells via 5-ethynyl-2′-deoxyuridine (EdU) incorporation. EdU, incorporated into chromosomal DNA during replication, was labeled by copper-catalyzed azide alkyne cycloaddition (CuAAC) with 6-FAM and imaged with an Operetta high-content screening (HCS) system. Representative images of BT474 cells are shown in (**A**). Scale bar represents 100 µm. Segmented nuclei from **Figure 2A** were classified as proliferating (green) or nonproliferating (red) based on EdU signal presence. It is clearly visible that only a small fraction of all surviving cells is still proliferating at high antibody concentrations. Results of quantification of proliferating cells and data fitting similar to data in **Figure 2** are shown for BT474 cells (**B**) and SKBR3 cells (**C**). The signal to background (S/B) ratio could be greatly improved for BT474 cells from 2.7 to 10 compared with surviving cell quantification (**Fig. 2**). SKBR3 cells exhibit an S/B ratio of 2.8, which is comparable to the value derived from 4′,6-diamidino-2-phenylindole (DAPI)–based quantification of surviving cells (2.7).

antiproliferative effect is weak. Nevertheless, it is also desirable to detect this weak proliferation inhibition with greater resolution. To address this need, we chose EdU incorporation for sensitive detection of proliferating cells.

Increased Assay Sensitivity via Quantification of EdU Incorporating Cells

Since DNA replication is a major characteristic of proliferation, we decided to use EdU incorporation as a marker for proliferating cells. Labeling EdU with a fluorescent dye allowed the distinction between proliferating and nonproliferating cells by fluorescence microscopy. Automated quantification of EdU-positive cells increased the S/B ratio to 10 for treated versus untreated BT474 cells (**Fig. 4B**). A concentration of half maximal inhibition (IC_{50}) of 4.9 nM was obtained from the fitted inhibition curve, whereas the maximal induction of proliferation inhibition was 90%. For SKBR3 cells, we observed a maximal induction of proliferation inhibition of 64% and IC_{50} of 3.9 nM. To ensure that the detected inhibition of proliferation was due to trastuzumab-mediated effects, we subjected a control cell line, MDA-MB-468, to the same treatment. As expected, we could not observe any difference in the proliferating fraction upon addition of trastuzumab (**Fig. 4B**,**C**). We could show that EdU incorporation-based detection of proliferating cells by microscopy greatly increases the S/B ratio compared with detecting surviving cells and improves the inhibition curve parameters such as Hill slope in the case of SKBR3 (**Fig. 4C**). A 10-fold change in proliferation has recently also been demonstrated with a DELFIA-BrdU–based assay.[9] However, the assay described in the present article uses the more sensitive and mild EdU staining method, provides the possibility for multiplexed readout of

various parameters, and increases the assay resolution by the detection of single cells instead of averaging over a bulk population.

In summary, we could show that EdU-based labeling of proliferating cells with subsequent automated imaging and analysis combined with DAPI-based cell cycle profiling is a simple and sensitive way for parallel investigation of anti-proliferative potency and mode of action of therapeutic antibodies.

Acknowledgments

We thank Dr. Shane Miersch for providing cell lines and advice on assay setup.

Declaration of Conflicting Interests

The authors declared no potential conflicts of interest with respect to the research, authorship, and/or publication of this article.

Funding

The authors disclosed receipt of the following financial support for the research, authorship, and/or publication of this article: This work was supported by a grant from the Priority Program SPP1623 of the Deutsche Forschungsgemeinschaft by H. L. A. S. was trained and supported by the graduate school GRK1721 of the Deutsche Forschungsgemeinschaft as an associate member.

References

1. Schumacher, D.; Hackenberger, C. P.; Leonhardt, H.; et al. Current Status: Site-Specific Antibody Drug Conjugates. *J. Clin. Immunol*. **2016**, *36*(Suppl 1), 100–107.
2. Shi, S. Biologics: An Update and Challenge of Their Pharmacokinetics. *Curr. Drug Metab*. **2014**, *15*, 271–290.
3. Crombet-Ramos, T.; Rak, J.; Perez, R.; et al. Antiproliferative, Antiangiogenic and Proapoptotic Activity of h-R3: A Humanized Anti-EGFR Antibody. *Int. J. Cancer* **2002**, *101*, 567–575.
4. Vega-Avila, E.; Pugsley, M. K. An Overview of Colorimetric Assay Methods Used to Assess Survival or Proliferation of Mammalian Cells. *Proc. West Pharmacol. Soc*. **2011**, *54*, 10–14.
5. Dehlinger, D.; Suer, L.; Elsheikh, M.; et al. Dye Free Automated Cell Counting and Analysis. *Biotechnol. Bioeng*. **2013**, *110*, 838–847.
6. Mosmann, T. Rapid Colorimetric Assay for Cellular Growth and Survival: Application to Proliferation and Cytotoxicity Assays. *J. Immunol. Methods* **1983**, *65*, 55–63.
7. Crouch, S. P.; Kozlowski, R.; Slater, K. J.; et al. The Use of ATP Bioluminescence as a Measure of Cell Proliferation and Cytotoxicity. *J. Immunol. Methods* **1993**, *160*, 81–88.
8. Porstmann, T.; Ternynck, T.; Avrameas, S. Quantitation of 5-Bromo-2-Deoxyuridine Incorporation into DNA: An Enzyme Immunoassay for the Assessment of the Lymphoid Cell Proliferative Response. *J. Immunol. Methods* **1985**, *82*, 169–179.
9. Lu, X.; Bergelson, S. Development of a Sensitive Potency Assay to Measure the Anti-Proliferation Effect of an Anti-HER2 Antibody. *J. Immunol. Methods* **2014**, *415*, 80–85.
10. Fraietta, I.; Gasparri, F. The Development of High-Content Screening (HCS) Technology and Its Importance to Drug Discovery. *Expert Opin. Drug Discov*. **2016**, *11*, 501–514.
11. Dodev, T. S.; Karagiannis, P.; Gilbert, A. E.; et al. A Tool Kit for Rapid Cloning and Expression of Recombinant Antibodies. *Sci. Rep*. **2014**, *4*, 5885.
12. Browne, B. C.; O'Brien, N.; Duffy, M. J.; et al. HER-2 Signaling and Inhibition in Breast Cancer. *Curr. Cancer Drug Targets* **2009**, *9*, 419–438.
13. Vu, T.; Claret, F. X. Trastuzumab: Updated Mechanisms of Action and Resistance in Breast Cancer. *Front. Oncol*. **2012**, *2*, 62.
14. Brockhoff, G.; Heckel, B.; Schmidt-Bruecken, E.; et al. Differential Impact of Cetuximab, Pertuzumab and Trastuzumab on BT474 and SK-BR-3 Breast Cancer Cell Proliferation. *Cell Prolif*. **2007**, *40*, 488–507.
15. Lane, H. A.; Motoyama, A. B.; Beuvink, I.; et al. Modulation of p27/Cdk2 Complex Formation through 4D5-Mediated Inhibition of HER2 Receptor Signaling. *Ann. Oncol*. **2001**, *12*(Suppl 1), S21–S22.

Supplementary Information

A Simple and Sensitive High Content Assay for the Characterization of Anti-Proliferative Therapeutic Antibodies

Andreas Stengl[1], David Hörl[1], Heinrich Leonhardt[1], Jonas Helma[1]*

[1] Department of Biology II, LMU Munich, Grosshadernerstrasse 2, 82152 Planegg-Martinsried, Germany

* Corresponding author: helma@biologie.uni-münchen.de

Keywords: therapeutic antibodies, cell-based, high-content assay, EdU, proliferation

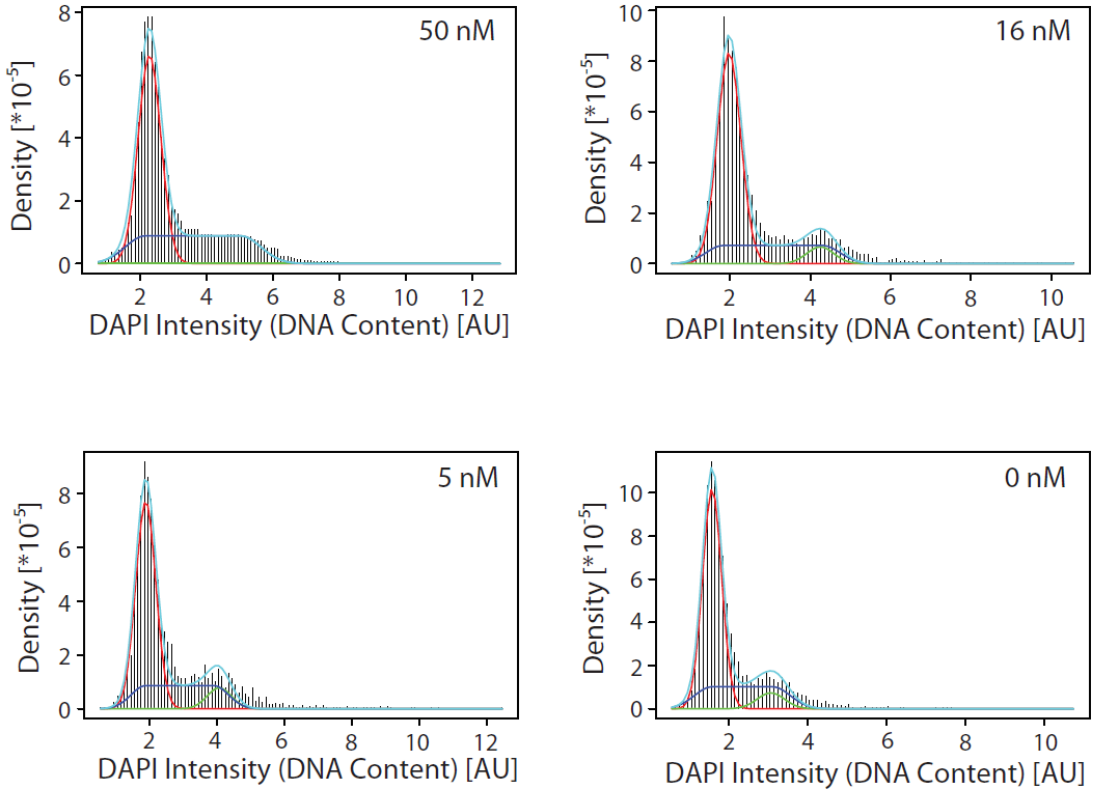

Figure S1 Histograms of total nuclear DAPI intensities and fitted cell cycle phase curves. Total DAPI intensities per nucleus were calculated for SKBR3 cells and plotted as probability density histograms at four different trastuzumab concentrations. A prominent peak for G1 phase was observed, a plateau representing S phase and a smaller peak at approximately two times the DNA content of G1 phase cells, consisting of cells in G2/M phase. Solid line graphs represent either the G1 phase term (red), S phase term (blue) or G2/M phase term (green) of the resulting fit (cyan). Integration over the individual terms yielded relative quantities for each cell cycle phase (see Figure 2).

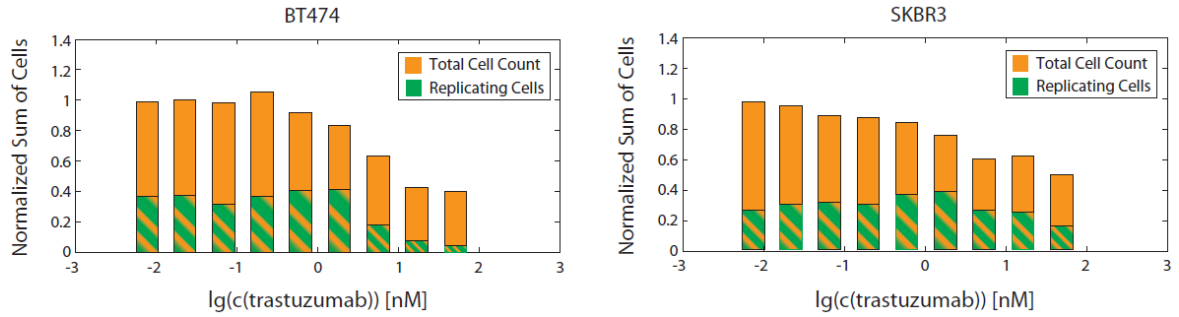

Figure S2 Quantification of proliferating cells improves assay sensitivity compared to counting total surviving cells. Total cell count (orange) and proliferating cell fraction (green) are depicted for different trastuzumab concentrations. With increasing antibody concentration the number of cells surviving treatment is decreased for BT474 as well as for SKBR3 cells. Even more pronounced is the decrease in proliferating cells of the surviving cell population illustrating the increased sensitivity demonstrated with the described assay. These data reflect the assay schematic given in Figure 1.

4.2 TuPPL: Tub-tag mediated C-terminal Protein-Protein-Ligation Using Complementary Click-Chemistry Handles

Volume 17 | Number 20 | 28 May 2019 | Pages 4923–5162

Organic & Biomolecular Chemistry

rsc.li/obc

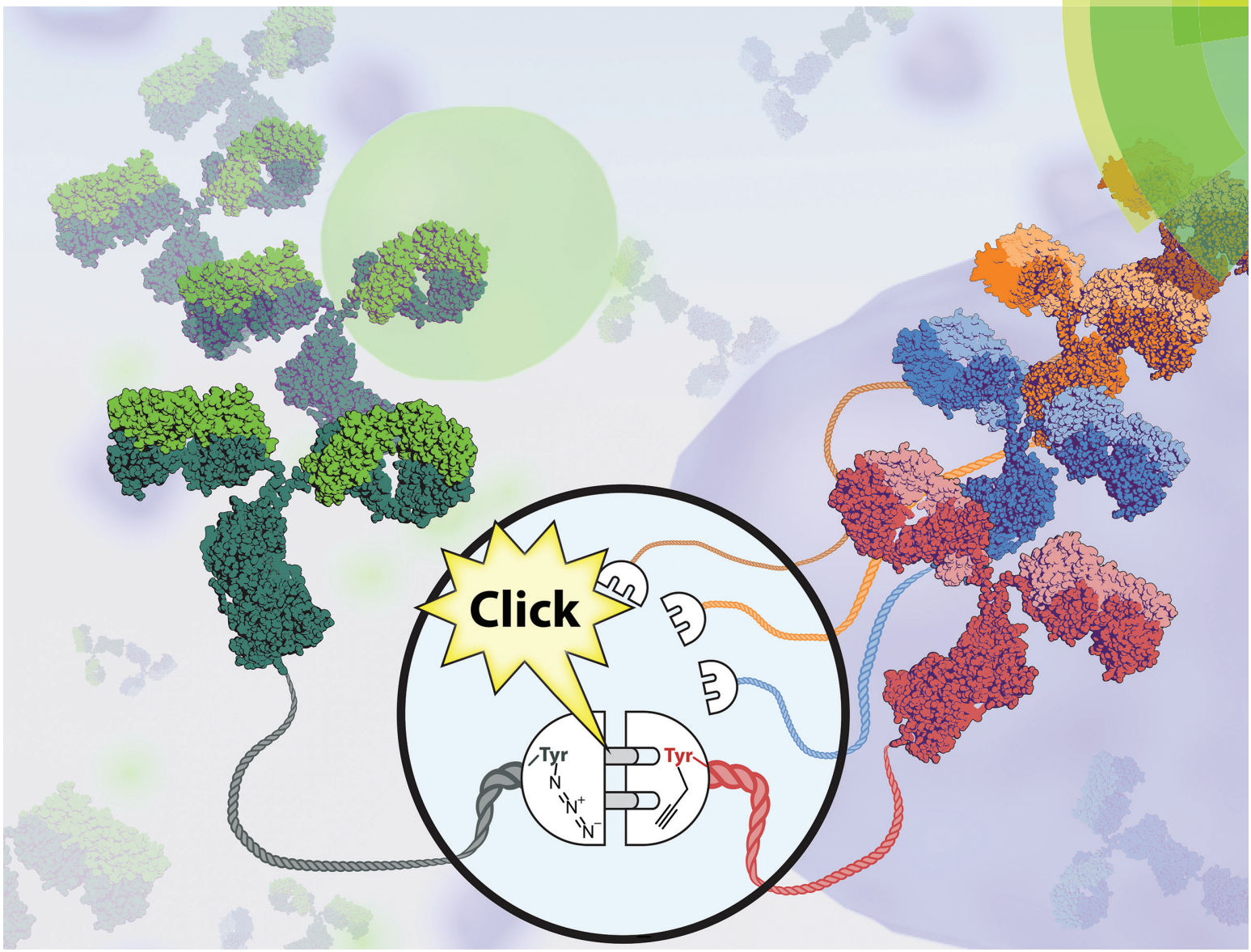

ISSN 1477-0520

ROYAL SOCIETY OF CHEMISTRY | Celebrating IYPT 2019

COMMUNICATION
Dominik Schumacher, Jonas Helma *et al.*
TuPPL: Tub-tag mediated C-terminal protein–protein-ligation using complementary click-chemistry handles

Organic & Biomolecular Chemistry

COMMUNICATION

Cite this: *Org. Biomol. Chem.*, 2019, **17**, 4964

Received 1st March 2019,
Accepted 5th March 2019

DOI: 10.1039/c9ob00508k

rsc.li/obc

TuPPL: Tub-tag mediated C-terminal protein–protein-ligation using complementary click-chemistry handles†

Andreas Stengl,[a] Marcus Gerlach,[a] Marc-André Kasper,[b,c] Christian P. R. Hackenberger,[b,c] Heinrich Leonhardt,[a] Dominik Schumacher *[a] and Jonas Helma*[a]

We introduce a chemoenzymatic strategy for straightforward *in vitro* generation of C-terminally linked fusion proteins. Tubulin tyrosine ligase is used for the incorporation of complementary click chemistry handles facilitating subsequent formation of functional bispecific antibody-fragments. This simple strategy may serve as central conjugation hub for a modular protein ligation platform.

Recombinant fusion proteins have recently emerged as highly promising biopharmaceuticals.[1,2] A prominent example are therapeutic antibody formats, such as Bispecific T-cell Engagers (BiTEs), a novel class of therapeutics, combining the antigen binding domains of two different antibodies to redirect immune cells to tumor cells.[3,4] Individual proteins and their functionalities can be combined into a single biomolecule, however, how these proteins are connected is crucial but not trivial.[1,5] Commonly, proteins are genetically fused as a single polypeptide. Even though genetic fusions are straightforward to construct, this approach comes with limitations such as strict C- to N-terminal linkage or the necessity of a mutual expression and purification strategy for both fusion partners.[6] To circumvent these limitations alternative strategies have been described for *in vitro* conjugation. Although, amine or thiol reactive crosslinking reagents can serve as adaptors to covalently link proteins,[7] occurring heterogeneity in conjugation site and stoichiometry can be detrimental to protein function. Chemical ligation methods like native chemical ligation (NCL) or expressed protein ligation (EPL) form native amide bonds and are established methods to increase conjugate homogeneity.[8,9] However, like genetic fusions, they are also limited to N- to C-terminal linkage. The site of linkage and the relative orientation of the fusion partners can influence conjugation efficiency and functional activity.[10] Therefore, different connections, such as N-to-N, C-to-C or AA_x-to-AA_y fusions are of high interest and became available by the development of several site-specific, bioorthogonal methods,[11] for example, the incorporation of unnatural amino acids (UAAs) by amber suppression.[12] Alternatively, peptide-tag based systems, have been developed for enzyme catalyzed, site-specific incorporation of bioorthogonal handles[13] and applied for protein–protein-ligation.[14–17] In contrast to amber suppression, tag-based systems do not require engineered expression systems and often allow the incorporation of bioorthogonal reporters of choice after expression, resulting in highly modular ligation platforms.[18,19] We have recently developed the Tub-tag technology for site-specific modification of recombinant proteins.[20,21] The Tub-tag system utilizes the tubulin tyrosin ligase (TTL) and an alpha-tubulin derived C-terminal recognition sequence for the incorporation of unnatural tyrosine derivatives for chemoselective conjugation.[22] For example, 3-azido-L-tyrosine was efficiently ligated to several proteins and enabled their modification by strain promoted click chemistry. Moreover, we were able to show that TTL is promiscuous towards a number of different bioorthogonal handles including *O*-propargyl-L-tyrosine allowing the ligation of compounds complementary for copper catalyzed click chemistry (copper(I)-catalyzed alkyne–azide cycloaddition (CuAAC)) (Fig. 1A).[23] Whereas incorporation efficiency of 3-azido-L-tyrosine to a fluorescently labeled 14-mer C-terminal tubulin peptide (Tub tag peptide) is reported as >90%, under identical reaction conditions the incorporation of *O*-propargyl-L-tyrosine is less efficient.[23] To improve incorporation on the Tub-tag peptide we investigated its dependence of the tyrosine derivative concentration. While the already high incorporation efficiency of 3-azido-L-tyrosine is only slightly improved, we observe a pronounced enhancement for *O*-propargyl-L-tyrosine from 25% to 95% when increasing the concentration from 1 mM to 16 mM (Fig. 1B and C). In a subsequent CuAAC reaction, *O*-propargyl-L-tyrosine is efficiently

[a]*Department of Biology II and Center for Integrated Protein Science Munich (CIPSM), Ludwig-Maximilians-Universität München, 82152 Planegg, Martinsried, Germany. E-mail: schumacher@biologie.uni-muenchen.de, helma@biologie.uni-muenchen.de*
[b]*Leibniz-Forschungsinstitut für Molekulare Pharmakologie (FMP), Chemical Biology Department, Robert-Rössle-Strasse 10, 13125 Berlin, Germany*
[c]*Humboldt Universität zu Berlin, Department of Chemistry, Brook-Taylor-Str. 2, 12489 Berlin, Germany*

†Electronic supplementary information (ESI) available. See DOI: 10.1039/c9ob00508k

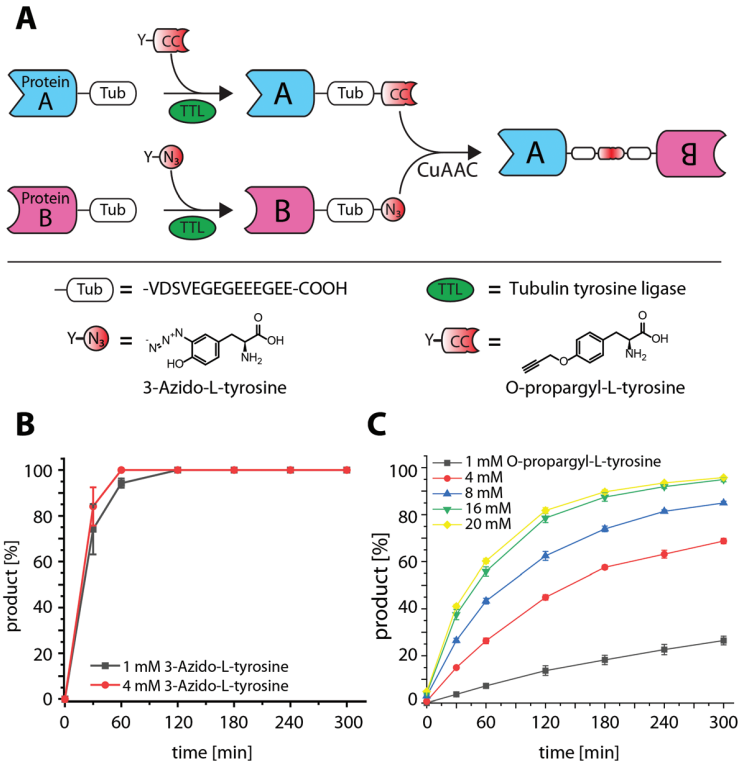

Fig. 1 Tub-tag mediated protein–protein ligation (TuPPL) process and TTL catalyzed ligation of 3-azido- and *O*-propargyl-L-tyrosine with a Tub-tag peptide. (A) Schematic depiction of TuPPL. Tubulin tyrosine ligase (TTL) catalyzes the site-specific incorporation of tyrosine derivatives on a C-terminal peptide tag (Tub-tag). Incorporation of derivatives carrying complementary click chemistry handles on Tub-tagged proteins enables their C-terminal ligation by CuAAC, (B) ligation of 3-azido- and (C) *O*-propargyl-L-tyrosine to the Tub-tag peptide (CF-VDSVEGEGEEEGEE). Samples were taken at different time points of the TTL reaction and analyzed with RP-UPLC. Quantitation of substrate and product was performed through peak integration as described before.[17] The mean values and standard deviations of three replicate reactions are shown.

conjugated to 3-azido-L-tyrosine-modified Tub-tag peptide. After 32 minutes full conversion was achieved as monitored by RP-UPLC (Fig. S2†). Based on these observations, we decided to examine 3-azido- and *O*-propargyl-L-tyrosine as orthogonal handles for the generation of C-terminal fusion proteins. Therefore, we evaluated the TTL catalyzed incorporation of 3-azido- and *O*-propargyl-L-tyrosine on C-terminally Tub-tagged GFP-Binding Protein (GBP)[24–26] and the reactivity of the installed handles in subsequent CuAAC reactions. We observed improved incorporation at 4 mM 3-azido-L-tyrosine, whereas 1 mM is sufficient to achieve full conversion after 3 h at 37 °C. Again, we found a strong concentration dependence on the incorporation efficiency of *O*-propargyl-L-tyrosine as monitored by SDS-PAGE and validated using MS analysis (Fig. S3 and S4†). Based on these findings we decided to perform all subsequent experiments with 1 mM 3-azido- and 10 mM *O*-propargyl-L-tyrosine for 3 h at 37 °C.

To validate reactivity of installed handles, we used CuAAC to conjugate 6-Carboxyfluorescein-azide (N_3-6FAM) to *O*-propargyl-L-tyrosine modified GBP (alkynyl-GBP). Conversion from unlabeled to 6FAM labeled GBP was determined by band shifts in Coomassie stained SDS-gels and in-gel fluorescence (Fig. 2A). Quantitative formation of GBP-6FAM in 60 min demonstrated that *O*-propargyl-L-tyrosine can efficiently be ligated to Tub-tagged proteins and that the installed alkyne-handle is reactive for the subsequent CuAAC conjugation. In the same manner, efficient incorporation of 3-azido-L-tyrosine and reactivity was demonstrated by generating 3-azido-L-tyrosine modified GBP (azido-GBP) and subsequent labeling with biotin-PEG_4-alkyne at >99% efficiency in ≤10 min (Fig. 2B). These results show that C-terminally Tub-tagged proteins can be equipped with highly CuAAC-reactive alkyne- and azide-handles by incorporation of respective tyrosine derivatives.

Encouraged by these observations we set out to generate a homodimeric fusion protein consisting of two GBP entities. In this regard, Tub-tagged GBP was functionalized either with 3-azido- or *O*-propargyl-L-tyrosine in two individual, but procedural similar, TTL-catalyzed reactions. In a second step, CuAAC of alkynyl-GBP and azido-GBP generated the C-terminally linked GBP-homodimer, as illustrated in Fig. 3A. We followed the click reaction over time by SDS-PAGE analysis and observed the formation of the homodimeric product GBP-GBP (Fig. 3B). Since our initial coupling conditions (2 h, 30 °C in PBS) gave only moderate conversion (~20%) we set out to optimize the CuAAC conditions (Fig. S5†). From this screen two conditions turned out to be beneficial; firstly, lowering the pH to 5.5 with MES as buffer component and,

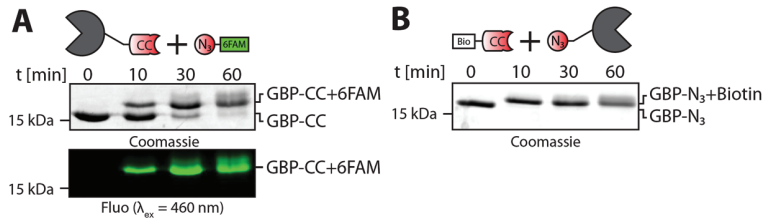

Fig. 2 CuAAC reactivity of alkynyl-GBP and azido-GBP with complementary small molecules 6FAM-azide or biotin-PEG$_4$-alkyne, respectively. (A) Alkynyl-GBP reactivity in CuAAC reactions is demonstrated by conjugation of 6FAM-azide. The increase in molecular weight upon conjugation is observed as a band shift in SDS-PAGE analysis and detection of 6FAM fluorescence. Over 95% conversion is reached after 60 min estimated by densitometric analysis, (B) azido-GBP reactivity in CuAAC reactions is demonstrated by the conjugation of biotin-PEG$_4$-alkyne with over 99% efficacy in ≤10 min.

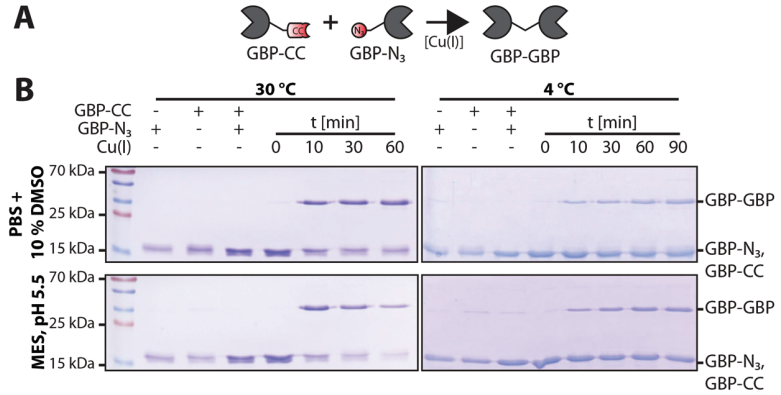

Fig. 3 GBP-homodimer formation by CuAAC mediated ligation of alkynyl-GBP and azido-GBP. (A) Schematic of Cu(I) catalyzed C-terminal ligation of alkynyl-GBP (GBP-CC) and azido-GBP (GBP-N$_3$) to form a covalently linked GBP-homodimer. (B) SDS-PAGE time course analysis of GBP-homodimer formation at 30 °C or 4 °C. The monomeric substrates, alkynyl-GBP and azido-GBP(~17 kDa) form a dimeric product (GBP–GBP, ~35 kDa). At 30 °C the reactions reach ~60% conversion (pH 5.5, MES) or ~50% conversion (PBS/10% DMSO) after 10 min with a loss of total protein observable in MES, pH 5.5 but not in PBS/10% DMSO. At 4 °C we also observe efficient coupling with ~50% conversion after 90 min without any significant loss of protein. Control reactions confirm that dimer formation is dependent on the presence of (i) both complementary functionalized GBP monomers and (ii) Cu(I) as a catalyst.

secondly, the addition of 10% DMSO when using PBS, pH 7.4 as buffer component. At 30 °C GBP-dimer formation reaches ~60% conversion (pH 5.5, MES) or ~50% conversion (PBS/10% DMSO) after 10 min (Fig. 3B). We observed a slight loss of protein over time in MES, pH 5.5 presumably due to protein aggregation; however, this effect was not observed in PBS/10% DMSO. At 4 °C we also observe efficient coupling with ~50% conversion after 90 min without any significant loss of protein. Control reactions confirm that dimer formation is dependent on the presence of both complementary functionalized GBP monomers and Cu(I) as a catalyst. These results show that by using the TuPPL workflow C-terminally linked homodimers can be generated efficiently at equimolar protein concentrations. We confirmed homodimer formation by MS-analysis (Fig. S6†). To evaluate the preserved binding of the GBP-dimers to their antigen eGFP, GBP-dimers were purified by preparative size exclusion chromatography (Fig. 4A). Due to the C-terminal linkage, both N-terminal eGFP binding sites of the GBP-dimer face opposite directions, thus, functional GBP-dimers bind two eGFP molecules.[15] To test this bivalent eGFP-binding we performed analytic size exclusion chromatography of GBP-dimer incubated with eGFP at different molar ratios. At a 1 : 1 molar ratio of eGFP to GBP-dimer we observed three products: (i) GBP-dimer, (ii) GBP-dimer bound to a single eGFP and (iii) to two eGFP molecules (Fig. 4B). A molar excess of 4 : 1 eGFP over GBP-dimer leads to saturation of all binding sites, confirming functional bivalency of the purified GBP-homodimer. Furthermore, we would like to emphasize the near-quantitative eGFP binding of almost all GBP-dimer molecules. This highlights that the C-terminal linkage allows quantitative bivalent binding of two molecules which has been reported to be problematic in genetic N-to-C fusions of antibodies[27] and that the mild conjugation procedure fully preserves the antibodies' antigen binding properties.

In vitro ligation is especially beneficial for fusing proteins that require different production strategies. Thus, we finally set out to ligate two different antibody fragments isolated from different bacterial compartments. On the one hand we purified GBP from whole cell lysate and on the other hand a trastuzumab derived single chain Fragment variable (TscFv) from the periplasm. Subsequently, we functionalized both proteins with *O*-propargyl- or 3-azido-L-tyrosine, respectively, to

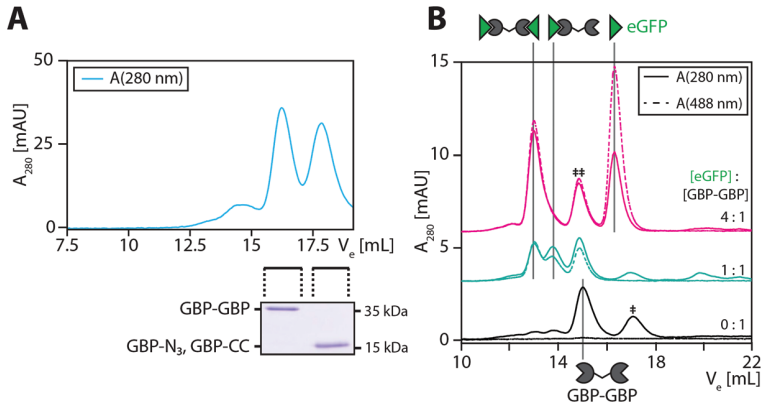

Fig. 4 Purification of GBP-homodimer and confirmation of bivalent antigen binding. (a) Size exclusion chromatogram of GBP-homodimer preparation after TuPPL and SDS-PAGE analysis of pooled peak fractions. (b) Size exclusion chromatogram of eGFP incubated with GBP-homodimer in a molar ratio of 0 : 1 (black), 1 : 1 (cyan) or 4 : 1 (magenta). At a 1 : 1 molar ratio the following species can be observed: GBP–GBP bound to (i) no, (ii) one or (iii) two eGFP molecules, whereas, complexes containing eGFP can be identified by following the absorbance at 488 nm (dashed line). A molar excess of 4 : 1 eGFP over GBP–GBP leads to saturation of all binding sites, confirming functional bivalency of the purified GBP-homodimer. Impurities of monomeric GBP (‡) and GBP : eGFP complex (‡‡) are present.

generate alkynyl-GBP and azido-TscFv (MS analysis see Fig. S4†). Ligation of alkynyl-GBP and azido-TscFv by TuPPL was achieved by CuAAC (Fig. 5B) with a conjugation efficacy of 62% after 30 min and generated heterodimers (GBP-TscFv) were purified by SEC. Removal of residual copper ions was achieved by dialysis against EDTA containing buffer and confirmed by ICP-OES (Table S1†). A functional GBP-TscFv heterodimer is bispecific, whereas one paratope binds eGFP and the other the extracellular domain of the Her2-receptor. Fluorescence microscopy, shows that GBP-TscFv heterodimers recruit eGFP to the plasma membrane of Her2 overexpressing cells (SKBR3), but not to Her2 low expressing cells (MDAMB468) (Fig. 5C). These results demonstrate the functional integrity of both fusion partners after ligation, thus, confirming the applicability of TuPPL for the generation of C-terminally linked bispecific fusion proteins.

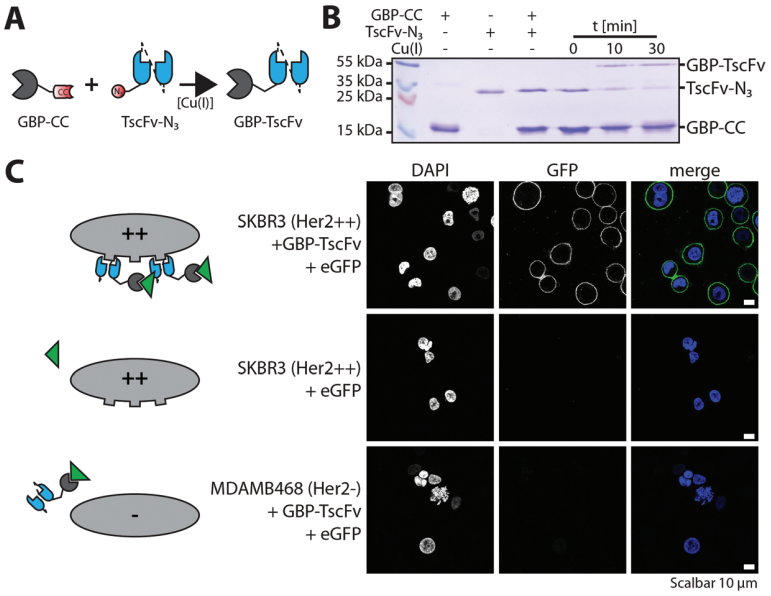

Fig. 5 C-Terminally linked GBP-TscFv heterodimer recruits eGFP to the plasma membrane of Her2 overexpressing (SKBR3) but not Her2 low expressing cells (MDAMB468). (A) Schematic of Cu(I)-catalyzed C-terminal ligation of alkynyl-GBP and azido-TscFv (single-chain fragment variable derived from the Her2 binding antibody trastuzumab) to form a bispecific heterodimer. (b) SDS-PAGE time course analysis of GBP-TscFv heterodimer formation at 30 °c. (C) eGFP recruitment of GBP-TscFv heterodimer to fixed Her2 overexpressing cells is demonstrated by fluorescence microscopy and verifies the functional integrity of both paratopes of the heterodimer. No recruitment can be observed when either (i) the heterodimer is excluded or (ii) Her2 low expressing cells (MDAMB468) are used. Scalebars represent 10 µm.

Herein, we describe TuPPL as a modular site-specific conjugation approach for the C-terminal ligation of proteins post expression. The modularity of TuPPL allows parallel generation of azido- and alkynyl-functionalized proteins as well as straightforward ligation of proteins that are produced in different expression systems. We showed that TTL catalyzed incorporation of 3-azido-L- and *O*-propargyl-L-tyrosine in combination with CuAAC chemistry enables the convenient generation of homodimeric and heterodimeric antibody-fragments without diminishing the protein's function and no residual copper contaminants. Since the relative orientation of binding sites in a multimeric complex has been shown to influence their binding ability,[10] fusion proteins in general might benefit from C-to-C-terminal linkage generated by TuPPL. Especially for antibodies this C-to-C linkage will be beneficial since N-terminal fusion, as generated by standard genetic fusion or EPL, can impair antigen binding due to steric obstruction of the paratope.[27] In addition, our approach may readily be combined with other site-specific protein modification techniques due to the use of universal bioorthogonal handles. Future work may include the use of alternative bioorthogonal handles and conjugation reactions to expand TuPPL's modularity. Moreover, the use of TuPPL can be expanded to many more proteins such as antibodies, enzymes or proteinaceous toxins. In this case, a set of pre-functionalized proteins could serve as building blocks for a modular and scalable protein ligation platform in which TuPPL serves as a central conjugation hub.

Conflicts of interest

The Tub-tag technology is part of a patent application filed by D.S., J.H, C.P.R.H and H.L. and subject to the spin-off project Tubulis.

Acknowledgements

We thank J. Koch and H. Flaswinkel for providing recombinant eGFP and H. Mescheder and T. Stoschek for critical scientific discussions. A. S. was trained and supported by the graduate school GRK1721 of the Deutsche Forschungsgemeinschaft (DFG). This work was further supported by the DFG with grants to H. L. (SFB1243, SPP1623) and C. P. R. H. (SPP1623), the Einstein Stiftung Berlin (Leibniz-Humboldt Professorship) to C. P. R .H., the Boeringer Ingelheim Fond (Plus 3 award) to C. P. R. H., by the Leibniz Association with the Leibniz Wettbewerb to C. P. R. H. and H. L. and by the German Federal Ministry for Economic Affairs and Energy with grants to D. S. and J. H. (EXIST FT I).

Notes and references

1 U. Brinkmann and R. E. Kontermann, *mAbs*, 2017, **9**, 182–212.
2 K. Garber, *Nat. Rev. Drug Discovery*, 2014, **13**, 799–801.
3 P. A. Baeuerle and C. Reinhardt, *Cancer Res.*, 2009, **69**, 4941–4944.
4 M. Mack, G. Riethmuller and P. Kufer, *Proc. Natl. Acad. Sci. U. S. A.*, 1995, **92**, 7021–7025.
5 S. Berger, P. Lowe and M. Tesar, Centre d'Immunologie Pierre Fabre, in *MAbs*, Taylor & Francis Group, LLC, 2015, vol. 7, pp. 456–460.
6 M. Schmittnaegel, E. Hoffmann, S. Imhof-Jung, C. Fischer, G. Drabner, G. Georges, C. Klein and H. Knoetgen, *Mol. Cancer Ther.*, 2016, **15**, 2130–2142.
7 S. Panowski, S. Bhakta, H. Raab, P. Polakis and J. R. Junutula, *mAbs*, 2014, **6**, 34–45.
8 S. B. Kent, *Chem. Soc. Rev.*, 2009, **38**, 338–351.
9 T. W. Muir, D. Sondhi and P. A. Cole, *Proc. Natl. Acad. Sci. U. S. A.*, 1998, **95**, 6705–6710.
10 B. M. Hutchins, S. A. Kazane, K. Staflin, J. S. Forsyth, B. Felding-Habermann, P. G. Schultz and V. V. Smider, *J. Mol. Biol.*, 2011, **406**, 595–603.
11 D. Schumacher, C. P. Hackenberger, H. Leonhardt and J. Helma, *J. Clin. Immunol.*, 2016, **36**(Suppl. 1), 100–107.
12 K. Lang and J. W. Chin, *Chem. Rev.*, 2014, **114**, 4764–4806.
13 D. M. Patterson, L. A. Nazarova and J. A. Prescher, *ACS Chem. Biol.*, 2014, **9**, 592–605.
14 K. Wagner, M. J. Kwakkenbos, Y. B. Claassen, K. Maijoor, M. Bohne, K. F. van der Sluijs, M. D. Witte, D. J. van Zoelen, L. A. Cornelissen, T. Beaumont, A. Q. Bakker, H. L. Ploegh and H. Spits, *Proc. Natl. Acad. Sci. U. S. A.*, 2014, **111**, 16820–16825.
15 M. D. Witte, J. J. Cragnolini, S. K. Dougan, N. C. Yoder, M. W. Popp and H. L. Ploegh, *Proc. Natl. Acad. Sci. U. S. A.*, 2012, **109**, 11993–11998.
16 J. E. Hudak, R. M. Barfield, G. W. de Hart, P. Grob, E. Nogales, C. R. Bertozzi and D. Rabuka, *Angew. Chem., Int. Ed.*, 2012, **51**, 4161–4165.
17 D. A. Levary, R. Parthasarathy, E. T. Boder and M. E. Ackerman, *PLoS One*, 2011, **6**, e18342.
18 T. Kruger, S. Weiland, G. Falck, M. Gerlach, M. Boschanski, S. Alam, K. M. Muller, T. Dierks and N. Sewald, *Angew. Chem., Int. Ed.*, 2018, **57**, 7245–7249.
19 J. Lotze, U. Reinhardt, O. Seitz and A. G. Beck-Sickinger, *Mol. BioSyst.*, 2016, **12**, 1731–1745.
20 D. Schumacher, J. Helma, F. A. Mann, G. Pichler, F. Natale, E. Krause, M. C. Cardoso, C. P. Hackenberger and H. Leonhardt, *Angew. Chem., Int. Ed.*, 2015, **54**, 13787–13791.
21 M. Effenberger, A. Stengl, K. Schober, M. Gerget, M. Kampick, T. R. Muller, D. Schumacher, J. Helma, H. Leonhardt and D. H. Busch, *J. Immunol.*, 2019, DOI: 10.4049/jimmunol.1801435.
22 A. Banerjee, T. D. Panosian, K. Mukherjee, R. Ravindra, S. Gal, D. L. Sackett and S. Bane, *ACS Chem. Biol.*, 2010, **5**, 777–785.

23 D. Schumacher, O. Lemke, J. Helma, L. Gerszonowicz, V. Waller, T. Stoschek, P. M. Durkin, N. Budisa, H. Leonhardt, B. G. Keller and C. P. R. Hackenberger, *Chem. Sci.*, 2017, **8**, 3471–3478.
24 A. Kirchhofer, J. Helma, K. Schmidthals, C. Frauer, S. Cui, A. Karcher, M. Pellis, S. Muyldermans, C. S. Casas-Delucchi, M. C. Cardoso, H. Leonhardt, K. P. Hopfner and U. Rothbauer, *Nat. Struct. Mol. Biol.*, 2010, **17**, 133–138.
25 J. Helma, M. C. Cardoso, S. Muyldermans and H. Leonhardt, *J. Cell Biol.*, 2015, **209**, 633–644.
26 U. Rothbauer, K. Zolghadr, S. Tillib, D. Nowak, L. Schermelleh, A. Gahl, N. Backmann, K. Conrath, S. Muyldermans, M. C. Cardoso and H. Leonhardt, *Nat. Methods*, 2006, **3**, 887–889.
27 M. M. Harmsen and H. J. De Haard, *Appl. Microbiol. Biotechnol.*, 2007, **77**, 13–22.

Electronic Supplementary Material (ESI) for Organic & Biomolecular Chemistry.

-Electronic Supplementary Information-

TuPPL: Tub-tag mediated C-terminal Protein-Protein-Ligation Using Complementary Click-Chemistry Handles

Andreas Stengl[a], Marcus Gerlach[a], Marc-André Kasper[b],[c], Christian P. R. Hackenberger[b],[c], Heinrich Leonhardt[a], Dominik Schumacher*[a] and Jonas Helma*[a]

[a]LMU Biozentrum, Department II, Human Biology and BioImaging, Großhadernerstr. 2, Planegg
[b]Leibniz-Forschungsinstitut für Molekulare Pharmakologie (FMP), Chemical Biology Department, Robert-Rössle-Strasse 10, 13125 Berlin (Germany)
[c]Humboldt Universität zu Berlin, Department of Chemistry, Brook-Taylor-Str. 2, 12489 Berlin (Germany)
* Co-corresponding

Supplementary Figures and Tables

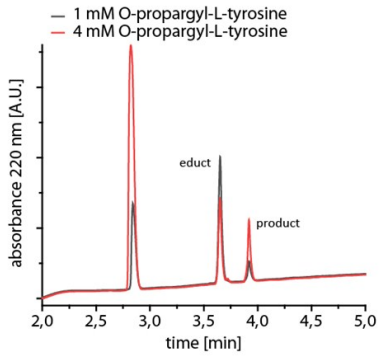

Figure S1. TTL mediated ligation of O-propargyl-L-tyrosine to the Tub-tag peptide (CF-VDSVEGEGEEEEGEE). Exemplary chromatogram recorded at 220 nm (black: 1 mM, red: 4 mM O-propargyl-*L*-tyrosine. The product peptide with O-propargyl-*L*-tyrosine elutes at 3.94 min and the sample with a substrate concentration of 4 mM showed an increased product-yield.

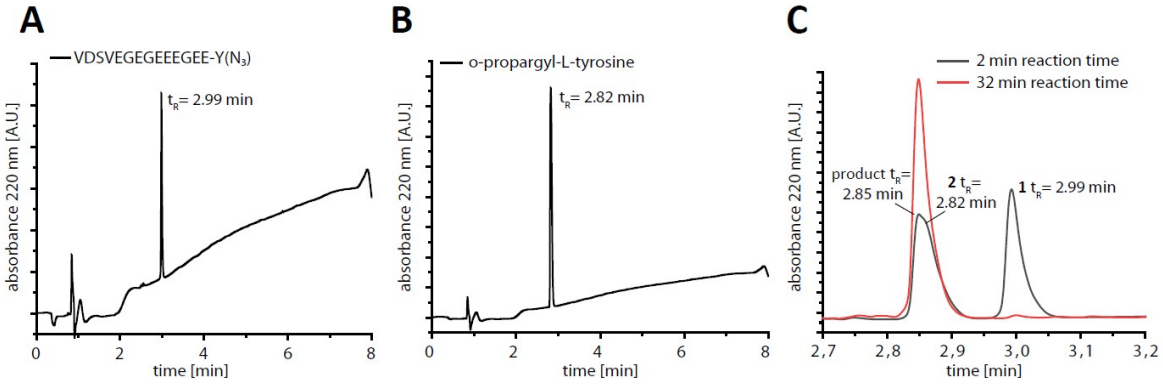

Figure S2. CuAAC model-reaction with Tub-tag peptide. 3-azido-L-tyrosine was incorporated C-terminally at the Tub-tag peptide (VDSVEGEGEEEGEE) using previously described conditions (Schumacher et al. 2015). A) After purification with RP-HPLC a pure azide-containing peptide t_R = 2.99 min was isolated. B) O-propargyl-*L*-tyrosine has an elution time of t_R = 2.82 min. The progress of the CuAAC reaction of these two educts was analyzed with RP-UPLC. C) Chromatogram of the reaction after two (black) and 32 minutes (red). Full conversion of the azide-containing peptide was achieved after 32 minutes.

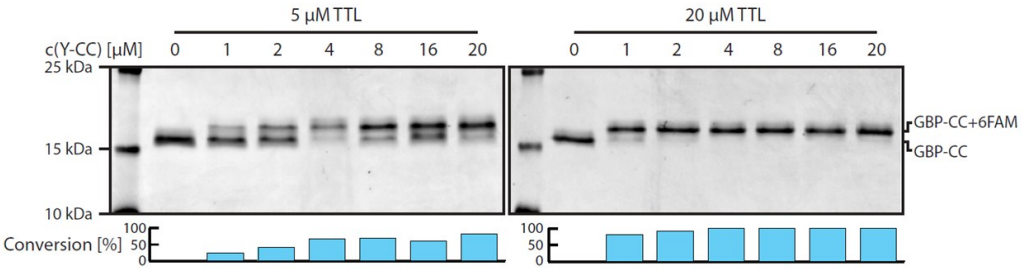

Figure S3. Concentration dependent, TTL catalyzed, ligation of O-propargyl-L-tyrosine to Tub-tagged GBP. Increasing O-propargyl-*L*-tyrosine concentration leads to increased incorporation efficacy using 5 µM TTL and 100 µM GBP at 30 °C after 3 h. Incorporation is demonstrated by CuAAC of 6FAM-azide and subsequent SDS-PAGE analysis. Complete conversion is reached at all tested O-propargyl-*L*-tyrosine concentrations when increasing the TTL concentration to 20 µM.

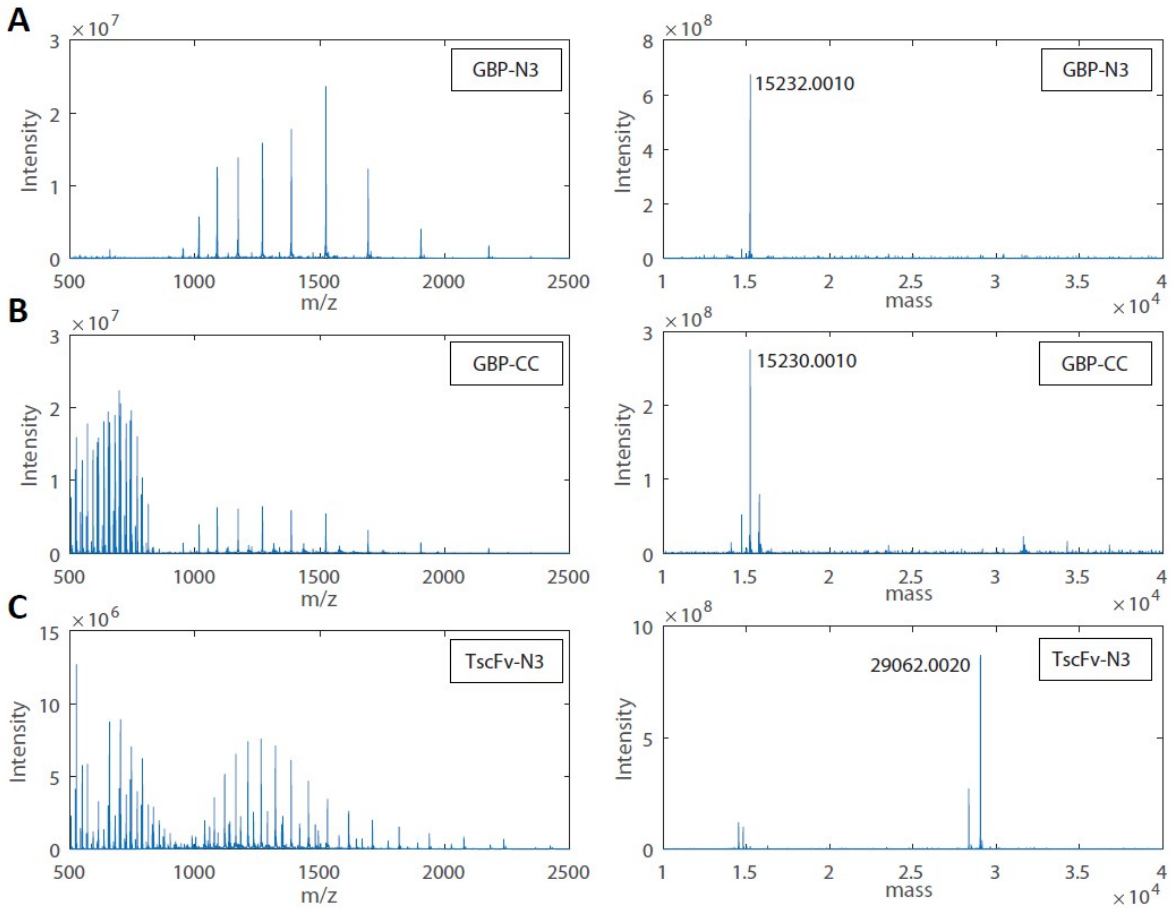

Figure S4. Intact MS analysis of tyrosine derivative modified proteins. Raw (left) and deconvoluted (right) MS spectra of GBP-Tub conjugated with 3-azido-*L*-tyrosine (GBP-N3) or O-propargyl-*L*-tyrosine (GBP-CC) and TscFv-Tub conjugated with 3-azido-*L*-tyrosine (TscFv-N3). GBP-N3 expected: 15232 Da = 15028 Da (GBP-Tub) + 222 Da (3-azido-*L*-tyrosine) – 18 Da

(H_2O). GBP-CC expected: 15229 Da = 15028 Da (GBP-Tub) + 219 Da (O-propargyl-*L*-tyrosine) – 18 Da (H_2O). TscFv-N3 expected: 29066 Da

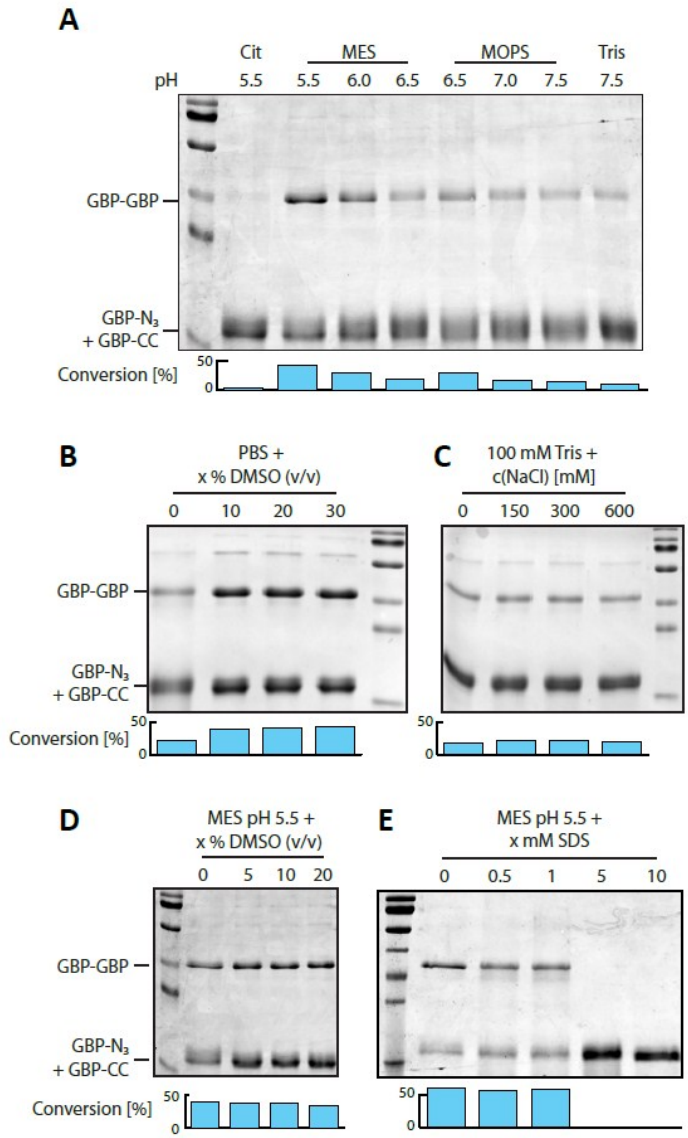

Figure S5. Optimization of CuAAC reaction conditions for protein-protein conjugation. SDS-PAGE analysis of GBP-homodimer formation under various conditions. Conversion efficacy was estimated by densitometric analysis. **A)** We observed a clear effect of buffer component as well as pH value on conjugation efficacy. Citrate almost completely abolished conjugation most probably due to its Cu ion complexation potential. Tris also has been shown to complex Cu ions which might explain the observed low conjugation efficacy in our experiment. When using MES or MOPS (two non-chelating compounds) we observe an increase in conjugation efficacy and in addition a clear pH dependence. Lower pH values are favored with

pH 5.5 giving the best results of all tested conditions. However, we observed slight aggregation at low pH this effect was reversible upon pH neutralization. **B)** Since this low pH might not be tolerated by all proteins we also assessed the effect of the miscible organic solvent DMSO under physiological buffer conditions (1x PBS, pH 7.4). Addition of 10 % (v/v) DMSO doubled the conjugation efficacy whereas higher concentrations did not further increase efficacy. **C)** NaCl concentration did not significantly influence the conjugation in the tested range and also **D)** the combination of the two beneficial conditions, MES pH 5.5 and 10 % (v/v) DMSO did not have an additive effect. **E)** We also could not observe a further beneficial effect of low concentrations of SDS which has been shown to increase protein protein conjugation involving ubiquitin (Schneider, Schneider et al. 2016). 5 mM and 10 mM SDS seemed to completely prevent conjugation.

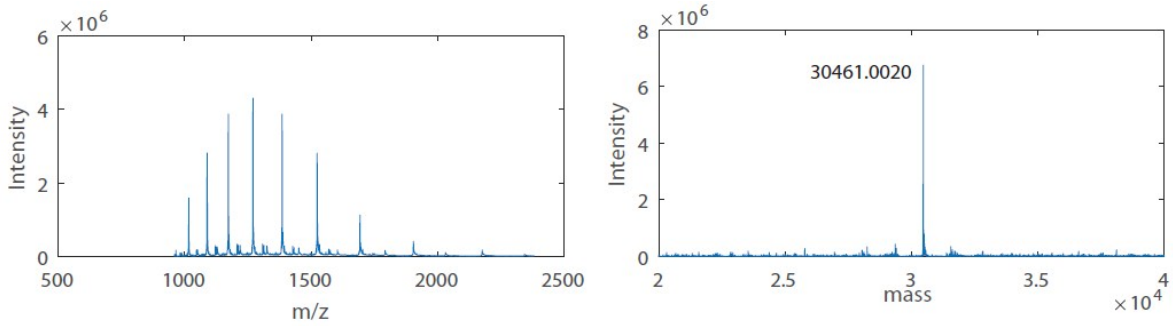

Figure S6. Raw (left) and deconvoluted (right) MS spectrum of GBP-GBP. Calculated Mass: 30461 Da = 15232 Da (GBP-N3) + 15229 Da (GBP-CC)

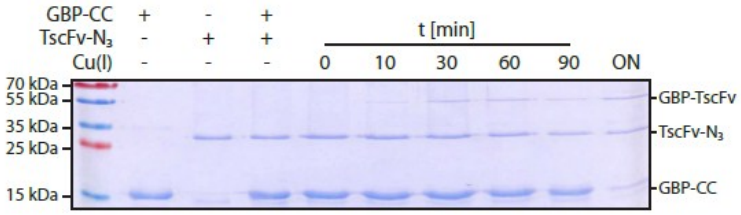

Figure S7. GBP-TscFv heterodimer formation by CuAAC at 4 °C. SDS-PAGE time course analysis of GBP-TscFv heterodimer formation. The monomeric substrates, alkynyl-GBP and azido-TscFv, of approx. 17 kDa and 30 kDa respectively, form a dimeric product (GBP-TscFv) in CuAAC.

	Cu 224.7 nm **µg/ml**	**Cu** 324.8 nm **µg/ml**
GBP-TscFv	<LOD	<LOD
GBP-TscFv + 0.25 mM CuSO4	17.38	17.22
LOD(µg/ml)	0.01	0.06

Table S1. Copper content analysis by ICP-OES. Samples were diluted 1:5 in dialysis buffer. Samples were prepared by addition of 5 volumes 3 % HNO_3 and copper emission was recorded at two wavelengths (224.7 nm and 324.8 nm) on a Varian Vista-PRO CCD Simultaneous ICP-OES instrument. No residual copper was detected in the dialyzed sample. The same sample spiked with 0.25 mM $CuSO_4$ (equals $CuSO_4$ concentration in click reaction) served as a positive control. Measurements were performed by J. Obel (Dept. of Chemistry, LMU Munich)

Experimental Section

Chemical synthesis

The Carboxyfluorescein–Tub-tag peptide (CF-VDSVEGEGEEEGEE) was synthesized as previously described[1] using standard Fmoc based SPPS. The synthesis of O-propargyl-*L*-tyrosine was carried out according to a known procedure in literature.[2]

Cell lines

HER2 overexpression cell line SKBR3 (ATCC HTB30) and a control cell line with neglectable HER2 expression levels (1000 fold less than SKBR3), MDA-MB-468 (ATCC HTB-132), were cultured in DMEM/F12 + Glutamax-I (Gibco) supplemented with 10 % FCS at 37 °C, 5% CO_2.

Protein expression, purification and SDS-PAGE analysis

TTL was expressed and purified according to a published protocol as follows [1]. TTL was expressed from a pET28 vector in *E. coli* BL21(DE3) as Sumo-TTL fusion protein with an N-terminal His-Tag. Cells were induced with 0.5 mM IPTG and incubated at 18°C for 18 h. Lysis was performed in presence of Lysozyme (100 µg/ml), DNAse (25 µg/ml) and PMSF (2 mM) followed by sonification (Branson® Sonifier; 5 times 7 x 8 sec, 40 % amplitude) and debris centrifugation at 20.000 g for 30 min. His-SUMO-TTL was purified using a 5 ml His-Trap (GE Healthcare). Purified protein was desalted on a PD10 column (GE Healthcare) by buffer exchange to MES/K pH 7.0 (20 mM MES, 100 mM KCl, 10 mM $MgCl_2$) supplemented with 50 mM L-glutamate, 50 mM L-arginine and 3 mM β-mercaptoethanol. Protein aliquots were shock-frozen and stored at -80°C.

Tub-tagged **GBP** (GFP binding protein) nanobody was expressed with a N-terminal His-tag in *E.coli* JM109 as described previously.[1]

N-terminally His-tagged **eGFP** (enhanced green fluorescent protein) was expressed from a pRSET5D expression vector in *E.coli* JM109 following the GBP expression and purification protocol.

Tub-tagged **TscFv**, a single chain Fragment variable of the variable domains of the Her2 binding antibody Trastuzumab, was assembled from VL and VH coding PCR fragments and cloned into a pNE phagmid vector suitable for periplasmatic expression[3] (kindly provided by Andreas Ernst) with standard molecular cloning techniques adopted from [4]. The construct has the following topology: SS---His-tag---T(V_L-$(G_4S)_4$-V_H)---Tub-tag with an N-terminal signal sequence (SS) for periplasmatic expression. Expression in *E. coli* BL21 (DE3) was induced at OD_{600} = 0.6 - 0.8 with 1 mM IPTG. Cells were incubated at 30 °C overnight. For periplasmic extraction cells were pelleted, resuspended in periplasmic extraction buffer I (20 % w/v Sucrose, 100 mM Tris.HCl, 1mM EDTA, pH 8.0) and incubated for 10 min at 4 °C. Cells were pelleted again, resuspended in periplasmic extraction buffer II (5 mM $MgCl_2$ in H_2O) and incubated for 20 min at 4 °C. Both extraction fractions were pooled and His-tagged TscFv-tub was purified using a 1 ml His-Trap column (GE Healthcare) followed by gel filtration on a Superdex 200 Increase 10/300 GL (GE Healthcare) using PBS as a running buffer. Protein preparation was concentrated with Amicon ultra filter units (MWCO 10 kDa, Merck Millipore) and stored at 4 °C.

Intact protein MS

Intact proteins were analyzed using a Waters H-class instrument equipped with a quaternary solvent manager, a Waters sample manager-FTN, a Waters PDA detector and a Waters column manager with an Acquity UPLC protein BEH C4 column (300 Å, 1.7 µm, 2.1 mm x 50 mm). Proteins were eluted with a flow rate of 0.3 mL/min and a column temperature of 80°C. The following gradient was used: A: 0.01% FA in H2O; B: 0.01% FA in MeCN. 5-95% B 0-6 min. Mass analysis was conducted with a Waters XEVO G2-XS QTof analyzer. Proteins were ionized in positive ion mode applying a cone voltage of 80 kV. Raw data was analyzed with MaxEnt 1 and deconvoluted between 10.000 and 40.000 Da with an accuracy of 1 Da/channel and 0.1 Da/channel for the GBP dimer.

Chemoenzymatic labeling of Tub-tag peptide with O-propargyl-*L*-tyrosine or 3-azido-*L*-tyrosine

TTL reactions with the substrate peptide CF-VDSVEGEGEEEGEE (0.2 mM) were performed in MOPS/K buffer (20 mM MOPS/K, 100 mM KCl, 10 mM $MgCl_2$, 2.5 mM ATP, 5 mM reduced GSH) at pH 7. The concentration of the respective tyrosine derivative was varied from 1 mM to 20 mM. To start the reaction 1 µM TTL was added and the reaction was incubated at 37°C. Aliquots (25 µL) were taken at defined time points and mixed with equal volume of ACN/ddH_2O 1:1, 0.2% TFA, thereupon subjected to RP-UPLC analysis.

Analytical RP-UPLC

RP-UPLC analysis was conducted on a Vanquish Flex UHPLC System with a DAD detector, Split Sampler FT, Column Compartment H and binary pump F (Thermo Fisher Scientific, USA) using a Hypersil Gold Vanquish 1.9 µM, 150 x 2.1 mm RP-UPLC-column (Thermo Fisher Scientific, USA) with a flow rate of 0.5 mL/min. The following gradient was used: (A= H_2O + 0.1% FA, B = ACN + 0.1% FA) 5% B -1.0 - 0.0 min, 5% B 0.0 – 0.5 min, 5-95% B 0.5 - 5.5 min, 95% B 5.5 – 6.5 min, 95-5% B 6.5 – 7.0 min, 5% B 7.0 – 8.0 min. UV chromatograms were recorded at 220 nm.

Preparative HPLC

Preparative HPLC was conducted on a Dionex Ultimate 3000 HPLC System with a UltiMate 3000 AFC automated fraction collector (Thermo Fisher Scientific, USA) using a ReproSil-XR 120 C18, 5 µM, 250 x 6,5 mm column (Dr. Maisch, Germany) with a flow rate of 2 mL/min. The following gradient was used: (A= H_2O + 0.1% TFA, B = ACN + 0.1% TFA) 5% B -5.0 - 0.0 min, 5% B 0.0 – 1 min, 5-95% B 1 - 60 min, 95% B 60 – 64 min, 95-5% B 64 – 65 min, 5% B. UV chromatograms were recorded at 220 nm.

Chemoenzymatic labeling of GBP-tub and TscFv-tub with 3-azido-*L*-tyrosine

TTL catalyzed ligation of 3-azido-L-tyrosine (Watanabe Chemical Industries LTD) to Tub-tagged proteins was performed in 25 - 500 uL reactions consisting of 50 µM TscFv-tub or 100 µM GBP-tub , 1/5 equivalent TTL and 1 mM 3-azido-L-tyrosine in TTL-reaction buffer (20 mM MES, 100 mM KCl, 10 mM $MgCl_2$, 2.5 mM ATP and 5 mM reduced glutathione) at 30°C for 3 h. TTL and excess 3-azido-L-tyrosine was removed by size exclusion chromatography on a Superdex 200 Increase 10/300 GL column (GE Healthcare) using PBS as a running buffer.

Chemoenzymatic labeling of GBP-tub with O-propargyl-*L*-tyrosine

TTL catalyzed ligation of O-propargyl-*L*-tyrosine to GBP-tub was performed in 25 - 500 uL reactions consisting of 100 µM GBP-tub, 20 µM TTL and 10 mM O-propargyl-*L*-tyrosine in TTL-reaction buffer (20 mM MES, 100 mM KCl, 10 mM $MgCl_2$, 2.5 mM ATP and 5 mM reduced glutathione) at 30°C for 3 h followed by size exclusion chromatography on a Superdex 200 Increase 10/300 GL column (GE Healthcare). For optimization experiments the reactions were carried out in the same manner with O-propargyl-*L*-tyrosine concentration ranging from 1 mM to 20 mM and TTL concentrations of 5 µM and 20 µM. Reaction mixtures were desalted by buffer exchange to PBS with Zeba Spin desalting columns (7K MWCO, Thermo Scientific).

CuAAC for small molecule labeling of azido-GBP and alkynyl-GBP

CuAAC reactions were performed with 100 µM azido-GBP or alkynyl-GBP and 1 mM biotin-PEG_4 -alkyne (Sigma-Aldrich) or 1 mM 6-FAM-azide (6-Carboxyfluorescein azide, baseclick), respectively, 0.25 mM $CuSO_4$, 1.25 mM THPTA (Tris(benzyltriazolylmethyl)amine), 5 mM aminoguanidine, 5 mM sodium ascorbate in 1x PBS at room temperature. Reactions were quenched at different timepoints by buffer exchange to PBS. Proteins were separated by SDS-PAGE and stained with Coomassie stain. 6-FAM-conjugates were additionally visualized by detection of in-gel fluorescence on an Amersham Imager 600 system (GE Healthcare).

CuAAC for GBP-GBP homodimer formation

CuAAC reactions for GBP homodimer formation were performed with 20 µM azido-GBP, 20 µM alkynyl-GBP, 0.25 mM $CuSO_4$, 1.25 mM THPTA, 5 mM aminoguanidine, 5 mM sodium ascorbate in either 100 mM MES pH 5.5 or 1x PBS/10 %(v/v) DMSO at 4 °C and 30 °C. Reactions were quenched at different timepoints by addition of 125 mM EDTA and buffer exchange to PBS. Proteins were separated by SDS-PAGE and stained with Coomassie stain. Conversion efficacy was estimated by densitometric analysis of coomassie stained SDS-PAGE gels. For preparative isolation of GBP-GBP dimers CuAAC reactions were quenched with 125 mM EDTA (Ethylenediaminetetraacetic acid) after 3 h and subjected to size exclusion chromatography as described above. To optimize the CuAAC reaction various buffer components, pH values and additives were tested. The common set up of these reactions was 15 µM azido-GBP, 15 µM alkynyl-GBP, 0.25 mM $CuSO_4$, 1.25 mM THPTA, 5 mM aminoguanidine, 5 mM sodium ascorbate, 100 mM buffer component X, pH X at 25 °C for 2 h. The effect of DMSO was assessed in 1x PBS, of NaCl in 20 mM Tris pH 7.5 and of SDS in 100 mM MES pH 5.5. CuAAC reactions were quenched with 125 mM EDTA and buffer exchanged to PBS with Zeba Spin desalting columns (7K MWCO, Thermo Scientific). Samples were analysed by SDS-PAGE as described above.

Conjugation efficiencies were assessed from scanned Coomassie stained SDS-PAGE gels. For this, the Gel Analyzer plugin of the Fiji software was used to quantify band intensities. For small molecule conjugation efficiency was calculated using the following equation: Intensity conjugate / (intensity conjugate + intensity unconjugated protein). For protein-protein conjugation the following equation was used: Intensity conjugate x (M_w(protein A)/M_w(protein A+B)) / (intensity protein A + intensity conjugate x (M_w(protein A)/M_w(protein A+B))), where protein B was used in excess to protein A.

CuAAC for GBP-TscFv heterodimer formation

CuAAC reactions for TscFv-GBP heterodimer formation were performed with 15 µM azido-TscFv, 60 µM alkynyl-GBP, 0.25 mM $CuSO_4$, 1.25 mM THPTA (Tris(benzyltriazolylmethyl)amine), 5 mM aminoguanidine, 5 mM sodium ascorbate in 100 mM MES pH 5.5 at 4 °C and 30 °C. Reactions were quenched at different timepoints by addition of 125 mM EDTA and buffer exchange to PBS. Proteins were separated by SDS-PAGE and stained with Coomassie stain. Conversion efficacy was estimated by densitometric analysis of coomassie stained SDS-PAGE gels. GBP-TscFv samples were dialyzed two times against 2 L 20 mM Tris, 50 mM EDTA, pH 8.0 over night at 4 °C to remove copper ions.

eGFP binding assay and analytic size-exclusion chromatography

9 µM purified GBP-GBP was mixed with 0, 1 or 4 equivalents of eGFP in PBS and incubated for 10 min at room temperature. Complex formation was assessed by size exclusion chromatography on an Aekta Pure system equipped with a Superdex 200 Increase 10/300 GL column. Absorption at 280 nm and 488 nm was monitored to detect proteins and eGFP containing complexes.

Her2 binding assay and fluorescence microscopy

SKBR3 and MDAMB468 cells were seeded on sterile coverslips and incubated overnight at 37 °C, 5 % CO2 for cell attachment. Cells were washed three times with 1x PBS prior to fixation for 10 min in 1x PBS/4% PFA (formaldehyde). Fixation was stopped by addition of an equal volume 1x PBST (PBS + 0.05 % Tween20) followed by two more washes with PBST. TscFv-GBP heterodimer was added and incubated for 1 h at room temperature (RT). Unbound TscFv-GBP was removed by three washes with PBS. eGFP was added and incubated for 30 min at RT followed by three washes with PBS. Coverslips were mounted on glass slides and images were acquired on a Leica SP5 confocal microscopy system equipped with a 63x1.40 oil immersion objective. Laserlines 405 nm and 488 nm were used in combination with standard DAPI and GFP filter settings. Image processing was carried out with ImageJ 1.5.1h software extended by the Fiji processing package.

References

1. D. Schumacher, J. Helma, F. A. Mann, G. Pichler, F. Natale, E. Krause, M. C. Cardoso, C. P. Hackenberger and H. Leonhardt, *Angew Chem Int Ed Engl*, 2015, **54**, 13787-13791.
2. D. Schumacher, O. Lemke, J. Helma, L. Gerszonowicz, V. Waller, T. Stoschek, P. M. Durkin, N. Budisa, H. Leonhardt, B. G. Keller and C. P. R. Hackenberger, *Chem Sci*, 2017, **8**, 3471-3478.
3. A. Ernst, G. Avvakumov, J. Tong, Y. Fan, Y. Zhao, P. Alberts, A. Persaud, J. R. Walker, A. M. Neculai, D. Neculai, A. Vorobyov, P. Garg, L. Beatty, P. K. Chan, Y. C. Juang, M. C. Landry, C. Yeh, E. Zeqiraj, K. Karamboulas, A. Allali-Hassani, M. Vedadi, M. Tyers, J. Moffat, F. Sicheri, L. Pelletier, D. Durocher, B. Raught, D. Rotin, J. Yang, M. F. Moran, S. Dhe-Paganon and S. S. Sidhu, *Science*, 2013, **339**, 590-595.
4. R. Rouet, D. Lowe, K. Dudgeon, B. Roome, P. Schofield, D. Langley, J. Andrews, P. Whitfeld, L. Jermutus and D. Christ, *Nat Protoc*, 2012, **7**, 364-373.

4.3 Cysteine-selective Phosphonamidate Electrophiles for Modular Protein Bioconjugations

Protein Modification

International Edition: DOI: 10.1002/anie.201814715
German Edition: DOI: 10.1002/ange.201814715

Cysteine-Selective Phosphonamidate Electrophiles for Modular Protein Bioconjugations

*Marc-André Kasper, Maria Glanz, Andreas Stengl, Martin Penkert, Simon Klenk, Tom Sauer, Dominik Schumacher, Jonas Helma, Eberhard Krause, M. Cristina Cardoso, Heinrich Leonhardt, and Christian P. R. Hackenberger**

Dedicated to Professor Hans-Ulrich Reißig on the occasion of his 70th birthday

Abstract: *We describe a new technique in protein synthesis that extends the existing repertoire of methods for protein modification: A chemoselective reaction that induces reactivity for a subsequent bioconjugation. An azide-modified building block reacts first with an ethynylphosphonite through a Staudinger-phosphonite reaction (SPhR) to give an ethynylphosphonamidate. The resulting electron-deficient triple bond subsequently undergoes a cysteine-selective reaction with proteins or antibodies. We demonstrate that ethynylphosphonamidates display excellent cysteine-selective reactivity combined with superior stability of the thiol adducts, when compared to classical maleimide linkages. This turns our technique into a versatile and powerful tool for the facile construction of stable functional protein conjugates.*

Chemical attachment of synthetic molecules to a distinct site of a protein is essential for a plethora of applications in the life sciences, in particular for the investigation of biological processes and the development of targeted therapeutics.[1] Protein modification can in principle be achieved by one of two strategies: incorporation of unnatural amino acids or peptide sequences, which possess distinct reactivities to chemical or enzymatic reactions, or reactions that rely on specific chemical properties of the side chains of proteinogenic amino acids.[2] The former requires sometimes tedious biochemical manipulations such as amber suppression or additional enzymatic transformations, while the latter is only residue-specific and can produce protein mixtures with a different degree of modification and several regioisomers being formed.[3] Despite recent advancements in the engineering of new residue-specific reactions, including the modification of tyrosine,[4] tryptophan,[5] and methionine,[6] the targeting of cysteine (Cys) residues for chemical protein modification still offers many advantages. Cys residues have a low natural abundance in a reduced form on accessible protein surfaces and can be readily incorporated into a given protein or antibody through facile mutagenesis.[7] Moreover, the unique nucleophilic properties of its sulfhydryl group have been exploited in the development of several Cys-selective modification techniques,[7,8] including metal-catalyzed reactions[9] and radical transformations.[10] Several compound classes have been employed, including the prominent electrophilic maleimides[11] and α-halo acetamides,[8] as well as a recent report on perfluorophenyl reagents.[12]

Among other techniques, maleimides remain the most widely used method for chemical modification on Cys residues,[7] mostly due to their rapid kinetics in reactions with sulfhydryl groups.[13] However, one of the biggest drawbacks of maleimide conjugates is their instability caused by a retro-Michael addition in the presence of external thiols.[14] Recently developed alternatives include self-hydrolyzing maleimides,[15] structurally refined Michael-type acceptors such as carbonyl acrylic derivatives,[16] or exocyclic maleimides.[17] These Michael-type acceptors yield stable sulfhydryl adducts; however, challenges remain, since stereo- or regioisomers are formed[18] and their incorporation into functional molecules usually requires protecting-group manipulations.

Previous work from our laboratory has shown that phosphonamidates can be chemoselectively installed into a given azide-containing protein with high functional-group tolerance through a Staudinger-phosphonite reaction (SPhR).[19] By taking advantage of this, we have used borane-protected ethynylphosphonites for the sequential coupling of two azide-containing molecules, including probes, polymers, or proteins.[20] Based on these findings, we now report a method that enables the chemoselective installation of a highly Cys-selective handle into a given azide-containing molecule through SPhR with unprotected ethynylphosphonites. Most importantly, the chemoselective

[*] M.-A. Kasper, M. Glanz, M. Penkert, S. Klenk, T. Sauer, Dr. D. Schumacher, Dr. E. Krause, Prof. Dr. C. P. R. Hackenberger
Chemical Biology Department
Leibniz-Forschungsinstitut für Molekulare Pharmakologie (FMP)
Robert-Rössle-Strasse 10, 13125 Berlin (Germany)
E-mail: hackenbe@fmp-berlin.de
M.-A. Kasper, M. Glanz, M. Penkert, S. Klenk, Dr. D. Schumacher, Prof. Dr. C. P. R. Hackenberger
Department of Chemistry, Humboldt Universität zu Berlin
Brook-Taylor-Str. 2, 12489 Berlin (Germany)
A. Stengl, Dr. D. Schumacher, Dr. J. Helma, Prof. Dr. H. Leonhardt
Department of Biology II, and Center for Integrated Protein Science Munich, Ludwig-Maximilians-Universität München
Großhadenerstr. 2, 82152 Martinsried (Germany)
Prof. Dr. M. C. Cardoso
Department of Biology, Technische Universität Darmstadt
Schnittspahnstrasse 10, 64287 Darmstadt (Germany)
Supporting information and the ORCID identification number(s) for the author(s) of this article can be found under: https://doi.org/10.1002/anie.201814715.

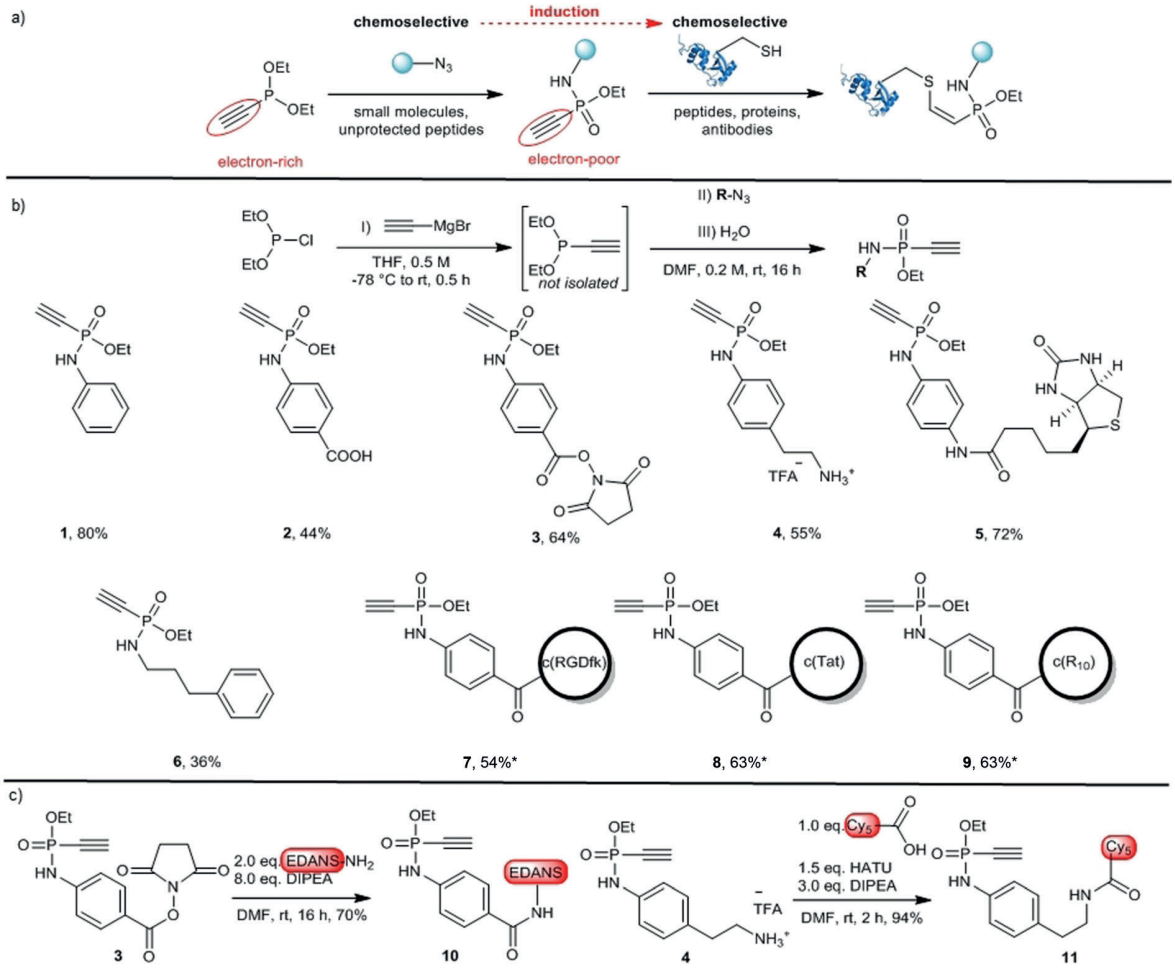

Figure 1. a) Principle of chemoselective reactivity induction for Cys. b) Yields of isolated product from one-pot SPhR with different unprotected azides. Unless stated otherwise 1.2 equiv of phosphonite were used with respect to the azide; reactions were carried out in THF at room temperature overnight. * 4 equiv phosphonite were used, reactions were carried out in DMSO. c) Modular building blocks (**3**, **4**) to attach ethynylphosphonamidates to other functional modules via amide bonds.

SPhR turns the electron-rich triple bond of an ethynylphosphonite into an electron-poor ethynylphosphonamidate and thereby induces reactivity for subsequent thiol addition (Figure 1 a). With this unique reaction sequence of two subsequent chemoselective transformations, we developed a modular method that simplifies the attachment of functional molecules to proteins and antibodies with superior stability.

At the outset of our studies, we validated our proposed concept by reacting readily available diethyl ethynylphosphonite with different azides containing various functional groups. In comparison to other P^{III} species such as phosphites, auto-oxidation of phosphonites is more rapid.[21] This issue was previously addressed by isolating air-stable borane protected phosphonites that had to be deprotected with strong bases prior SPhR.[19,20] Now, we developed a one-pot synthesis starting from commercially available diethyl chlorophosphite and ethynylmagnesium bromide followed by azide addition and hydrolysis without isolation of the phosphonite intermediate (Figure 1 b. We observed that polar aprotic solvents generally worked best for the SPhR as they gave the best yields and ensured solubility of all tested azides. The desired ethynylphosphonamidates **1**–**6** were isolated in good overall yields, with a better performance in the formation of N-phenylphosphonamidates compared to the alkyl derivative **6**. Nucleophilic functional groups such as amines, alcohols, carboxylic acids, and electrophilic NHS esters were well tolerated. Even unprotected azide-containing peptides, including cyclic RGD and cyclic cell-penetrating peptides (cCPPs) could be converted into the desired ethynylphosphonamidates **7**–**9** in very good yields of isolated product, with HPLC analysis verifying the formation of a single reaction product.

The purified ethynylphosphonamidates showed excellent stability in solution at neutral pH over several days (Figure S1 in the Supporting Information) and could be stored at 4 °C for several months without any observable decomposition. Furthermore, we were able to demonstrate that compounds **3** and **4** can be further used as modular building blocks to attach ethynylphosphonamidates to other functional modules in high yields, as exemplified by the synthesis of phosphonami-

date derivatives of the fluorescent dyes EDANS (**10**) and Cy5 (**11**) in 70 % and 94 % yield of isolated product, respectively (Figure 1 c).

Previously, Gao et al. observed that vinylphosphonamidates do not undergo thiol addition under their tested conditions.[22] Since we envisioned ethynylphosphonamidates to be more reactive, we carried out model reactions with the *N*-phenyl derivative **1** and glutathione under varying pH conditions and monitored the progress by UPLC-UV. It was observed that the conversion rate increases from pH 7.4 to 9.0 with only a slight increase from pH 8.5 to 9.0 (Figure S2 in the Supporting Information). Considering decreased protein stability at higher pH, we decided to continue our studies at pH 8.5. Full conversion to the desired thiol adduct was observed at pH 8.5 after 30 minutes at a concentration of 10 mM *N*-phenyl derivative **1** (Figure 2 a and Figure S2 in the Supporting Information). The second-order rate constant for the thiol addition reaction was determined by fluorescence HPLC with the *N*-phenyl-EDANS-phosphonamidate derivative **10** at a concentration of 0.1 mM to $0.62 \pm 0.01\,M^{-1}s^{-1}$ (Figure S3 in the Supporting Information). It should be noted that the thiol adduct is formed with a high *Z* selectivity (> 97 %) in aqueous systems, as studied for the addition of ethanethiol to **1** (Figure S4 in the Supporting Information). Similar observations for the formation of the *Z* isomer have been made for other electron-deficient alkynes earlier.[23] DFT calculations revealed a higher activation barrier for the *E* product and can therefore explain the high *Z* selectivity (Figure S5 in the Supporting Information).

To test the applicability of our reaction to the construction of protein conjugates, we proceeded in a proof-of-principle study with the Her2-addressing IgG monoclonal antibody trastuzumab. For antibody modification, we applied a previously described protocol, which reduces and alkylates interchain disulfide bonds of IgG antibodies.[24] In our studies, we probed the modification of trastuzumab with different electrophilic biotin derivatives, including a maleimide, an iodoacetamide, and the ethynylphopshonamidate **5**. All antibody modifications were carried out at concentrations between 3 and 6 μM. Anti-biotin western-blot analysis revealed labeling of the light and heavy chains with DTT-reduced trastuzumab for all of the tested biotin derivatives when using the reported conditions of 1.1 equiv. of labeling reagent per free Cys.[24] Probably due to slower reaction kinetics ($0.62\,M^{-1}s^{-1}$ for phosphonamidates vs. $734\,M^{-1}s^{-1}$ for maleimides),[25] decreased labelling efficiency was observed for **5** compared to the maleimide derivative (Figure S6 in the Supporting Information). Therefore, we screened various phosphonamidate equivalents and monitored the degree of modification by intact protein MS. Optimal conditions for the phosphonamidate labelling were identified with 10 equiv of phosphonamidate per free Cys, which corresponds to 80 equiv with respect to the antibody (Figure S7 in the Supporting Information). Side reactions of other nucleophilic amino acid residues with common Cys-labeling techniques have been reported earlier[26] and have been shown to be very problematic in certain applications.[27,26b] To confirm the chemoselectivity of the phosphonamidate labeling technique, reactions were carried out without prior reduction of the antibody

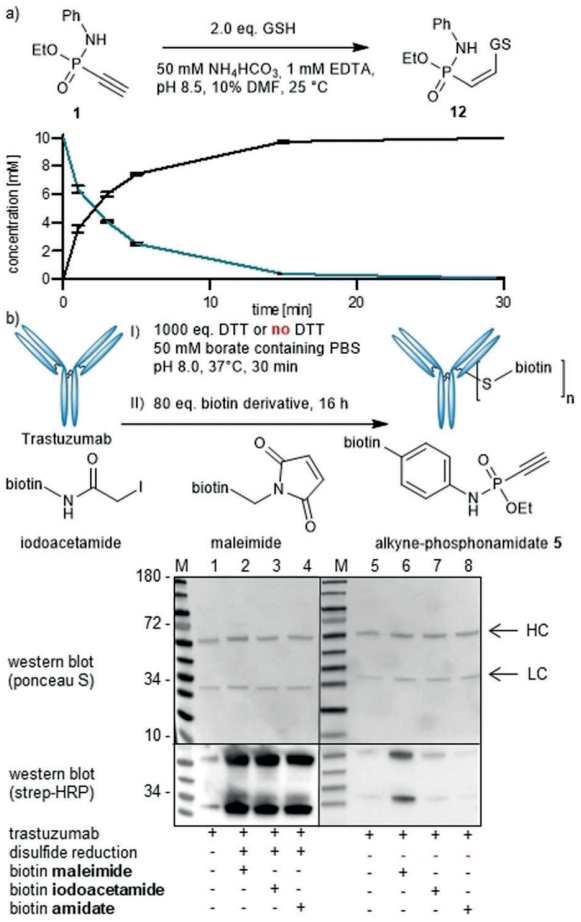

Figure 2. a) Reaction of glutathione (GSH) with phosphonamidate **1**. 10 mM phosphonamidate were reacted with 20 mM GSH at pH 8.5 (NH_4HCO_3-buffer). Concentrations of the starting material **1** (cyan) and product **12** (black) over time are sown as a mean and error from three independent measurements, as monitored by UPLC-UV. b) Trastuzumab modification with three different Cys-reactive biotin derivatives. Reactions were carried out with 80 equiv biotin derivative. Western-blot analysis: Lanes 1 and 5: untreated antibody. Lanes 2–4: prior DTT treatment. Lanes 6–8: Control reactions without prior DTT treatment. HC = Antibody heavy chain, LC = light chain.

disulfide bonds. Compared to other Cys-conjugation techniques at neutral pH, outstanding selectivity for Cys residues was observed for the labeling reaction with 1.1 equiv ethynylphosphonamidate per free cysteine residue at pH 8.5 when carried out without prior reduction of the antibody disulfide bonds (Figure S6 in the Supporting Information). In contrast to a maleimide reagent, even a larger excess of 10 equiv ethynylphosphonamidate per free cysteine did not lead to any unspecific labeling (Figure 2 b). The selectivity was further confirmed by mass spectrometry (LC-MS/MS) after trypsin digestion of the modified antibody. Only interchain-disulfide-forming cysteines were modified after reduction and alkylation with an excess of **1**, and no modification on any amino acid was found without prior reduction (Figure S8 in the Supporting Information). Taken together, the intrinsic Cys selectivity of this reaction allows ethynylphosphonamidates to be employed in bioconjugation reactions even in larger

excess without running into the risk of unselective labeling, which is advantageous when the exact concentration of the protein or antibody probe is difficult to determine.

The linkage stability of the Cys conjugates is crucial for many applications and in particular for drug delivery applications to prevent hazardous off-target effects, especially during circulation in the blood stream.[7] To test the stability of our phosphonamidate–thiol adducts a fluorescence-quenching assay was carried out in which a fluorescent signal was generated upon cleavage of the conjugates (Figure 3a). Quenched probes were synthesized through the addition of a DABCYL-modified peptide to the fluorescent phosphonamidate **10**. The phosphonamidate adducts show a high stability in PBS buffer, HEK cell lysate, and human serum over several days. Since P–N bonds are generally susceptible to hydrolysis under acidic conditions,[28] very harsh conditions

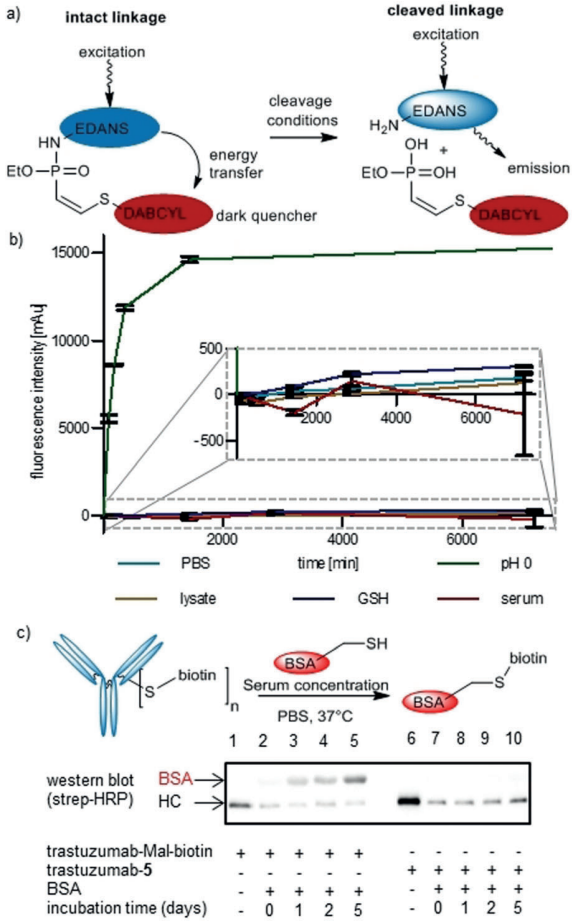

Figure 3. a) Set-up of the fluorescence-quenching assay for stability measurements of the thiol adducts. b) Fluorescence increase was monitored over time. Measurements were performed at least in triplicate. Cyan: PBS, green: pH 0 (1 N HCl), brown: cell-lysate, blue: GSH (1000 equiv of glutathione in PBS), red: human serum. c) Transfer of the antibody modification to serum proteins. Trastuzumab–biotin conjugates were incubated at a concentration of 3 μM with 500 μM BSA in PBS at 37 °C. Lane 1: Untreated maleimide conjugate. Lanes 2–5: BSA-exposed maleimide adduct after 0, 1, 2 and 5 days. Lane 6: Untreated phosphonamidate conjugate. Lanes 7–10: BSA-exposed phosphonamidate adduct after 0, 1, 2 and 5 days.

of pH 0 were applied, which led to to cleave the phosphonamidate adduct within 24 h (Figure 3b). Previously, thiol adducts of electron-deficient alkynes such as propynamides were described as susceptible to exchange with other thiols.[23] However, with the ethynylphosphonamidates, high stability upon exposure to excess thiols was observed, with a superior performance in a direct comparison to a maleimide conjugate (Figure S9 in the Supporting Information). Next, we probed the stability of phosphonamidite- versus maleimide-labelled antibodies under physiologically relevant concentrations of serum proteins. This is of particular importance, since the transfer of maleimide-modified drugs to serum albumin has been described before and poses a serious risk for off-target toxicity when applied to drug delivery.[14,29] Biotin-modified antibodies were exposed to bovine serum albumin (BSA) at 37 °C under physiological conditions and the potential transfer to BSA was monitored by western blotting (Figure 3c and Figure S10 in the Supporting Information). After several days of incubation, a significant transfer of the biotin to BSA was observed for the maleimide linkage whereas the phosphonamidate linkage was stable under the tested conditions. Taken together with the previously described stability experiments with quenched fluorescent probes, these results clearly point to excellent stability of the phosphonamidate conjugates, especially when compared to conventional maleimide-linked conjugates.

Encouraged by the outstanding thiol selectivity and the high stability of the Cys–phosphonamidate adducts, we proceeded with the functional evaluation of phosphonamidite-based antibody conjugates. We modified trastuzumab, an anti-Her2 antibody, with the fluorescent Cy5 phosphonamidate **11** to generate an antibody–fluorophore conjugate (AFC). Trastuzumab modification was carried out by using the above-mentioned reduction and alkylation of the interchain disulfide bonds (Figure 4a). Successful modification was confirmed by in-gel fluorescence measurements of the antibody heavy and light chains (Figure S11 in the Supporting Information). Immunostaining experiments with the AFC constructs show excellent target selectivity for the Her2-receptor on the outer cell membrane (Figure 4b). This experiment clearly shows that our modification strategy does not affect the antibody's performance and provides a simple conjugation approach for diagnostic reagents.

Finally, we applied our strategy to the attachment of cCPPs to eGFP for functional protein delivery into living cells, in a manner similar to that previously described.[30] An eGFP mutant with a single addressable cysteine was obtained by consecutive point mutation of Cys 70 to Met and Ser 147 to Cys, and the mutant protein was almost quantitatively modified with 20 equiv of the phosphonamidate cTAT or cR_{10} peptides **8** and **9** after reaction for three hours at 37 °C in PBS at a protein concentration of 100 μM (Figure 4c,d). With the eGFP–cCPP conjugates in hand, we performed cellular uptake studies monitored by live-cell microscopy in HeLa cells. Unconjugated eGFP was not taken up, whereas a green fluorescence signal was detected in the cytosol and the nucleoli for both eGFP–cCPP conjugates following incubation with 50 μM of the constructs, which is in accordance with previous observations using CuAAC conjugation for the

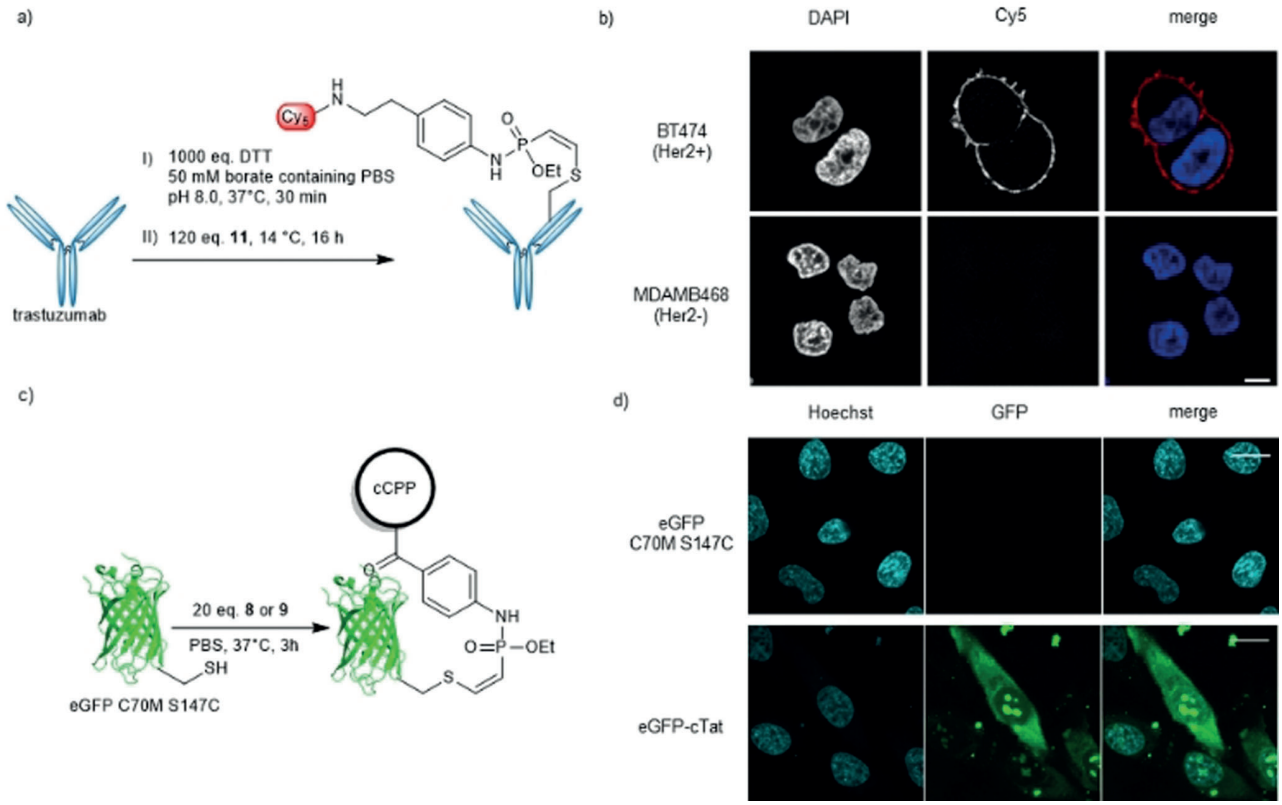

Figure 4. a) Synthetic scheme for phosphonamidate attachment of the Cy5 fluorophore to trastuzumab (anti-Her2 antibody) to generate an AFC. b) Immunostaining of fixed cells either over-expressing the cell-surface receptor Her2 (BT474) or exhibiting low Her2 expression levels (MDAMB468). The merged images show the signal from the DNA stain DAPI in blue and the Cy5 signal in red. Scale bar: 10 μm. c) Synthetic scheme for the attachment of phosphonamidite-modified cCPPs **8** and **9** to a eGFP mutant with a single addressable cysteine. d) Fluorescence imaging of HeLa cells after incubation with eGFP alone and eGFP–cTat at 50 μM. Images show the GFP channel in green and the Hoechst 33342 nuclear stain in blue. Scale bar: 20 μm. For further information see the Supporting Information.

attachment of cTAT (Figure 4e).[30a] With these results, we demonstrated that our method enables the straightforward synthesis of functional protein–cCPP conjugates for intracellular protein delivery.

In summary, we present a unique reaction sequence that first incorporates a thiol-reactive ethynylphosphonamidate into a given molecule through an initial chemoselective SPhR and subsequently modifies Cys residues smoothly in aqueous systems with outstanding selectivity towards sulfhydryl groups. This approach enables the facile conjugation of complex molecules to proteins, as exemplified by the conjugation of biotin, fluorophores, and peptides to antibodies and proteins. In contrast to the widespread maleimide labeling, our thiol adducts showed excellent stability to thiol exchange with GSH and albumin in the presence of human serum and cell lysate. The applicability of our method was demonstrated by the synthesis of a functional AFC for selective staining of antigen-presenting cells and eGFP–CPP conjugates for efficient protein delivery into cells. This method combines facile synthetic access with high flexibility, chemoselectivity, and superior linkage stability and is therefore a powerful and versatile tool for selective protein conjugation.

Acknowledgements

We thank K. K. Hassanin for excellent technical assistance, B. Keller for discussion on the computational modelling and P. Schmieder for helpful discussions on NMR-spectra. This work was supported by grants from the Deutsche Forschungsgemeinschaft (SPP1623) to C.P.R.H. (HA 4468/9-1) and H.L. (LE 721/13-2), (RTG1721) to H.L., the Einstein Foundation Berlin (Leibniz-Humboldt Professorship), the Boehringer-Ingelheim Foundation (Plus 3 award) and the Fonds der Chemischen Industrie to C.P.R.H. A.S. was trained and supported by the graduate school GRK1721 of the Deutsche Forschungsgemeinschaft (DFG).

Conflict of interest

The technology described in the manuscript is part of a pending patent application by M.-A.K., M.G., T.S., D.S., J.H., A.S, H.L and C.P.R.H.

Keywords: bioconjugation · bioorganic chemistry · bioorthogonal chemistry · cysteine-selective modification · protein modification

[1] a) R. D. Row, J. A. Prescher, *Acc. Chem. Res.* **2018**, *51*, 1073 – 1081; b) N. Krall, F. P. da Cruz, O. Boutureira, G. J. L. Bernardes, *Nat. Chem.* **2016**, *8*, 103; c) E. M. Sletten, C. R. Bertozzi, *Angew. Chem. Int. Ed.* **2009**, *48*, 6974 – 6998; *Angew. Chem.* **2009**, *121*, 7108 – 7133.

[2] C. D. Spicer, B. G. Davis, *Nat. Commun.* **2014**, *5*, 4740.

[3] a) K. Lang, J. W. Chin, *Chem. Rev.* **2014**, *114*, 4764 – 4806; b) E. Baslé, N. Joubert, M. Pucheault, *Chem. Biol.* **2010**, *17*, 213 – 227.

[4] H. Ban, J. Gavrilyuk, C. F. Barbas, *J. Am. Chem. Soc.* **2010**, *132*, 1523 – 1525.

[5] J. M. Antos, M. B. Francis, *J. Am. Chem. Soc.* **2004**, *126*, 10256 – 10257.

[6] S. Lin, X. Yang, S. Jia, A. M. Weeks, M. Hornsby, P. S. Lee, R. V. Nichiporuk, A. T. Iavarone, J. A. Wells, F. D. Toste, C. J. Chang, *Science* **2017**, *355*, 597 – 602.

[7] S. B. Gunnoo, A. Madder, *ChemBioChem* **2016**, *17*, 529 – 553.

[8] J. M. Chalker, G. J. L. Bernardes, Y. A. Lin, B. G. Davis, *Chem. Asian J.* **2009**, *4*, 630 – 640.

[9] E. V. Vinogradova, C. Zhang, A. M. Spokoyny, B. L. Pentelute, S. L. Buchwald, *Nature* **2015**, *526*, 687.

[10] C. E. Hoyle, C. N. Bowman, *Angew. Chem. Int. Ed.* **2010**, *49*, 1540 – 1573; *Angew. Chem.* **2010**, *122*, 1584 – 1617.

[11] J. E. Moore, W. H. Ward, *J. Am. Chem. Soc.* **1956**, *78*, 2414 – 2418.

[12] C. Zhang, M. Welborn, T. Zhu, N. J. Yang, M. S. Santos, T. Van Voorhis, B. L. Pentelute, *Nat. Chem.* **2016**, *8*, 120.

[13] L.-T. T. Nguyen, M. T. Gokmen, F. E. Du Prez, *Polym. Chem.* **2013**, *4*, 5527 – 5536.

[14] B.-Q. Shen, K. Xu, L. Liu, H. Raab, S. Bhakta, M. Kenrick, K. L. Parsons-Reponte, J. Tien, S.-F. Yu, E. Mai, D. Li, J. Tibbitts, J. Baudys, O. M. Saad, S. J. Scales, P. J. McDonald, P. E. Hass, C. Eigenbrot, T. Nguyen, W. A. Solis, R. N. Fuji, K. M. Flagella, D. Patel, S. D. Spencer, L. A. Khawli, A. Ebens, W. L. Wong, R. Vandlen, S. Kaur, M. X. Sliwkowski, R. H. Scheller, P. Polakis, J. R. Junutula, *Nat. Biotechnol.* **2012**, *30*, 184 – 189.

[15] P. A. Szijj, C. Bahou, V. Chudasama, *Drug Discovery Today* **2018**, *30*, 27 – 34.

[16] B. Bernardim, P. M. S. D. Cal, M. J. Matos, B. L. Oliveira, N. Martínez-Sáez, I. S. Albuquerque, E. Perkins, F. Corzana, A. C. B. Burtoloso, G. Jiménez-Osés, G. J. L. Bernardes, *Nat. Commun.* **2016**, *7*, 13128.

[17] D. Kalia, P. V. Malekar, M. Parthasarathy, *Angew. Chem. Int. Ed.* **2016**, *55*, 1432 – 1435; *Angew. Chem.* **2016**, *128*, 1454 – 1457.

[18] O. Koniev, A. Wagner, *Chem. Soc. Rev.* **2015**, *44*, 5495 – 5551.

[19] M. R. J. Vallée, P. Majkut, I. Wilkening, C. Weise, G. Müller, C. P. R. Hackenberger, *Org. Lett.* **2011**, *13*, 5440 – 5443.

[20] a) M. R. J. Vallée, L. M. Artner, J. Dernedde, C. P. R. Hackenberger, *Angew. Chem. Int. Ed.* **2013**, *52*, 9504 – 9508; *Angew. Chem.* **2013**, *125*, 9682 – 9686; b) M. R. J. Vallée, P. Majkut, D. Krause, M. Gerrits, C. P. R. Hackenberger, *Chem. Eur. J.* **2015**, *21*, 970 – 974.

[21] W.-S. Hwang, J. T. Yoke, *J. Org. Chem.* **1980**, *45*, 2088 – 2091.

[22] F. Gao, X. Yan, K. Auclair, *Chem. Eur. J.* **2009**, *15*, 2064 – 2070.

[23] H.-Y. Shiu, T.-C. Chan, C.-M. Ho, Y. Liu, M.-K. Wong, C.-M. Che, *Chem. Eur. J.* **2009**, *15*, 3839 – 3850.

[24] S. O. Doronina, B. E. Toki, M. Y. Torgov, B. A. Mendelsohn, C. G. Cerveny, D. F. Chace, R. L. DeBlanc, R. P. Gearing, T. D. Bovee, C. B. Siegall, J. A. Francisco, A. F. Wahl, D. L. Meyer, P. D. Senter, *Nat. Biotechnol.* **2003**, *21*, 778 – 784.

[25] F. Saito, H. Noda, J. W. Bode, *ACS Chem. Biol.* **2015**, *10*, 1026 – 1033.

[26] a) C. F. Brewer, J. P. Riehm, *Anal. Biochem.* **1967**, *18*, 248 – 255; b) M. L. Nielsen, M. Vermeulen, T. Bonaldi, J. Cox, L. Moroder, M. Mann, *Nat. Methods* **2008**, *5*, 459 – 460.

[27] J. Václavík, R. Zschoche, I. Klimánková, V. Matoušek, P. Beier, D. Hilvert, A. Togni, *Chem. Eur. J.* **2017**, *23*, 6490 – 6494.

[28] J. Bertran-Vicente, R. A. Serwa, M. Schümann, P. Schmieder, E. Krause, C. P. R. Hackenberger, *J. Am. Chem. Soc.* **2014**, *136*, 13622 – 13628.

[29] J. F. Ponte, X. Sun, N. C. Yoder, N. Fishkin, R. Laleau, J. Coccia, L. Lanieri, M. Bogalhas, L. Wang, S. Wilhelm, W. Widdison, J. Pinkas, T. A. Keating, R. Chari, H. K. Erickson, J. M. Lambert, *Bioconjugate Chem.* **2016**, *27*, 1588 – 1598.

[30] a) N. Nischan, H. D. Herce, F. Natale, N. Bohlke, N. Budisa, M. C. Cardoso, C. P. R. Hackenberger, *Angew. Chem. Int. Ed.* **2015**, *54*, 1950 – 1953; *Angew. Chem.* **2015**, *127*, 1972 – 1976; b) H. D. Herce, D. Schumacher, A. F. L. Schneider, A. K. Ludwig, F. A. Mann, M. Fillies, M.-A. Kasper, S. Reinke, E. Krause, H. Leonhardt, M. C. Cardoso, C. P. R. Hackenberger, *Nat. Chem.* **2017**, *9*, 762 – 771.

Manuscript received: December 29, 2018
Accepted manuscript online: March 4, 2019
Version of record online: ■■ ■■, ■■■■

Communications

Protein Modification

M.-A. Kasper, M. Glanz, A. Stengl, M. Penkert, S. Klenk, T. Sauer, D. Schumacher, J. Helma, E. Krause, M. C. Cardoso, H. Leonhardt, C. P. R. Hackenberger* ____ ▮▮▮▮–▮▮▮▮

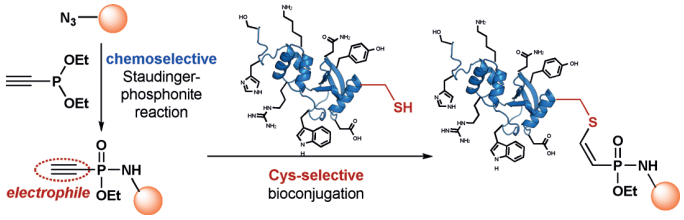

Cysteine-Selective Phosphonamidate Electrophiles for Modular Protein Bioconjugations

Staudinger—Ready—Go! Ethynylphosphonamidates can be chemoselectively incorporated into a given molecule through a Staudinger-phosphonite reaction, and they react specifically with cysteine residues on proteins to give thiol adducts that are stable under physiological conditions. This enables the facile fusion of complex molecules to proteins.

Communications

Protein Modification

M.-A. Kasper, M. Glanz, A. Stengl, M. Penkert, S. Klenk, T. Sauer, D. Schumacher, J. Helma, E. Krause, M. C. Cardoso, H. Leonhardt, C. P. R. Hackenberger* ____ ▮▮▮▮–▮▮▮▮

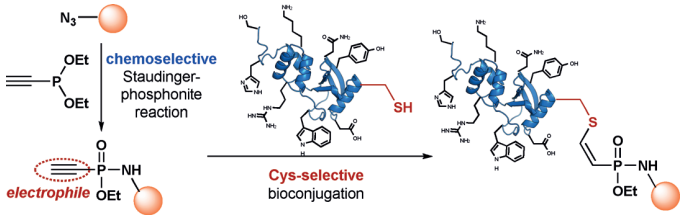

Cysteine-Selective Phosphonamidate Electrophiles for Modular Protein Bioconjugations

Staudinger—Ready—Go! Ethynylphosphonamidates can be chemoselectively incorporated into a given molecule through a Staudinger-phosphonite reaction, and they react specifically with cysteine residues on proteins to give thiol adducts that are stable under physiological conditions. This enables the facile fusion of complex molecules to proteins.

Angewandte Chemie
Eine Zeitschrift der Gesellschaft Deutscher Chemiker

Supporting Information

Cysteine-Selective Phosphonamidate Electrophiles for Modular Protein Bioconjugations

*Marc-André Kasper, Maria Glanz, Andreas Stengl, Martin Penkert, Simon Klenk, Tom Sauer, Dominik Schumacher, Jonas Helma, Eberhard Krause, M. Cristina Cardoso, Heinrich Leonhardt, and Christian P. R. Hackenberger**

anie_201814715_sm_miscellaneous_information.pdf

Table of contents

1. Supplementary Figures

1.1. Figure S1

pH-dependent stability of ethynylphosphonamidate **8** (0.3 mM). Stability was monitored by UPLC-UV by integration of the UV peaks in relation to an internal standard (tryptophan, 0.15 mM) over several days. Shown are mean and error of three independent measurements (n=3). Conditions: pH 1.0: 0.1 M HCl; pH 2.0: TFA in H_2O; pH 7.4: PBS; pH 9.0: 100 mM NH_4HCO_3, pH 12: 0.01 M NaOH.

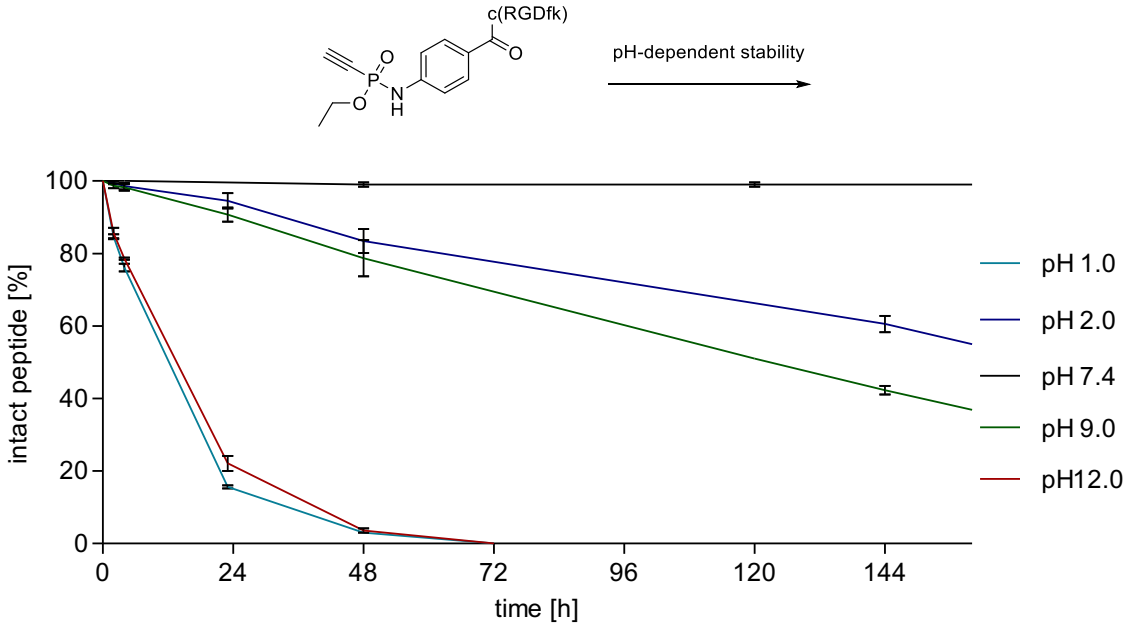

1.2. Figure S2

Glutathione addition to phosphonamidates. A) Concentration of starting material Ethyl-*N*-phenyl-*P*-ethynylphosphonamidate (**1**) under varying pH conditions over time monitored by UPLC/MS (pH 8.0, 8.5 and 9.0: 50mM NH_4HCO_3, 1mM EDTA; pH 7.4: Dulbecco's PBS, 1mM EDTA). Values were calculated by integration of the peaks in relation to an internal standard (inosin). Sample were drawn from the reaction mixture and immediately diluted into 50 mM NaOAc buffer at pH 3.5 to stop the reaction and subjected to UPLC analysis. Peaks were assigned by MS. Shown are mean and error of three independent measurements (n=3). B) Exemplaric UPLC/UV trace (254 nm) of the addition reaction at pH 8.5 after 0, 1, 5 and 30 min. Extinction of the starting material is lower than extinction of the glutathione adduct at 254 nm. C) Concentration of starting material **1** (black) and glutathione adduct (red) over time. Reaction performed at pH 8.5. Shown are mean and error of three independent measurements (n=3).

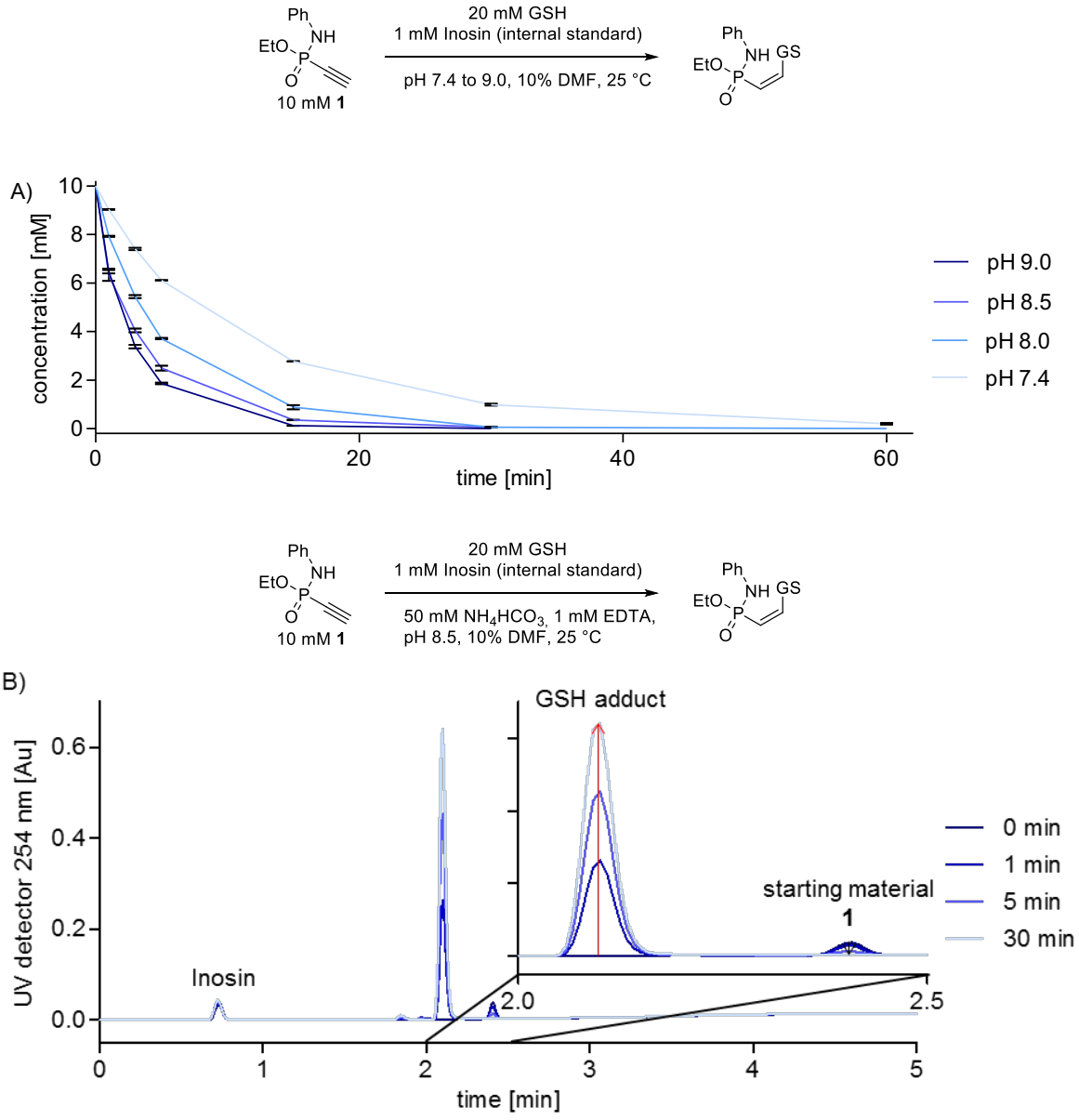

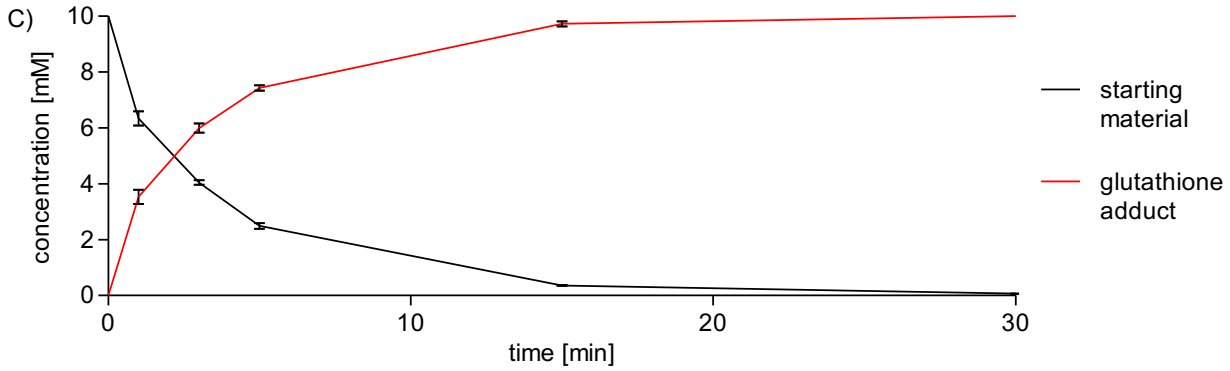

1.3. Figure S3

Determination of the second-order rate constant of the reaction between glutathione and EDANS phosphonamidate **11**. A) Reaction conditions. Reactions were performed in a volume of 0.5 ml. The first sample (t=0) was drawn before the addition of glutathione. Samples were taken after 15, 30, 60, 120, 240 and 480 min. Samples were drawn in a volume of 20 µl and immediately diluted into 80 µl of 50 mM NaOAc buffer at pH 3.5 to stop the reaction. Those samples were subjected to fluorescent HPLC analyses, injecting 20 µl each. B) Mathematic consideration for the determination of a second order rate constant with equal concentrations of the two reactants. C) Concentration of starting material over time. Calculated by integration of the peaks in relation to the internal standard (EDANS). Shown are mean and error of three independent measurements. (n=3) D) Graph: 1/c over time and

linear plot. Slope is the second order rate constant. Shown are mean and error of three independent measurements.

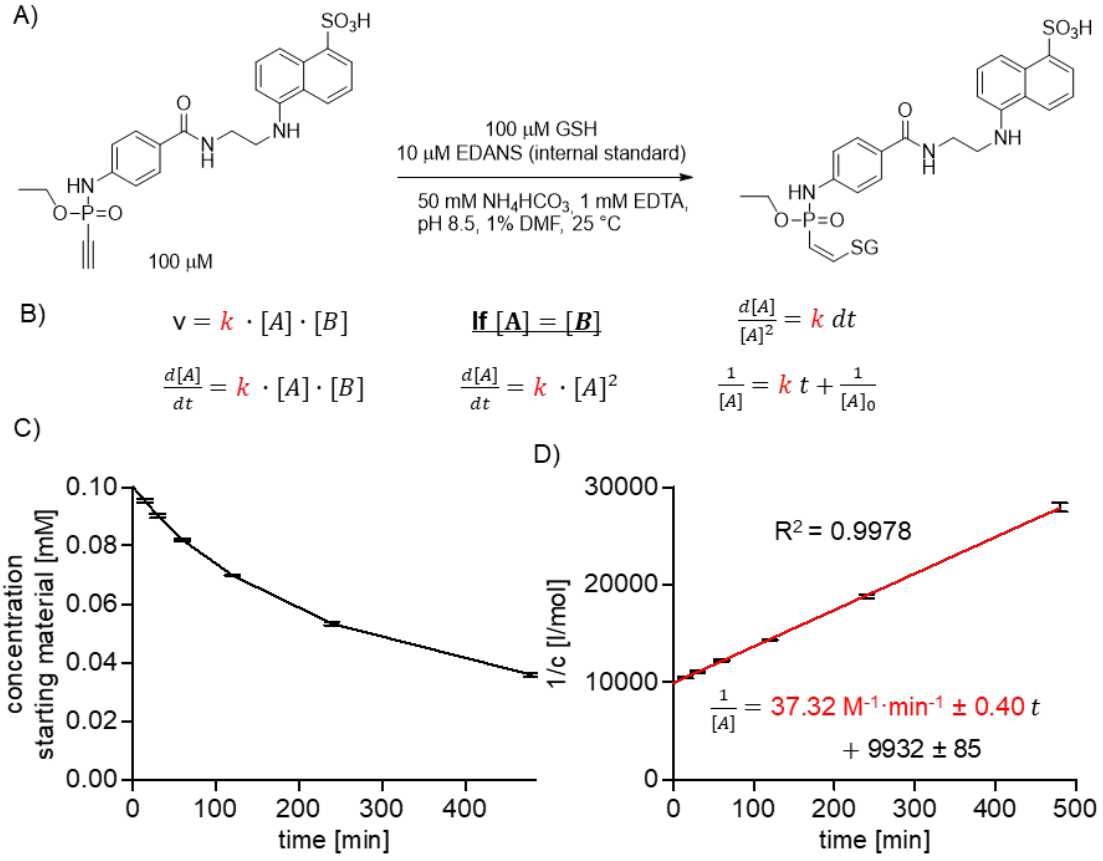

1.4. Figure S4

E/*Z*-selectivity of the thiol addition in dependence of the solvent system and different bases. a) Values measured by ^{31}P-NMR-signal integration of the crude reaction mixtures. b) ^{31}P peaks were assigned by comparison to spectra of isolated *E*- and *Z*-products (See chapter 4.18, 4.19 and 5 for synthesis details and NMR-spectra). The *E*-Product was synthesized via radical mediated thiol addition. Here, we measured almost identical *H*-*H* and *H*-*P*-coupling constants in comparison to a previously described *E*-thiol adduct of a phosphonate.[1] For the *Z*-product that was synthesized via base mediated thiol addition on the other hand, a lower $^{3}J_{HH}$ and a much higher $^{3}J_{PH}$ coupling constant was measured.

a)

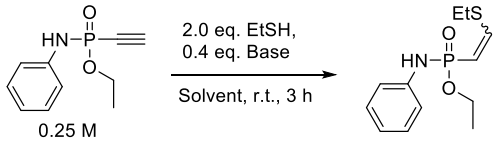

Entry	Base	DMSO E/Z	DMF/H_2O (1:1) E/Z
1	$MeNH_2$	5:95	3:97
2	Li_2CO_3	3:97	2:98
3	Na_2CO_3	6:94	1:99
4	K_2CO_3	12:88	2:98
5	Cs_2CO_3	17:83	2:98

b)

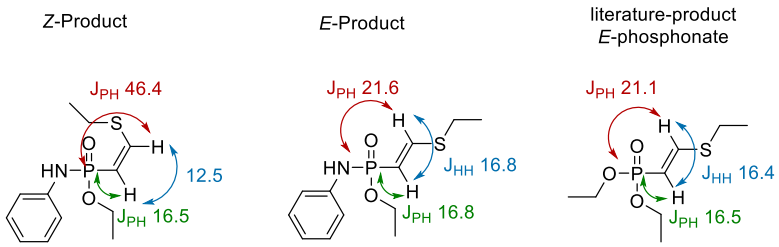

1.5. Figure S5

Computed *E* (red) and *Z* (blue) reaction paths for the addition of sodium methylthiolate to methylphosphonamidate. Calculations were performed with *O*-methyl substituted phosphonamidates and methyl thiol to simplify the calculations. The *E* addition pathway exhibits a 6.9 kcal/mol higher activation barrier than the *Z* pathway. (See chapter 6 for details)

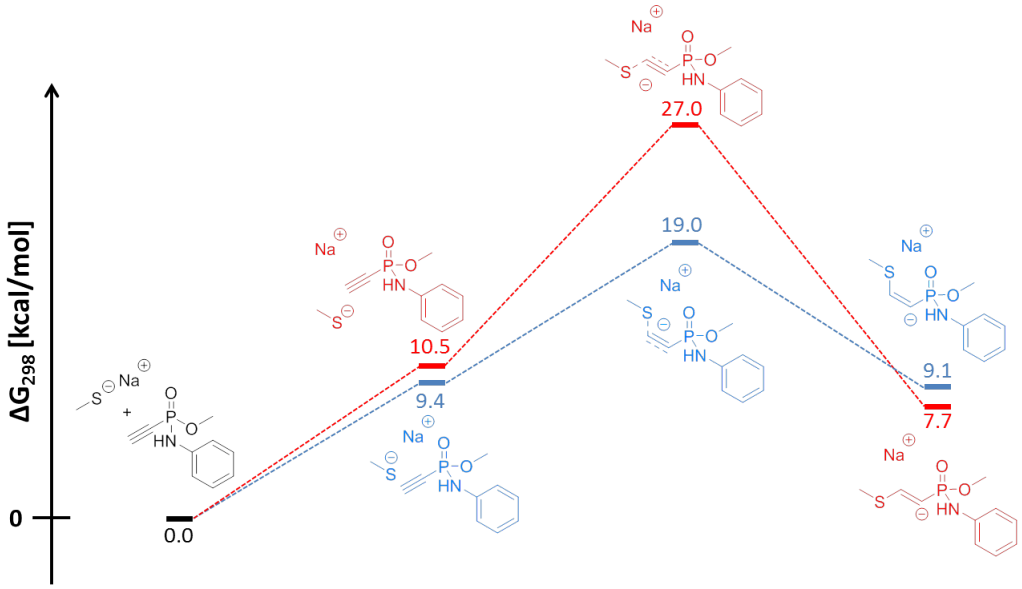

1.6. Figure S6

Trastuzumab modification with three different Cys-reactive biotin derivatives, applying the general procedure described in 3.2. Disulfide reduction was carried out with 1000 eq. DTT in 50 mM borate containing PBS for 30 min at 37°C. Excess DTT was removed with Zeba™ Spin Desalting Columns. Labelling was conducted with 8.8 eq. biotin derivative with a final DMSO content of 1% in a Buffer containing 50 mM NH_4HCO_3 and 1mM EDTA, pH 8.5 at 14°C for the phosphonamidate and PBS containing 1mM EDTA, pH 7.4 at 4°C for the maleimide and iodoacetamide labelling. Western blot analysis: Lane 1: untreated antibody. Lane 2-4: prior DTT treatment. Lane 5-7: Control reactions without prior DTT treatment. See chapter 3.1 for trastuzumab expression details)

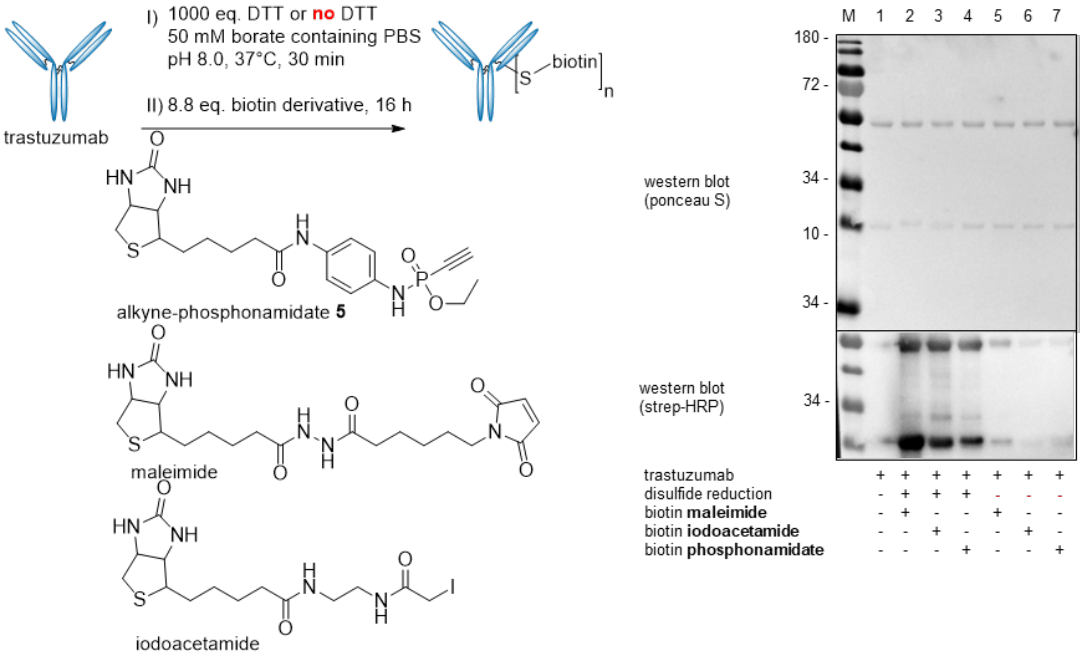

1.7. Figure S7

Influence of the phosphonamidate equivalents on the degree of antibody modification. Reactions were carried out, applying the general procedure described in 3.2 with varying equivalents of **5**. The degree of modification was calculated with the MS intensities with intact protein MS (See chapter 2.11) after deglycosylation and reduction (See chapter 3.3). An exemplary spectrum of the reaction with 80 eq. **5** is shown below (left: raw spectrum, right: deconvoluted). It should be noted that the degree of modification does not exceed 1 for the LC and 3 for the HC, clearly underlining the selectivity for inter-chain forming Cys-residues LC: Light Chain; HC: Heavy Chain, mod: modification with **5** (See chapter 3.1 for trastuzumab expression details).

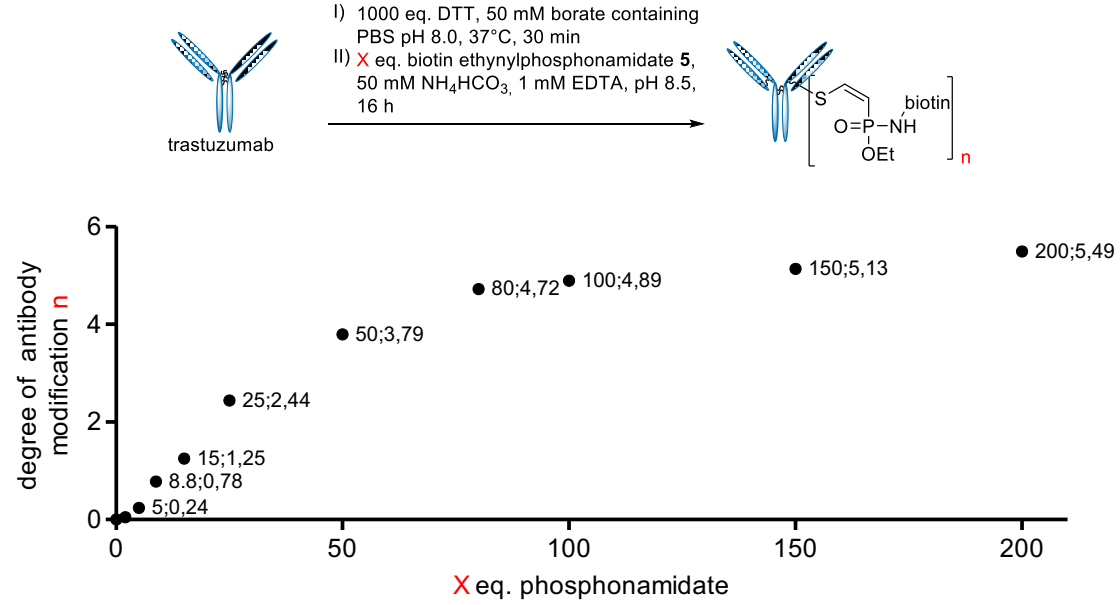

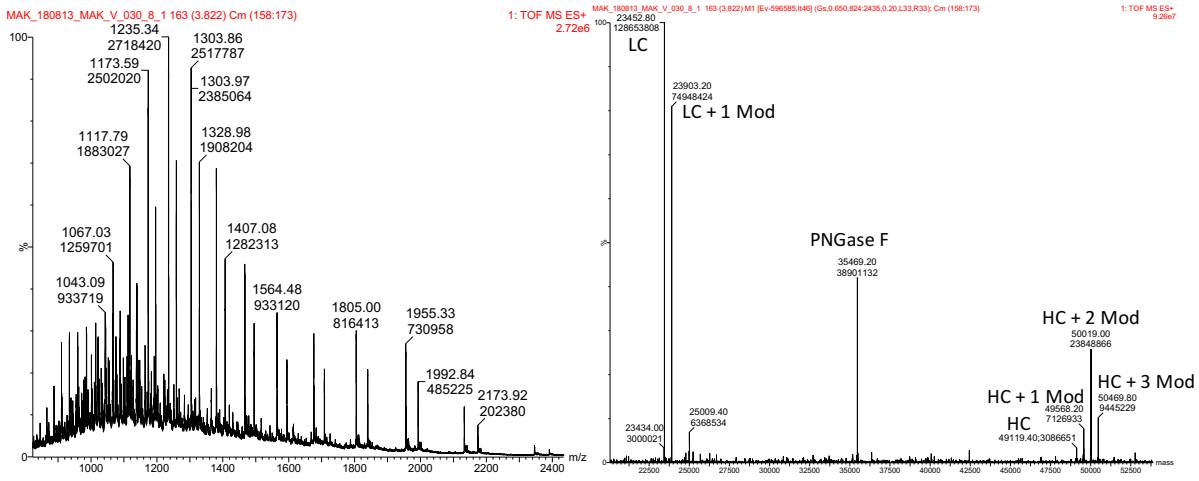

1.8. Figure S8

MS/MS experiments of trastuzumab, modified with Ethyl-*N*-phenyl-*P*-ethynylphosphonamidate (**1**), with and without prior reduction of the antibody as described in general procedure 2. In-gel digest of heavy and light chain separately after reducing SDS/Page as described earlier.[2] Oxidation of methionine, alkylation of cysteine via iodoacetamide and the phosphonamidate on Y, S, T, C, K, H & R were searched as variable modifications. (See chapter 2.9. for MS/MS details).

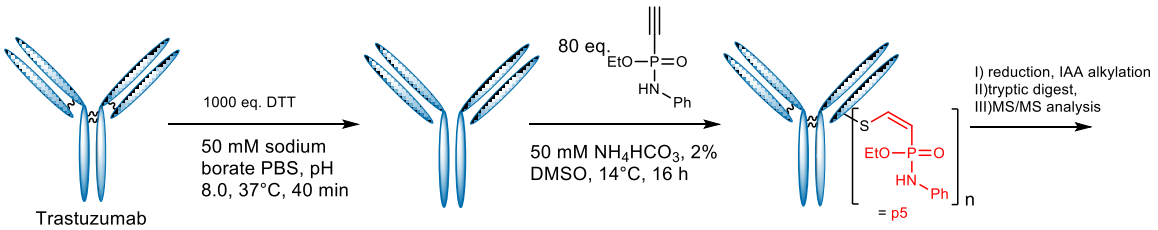

Light Chain: Sequence coverage: 94.39%; MS/MS recorded
Modifications: O: Methionine oxidation; C: Carbamidomethyl; p5: *N*-phenyl-phosphonamidate

O C
DIQMTQSPSSLSASVGDRVTITCRASQDVNTAVAWYQQKPGKAPKLLIYSASFLYSGVPSRFSGSR
C
SGTDFTLTISSLQPEDFATYYCQQHYTTPPTFGQGTKVEIKRTVAAPSVFIFPPSDEQLKSGTASV
C C
VCLLNNFYPREAKVQWKVDNALQSGNSQESVTEQDSKDSTYSLSSTLTLSKADYEKHKVYACEVTH
p5
QGLSSPVTKSFNRGEC

Peptide spectrum match of the modified peptide SFNRGEp5C (HCD MS/MS spectrum):

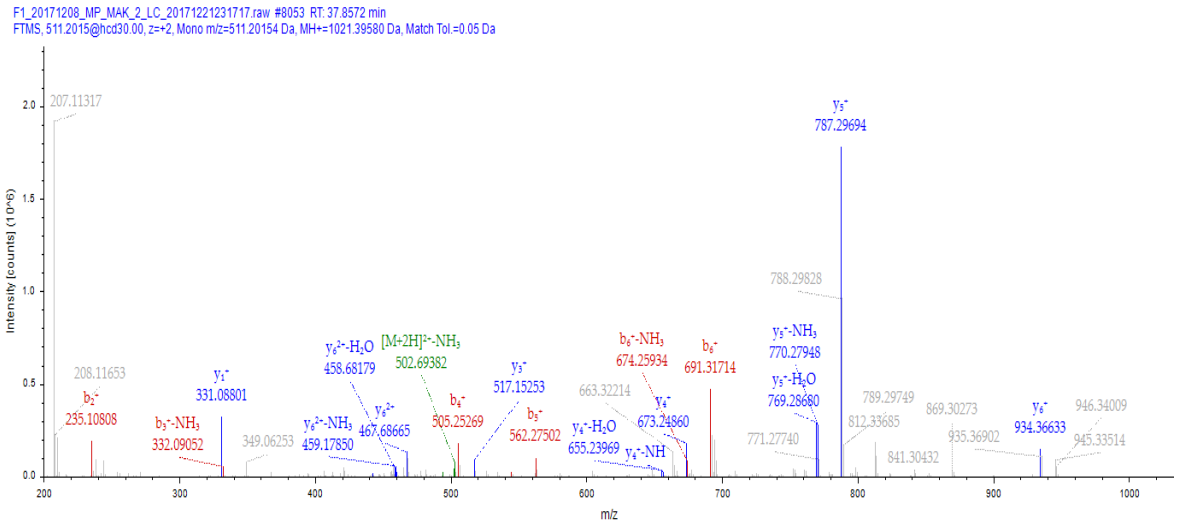

Peptide spectrum match of the modified peptide SFNRGEp5C (EthcD MS/MS spectrum):

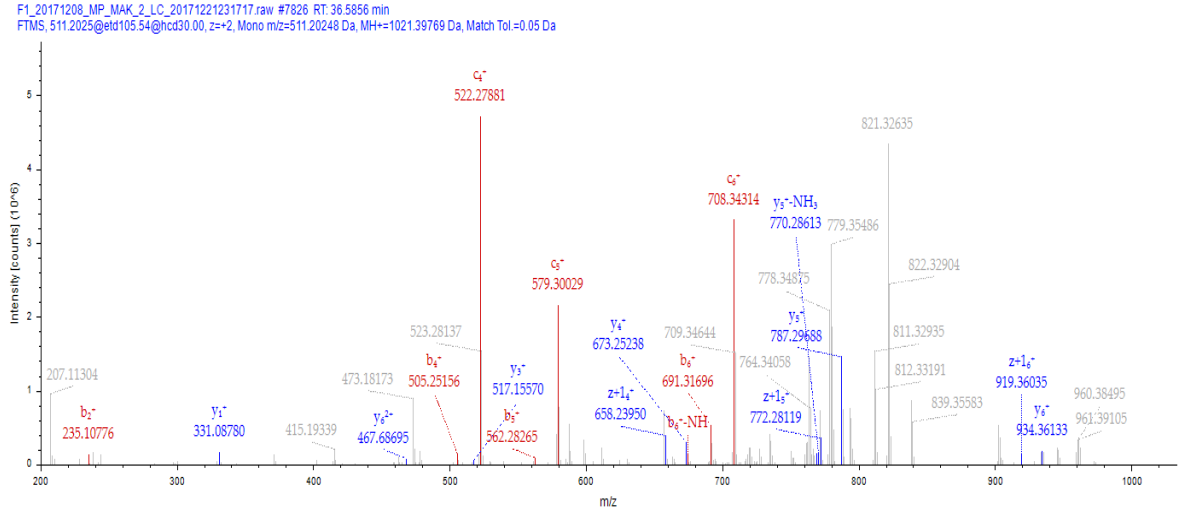

Heavy chain: Sequence coverage: 64.52%; MS/MS recorded

Modifications: O: Methionine oxidation; C: Carbamidomethyl; p5: *N*-phenyl-phosphonamidate

EVQLVESGGGLVQPGGSLRLSCAASGFNIKDTYIHWVRQAPGKGLEWVARIYPTNGYTRYADSVKGRFTISA
DTSKNTAYLQMNSLRAEDTAVYYCSRWGGDGFYAMDYWGQGTLVTVSSASTKGPSVFPLAPSSKSTSGGTAA
LGCLVKDYFPEPVTVSWNSGALTSGVHTFPAVLQSSGLYSLSSVVTVPSSSLGTQTYICNVNHKPSNTKVDK
KVEPPKSCDKTHTCPPCPAPELLGGPSVFLFPPKPKDTLMISRTPEVTCVVVDVSHEDPEVKFNWYVDGVEV
HNAKTKPREEQYNSTYRVVSVLTVLHQDWLNGKEYKCKVSNKALPAPIEKTISKAKGQPREPQVYTLPPSRE
LTKNQVSLTCLVKGFYPSDIAVEWESNGQPENNYKTTPPVLDSDGSFFLYSKLTVDKSRWQQGNVFSCSVMH
EALHNHYTQKSLSLSPGK

Peptide spectrum match of the modified peptide THTp5CPPcamCPAPELLGGPSVFLFPPKPK (EThcD MS/MS spectrum)

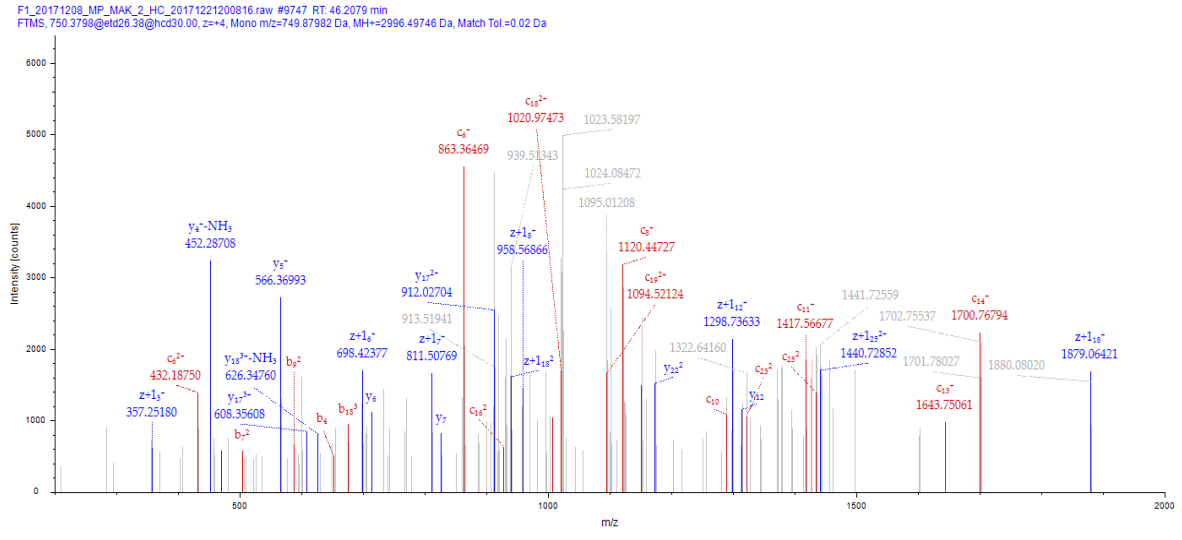

Peptide spectrum match of the modified peptide THTcamCPPp5CPAPELLGGPSVFLFPPKPK (EThcD MS/MS spectrum)

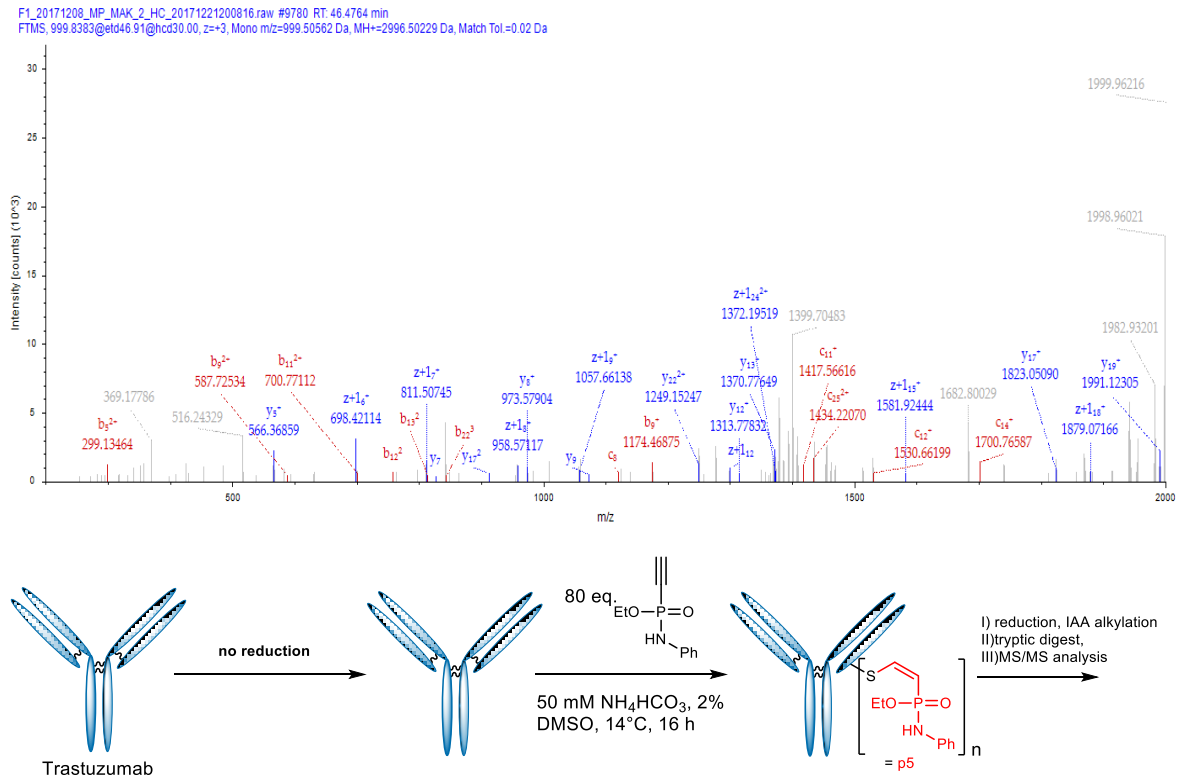

Light Chain: Sequence coverage: 92.06%

Modifications: O: Methionine oxidation; C: Carbamidomethyl; p5: *N*-phenyl-phosphonamidate

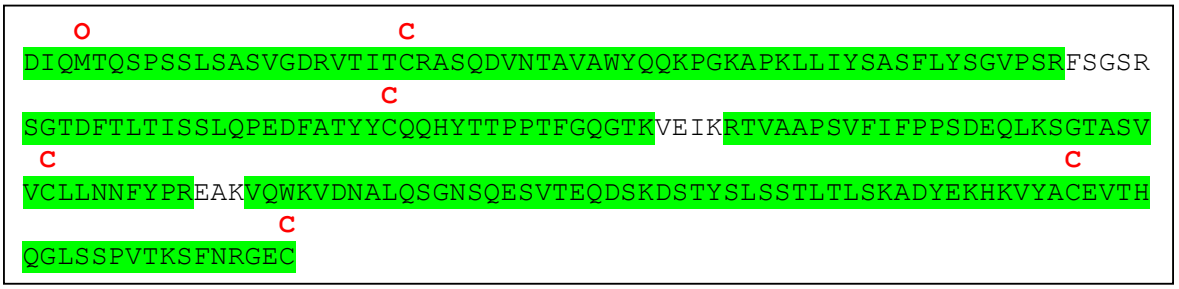

Heavy Chain: Sequence coverage: 64.52%

Modifications: O: Methionine oxidation; C: Carbamidomethyl; p5: *N*-phenyl-phosphonamidate

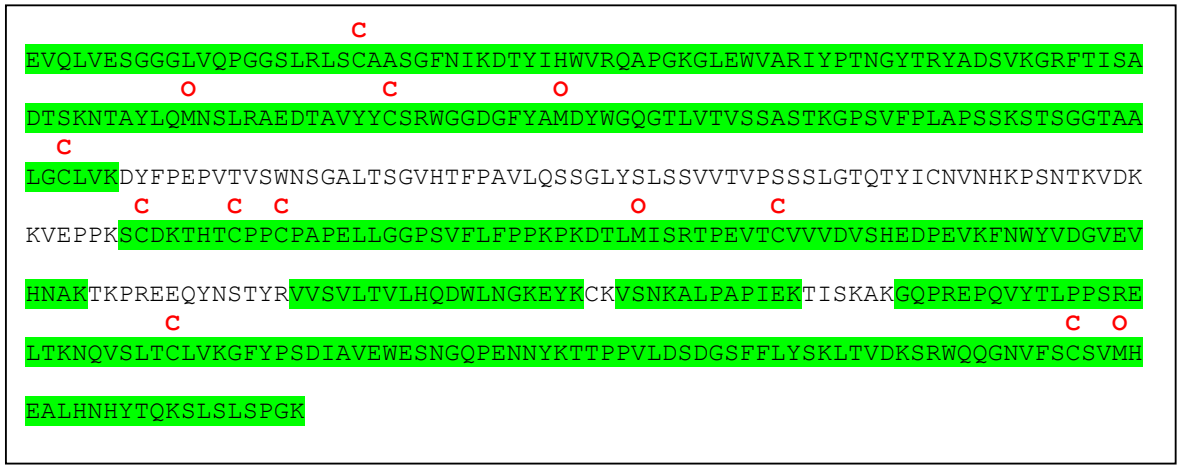

1.9. Figure S9

Fluorophore-quencher based assay to investigate the stability of phosphonamidate-thiol adducts. A: Structure of the phosphonamidate linked dye-quencher conjugate. B: Structure of the maleimide linked dye-quencher conjugate C: Principle of the fluorescence-quencher based readout. Conjugates were incubated at room temperature at a concentration of 10 µM. Measurements were performed at least in triplicates in a 96-well plate (n≥3). Normalization of the graphs by subtraction of the intensity at t=0min for each value. D: Fluorescence measurements for the phosphonamidate linkage (blue) and the maleimide linkage (orange) lysate was freshly prepared from HEK-cells, lysed in PBS. Serum originated from human blood. Glutathione was dissolved in 10 mM in PBS and pH was adjusted to 7.4. (See chapter 3.4 for details)

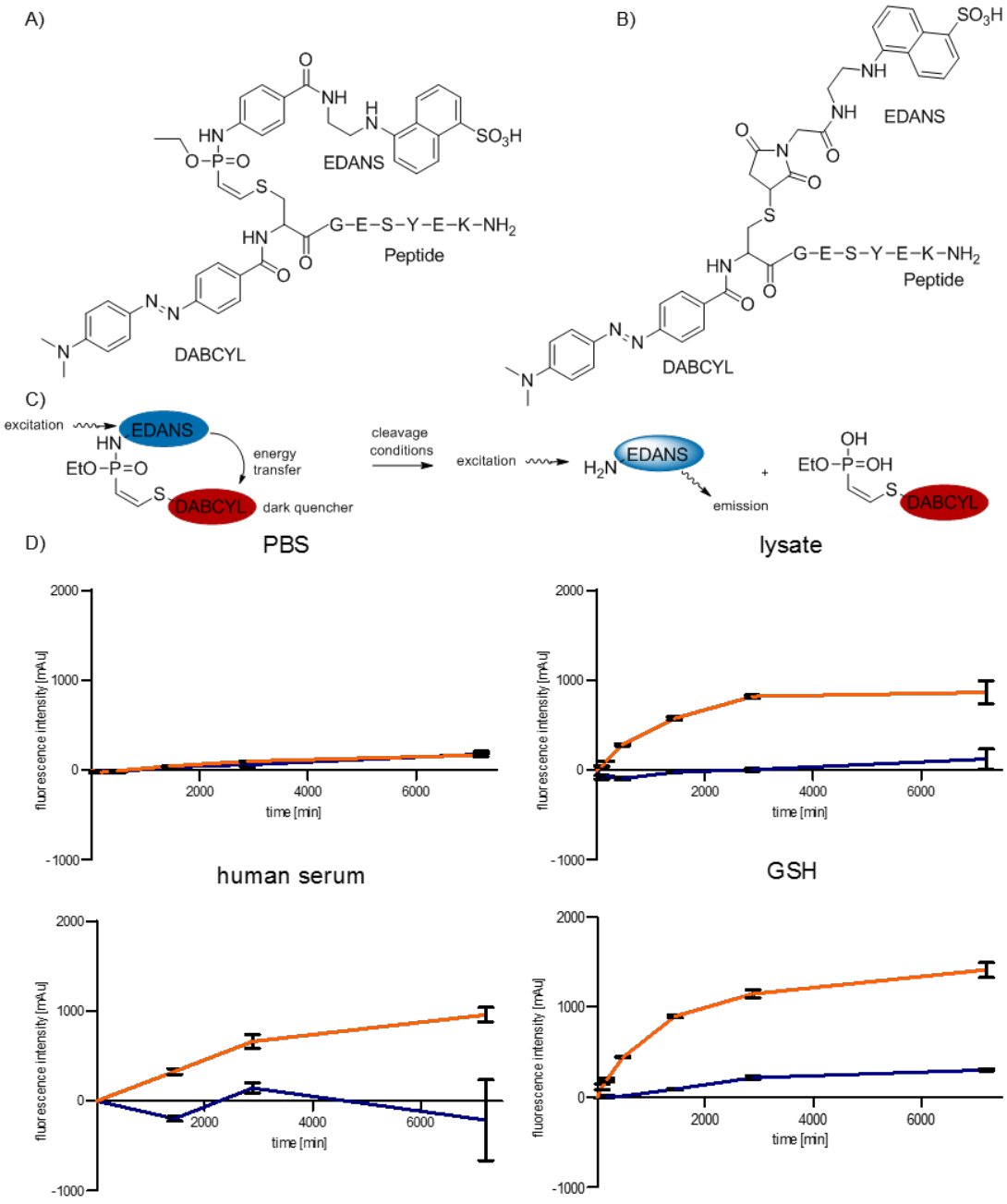

1.10. Figure S10

Stability of trastuzumab-biotin-conjugates towards modification transfer to serum proteins. Conjugates were incubated at a concentration of 3 µM in PBS with a final concentration of 3 µM and 0.5 mM BSA at 37 °C. Samples were drawn after 0, 1, 2 and 5 days, deep frozen in liquid N_2 and finally subjected to SDS/Page and western blot analysis. (See Chapter 3.5 for details)

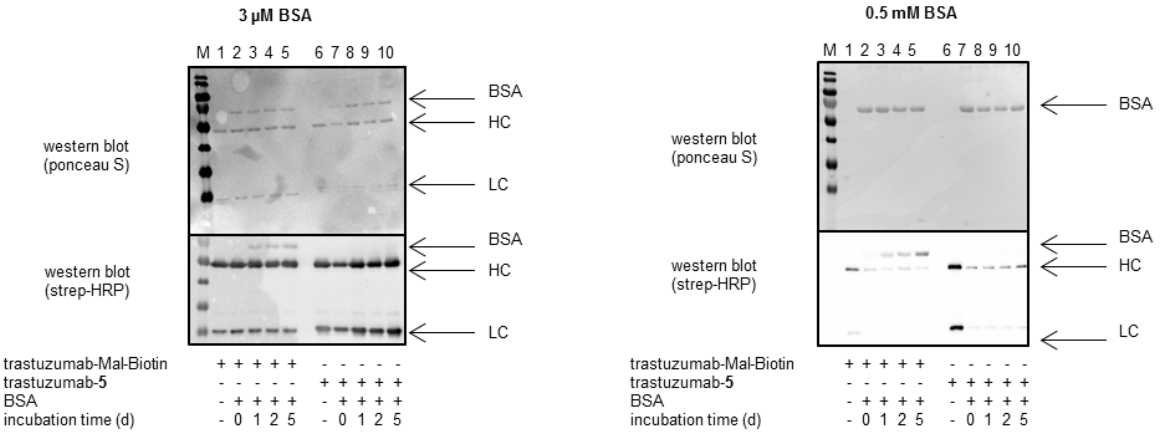

1.11. Figure S11

SDS-Page analysis and fluorescence microscopy of trastuzumab-phosphonamidate-Cy5 conjugates. Depicted are immunostainings of fixed cells over expressing the cell surface receptor Her2 (SKBR3). The antibody-flurophore-conjugate (AFC) Tras-P5-Cy5 shows clear localization to the plasma membrane for Her2+ cell lines. The merged images show the DAPI signal in blue and the Tras-phosphonamidate-Cy5 signal in red. Scale bar represents 10 µM. (See Chapter 3.6 for conjugation and microscopy details)

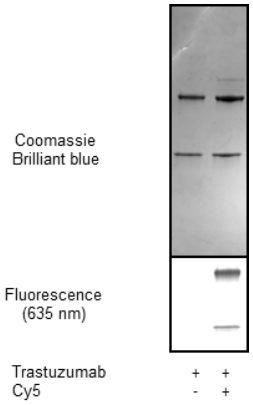

1.12. Figure S12

Fluoresence imaging of HeLa-cells after incubation with eGFP alone and eGFP-cR_{10} at 50 µM. Images show GFP channel in green and Hoechst 33342 in blue. Scale bar represents 20 µm.

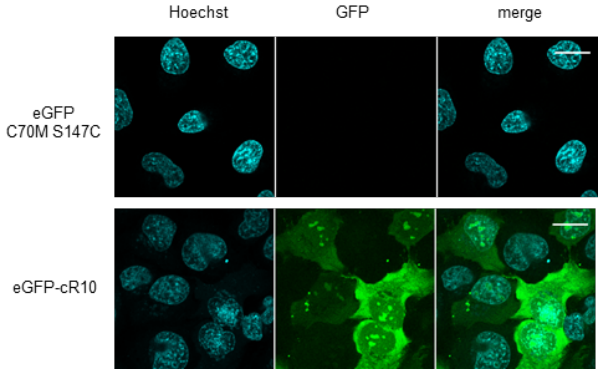

2. General Information

2.1. Chemicals and solvents

Chemicals and solvents were purchased from Merck (Merck group, Germany), TCI (Tokyo chemical industry CO., LTD., Japan) and Acros Organics (Thermo Fisher scientific, USA) and used without further purification. Dry solvents were purchased from Acros Organics (Thermo Fisher scientific, USA).

2.2. Flash- and thin layer chromatography

Flash column chromatography was performed, using NORMASIL 60® silica gel 40-63 µm (VWR international, USA). Glass TLC plates, silica gel 60 W coated with fluorescent indicator F254s were purchased from Merck (Merck Group, Germany). Spots were visualized by fluorescence depletion with a 254 nm lamp or manganese staining (10 g K_2CO_3, 1.5 g $KMnO_4$, 0.1 g NaOH in 200 ml H_2O), followed by heating.

2.3. Preparative HPLC

Preparative HPLC was performed on a Gilson PLC 2020 system (Gilson Inc, WI, Middleton, USA) using a VP 250/32 Macherey-Nagel Nucleodur C18 HTec Spum column (Macherey-Nagel GmbH & Co. Kg, Germany). The following gradients were used: Method C: (A = H_2O + 0.1% TFA (trifluoroacetic acid), B = MeCN (acetonitrile) + 0.1% TFA, flow rate 30 ml/min, 5% B 0-5 min, 5-90% B 5-60 min, 90% B 60-65 min. Method D: 0.1% TFA, flow rate 18 ml/min, 5% B 0-5 min, 5-90% B 5-60 min, 90% B 60-65 min, using a VP 250/21 Macherey-Nagel Nucleodur C18 HTec Spum column (Macherey-Nagel GmbH & Co. Kg, Germany)

2.4. Semi-preparative HPLC

Semi-preparative HPLC was performed on a Shimadzu prominence HPLC system (Shimadzu Corp., Japan) with a CBM20A communication bus module, a FRC-10A fraction collector, 2 pumps LC-20AP, and a SPD-20A UV/VIS detector, using a VP250/21 Macherey-Nagel Nucleodur C18 HTec Spum column (Macherey-Nagel GmbH & Co. Kg, Germany). The following gradients were used: Method E: (A = H2O + 0.1% TFA, B = MeCN + +0.1% TFA), flow rate 10 ml/min, 5% B 0-5 min, 5-99% B 5-65 min, 99% B 65-75 min.

2.5. NMR

NMR spectra were recorded with a Bruker Ultrashield 300 MHz spectrometer and a Bruker Avance III 600 MHz spectrometer (Bruker Corp., USA) at ambient temperature. Chemical shifts δ are reported in ppm relative to residual solvent peak ($CDCl_3$: 7.26 [ppm]; DMSO-d6: 2.50 [ppm]; acetone-d6: 2.05 [ppm]; CD_3CN 1.94 [ppm]; 4.79 D_2O [ppm] for ^{1}H-spectra and $CDCl_3$: 77.16 [ppm]; DMSO-d6: 39.52 [ppm]; acetone-d6: 29.84 [ppm]; CD3CN 1.32 [ppm]; for ^{13}C-spectra . Coupling constants *J* are stated in Hz. Signal multiplicities are abbreviated as follows: s: singlet; d: doublet; t: triplet; q: quartet; m: multiplet.

2.6. UPLC-UV/MS

UPLC-UV/MS traces were recorded on a Waters H-class instrument equipped with a quaternary solvent manager, a Waters autosampler, a Waters TUV detector and a Waters Acquity QDa detector with an Acquity UPLC BEH C18 1.7 µm, 2.1 x 50 mm RP column with a flow rate of 0.6 mL/min (Waters Corp., USA). The following gradient was used: A: 0.1% TFA in H_2O; B: 0.1% TFA in MeCN. 5% B 0 - 0.5 min, 5-95% B 0.5-3 min, 95% B 3-3.9 min, 5% B 3.9-5 min.

2.7. Analytical HPLC

Analytical fluorescence HPLC was conducted on a Shimadzu prominence HPLC system (Shimadzu Corp., Japan) with a CBM-20A communication bus module, a SIL-20A auto sampler, 2 pumps LC-20AT, and a SPD-M20A UV/VIS detector, a CTO-20A column oven and a RF-10AXL fluorescence detector, using an Agilent Eclipse C18 5 µm, 250 x 4.6 mm RR-HPLC column (Agilent Technologies, USA) with a flow rate of 1.0 ml/min. The following gradients were used: (A = H2O + 0.1% TFA, B = MeCN + +0.1% TFA), flow rate 1.0 ml/min, 2% B 0-5 min, 2-45% B 5-35 min, 45-95% B 35-36 min, 95% B 36-40 min, 95 to 2% B 40-41 min, 2% B 41-45 min. Fluorescence spectra with Ex/Em 336/490 were recorded.

2.8. HR-MS

High resolution ESI-MS spectra were recorded on an Agilent 6220 TOF Accurate Mass coupled to an Agilent 1200 LC (Agilent Technologies, USA) and were measured at 35°C between 100- 2000 m/z. The used column was an Accucore RP-MS (30 x 2,1 mm; 2.6 µm particle size) eluted with a flow of 0.8 mL/min and the following gradient (A = water, B = acetonitrile): 95%A + 5%B for 0.2 min, then 95% A + 5% B to 1% A + 99% B until 1.1 min, then 1% A + 99% B until 2.5 min.

2.9. Analytical HPLC-MS/MS

After in-gel digestion peptides were dissolved in water and analyzed by a reversed-phase capillary liquid chromatography system (Dionex Ultimate 3000 NCS-3500RS Nano, Thermo Scientific) connected to an Orbitrap Fusion mass spectrometer (Thermo Fisher Scientific, Germany). LC separations were performed with an in-house packed C18 column for reversed phase separation (column material: Poroshell 120 EC-C18, 2.7 µm (Agilent Technologies, USA) at an eluent flow rate of 300 µL/min using a gradient of 2-40% B in 38 min. Mobile phase A contained 0.1% formic acid in water, and mobile phase B 0.1% formic acid in acetonitrile. FT survey scans were acquired in a range of 350 to 1500 m/z with a resolution of 60000 (FMHM) and an AGC target value of 4e5. Precursor ions with charge states 2-4 were isolated with a mass selecting quadrupole (isolation window m/z 1.6). Precursor ions were fragmented in alternating mode using EThcD and HCD. HCD MS/MS spectra were acquired with 30% NCE. EThcD fragmentation was performed using charge dependent ETD parameters and the supplemental activation (sa) was set to 30%. For both fragmentation types the maximum injection time was set to 500 ms to collect 5e4 precursor ions. Fragment ion spectra were acquired with a resolution of 15000 (FWHM).

MS raw data were processed with Proteome Discoverer 2.2 software (Thermo Fisher Scientific, Germany). The non-fragment filter was applied with following parameters: Precursor ions and charged reduced precursors were removed within a 1 Da window and neutral losses within a 0.5 Da window. MS/MS spectra were search against a database containing trastuzumab heavy and light chain and some common contaminants using Sequest. Precursor mass tolerance and fragment mass tolerance were set to 6 ppm and 0.02 Da, respectively. Oxidation of methionine, alkylation of cysteine via iodoacetamide and the phosphonamidate (Y, S, T, C, K, H & R) were searched as variable modifications. Target Decoy PSM Validator was used to filter peptide spectrum matches (PSMs) with a false-discovery rate (FDR) of 0.05. Peptide spectrum matches displaying modification sites were manually verified.

2.10. Size-exclusion chromatography

Protein purification by size-exclusion chromatography was conducted with an ÄKTA FPLC system (GE Healthcare, United States) equipped with a P-920 pump system, a UPC-900 detector, a FRAC-950 fraction collector and a 5 ml HiTrap® desalting column, with a flow of 1.5 ml/min.

2.11. Intact protein MS

Intact proteins were analyzed using a Waters H-class instrument equipped with a quaternary solvent manager, a Waters sample manager-FTN, a Waters PDA detector and a Waters column manager with an Acquity UPLC protein BEH C4 column (300 Å, 1.7 µm, 2.1 mm x 50 mm). Proteins were eluted at a clomun temperature of 80°C with a flow rate of 0.3 mL/min. The following gradient was used: A: 0.01% FA in H_2O; B: 0.01% FA in MeCN. 5-95% B 0-6 min. Mass analysis was conducted with a Waters XEVO G2-XS QTof analyzer. Proteins were ionized in positive ion mode applying a cone voltage of 40 kV. Raw data was analyzed with MaxEnt 1.

2.12. MALDI-TOF MS

MALDI-TOF MS of intact protein samples was conducted with a Bruker Microflex™ LT benchtop system (Bruker, United States). Using a matrix of saturated DHAP (2',6'-Dihydroxyacetophenone) in acetonitrile.

2.13. Solid-Phase-Peptide Synthesis (SPPS)

SPPS was carried out manually or on a Tribute-UV peptide synthesizer (Protein technologies, USA) via standard Fmoc-based protocols.

3. Experimental procedures

3.1. Trastuzumab production

Trastuzumab expression and purification was executed as previously published with an additional final purification by gel filtration on a Superdex 200 Increase 10/300 from GE (GE life sciences, USA) with PBS and flow rate of 0.75 ml/min.[3]

3.2. General procedure for antibody modification with phosphonamidates via reduction and alkylation of inter-chain disulfides

Trastuzumab modification was carried out by incubating freshly expressed antibody (typical concentration c = 0.5 to 1.0 mg/ml) with 1000 eq. of DTT in a buffer containing 50 mM sodium borate in PBS (pH 8.0) with a total volume of 80 µl at 37 °C for 40 min. Excess DTT removal and buffer exchange to a solution containing 50 mM NH_4HCO_3 and 1mM EDTA (pH 8.5) was conducted afterwards using 0.5 mL Zeba™ Spin Desalting Columns with 7K MWCO (Thermo Fisher Scientific, USA). The desired

phosphonamidate, dissolved in DMSO was added quickly to reach a final DMSO content of no more than 5%. The mixture was shaken at 850 rpm and 14 °C for 16 hours. Excess reagent was again removed by buffer exchange to sterile PBS using 0.5 mL Zeba™ Spin Desalting Columns with 7K MWCO or size exclusion chromatography.

3.3. Deglycosylation, reduction and MS-analysis of trastuzumab conjugates

40 µl of the crude antibody modification mixture were purified by size-exclusion chromatography, eluting with 100 mM $NaHCO_3$ and 500 mM NaCl. The antibody containing fractions were pooled and concentrated by spin-filtration to 40 µl (MCWO: 10 kDa, 0.5 ml, Sartorius, Germany). 2 µl RapiGest™ solution (1% in H_2O) (Waters Corp., USA) were added and the solution was heated to 60 °C for 30 min. The solution was allowed to cool to room temperature, 1 µl PNGase-F solution (Pomega, Germany, Recombinant, cloned from Elizabethkingia miricola 10 u/µl) was added and the solution was incubated at 37 °C over night. Disulfide bridges were reduced by addition of 2 µl DTT solution (70 mM in H_2O) and incubation at 37°C for 30 min. Samples were diluted with 120 µl 1% HCl and subjected to intact protein MS.

3.4. Stability studies of the Dabcyl-EDANS adducts

Stability studies were conducted in 96-well plate (Corning 3615, black with clear, flat bottom) at least in triplicates. 5 µl of a 200 µM Stock solution of the Dabcyl-EDANS adducts and 95 µl of the respective test solutions were added to each well.

HEK cell lysate was generated from approximately $3,9*10^7$ cells, lysed in 2 mL PBS by sonification (final protein concentration: 1.7 mg/ml). Cells were grown on three 75 cm^2 cell culture plates, washed twice with PBS and harvested with a cell scraper. Human serum was purchased from Sigma Aldrich. Glutathione was dissolved at a concentration of 10 mM in PBS and the pH was adjusted to 7.4. 1N HCl studies were conducted at 200 µM, neutralized to pH 7 and diluted to 10 µM before fluorescence measurements.

Fluorescence was measured on a Tecan Safire plate reader. Excitation: 360 nm, emission: 508 nm, bandwidth: 5nm at 20 °C.

3.5. Incubation of trastuzumab-biotin conjugates with BSA

Trastuzumab-biotin conjugates were incubated at a concentration of 3 µM in PBS with a final concentration of 0.5 mM BSA at 37 °C. Samples were drawn after 0, 1, 2 and 5 days, deep frozen in liquid nitrogen and finally subjected to SDS-Page and western blot analysis.

3.6. Synthesis of trastuzumab-Cy5 conjugates and fluorescence microscopy

Trastuzumab-Cy5 conjugates were synthesized according to the general procedure 1 with the following slight modifications: the phosphonamidate equivalents (Cy5-*O*-ethyl-*P*-alkynyl-phosphonamidate) were raised to 130, and the DMSO content was raised to 5% to solubilize the Cy5. Samples were subjected to SDS-Page analysis and fluorescence microscopy.

BT474, SKBR3 and MDAMB468 were seeded on sterile cover slips and incubated ON at 37 °C, 5 % CO2 for cell attachment. Cells were washed three times with 1x PBS prior to fixation for 10 min in 1x PBS/4% PFA (formaldehyde). Fixation was stopped by the addition of an equal volume 1 x PBST (PBS + 0.05 % Tween20) followed by two more washes with PBST. AFCs were added to a final concentration of 5 µg/mL and incubated for 1 h at rt. Unbound AFC was removed by three washes with PBS. Images were acquired on a Leica SP5 confocal microscopy system equipped with a 63x1.40 oil immersion objective.

Laserlines 405 nm and 594 nm were used in combination with standard DAPI and Cy5 filter settings. Image processing was carried out with ImageJ 1.5.1h software extended by the Fiji processing package.

3.7. eGFP C70M S147C production

The eGFP mutant C70MS147C was generated allowing for single cysteine conjugation experiments. Even though this mutant obtains two cysteines (C48 and C147), the cysteine at position 48 was shown to be not addressable for different conjugation methods (data not shown).
For construction of the bacterial expression constructs coding for His-tagged eGFPC70MS147C, eGFP was cloned from pGEXeGFP (provided by Roland Kühne, FMP Berlin) into pET28a using XhoI and NdeI restriction endonuclease sites. The mutations were introduced with classical PCR by the use of complementary primer pairs (GTACAACTACAACTGCCACAACGTC and GACGTTGTGGCAGTTGT AGTTGTAC).
The protein was expressed in E. coli BL21(DE3) using LB medium containing 100 µg/mL ampicillin (LBAMP). Cells were grown at 37 °C, 180 rpm until OD_{600} reached approx. 0.8, induced with 0.3 mM IPTG and incubated at 18 °C for 19 h. Lysis was performed in Dulbecco's PBS (137 mM NaCl, 2.7 mM KCl, 10 mM Na2HPO4 and 1.8 mM KH2PO4) using a high-pressure homogenizer (Microfluidics LM10 Microfluidizer) and debris centrifuged at 20.000 g for 30 min. The protein was purified with a BioRad NGC system (BioRad, USA) using a 5 mL HisTrap FF (GE Healthcare, USA) column, peak fractions were collected and desalted to Dulbecco's PBS using a HiPrep 26/10 Desalting column (GE Healthcare, USA). Thrombin (1 µL/mL; Thrombin restriction grade, Merck Millipore, Germany) was added to the protein fractions and incubated for 16 h at 16 °C. The protein was concentrated to 1 mL using Vivaspin 20 (cut-off 19 kDa; Merck Millipore, Germany) and subjected to a final size exclusion chromatography using a Superdex 75 10/300 GL column (GE Healthcare, USA). The protein concentration was determined by NanoDrop® at 280 nm (ε = 21890 M-1 cm-1). The expressed protein was isolated in 15-20 mg yield for 1 L expression. Peak fractions were pooled, 0.1 mM PMSF added and aliquots were shock-frozen and stored at -80 °C until further use.

Deconvoluted HRMS: 27765 Da (calcd. MW: 27766 Da)

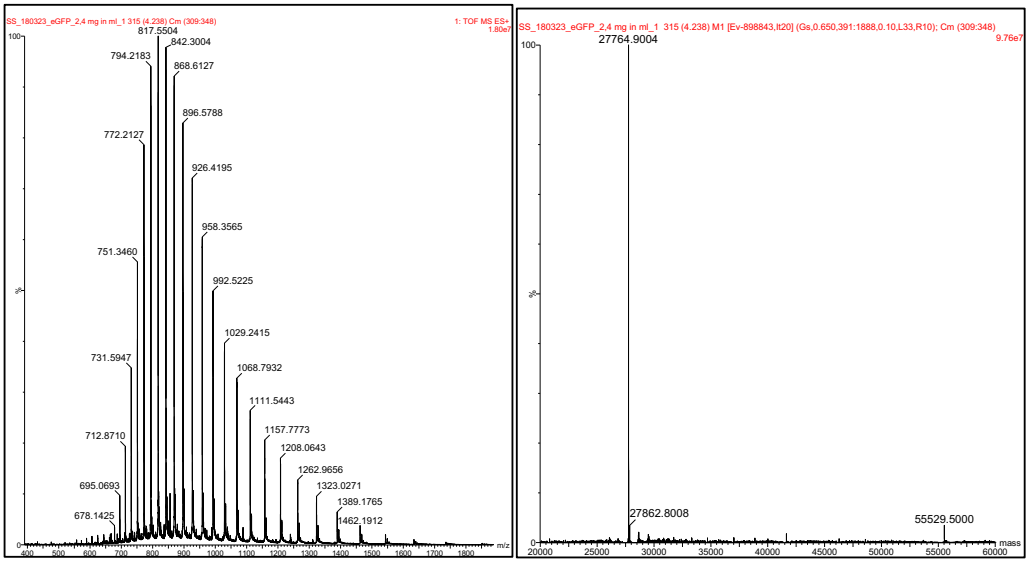

Protein sequence: His-tag highlighted in green; protease cleavage site highlighted in blue; eGFP highlighted in grey; C70M and S147C highlighted in red.

MGSSHHHHHHSSGLVPRGSHMGSIQMVSKGEELFTGVVPILVELDGDVNGHKFSVSGEGEGDATYGKLTLKFICTT
GKLPVPWPTLVTTLTYGVQMFSRYPDHMKQHDFFKSAMPEGYVQERTIFFKDDGNYKTRAEVKFEGDTLVNRIEL
KGIDFKEDGNILGHKLEYNYNCHNVYIMADKQKNGIKVNFKIRHNIEDGSVQLADHYQQNTPIGDGPVLLPDNHYL
STQSALSKDPNEKRDHMVLLEFVTAAGITLGMDELYK

3.8. Addition of the CPP-phosphonamidate peptides 8 and 9 to eGFP

To eGFP C70M S147C buffered in PBS, ethynylphosphonamidate-peptides (20 eq.) were added to give the final protein concentration of 100 µM protein and 2 mM peptide. The reaction mixture was shaken at 37°C and 800 rpm for 3 h. The excess peptide was removed by spinfiltration using Amicon Spin filters with a 10 kDa MWCO (Sartorius, Germany). The sample was filtered five times with PBS at 14000 rpm for 5 min to remove excess Peptide.

Cyclic-(Tat)-eGFP

Peptide **8** (3.06 mg as TFA-salt, 1.13 µmol, 20 eq.) was reacted with eGFP C70M S147C (56.3 nmol) according to the above stated procedure. After removal of excess peptide by spin filtration the sample was analyzed by MALDI-TOF after acetone precipitation and re-solvation in 10 mM ammonium bicarbonate buffer. Quantitative conversion to the product was observed.

MALDI TOF: expected (in Da): 29795.2 (M+H+); found (in Da): 29851.4 (M+H+)

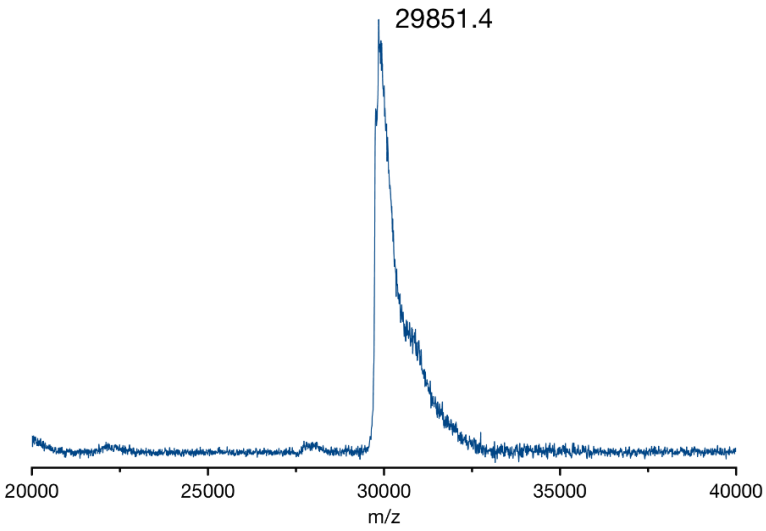

Cyclic-(R_{10})-eGFP

Peptide **9** (3.94 mg as TFA-salt, 1.13 µmol, 20 eq.) was reacted with eGFP C70M S147C (56.3 nmol) according to the above stated procedure. After removal of excess peptide by spin filtration the sample was analyzed by MALDI-TOF after acetone precipitation and re-solvation in 10 mM ammonium bicarbonate buffer. Quantitative conversion to the product was observed.

MALDI TOF: expected (in Da): 30106.4 ($M+H^+$); found (in Da): 30128.0 ($M+Na^+$).

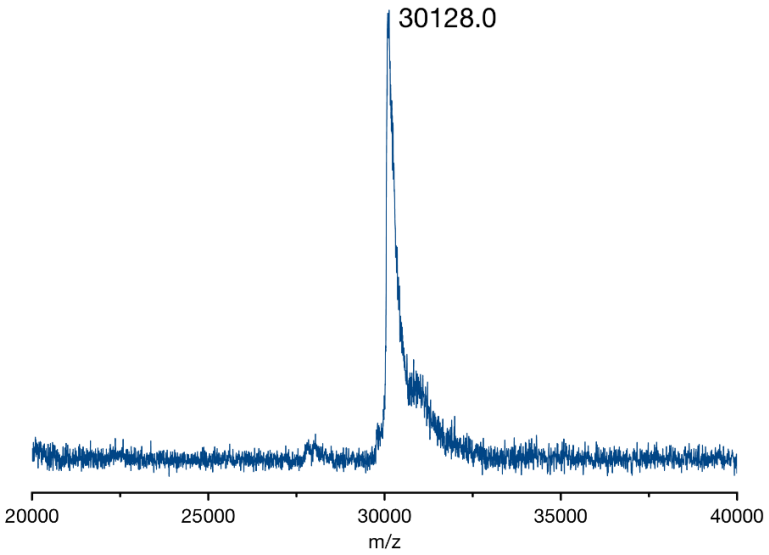

3.9. Cellular uptake experiments

All cellular uptake experiments were carried out with HeLa (ATCC CCL-2) cells cultured in Dulbecco's MEM medium supplemented with 10% FBS and 1% Penicillin Streptomycin. 70 000 cells were seeded in an uncoated glass bottom 8-well µ-slide (Ibidi) 24 hours prior to treatment. The cellular uptake was carried out by gently washing cells three times with HEPES buffer pH 7.5 (5 mM HEPES, 140 mM NaCl, 2.5 mM KCl, 5 mM glycine). The peptide-protein conjugate buffered in the same HEPES buffer was added to the cells in 200 µl at 50 µM and incubated for at 37°C in a 5% CO_2 atmosphere. After one hour cells were gently washed with 25 mM HEPES in Dulbecco's MEM supplemented with 10% FKS and cells were rested for 30 minutes at 37°C. The cell nucleus was stained with Hoechst 33342 and cells imaged with a Zeiss 710 confocal microscope.

4. Organic Synthesis

4.1. General procedure 1 for the synthesis of *O*-ethyl-ethynylphosphonamidates

A 25-ml Schlenk flask was charged with 173 µl diethyl chlorophosphite (1.20 mmol, 1.2 eq.) under an argon atmosphere, cooled to –78 °C and 2.00 ml ethynylmagnesium bromide solution (0.5 M in THF, 1.00 mmol, 1.0 eq.) was added drop wise. The solution was allowed to warm to room temperature and 1.00 mmol of azide (1.0 eq.) dissolved in 3.0 ml of THF or DMF was added and stirred over night at room temperature. 5 ml of water were added and stirred for another 2 h. The reaction mixture was extracted with EtOAc, the combined organic fractions dried ($MgSO_4$) and solvents were removed under reduced pressure. The crude product was purified by flash column chromatography on silica gel or preparative reversed phase HPLC.

4.2. Ethyl-*N*-phenyl-*P*-ethynylphosphonamidate (1)

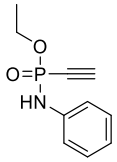

The compound was synthesized according to the general procedure 1 from 1.45 ml diethyl chlorophosphite (10.07 mmol) and 1.00 g phenyl azide (8.39 mmol). The crude phosphonamidate was purified by flash column chromatography on silicagel (50% *n*-hexan in EtOAc) and obtained as a yellowish solid. (1.4 g, 6.74 mmol, 80.3%)

^{1}H NMR (600 MHz, Chloroform-*d*) δ = 7.33 – 7.25 (m, 2H), 7.20 (d, *J*=7.6, 1H), 7.16 – 7.10 (m, 2H), 7.05 – 6.94 (m, 1H), 4.35 – 4.10 (m, 2H), 2.91 (d, *J*=12.9, 1H), 1.39 (t, *J*=7.1, 3H). ^{13}C NMR (151 MHz, Chloroform-*d*) δ = 139.18, 129.28, 122.23, 118.16 (d, *J*=7.6), 87.77 (d, *J*=48.8), 76.39 (d, *J*=272.9), 62.13 (d, *J*=5.1), 16.17 (d, *J*=7.4). ^{31}P NMR (243 MHz, Chloroform-*d*) δ = -8.75. HR-MS for $C_{10}H_{13}NO_2P^+$ $[M+H]^+$ calcd.: 210.0678, found 210.0680.

4.3. Ethyl-*N*-(4-carboxy-phenyl)-*P*-ethynylphosphonamidate (2)

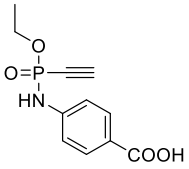

The compound was synthesized according to the general procedure 1 from 1.06 ml diethyl chlorophosphite (7.36 mmol) and 1.00 g 4-azidobenzoic acid (6.13 mmol). The crude phosphonamidate was purified by flash column chromatography on silicagel (5 to 20% MeOH in EtOAc) and obtained as a white solid. (0.68 g, 2.67 mmol, 43.5%)

^{1}H NMR (300 MHz, Acetone-d_6) δ 8.11 – 8.00 (m, 1H), 7.97 (d, *J* = 8.6 Hz, 2H), 7.30 (d, *J* = 8.6 Hz, 2H), 4.32 – 4.11 (m, 2H), 3.87 (d, *J* = 12.9 Hz, 1H), 1.36 (t, *J* = 7.1 Hz, 3H).^{13}C NMR (75 MHz, Acetone-d_6) δ = 167.65, 145.51 (d, *J*=1.5), 131.93, 124.63, 118.04 (d, *J*=7.8), 90.15 (d, *J*=47.6), 77.28 (d, *J*=267.2), 62.98 (d, *J*=5.1), 16.38 (d, *J*=7.1).^{31}P NMR (122 MHz, Acetone-d_6) δ -11.05. HR-MS for $C_{11}H_{13}NO_4P^+$ $[M+H]^+$ calcd.: 254.0577, found 254.0586.

4.4. Ethyl-*N*-(4-(2,5-dioxo-1-pyrrolidinyl)oxy-carbonyl-phenyl)-*P*-ethynylphosphonamidate (3)

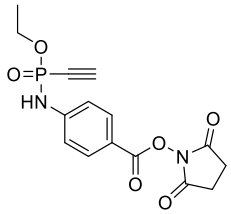

The compound was synthesized according to the general procedure 1 from 173 µl diethyl chlorophosphite (1.20 mmol) and 260 mg 4-azidobenzoic-acid-*N*-hydroxysuccinimide ester 1.00 mmol). The crude phosphonamidate was purified by flash column chromatography on silicagel (100% EtOAc) and obtained as a yellowish solid. (225 mg, 0.64 mmol, 64.3%)

^{1}H NMR (300 MHz, Chloroform-*d*) δ = 8.05 (d, *J*=8.6, 2H), 7.37 (d, *J*=7.4, 1H), 7.16 (d, *J*=8.6, 2H), 4.38 – 4.13 (m, 2H), 2.96 (d, *J*=13.2, 1H), 2.90 (s, 4H), 1.40 (t, *J*=7.1, 3H).^{13}C NMR (75 MHz, Chloroform-*d*) δ = 169.59, 161.51, 145.64, 132.55, 118.38, 117.59 (d, *J*=8.0), 88.69 (d, *J*=50.2), 62.93 (d, *J*=5.2), 25.82, 16.24 (d, *J*=7.3).^{31}P NMR (122 MHz, Chloroform-*d*) δ = -10.65. HR-MS for $C_{15}H_{16}N_2O_6P^+$ $[M+H]^+$ calcd.: 351.0740, found 351.0749.

Synthetic route to 2-(4-Azidophenyl)-ethylamine hydrochloride

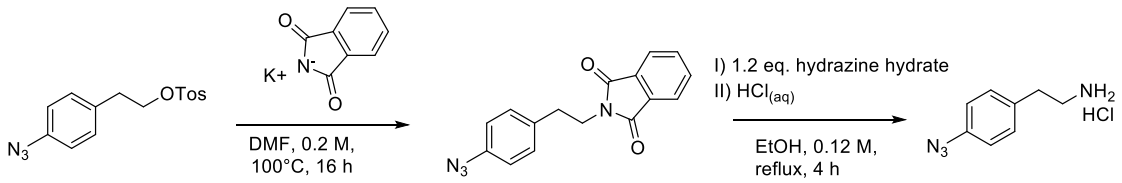

4.5. 2-(4-Azidophenyl)-ethyl phtalimide

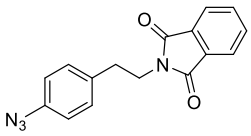

A 50-ml round-bottom flask was charged with 4.11 g of 2-(4-Azidophenyl)-ethyl-4-toluenesulfonate (12.95 mmol, 1.00 eq.), together with 3.60 g potassium phtalimide (19.42 mmol, 1.50 eq.) and dissolved in 60 ml DMF. The brown solution was stirred over night at 100 °C. All volatiles were removed under reduced pressure, 50 ml of water were added extracted three times with EtOAc, the combined organic fractions were washed two times with water, the organic layer was dried ($MgSO_4$) and all volatiles were removed under reduced pressure. The product was used in the next step without further purification. Pure product was obtained by flash column chromatography on silicagel (10% to 20% EtOAc in *n*-hexan) as a yellow solid (1.75 g, 5.99 mmol, 46.2%). ^{1}H NMR (600 MHz, Chloroform-*d*) δ = 7.85 (dd, *J*=5.4, 3.1, 2H), 7.73 (dd, *J*=5.4, 3.1, 2H), 7.25 (d, *J*=8.4, 2H), 6.96 (d, *J*=8.4, 2H), 3.93 (dd, *J*=8.3, 6.8, 2H), 3.00 (dd, *J*=8.3, 6.8, 2H). ^{13}C NMR (151 MHz, $CDCl_3$) δ = 168.12, 138.43, 134.76, 133.96, 132.00, 130.22, 123.26, 119.17, 39.14, 33.92.

4.6. 2-(4-Azidophenyl)-ethylamine hydrochloride

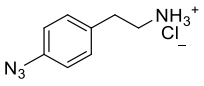

A 100-ml round-bottom flask was charged with 722 mg of 2-(4-Azidophenyl)-ethyl phtalimide (2.47 mmol, 1.00 eq.), 144 µl hydrazine hydrate (2.96 mmol, 1.20 eq.), dissolved in 20 ml of dry ethanol under argon atmosphere and the solution was refluxed for 4 h. Most of the solvent was removed under reduced pressure, 50 ml water was added and the suspension was basified with 1N NaOH. It was extracted three times with EtOAc, the combined organic fractions were washed two times with water, the organic layer was dried ($MgSO_4$) and all volatiles were removed under reduced pressure. Pure product was obtained by flash column chromatography on silicagel (10% MeOH in CH_2Cl_2 + 0.5% *N,N*-ethyldimethylamine) and lyohilisation from 1N HCl as yellowish solid (224 mg, 1.14 mmol, 46.2% over two steps). ^{1}H NMR (600 MHz, Deuterium Oxide) δ = 7.29 (d, *J*=7.6, 2H), 7.05 (d, *J*=7.6, 2H), 3.22 (t, *J*=7.2, 2H), 2.94 (t, *J*=7.2, 2H). ^{13}C NMR (151 MHz, D_2O) δ = 138.81, 133.24, 130.32, 119.40, 40.51, 32.13. NMR data was in accordance with literature values.[4]

4.7. Ethyl-*N*-(4-(2-aminoethyl)phenyl)-*P*-ethynylphosphonamidate TFA salt (4)

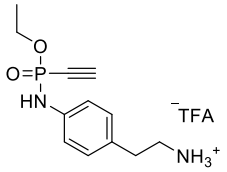

The compound was synthesized according to the general procedure 1 from 181 µl diethyl chlorophosphite (1.25 mmol) and 322 mg 2-(4-azidophenyl)ethyl amine hydrochloride (1.05 mmol). The crude phosphonamidate was purified by preparative RP-HPLC (Method C) and obtained as brown oil. (88 mg, 0.24 mmol, 22.9%)

^{1}H NMR (300 MHz, Acetonitrile-d_3) δ = 7.58 (s, 3H), 7.20 – 7.01 (m, 4H), 6.96 (d, *J*=8.5, 1H), 4.26 – 4.05 (m, 2H), 3.42 (d, *J*=12.8, 1H), 3.08 (d, *J*=7.8, 2H), 2.88 (dd, *J*=9.0, 6.4, 2H), 1.31 (t, *J*=7.1, 3H). ^{13}C NMR (75 MHz, Acetonitrile-d_3) δ = 161.38 (q, *J*=34.7), 139.20 (d, *J*=1.3), 131.75, 130.66, 119.63 (d, *J*=7.3), 90.09 (d, *J*=47.2), 77.02 (d, *J*=265.0), 63.54 (d, *J*=5.3), 41.92, 33.19, 16.41 (d, *J*=7.3). ^{31}P NMR (122 MHz, Acetonitrile-d_3) δ = -9.71. HR-MS for $C_{12}H_{18}N_2O_2P^+$ $[M+H]^+$ calcd.: 253.1100, found 253.1095.

4.8. *N*-(4-azidophenyl) biotinamide

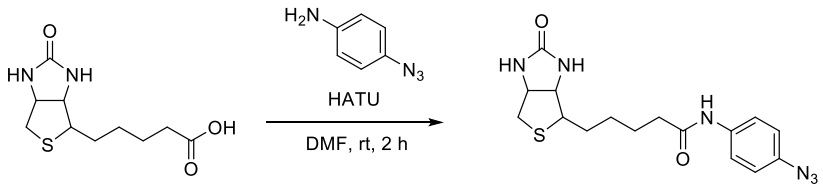

A 50-ml round-bottom flask was charged with 642 mg of D-biotin (2.63 mmol, 1.50 eq.) and 1.00 g of HATU (2.63 mmol, 1.50 eq.) under argon, dissolved in 5 ml of dry DMF and cooled to 0°C. 920 µl DIPEA (5.25 mmol, 3.0 eq.) were added and stirred for several min. A solution of 235 mg 4-azido aniline (1.75 mmol, 1.00 eq.) in 4 ml of dry DMF was added, the yellow solution was allowed to warm to room temperature and stirred for additional 2 h. The solvents were removed under reduced pressure and the crude product was purified by flash column chromatography on silicagel (5 to 12% MeOH in CH_2Cl_2). The product was obtained as white powder. (617 mg, 1,72 mmol, 98%)

^{1}H NMR (600 MHz, DMSO-d_6) δ = 9.96 (s, 1H), 7.64 (d, *J*=8.9, 2H), 7.07 (d, *J*=8.9, 2H), 6.44 (s, 1H), 6.37 (s, 1H), 4.42 – 4.28 (m, 1H), 4.21 – 4.08 (m, 1H), 3.21 – 3.07 (m, 1H), 2.84 (dd, *J*=12.4, 5.1, 1H), 2.60 (d, *J*=12.4, 1H), 2.31 (td, *J*=7.4, 1.8, 2H), 1.70 – 1.57 (m, 3H), 1.55 – 1.47 (m, 1H), 1.44 – 1.32 (m, 2H). ^{13}C NMR (151 MHz, DMSO) δ = 171.60, 163.20, 137.09, 134.00, 121.00, 119.83, 61.53, 59.69, 55.85, 40.31, 36.64, 28.70, 28.56, 25.55. HR-MS for $C16H21N_6O2S^+$ $[M+H]^+$ calcd.: 361.1441, found 361.1447.

4.9. Ethyl-*N*-(4-biotinamido-phenyl)-*P*-ethynylphosphonamidate (5)

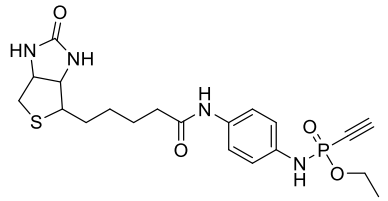

The compound was synthesized according to the general procedure 1 from 239 µl diethyl chlorophosphite (1.66 mmol) and 150 mg *N*-(4-azidophenyl) biotinamide (0.416 mmol). The crude phosphonamidate was purified by flash column chromatography on silicagel (12% MeOH in CH_2Cl_2) and obtained as white solid. (134 mg, 0.30 mmol, 71.5 %).

^{1}H NMR (600 MHz, DMSO-d_6) δ = 9.74 (s, 1H), 8.27 (d, *J*=8.6, 1H), 7.45 (d, *J*=8.6, 2H), 7.00 (d, *J*=8.6, 2H), 6.45 (bs, 2H), 4.39 – 4.30 (m, 2H), 4.19 – 4.01 (m, 3H), 3.17 – 3.10 (m, 1H), 2.84 (dd, *J*=12.4, 5.1, 1H), 2.60 (d, *J*=12.4, 1H), 2.28 (t, *J*=7.1, 2H), 1.73 – 1.55 (m, 3H), 1.55 – 1.46 (m, 1H), 1.44 – 1.32 (m, 2H), 1.29 (t, *J*=7.0, 3H). ^{13}C NMR (151 MHz, DMSO-d_6) δ = 171.21, 163.25, 135.56, 134.03, 120.64, 118.72 (d, *J*=7.4), 91.15 (d, *J*=44.8), 77.76 (d, *J*=257.8), 61.92 (d, *J*=3.6), 61.56, 59.72, 55.86, 40.31, 36.56, 28.71, 28.55, 25.65, 16.43 (d, *J*=6.8). ^{31}P NMR (243 MHz, DMSO) δ = -9.37. HR-MS for $C_{20}H_{28}N_4O_4PS^+$ $[M+H]^+$ calcd.: 451.1563, found 451.1565.

4.10. Ethyl-*N*-(3-phenyl-propyl)-*P*-ethynylphosphonamidate (6)

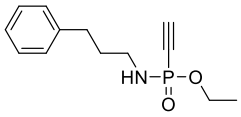

The compound was synthesized according to the general procedure 1 from 346 µl diethyl chlorophosphite (2.40 mmol) and 322 mg 3-phenyl-propyl azide (2.00 mmol). The crude phosphonamidate was purified by flash column chromatography on silicagel (50% *n*-hexan in EtOAc) and obtained as colourless oil. (180 mg, 0.72 mmol, 35.8%)

^{1}H NMR (300 MHz, Chloroform-*d*) δ = 7.33 – 7.25 (m, 2H), 7.24 – 7.16 (m, 3H), 4.20 – 4.05 (m, 2H), 3.31 (dd, *J*=11.8, 5.9, 1H), 3.07 – 2.93 (m, 2H), 2.88 (d, *J*=12.2, 1H), 2.68 (dd, *J*=8.7, 6.8, 2H), 1.88 (p, *J*=7.2, 2H), 1.35 (t, *J*=7.1, 3H). ^{13}C NMR (75 MHz, Chloroform-*d*) δ = 141.30, 128.33, 128.30, 125.87, 86.96 (d, *J*=45.5), 76.90 (d, *J*=257.0), 61.57 (d, *J*=5.1), 40.29, 32.84 (d, *J*=6.4), 32.78, 16.08 (d, *J*=7.3). ^{31}P NMR (122 MHz, Chloroform-*d*) δ = -2.23. HR-MS for $C_{13}H_{19}NO_2P^+$ $[M+H]^+$ calcd.: 252.1148, found 252.1154.

4.11. c(RGDfK)-azide

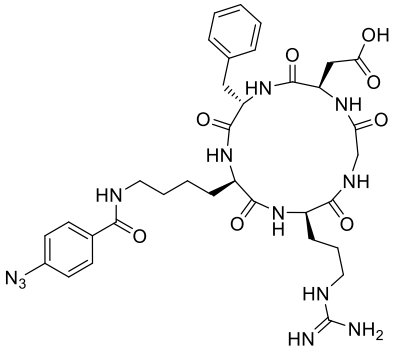

The cyclic RGDfK-azido peptide was synthesized manually on a NovaSynTGT alcohol resin with a loading of 0.26 mmol/g. First the resin was activated by stirring 480.7 mg resin in 2.5 ml toluene and 480 µl acetylchloride at 60°C for 3 h. Double coupling of Fmoc-Asp(OAll)-OH (123.56 mg, 0.3125 mmol, 2.5 eq) was performed in CH_2Cl_2 using DIPEA (212.6 µl, 1.25 mmol, 10 eq.) as activating base each for 1 h. Further amino acid couplings were performed by mixing amino acid (0.25 mmol, 2 eq.), HATU (0.25 mmol, 2 eq.) and DIPEA (0.5 mmol, 4 eq.) in DMF and coupling once for 30 min and once for one hour. Fmoc deprotection was accomplished with 20 % piperidine in DMF. After the final amino acid coupling the alloc deprotection was achieved by treating the resin with $Pd(P(Ph_3)_4)$ (433 mg, 0.375 mmol, 3 eq.) in chloroform/acetic acid/NMM (37:2:1;v:v:v) for 2 h in an argon atmosphere, followed by Fmoc deprotection and cyclisation with HATU (0.25 mmol, 2 eq.) and DIPEA (0.5 mmol, 4 eq.) in DMF for 16 h. To be able to install the aromatic azide on the lysine residue Fmoc-Lys(dde)-OH was used in the solid phase synthesis and was orthogonally deprotected on resin using 2% hydrazine in DMF three times for 3 min, followed by coupling of 4–azidobenzoic acid (81.65 mg, 0.5 mmol, 4 eq.) with HATU (190mg, 0.5 mmol, 4eq.) and DIPEA (1 mmol, 8 eq.) in DMF for 2 h. Cleavage from the resin was performed using

TFA/ CH_2Cl_2 (75:25;v:v) for 2.5 h. Precipitation was carried out in cold and dry ether. The crude was purified by preparative HPLC (Method C). LR-MS for $C_{34}H_{45}N_{12}O_3^+$ $[M+H]^+$ calcd.: 749.35, found 749.67.

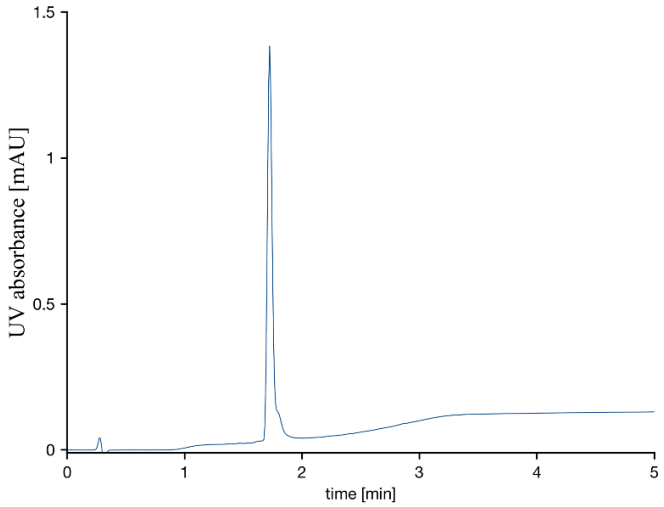

4.12. General procedure 2 for the synthesis of *O*-ethyl-alkynyl phosphonamidates from diethyl chlorophosphite with peptides

A 25-ml Schlenk flask was charged with 144 µl diethyl chlorophosphite (1.00 mmol, 5.0 eq.) under an argon atmosphere, cooled to –78 °C and 2.00 ml ethynylmagnesium bromide solution (0.5 M in THF, 1.00 mmol, 5.0 eq.) was added drop wise. The yellowish solution was allowed to warm to room temperature and 0.20 mmol of peptidic azide (1.0 eq.) dissolved in 5.0 ml of DMF or DMSO was added and stirred over night at room temperature. 5 ml of water were added and stirred for another 2 h. Solvents were removed under reduced pressure. The crude product was purified by preparative reversed phase HPLC.

4.13. Synthesis of c(RGDfK)-ethynylphosphonamidate 7

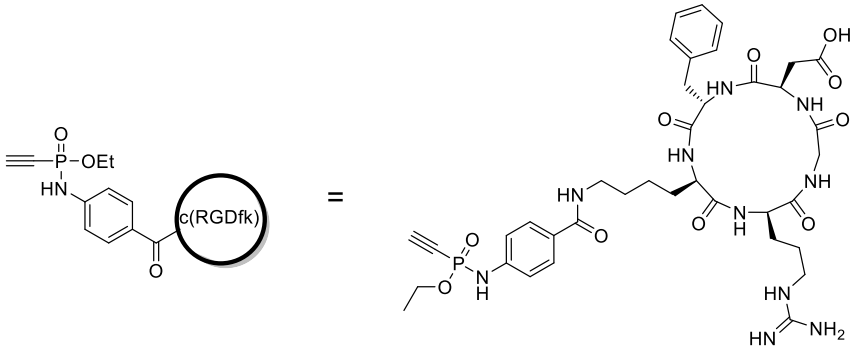

The compound was synthesized according to the general procedure 2 from 8.95 µl diethyl chlorophosphite (0.036 mmol, 4.0 eq.), 72 µl ethynylmagnesium bromide solution (0.5 M in THF, 0.036 mmol, 4.0 eq.) and 6.9 mg c(RGDfK)-azide (9.14 µmol, 1 eq.) . The crude phosphonamidate was purified by preparative HPLC (Method D) and obtained as a white solid after lyophilisation. (4.1 mg, 4.89 µmol, 53.5 % yield). HR-MS for $C_{38}H_{45}N_{10}O_{10}P^+$ $[M+H]^+$ calcd.: 839.3606, found 839.3636.

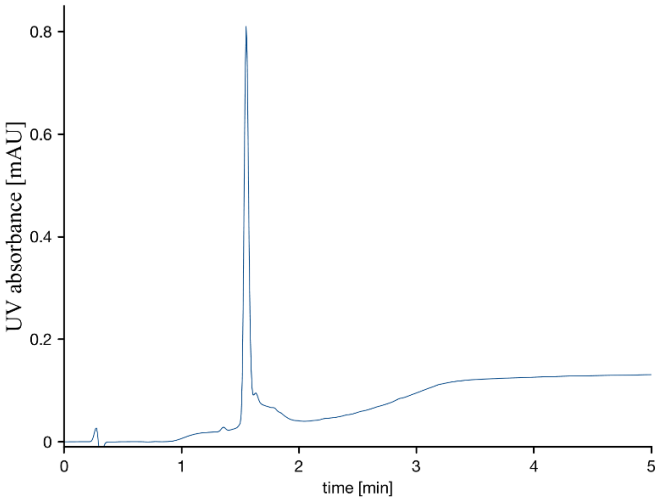

4.14. c-(Tat)-azide

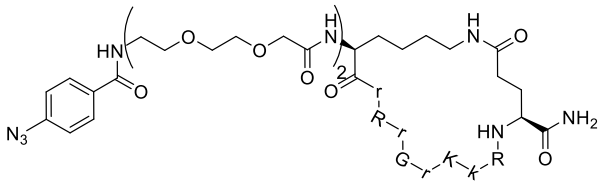

The cyclic-(Tat)-azido peptide was synthesized in a 0.1 mmol scale on a Rink amide resin with a loading of 0.78 mmol/g. The synthesis was carried out on a PTI synthesizer with single couplings of each amino acid (10 eq. amino acid for 40 min) in DMF. After the final PEG building block coupling the peptide, still Fmoc protected, was treated with Pd(PPh3)4 (24 mg, 20 µmol, 20 mol%) and phenylsilane (308 µl, 2.5 mmol, 2.5 eq.) in 4 ml dry CH_2Cl_2 for 1 h in order to cleave the alloc and allyl protecting groups in one step. After confirmation of full deprotection by test cleavage, cyclization with 2 eq. HATU 4 eq. DIPEA was carried for 4 h in DMF. The peptide was then Fmoc-deprotected using 20% piperidine in DMF and the 4-azidobenzoic acid (81.6 mg, 0.5 mmol, 5 eq.) was coupled to the *N*-terminus with HATU (190.1 mg, 0.5 mmol, 5 eq.) and DIPEA (170 µl, 1.0 mmol, 10 eq.) for 1 h. Finally the peptide was cleaved from the resin by treatment with 4 ml of a TFA:TIS:H2O (95:2.5:2.5) mixture for 3 h and precipitated in cold diethylether. The crude peptide was purified by preparative HPLC (Method D). The product was gained as white powder (30.0 mg as TFA-salt, 11.4 µmol, 11.4% yield) MS: m/z: 648.49 $[M+3H]^{3+}$ (calcd. m/z: 648.0569).

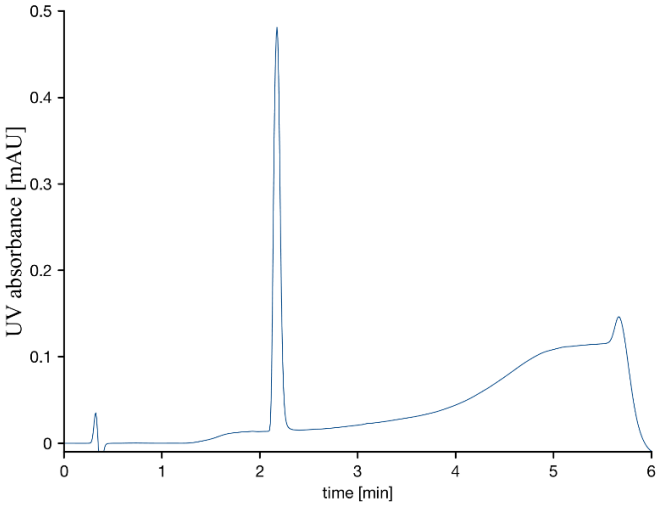

4.15. c-(Tat)-ethynylphosphonamidate 8

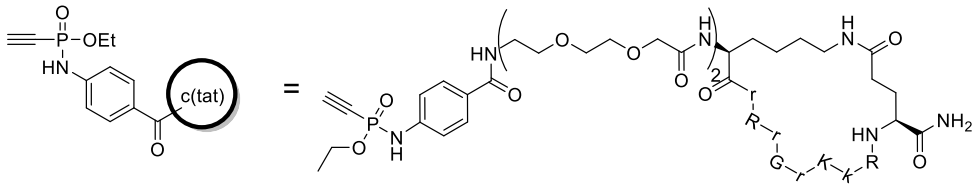

The compound was synthesized according to the general procedure 2 from 8.95 µl diethyl chlorophosphite (0.030 mmol, 4.0 eq.), 72 µl ethynylmagnesium bromide solution (0.5 M in THF, 0.030 mmol, 4.0 eq.) and 20 mg c(Tat)-azide (7.6 µmol, 1 eq.). The product was gained after semi-preparative HPLC (Method D) as white powder (13 mg, 4.8 µmol, 62.9% yield). HRMS: m/z: 678.0569 $[M+3H]^{3+}$ (calcd. m/z: 678.0610).

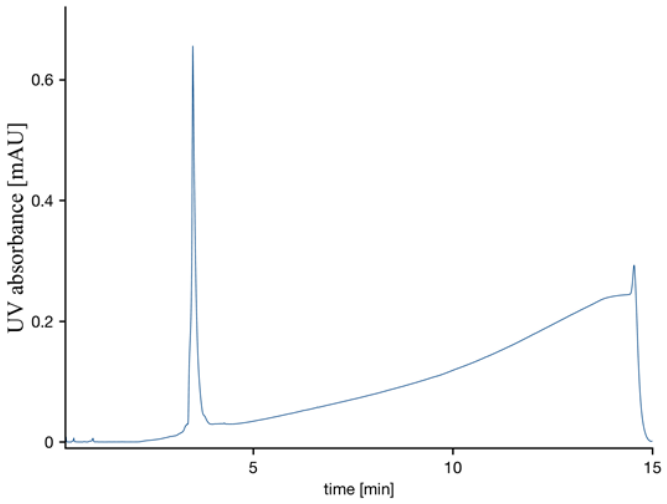

4.16. c(R_{10})-azide

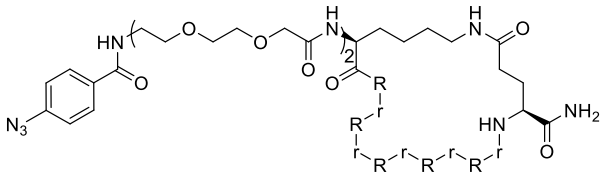

The cyclic-(R10)-azido peptide was synthesized in a 0.1 mmol scale on a Rink amide resin with a loading of 0.78mmol/g. The synthesis was carried out on a PTI synthesizer with double couplings of each amino acid (5 eq. amino acid for 40 min) in DMF. After the final PEG building block coupling the peptide, still Fmoc protected, was treated with Pd(PPh3)4 (24 mg, 20 µmol, 20 mol%) and phenylsilane (308 µl, 2.5 mmol, 2.5 eq.) in 4 ml dry CH_2Cl_2 for 1 h in order to cleave the alloc and allyl protecting groups in one step. After confirmation of full deprotection by test cleavage, cyclization with 2 eq. HATU 4 eq. DIPEA was carried out overnight in DMF. The peptide was then Fmoc-deprotected using 20% Piperidine in DMF and the 4-azidobenzoic acid (81.6 mg, 0.5 mmol, 5 eq.) was coupled to the *N*-terminus with HATU (190.1 mg, 0.5 mmol, 5 eq.) and DIPEA (170 µl, 1.0 mmol, 10 eq.) for 1 h. Finally the peptide was cleaved from the resin by treatment with 4 ml of a TFA:TIS:H2O (95:2.5:2.5) mixture for 3 h and precipitated in cold diethylether. The crude peptide was purified by preparative HPLC (Method D) and gained as white powder (62 mg as TFA-salt, 18.3 µmol 18.3% yield). MS: m/z: 752.35 $[M+3H]^{3+}$ (calcd. m/z: 751.7879)

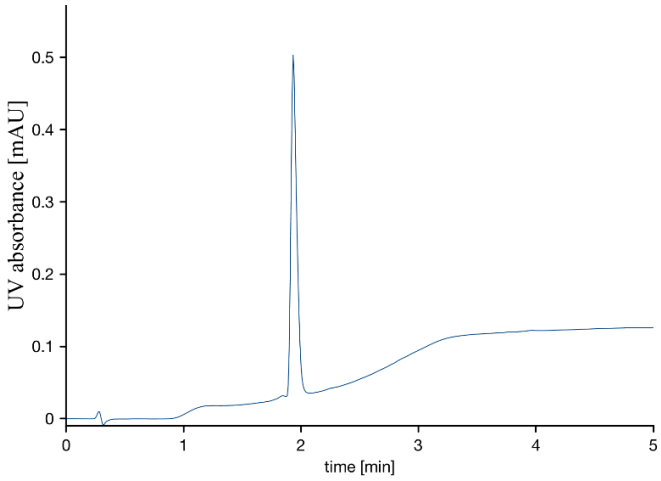

4.17. c-(R10)-ethynylphosphonamidate 9

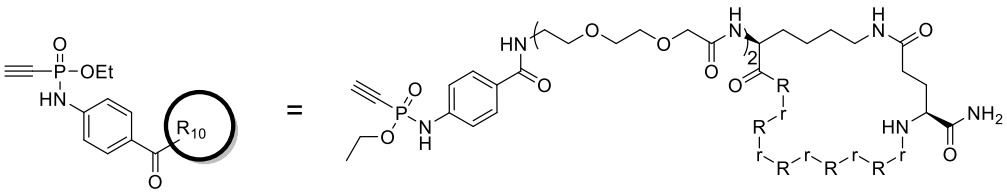

The compound was synthesized according to the general procedure 2 from 8.95 µl diethyl chlorophosphite (0.041 mmol, 4.0 eq.), 72 µl ethynylmagnesium bromide solution (0.5 M in THF, 0.041 mmol, 4.0 eq.) and 35 mg c(R10)-azide (7.6 µmol, 1 eq.). The product was gained after semi-preparative HPLC (Method D) as white powder (13 mg, 4.79 µmol, 62.9% yield). HRMS: m/z: 781.7965 $[M+3H]^{3+}$ (calcd. m/z: 781.7920).

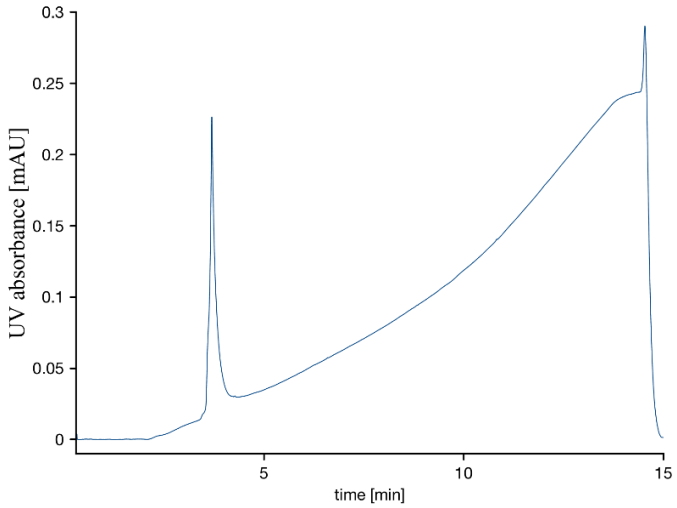

4.18. 5-((2-(*O*-Ethyl-*P*-ethynyl-phosphonamidato-*N*-benzoyl)ethyl)amino)naphthalene-1-sulfonic acid (10)

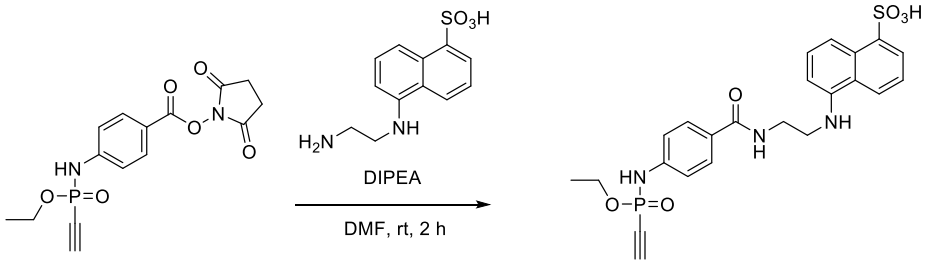

The reaction was carried out in DMF. 265 µl of a 100 mM solution of Ethyl-*N*-(4-(2,5-dioxo-1-pyrrolidinyl)oxy-carbonyl-phenyl)-*P*-ethynylphosphonamidate (0.0265 mmol, 1.00 eq.) and 1.06 ml of a 50 mM solution of 5-((2-Aminoethyl)aminonaphthalene-1-sulfonate (EDANS) (0.0530 mmol, 2.00 eq.) together with 795 µl DMF was premixed and 530 µl of a solution of 200 mM DIPEA (0.1060 mmol, 4.00 eq.) was added. The mixture was shaken for 2 h at room-temperature, all volatiles were removed under reduced pressure, the crude mixture was purified by semi-preparative HPLC using method D and the desired compound obtained as a white solid after lyophilisation. (9.30 mg, 0.0186 mmol, 70.0%)

^{1}H NMR (600 MHz, DMSO-d_6) δ = 8.78 (d, *J*=8.5, 1H), 8.57 (t, *J*=5.7, 1H), 8.36 (d, *J*=8.6, 1H), 8.11 (d, *J*=8.4, 1H), 7.99 (d, *J*=7.0, 1H), 7.80 (d, *J*=8.7, 2H), 7.43 (dd, *J*=8.5, 7.1, 1H), 7.38 (t, *J*=8.1, 1H), 7.14 (d, *J*=8.7, 2H), 6.92 (d, *J*=7.5, 1H), 4.43 (d, *J*=12.7, 1H), 4.21 – 4.05 (m, 2H), 3.62 (q, *J*=6.3, 2H), 3.46 (t, *J*=6.6, 2H), 1.31 (t, *J*=7.0, 3H). ^{13}C NMR (151 MHz, DMSO-d_6) δ = 167.03, 144.64, 143.48, 141.01, 130.59, 128.98, 127.65, 126.47, 125.13, 124.62, 123.86, 123.13, 119.62, 117.34 (d, *J*=7.8), 107.91, 91.69 (d, *J*=45.5), 77.26 (d, *J*=260.8), 62.31 (d, *J*=5.0), 45.51, 38.15, 16.42 (d, *J*=6.9). ^{31}P NMR (243 MHz, DMSO) δ = -10.35. HR-MS for $C_{23}H_{25}N_3O_6PS^+$ $[M+H]^+$ calcd.: 502.1196, found 502.1195.

4.19. Cy5-*O*-ethyl-*P*-alkynyl-phosphonamidate 11

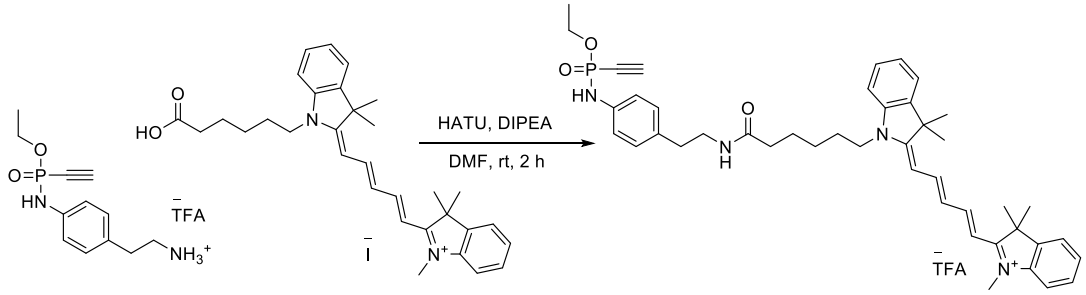

The Cy5-COOH was synthesized according to a procedure, previously published by our lab.[5] A 5-ml-round bottom flask was charged with 33.2 mg Cy5-COOH (0.0628 mmol, 1.00 eq.), 35.8 mg HATU (0.0942 mmol, 1.5 eq.) and 200 µl DMF. The deep blue solution was cooled to 0 °C and 32 µl DIPEA (0.1884 mmol, 3.0 eq.) were added. After 5 min a solution of 23 mg Ethyl-*N*-(4-(2-aminoethyl)phenyl)-*P*-ethynylphosphonamidate TFA salt (0.0628 mmol, 1.00 eq.) in 300 µl DMF were added drop-wise. The solution was allowed to warm to room-temperature and stirred for 2 h. All volatiles were removed under reduced pressure and the crude product was purified by flash column chromatography on silicagel (0% to 5% MeOH in CH_2Cl_2) and obtained as blue solid. (45 mg, 0.0590 mmol, 93.9 %).

^{1}H NMR (600 MHz, Chloroform-*d*) δ = 7.88 (td, *J*=13.0, 4.9, 2H), 7.43 – 7.33 (m, 4H), 7.23 (t, *J*=7.4, 2H), 7.15 – 7.07 (m, 4H), 7.01 (d, *J*=8.4, 2H), 6.72 (t, *J*=12.5, 1H), 6.46 (bs, 1H), 6.18 (dd, *J*=13.6, 8.5, 2H), 6.11 (q, *J*=7.6, 1H), 4.27 – 4.09 (m, 2H), 3.98 (t, *J*=7.6, 2H), 3.56 (s, 3H), 3.43 (q, *J*=6.9, 2H), 2.97 (d, *J*=12.8, 1H), 2.75 (t, *J*=7.5, 2H), 2.25 (t, *J*=7.3, 2H), 1.81 (p, *J*=8.0, 2H), 1.73 – 1.67 (m, 2H), 1.70 (s, 6H),

1.69 (s, 6H), 1.55 – 1.42 (m, 2H), 1.35 (t, *J*=7.1, 3H). ^{13}C NMR (151 MHz, CDCl3) δ = 173.64, 173.19, 173.11, 153.34, 152.99, 142.72, 141.90, 141.17, 140.89, 136.88, 133.32, 129.69, 128.78, 128.66, 126.32, 126.22, 125.34, 125.15, 122.21, 122.13, 118.60, 118.53, 110.83, 110.36, 103.77, 103.64, 88.54, 88.23, 75.27, 62.46, 49.40, 49.17, 44.22, 41.03, 35.94, 34.78, 27.96, 27.90, 27.84, 27.09, 26.32, 25.24, 16.17, 16.11, 16.04. ^{31}P NMR (243 MHz, CDCl3) δ = -9.08. HR-MS for $C_{44}H_{54}N_4O_3P^+$ $[M]^+$ calcd.: 717.3928, found 717.3895.

4.20. Ethyl-*N*-phenyl-*P*-(*Z*-ethylthioethenyl) phosphonamidate

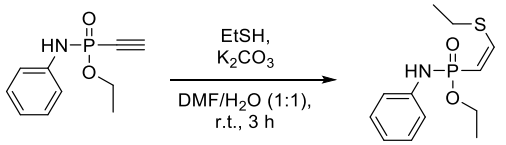

A 5-ml round bottom flask was charged with 50 mg Ethyl-*N*-phenyl-*P*-ethynylphosphonamidate (0.239 mmol, 1.0 eq.), 13.2 mg potassium carbonate (0.096 mmol, 0.4 eq.), 0.5 ml DMF and 0.5 ml water. 26.5 µl ethane thiol (0.359 mmol, 1.5 eq.) were added through a microliter syringe and the solution was stirred for 3 h at room temperature. All volatiles were removed under reduced pressure and the crude product was purified by flash column chromatography on silicagel (70% EtOAc in *n*-hexan to 100% EtOAc) and obtained as a yellowish solid. (56.0 mg, 0.206 mmol, 86.3%)

^{1}H NMR (600 MHz, Chloroform-*d*) δ 7.22 (t, *J* = 7.9 Hz, 2H), 7.12 (dd, *J* = 46.4, 12.5 Hz, 1H), 7.05 – 6.99 (m, 2H), 6.92 (t, *J* = 7.4 Hz, 1H), 6.65 (d, *J* = 6.1 Hz, 1H), 5.77 (dd, *J* = 16.5, 12.5 Hz, 1H), 4.40 – 3.97 (m, 2H), 2.73 (q, *J* = 7.4 Hz, 2H), 1.35 (t, *J* = 7.1 Hz, 3H), 1.26 (t, *J* = 7.4 Hz, 3H). ^{13}C NMR (75 MHz, Chloroform-d) δ 149.92, 140.44 (d, J = 1.0 Hz), 129.07, 121.03, 117.39, 117.30, 113.32, 110.94, 60.25 (d, J = 6.0 Hz), 29.42, 16.30 (d, J = 7.0 Hz), 15.40. ^{31}P NMR (122 MHz, CDCl3) δ 14.73. HR-MS for $C_{12}H_{19}NO_2PS^+$ $[M+H]^+$ calcd.: 272.0869, found 272.0856.

4.21. Ethyl-*N*-phenyl-*P*-(*E*-ethylthioethenyl) phosphonamidate

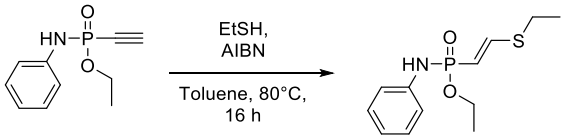

A 5-ml round bottom flask was charged with 40 mg Ethyl-*N*-phenyl-*P*-ethynylphosphonamidate (0.191 mmol, 1.0 eq.), 12.6 mg azobisisobutyronitrile (0.076 mmol, 0.4 eq.), 16.5 µl ethane thiol (0.229 mmol, 1.2 eq.) and 0.8 ml toluene. The brownish solution was heated to 80 °C over night. The reaction mixture was purified by flash column chromatography on silicagel (70% EtOAc in *n*-hexan to 100% EtOAc) and obtained as a yellowish solid. (22.0 mg, 0.081 mmol, 42.1%)

^{1}H NMR (300 MHz, Chloroform-*d*) δ 7.44 (dd, *J* = 21.6, 16.8 Hz, 1H), 7.28 – 7.20 (m, 2H), 7.03 – 6.90 (m, 3H), 6.33 (d, *J* = 6.0 Hz, 1H), 5.74 (t, *J* = 16.8 Hz, 1H), 4.40 – 3.85 (m, 2H), 2.75 (q, *J* = 7.4 Hz, 2H), 1.34 (t, *J* = 7.0 Hz, 3H), 1.28 (t, *J* = 7.4 Hz, 3H). ^{13}C NMR (75 MHz, Chloroform-*d*) δ 148.42 (d, *J* = 9.1 Hz), 140.34, 129.34, 121.23, 117.25, 117.16, 111.53, 109.13, 60.55 (d, *J* = 6.0 Hz), 25.76, 16.27 (d, *J* = 7.1 Hz), 13.64. ^{31}P NMR (122 MHz, $CDCl_3$) δ 15.42. HR-MS for $C_{12}H_{19}NO_2PS^+$ $[M+H]^+$ calcd.: 272.0869, found 272.0856.

4.22. DABCYl-Cys peptide

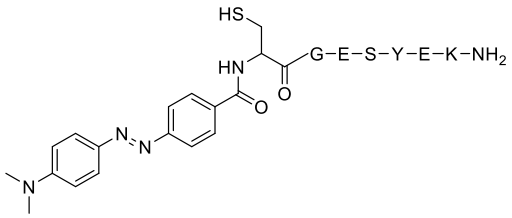

DABCYl-Cys peptide was synthesized by standard Fmoc-based chemistry in a linear synthesis by manual coupling. 0.1 mmol of Rink amide resin (subst: 0.4 mmol/g) was added to a reaction vessel and synthesis was performed with five-fold amino acid excess. Fmoc de-blocking was achieved by resin treatment with 20% piperidine in DMF twice for 5 min. Coupling was achieved by addition of HOBt/HBTU/DIPEA (5 eq./5 eq./10 eq) in DMF for 45 min. After the final Cys coupling, 5 eq. of the DABCYL acid was coupled with 5 eq. HATU and 10 eq. DIPEA in DMF for 45 min. The peptide was cleaved of the resin by addition of TFA/DTT/TIS (95/2.5/2.5, *w*,*w*,*w*) within 3 h. Subsequently, the peptide was precipitated by the addition of ice-cold diethyl ether. The precipitate was collected by centrifugation, dried and purified by preparative HPLC (method C). The peptide was obtained as a red solid in a yield of 35.8% (38.2 mg, 35.8 µmol). ESI-MS for $C_{48}H_{66}N_{12}O14S^{+}$ $[M+2H]^{+}$ calcd.: 533.23, found 533.34.

4.23. DABCYl-Cys peptide phosphonamidate EDANS adduct

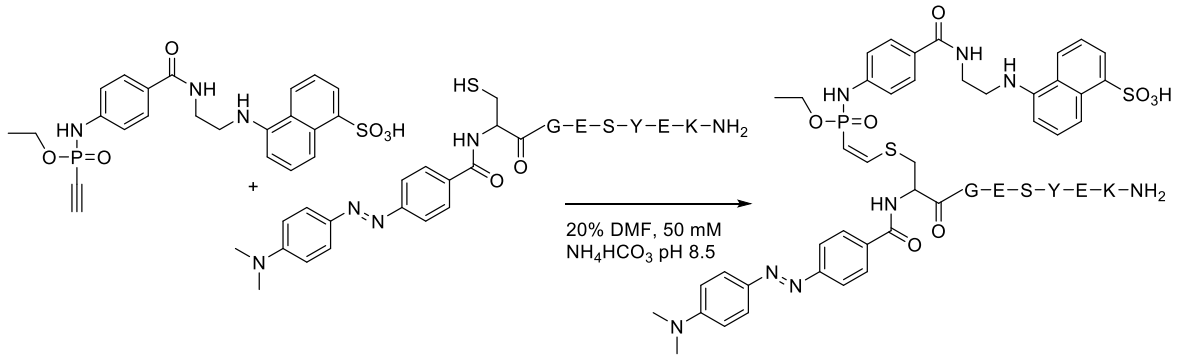

A 1.5-ml Eppendorf tube was charged with 263 µl of a solution of DABCYL-Cys peptide (20 mM) in 50 mM NH_4HCO_3 at a pH of 8.5. 158 µl 50 mM NH_4HCO_3 at a pH of 8.5 and 105 µl of a solution of EDANS phosphonamidate (100 mM) in DMF was added to give a final concentration of 20 mM peptide and 10 mM phosphonamidate in 20% DMF/Buffer. The tube was shaken at 800 rpm at room temperature for 3 h. All volatiles were removed under reduced pressure and the crude product purified by semi-preparative HPLC (method E). The peptide was obtained as a red solid. HR-MS for $C_{71}H_{90}N_{15}O_{20}PS_2^{2+}$ $[M+2H]^{2+}$ calcd.:783.7827, found 783.7804.

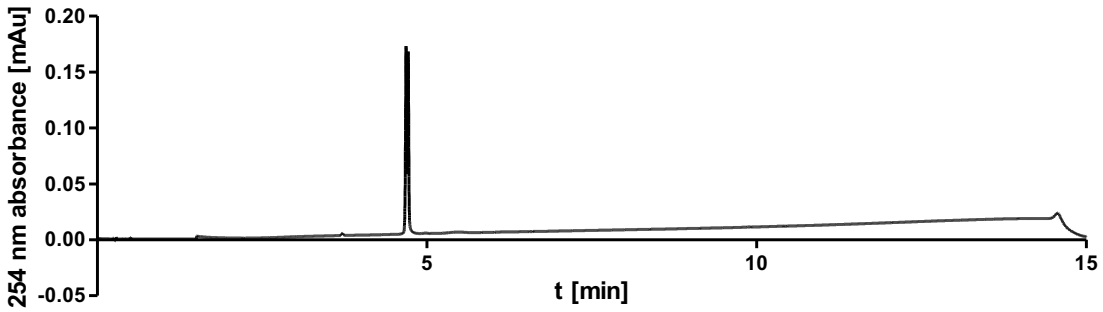

4.24. DABCYl-Cys peptid maleimide EDANS adduct

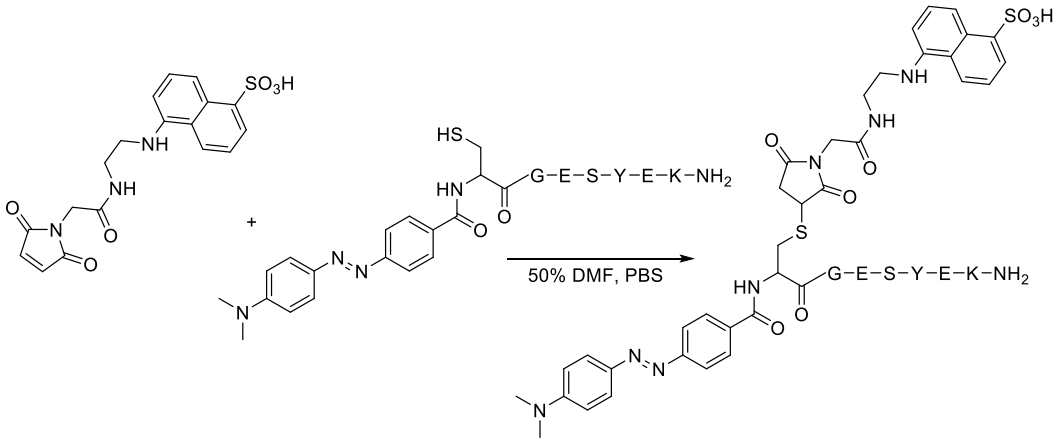

A 1.5-ml Eppendorf tube was charged with 188 µl of a solution of DABCYl-Cys peptide (20 mM) in PBS. 188 µl of a solution of EDANS maleimide (40 mM) in DMF was added to give a final concentration of 10 mM peptide and 20 mM maleimide in 50% DMF/buffer. The tube was shaken at 800 rpm at room temperature for 3 h. All volatiles were removed under reduced pressure and the crude product purified by semi-preparative HPLC (method E). The peptide was obtained as a red solid. HR-MS for $C_{66}H_{83}N_{15}O_{20}S_2^{2+}$ $[M+2H]^{2+}$ calcd. 734.7685, found. 734.7698.

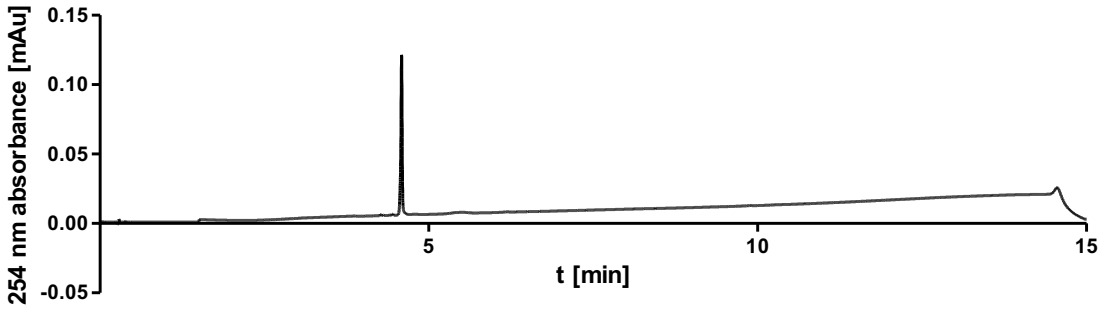

5. NMR spectra

Diethyl ethynylphosphonite (crude reaction mixture)

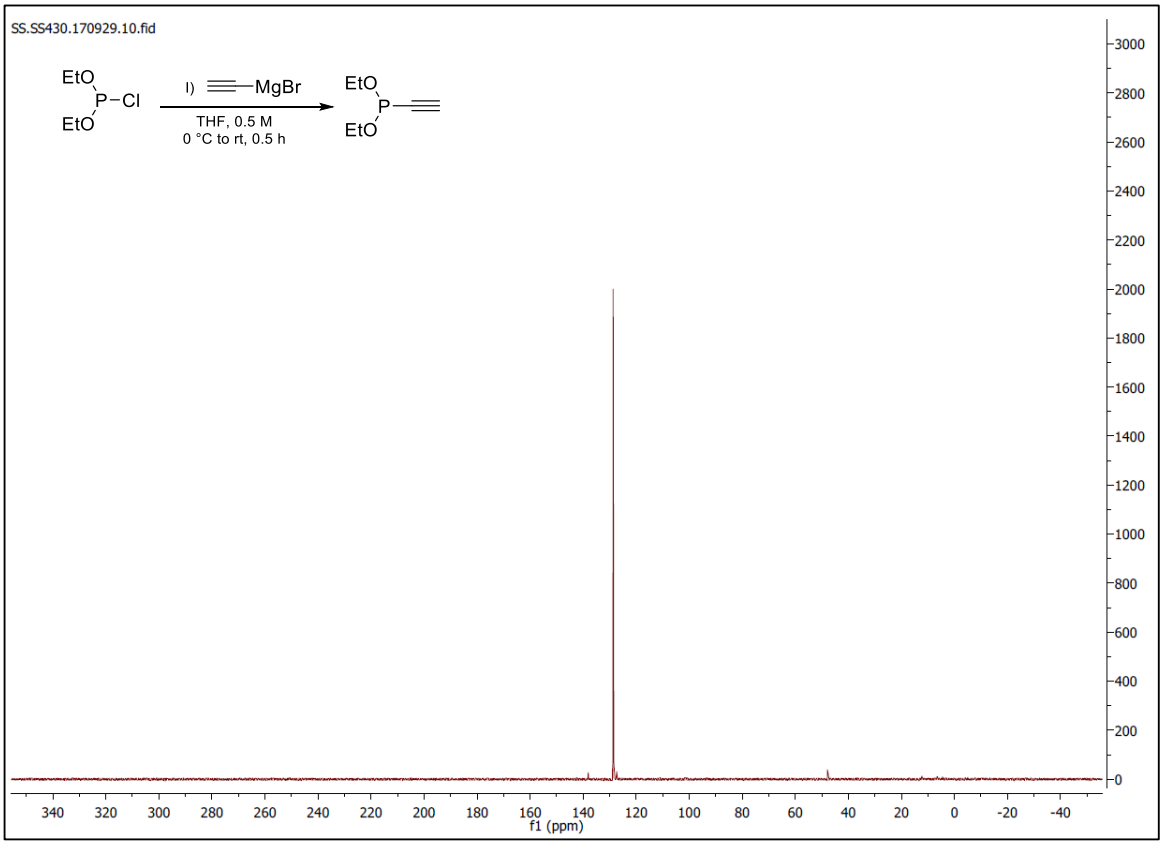

Ethyl-*N*-phenyl-*P*-ethynylphosphonamidate (**1**)

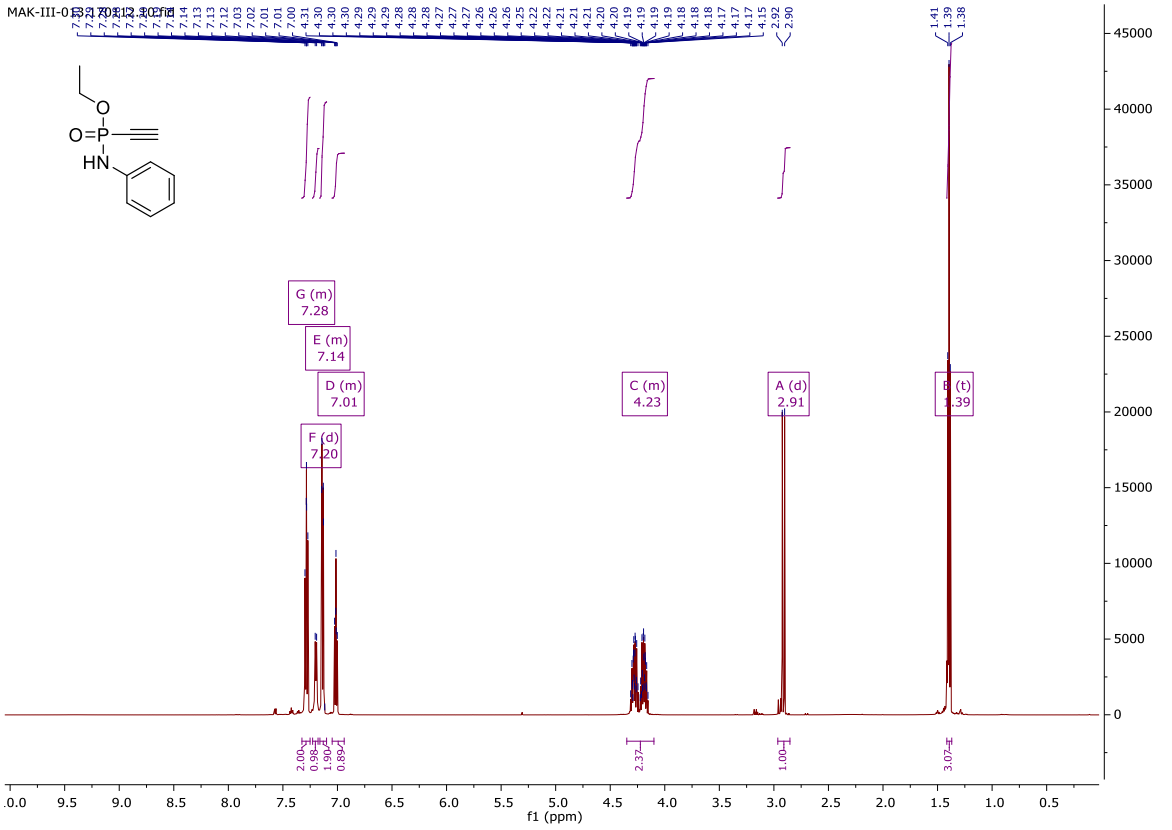

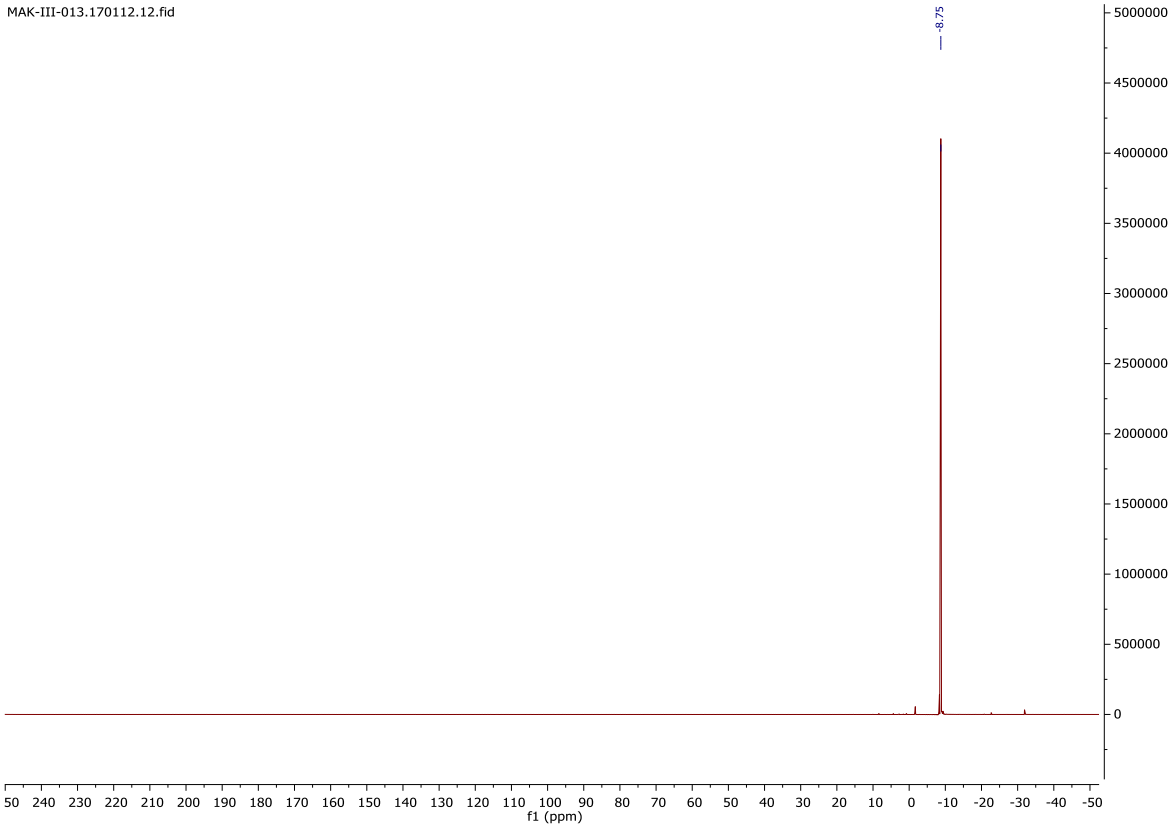

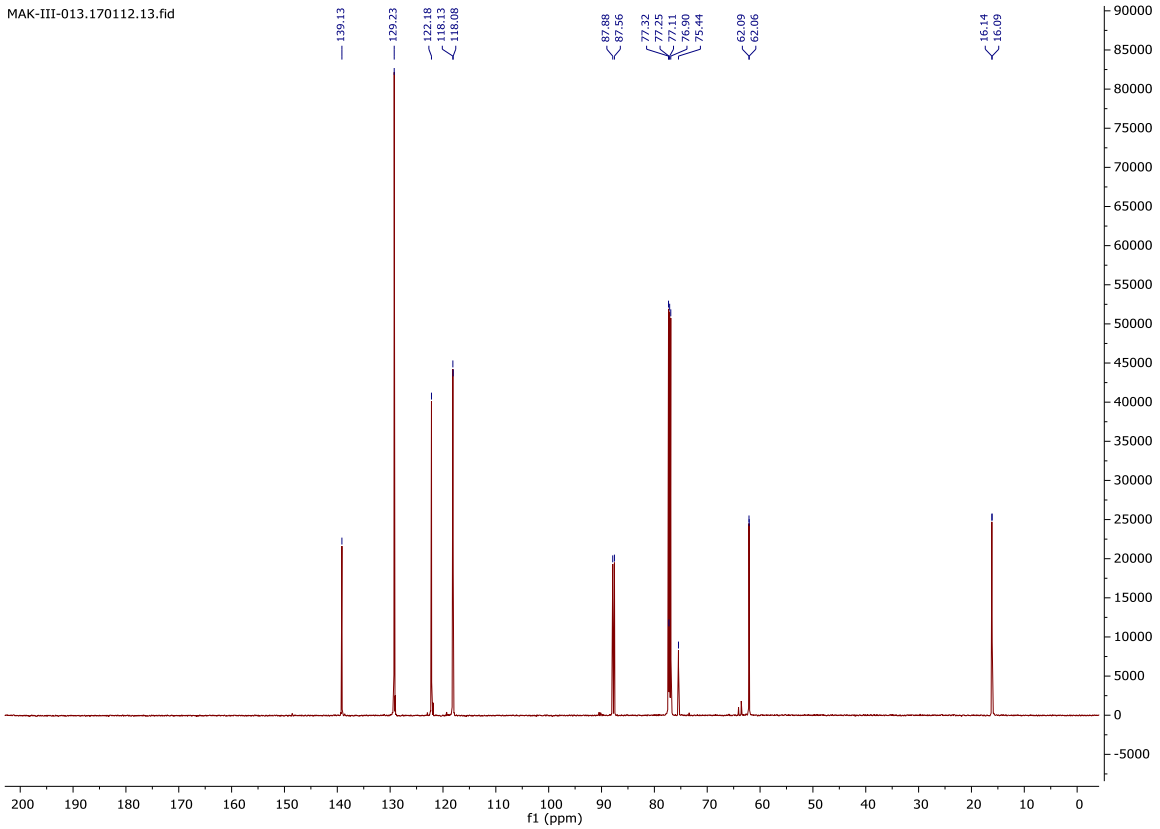

Ethyl-*N*-(4-carboxy-phenyl)-*P*-ethynylphosphonamidate (**2**)

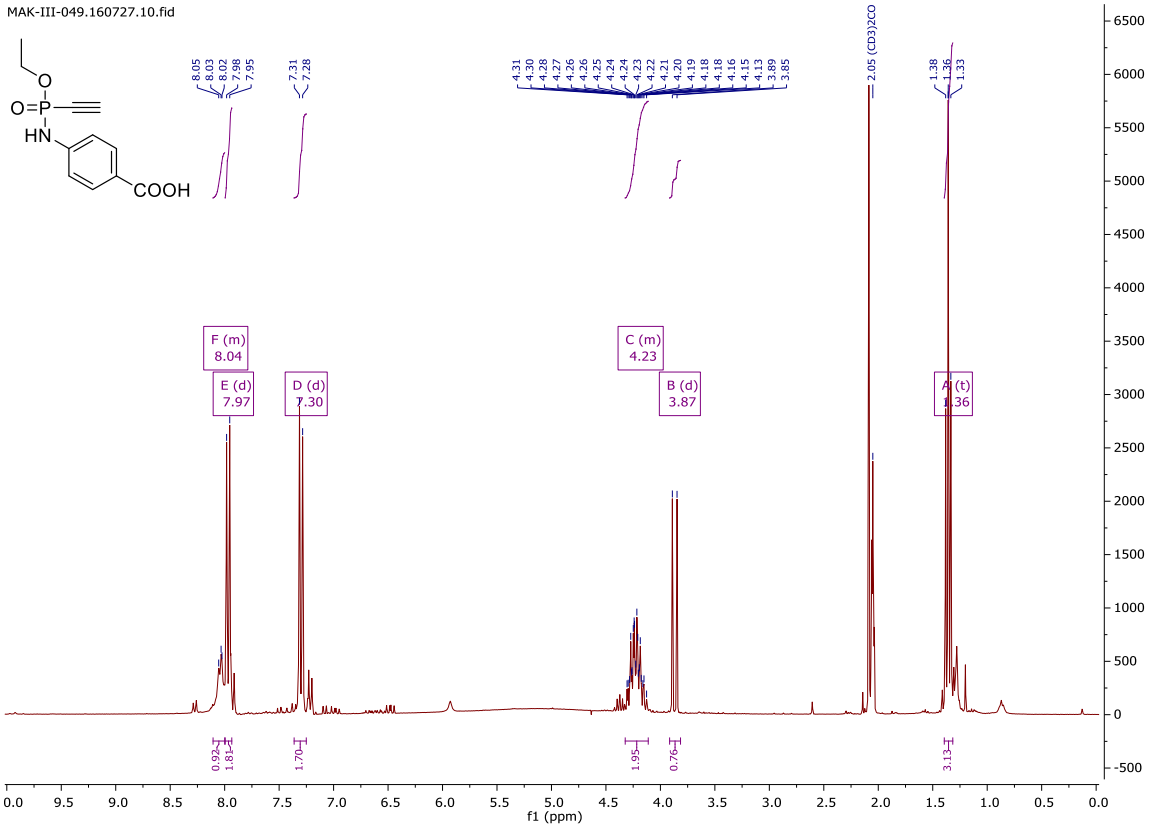

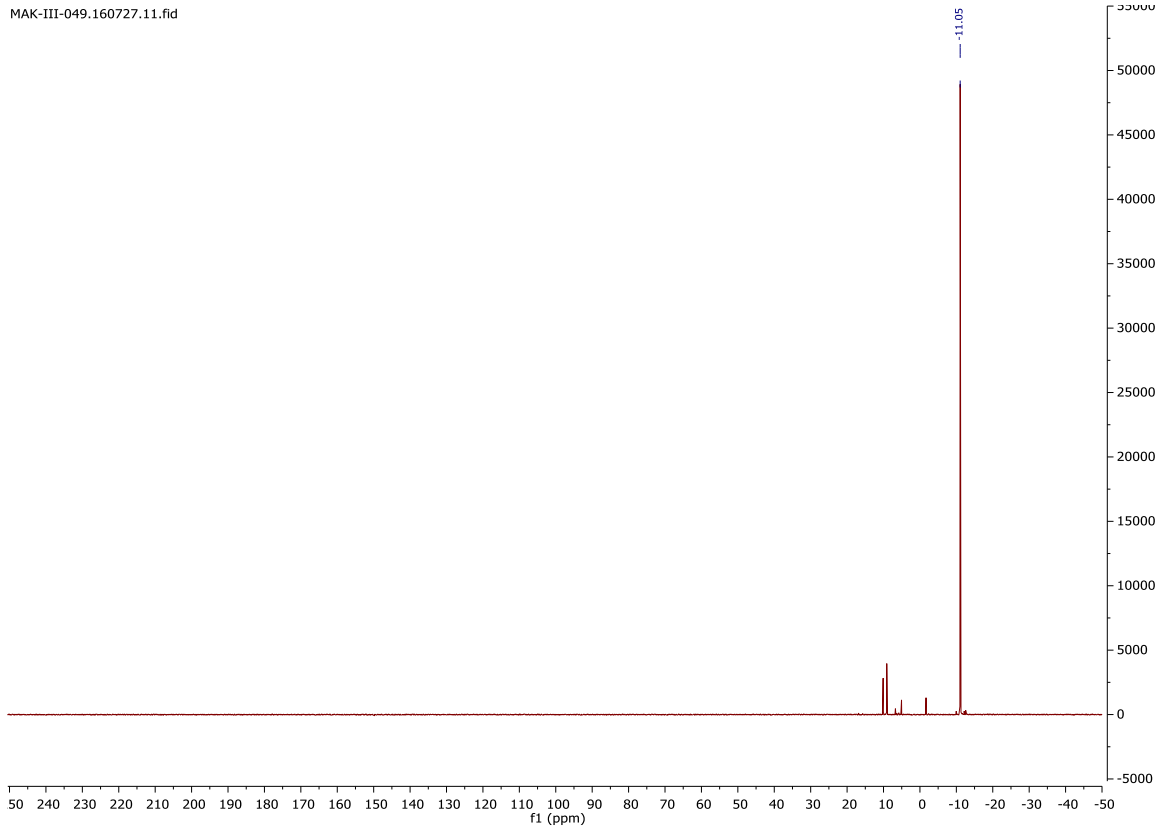
MAK-III-049.160727.11.fid
-11.05
f1 (ppm)

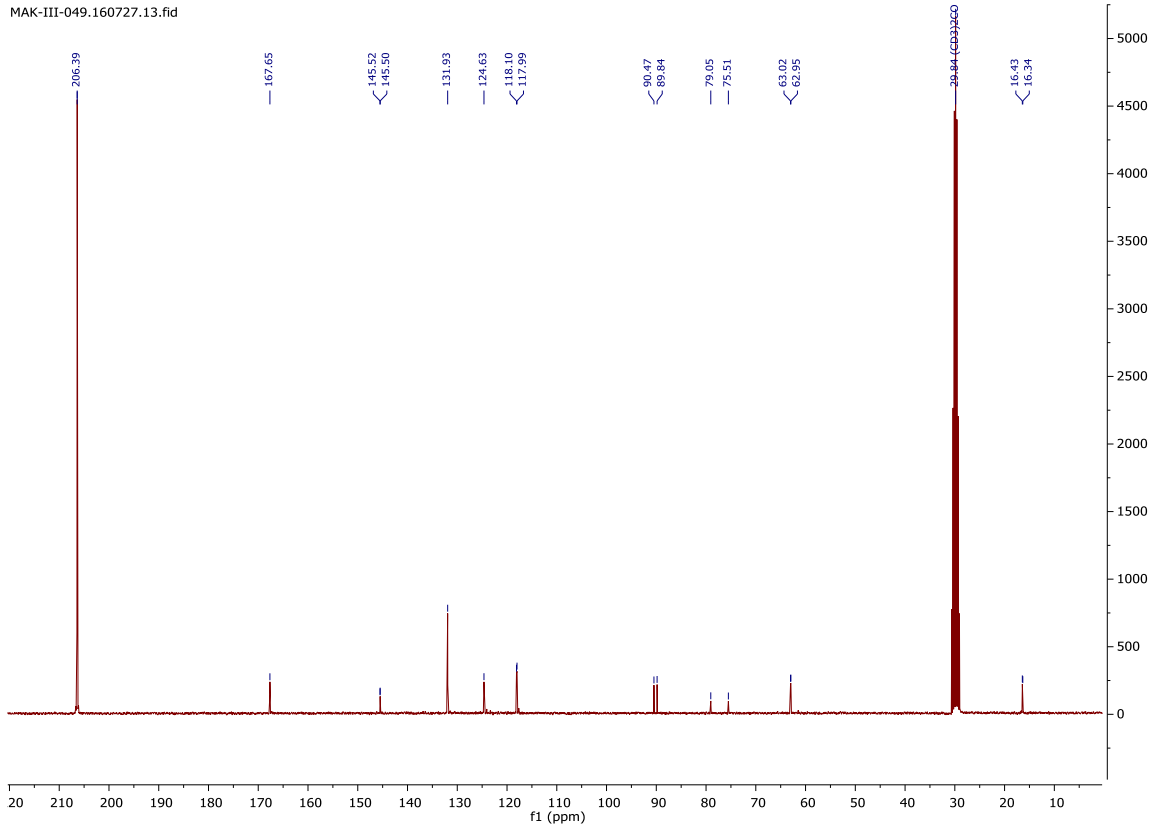
MAK-III-049.160727.13.fid
206.39
167.65
145.52
145.50
131.93
124.63
118.10
117.99
90.47
89.84
79.05
75.51
63.02
62.95
29.84 (CD3)2CO
16.43
16.34
f1 (ppm)

Ethyl-*N*-(4-(2,5-dioxo-1-pyrrolidinyl)oxy-carbonyl-phenyl)-*P*-ethynylphosphonamidate (**3**)

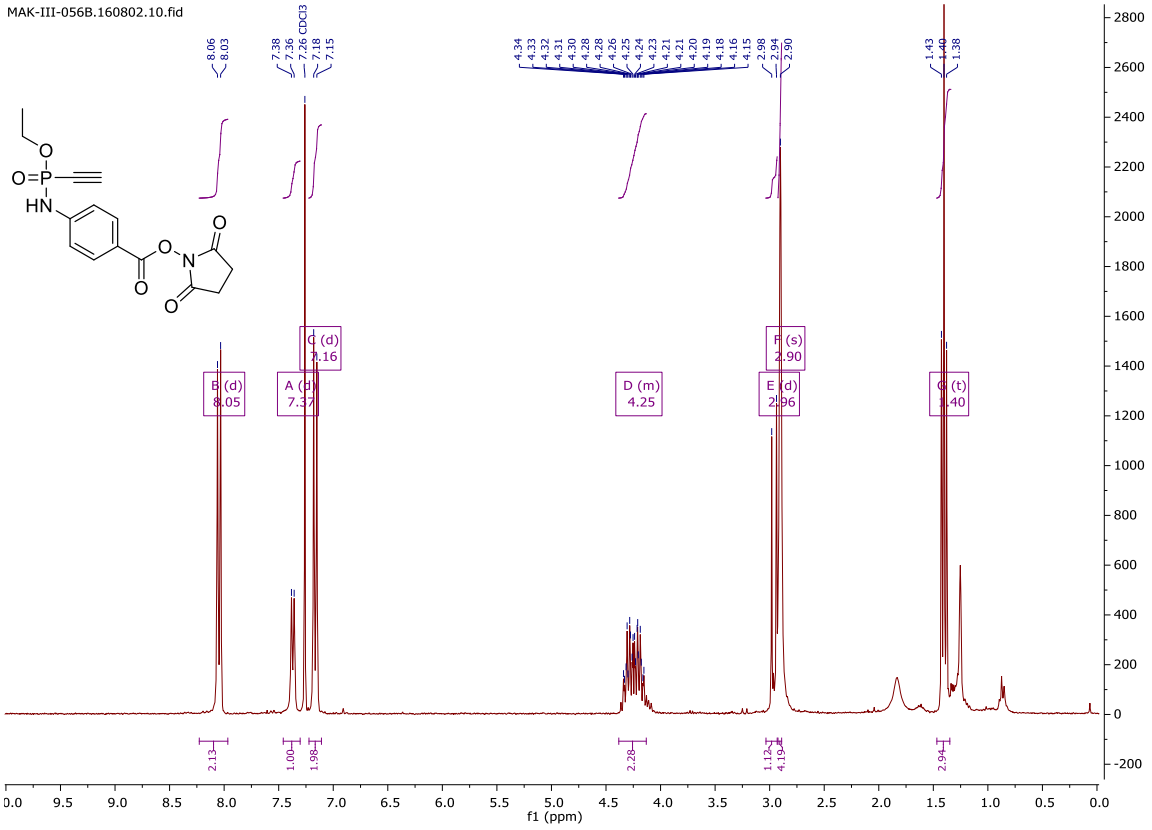

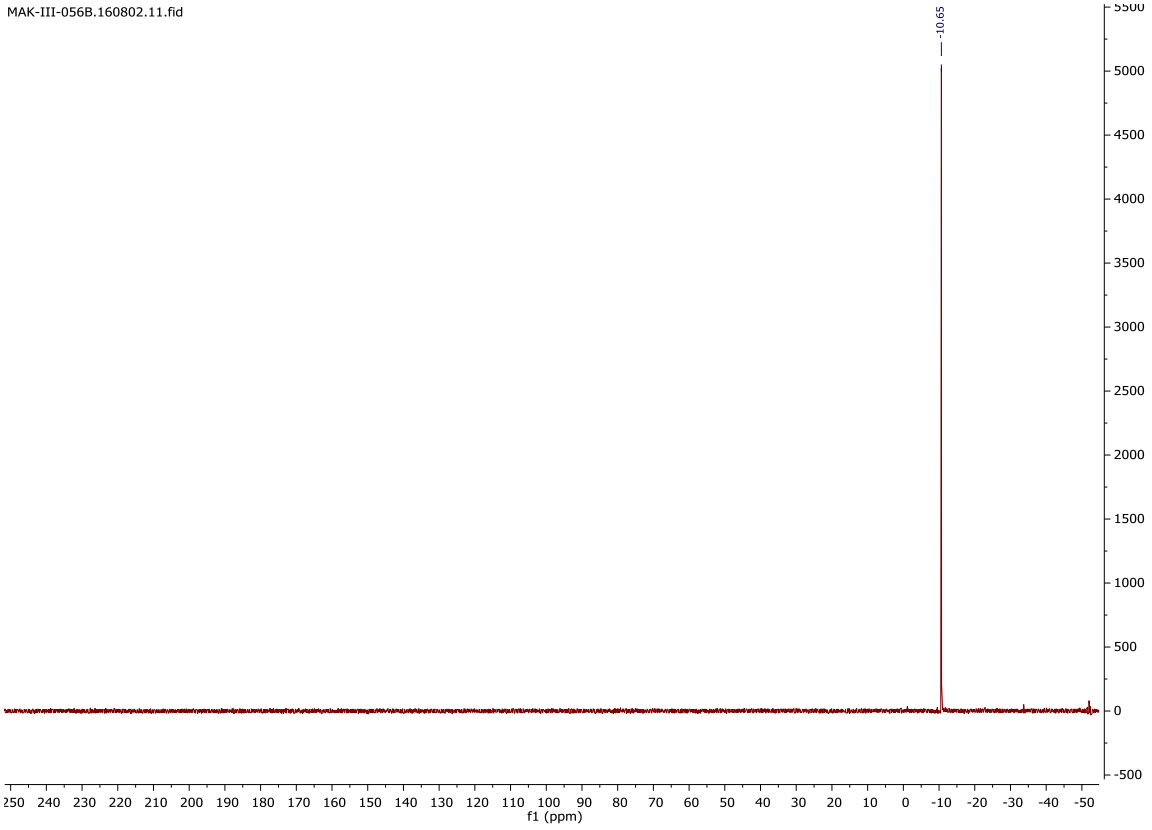

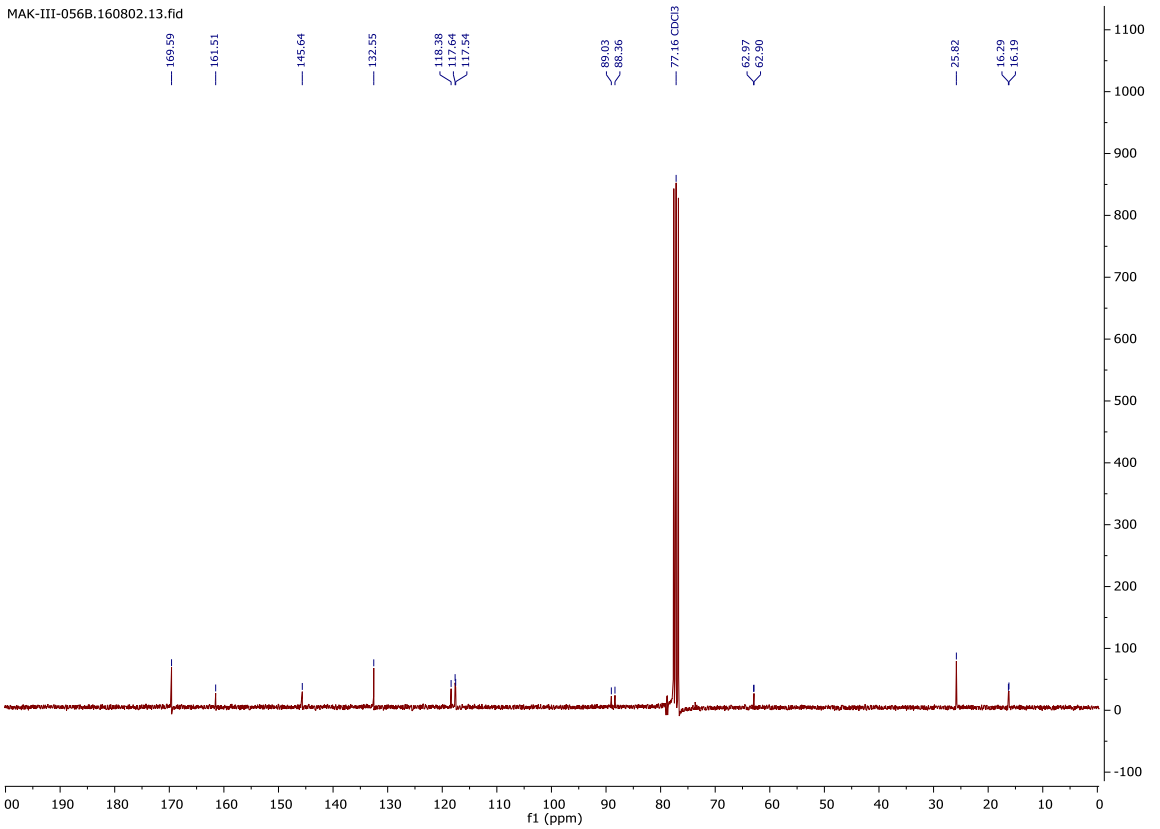

2-(4-Azidophenyl)-ethyl phtalimide

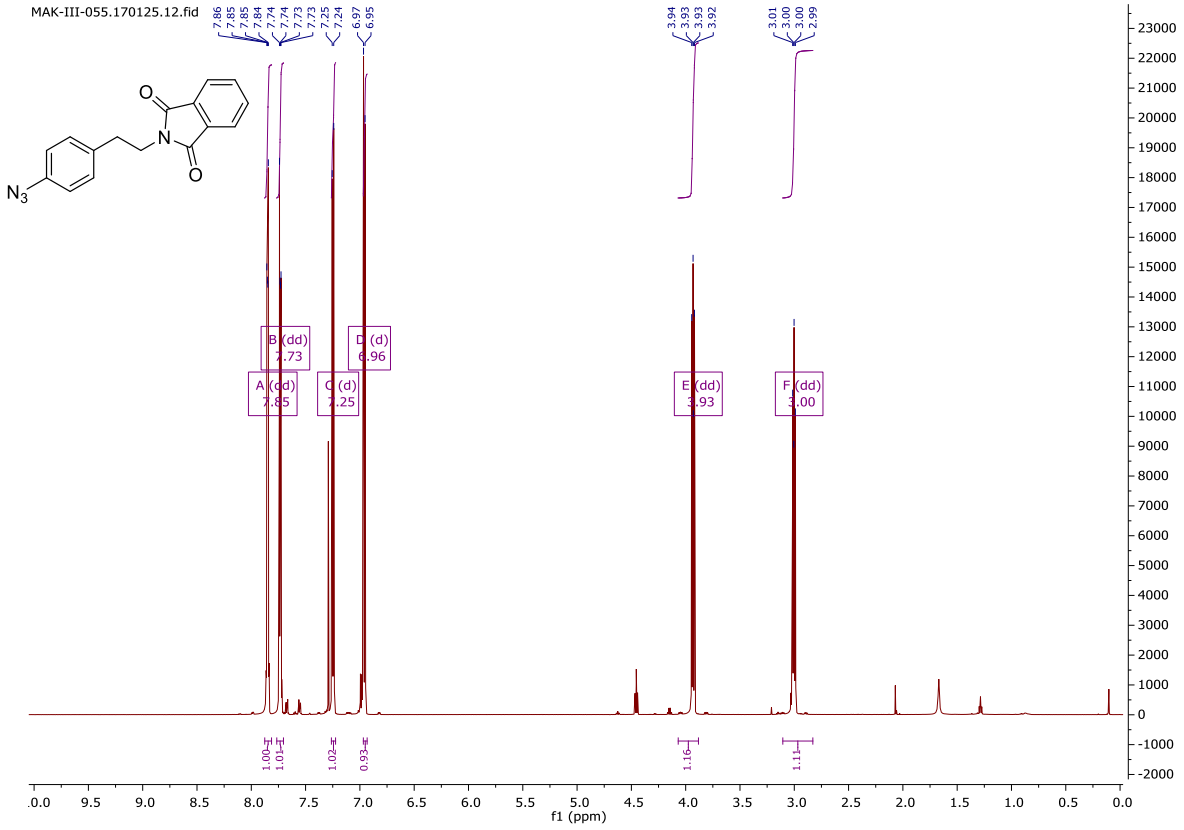

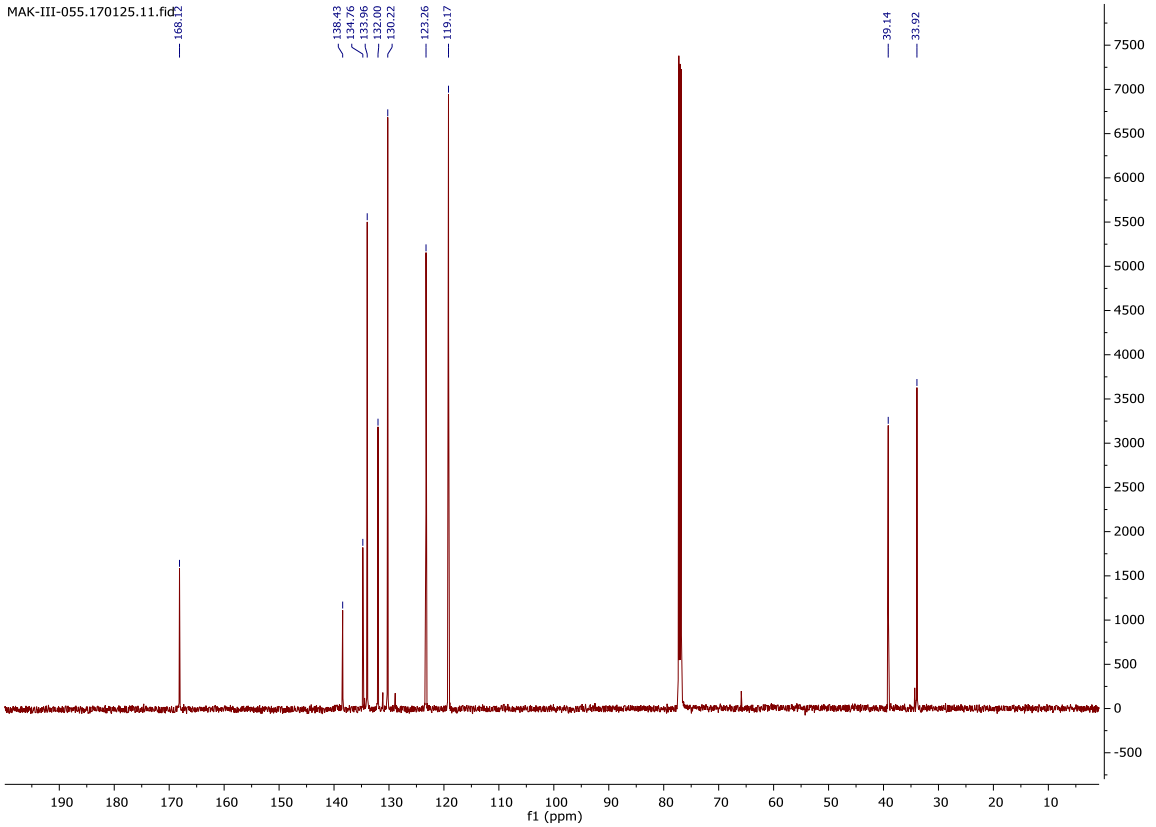

Ethyl-*N*-(4-(2-aminoethyl)phenyl)-*P*-ethynylphosphonamidate TFA salt (**4**)

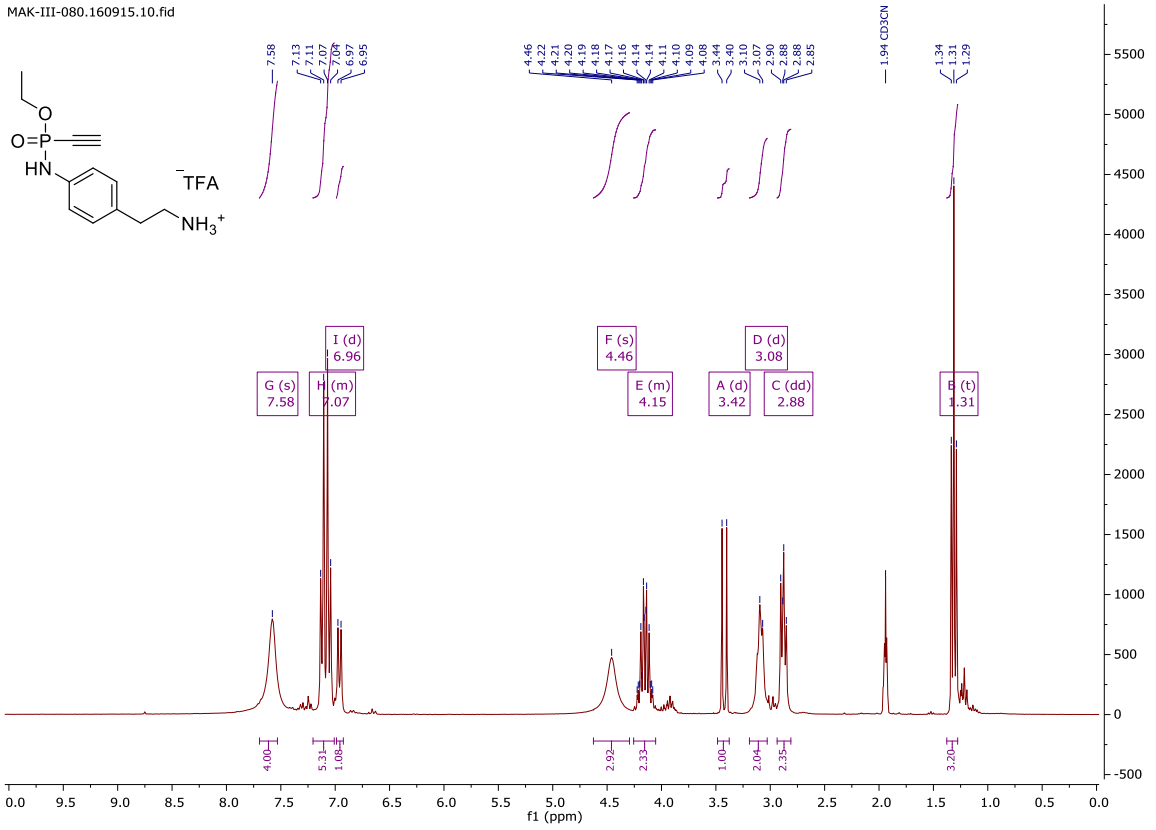

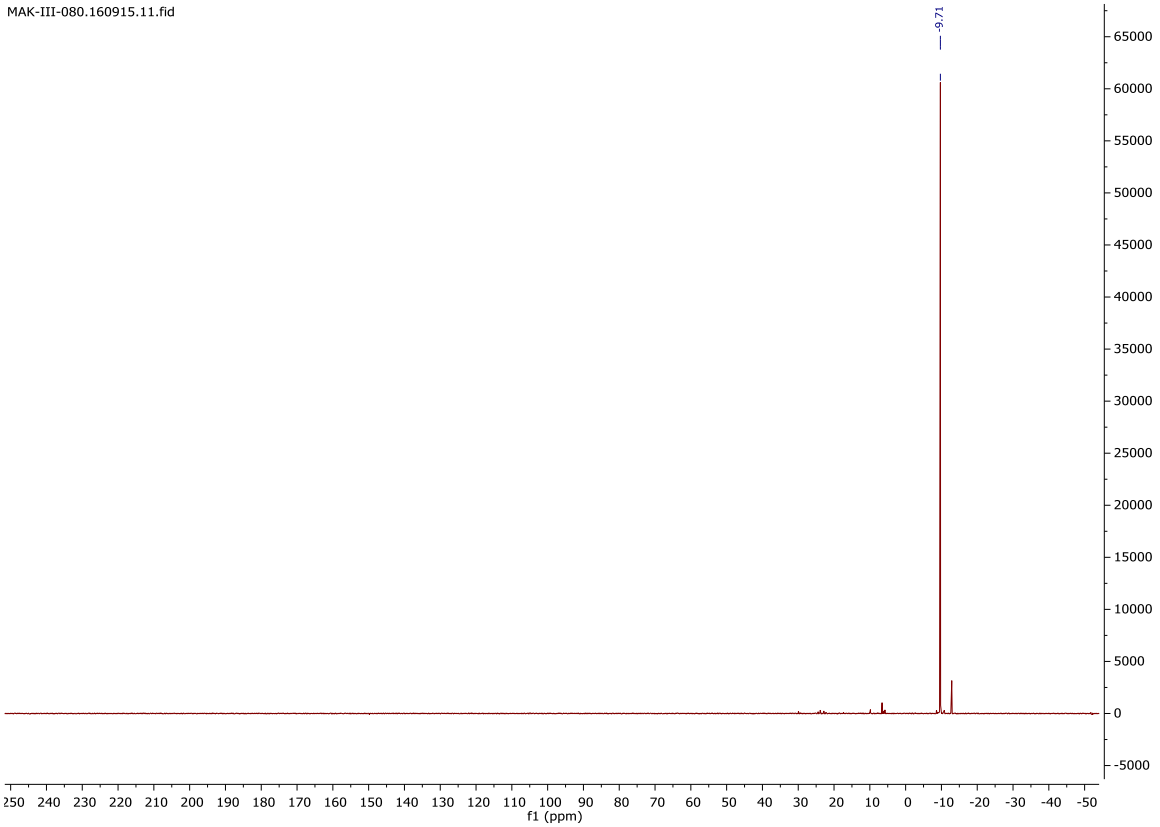
MAK-III-080.160915.11.fid
-9.71
f1 (ppm)

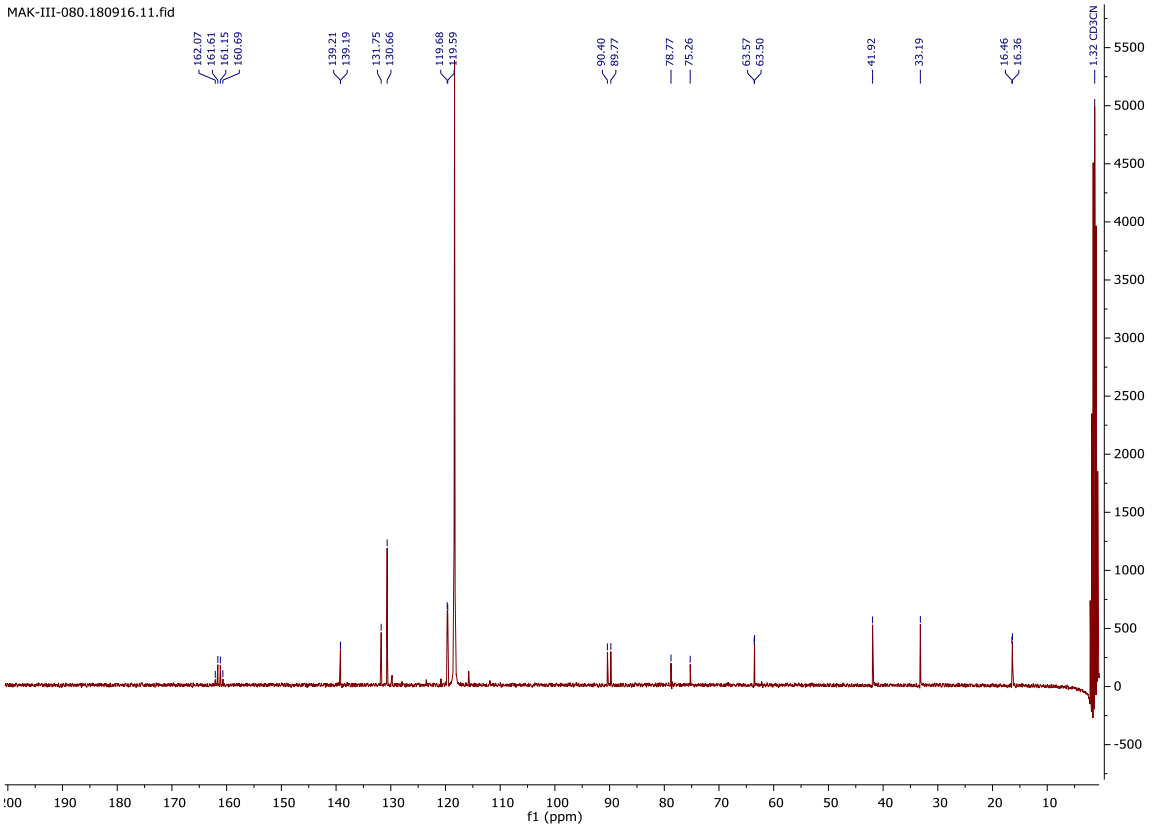
MAK-III-080.180916.11.fid
162.07
161.61
161.15
160.69
139.21
139.19
131.75
130.66
119.68
119.59
90.40
89.77
78.77
75.26
63.57
63.50
41.92
33.19
16.46
16.36
1.32 CD3CN
f1 (ppm)

N-(4-azidophenyl) biotinamide

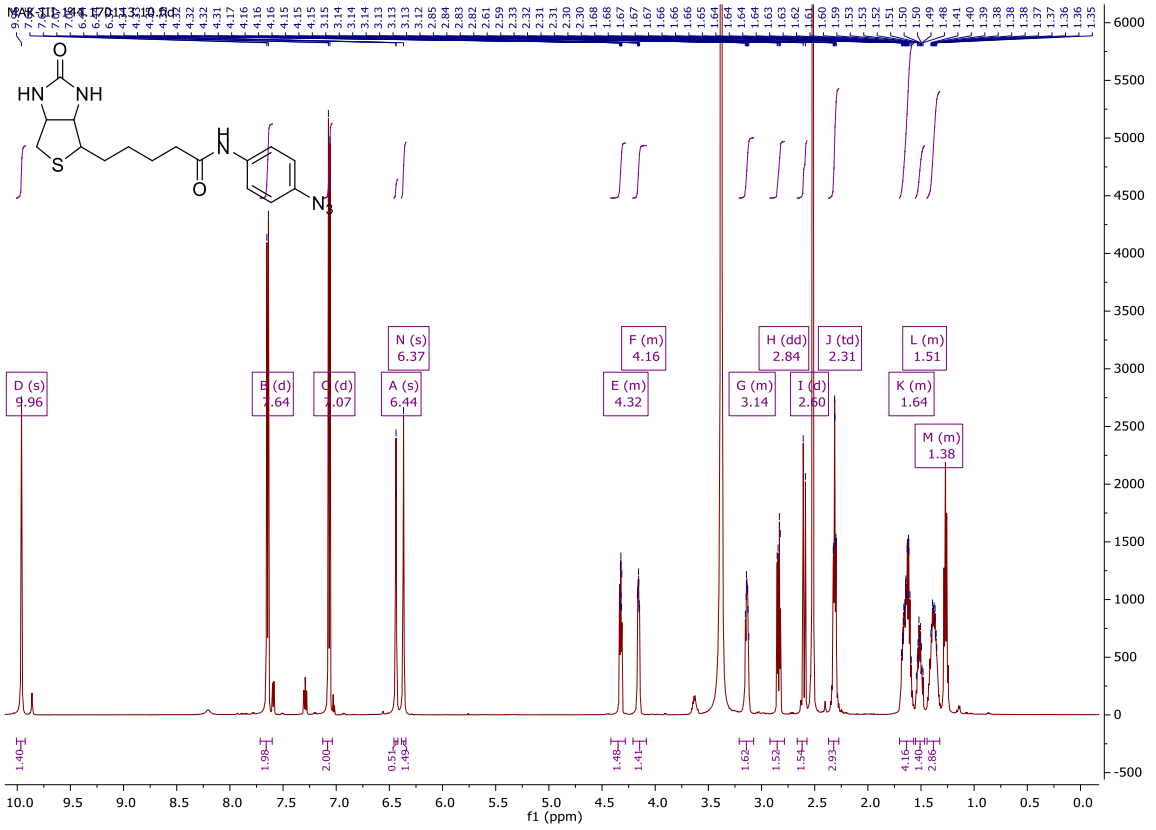

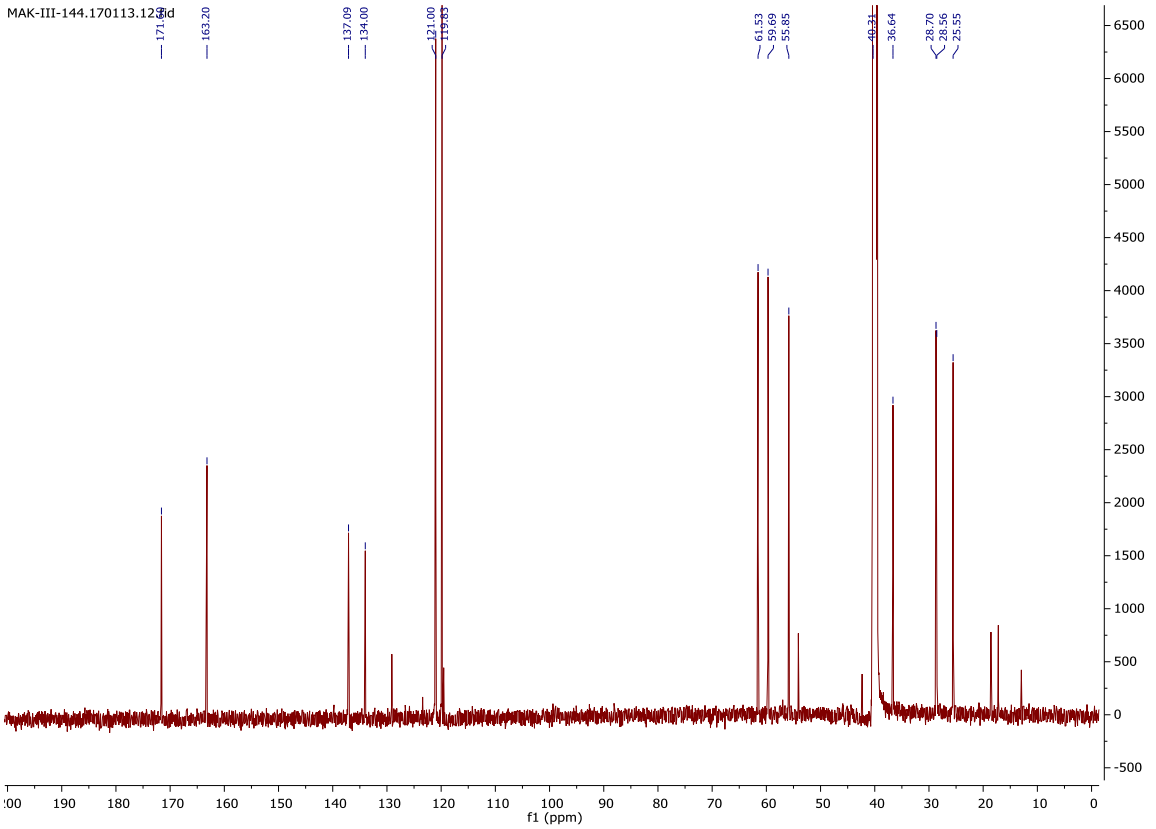

Ethyl-*N*-(4-biotinamido-phenyl)-*P*-ethynylphosphonamidate (**5**)

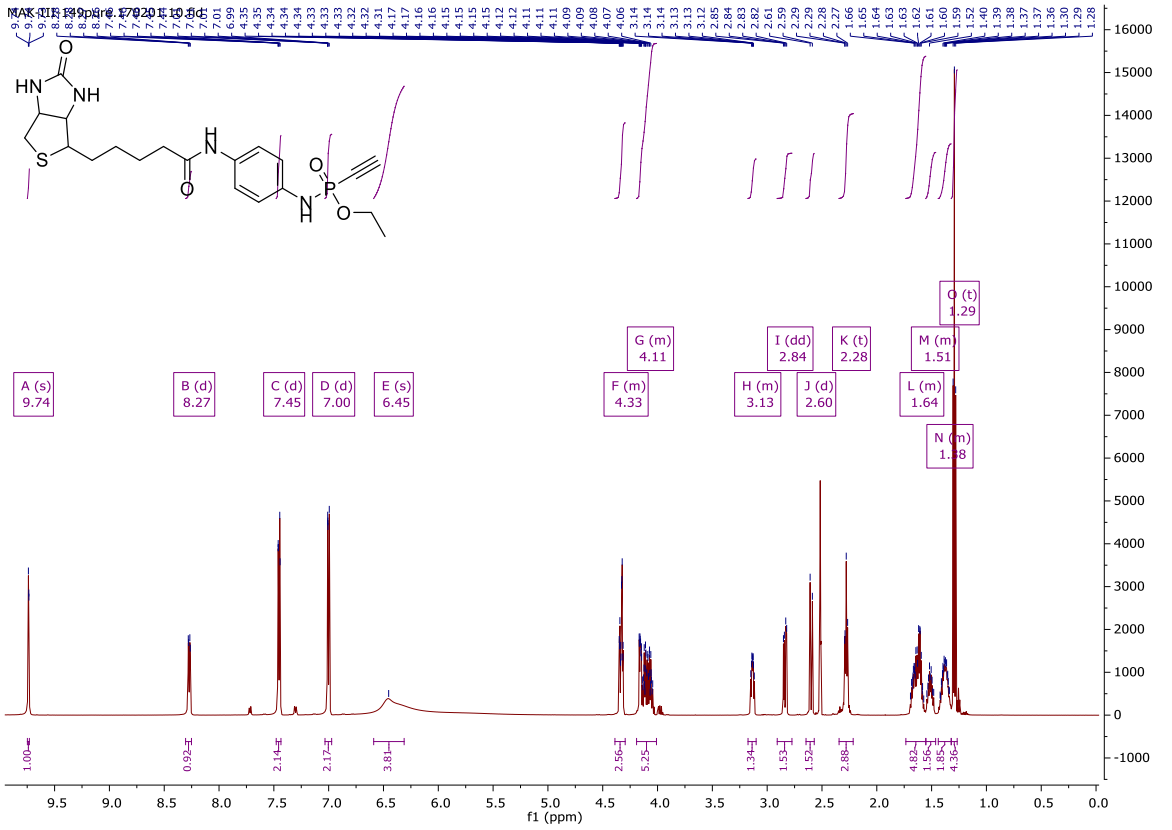

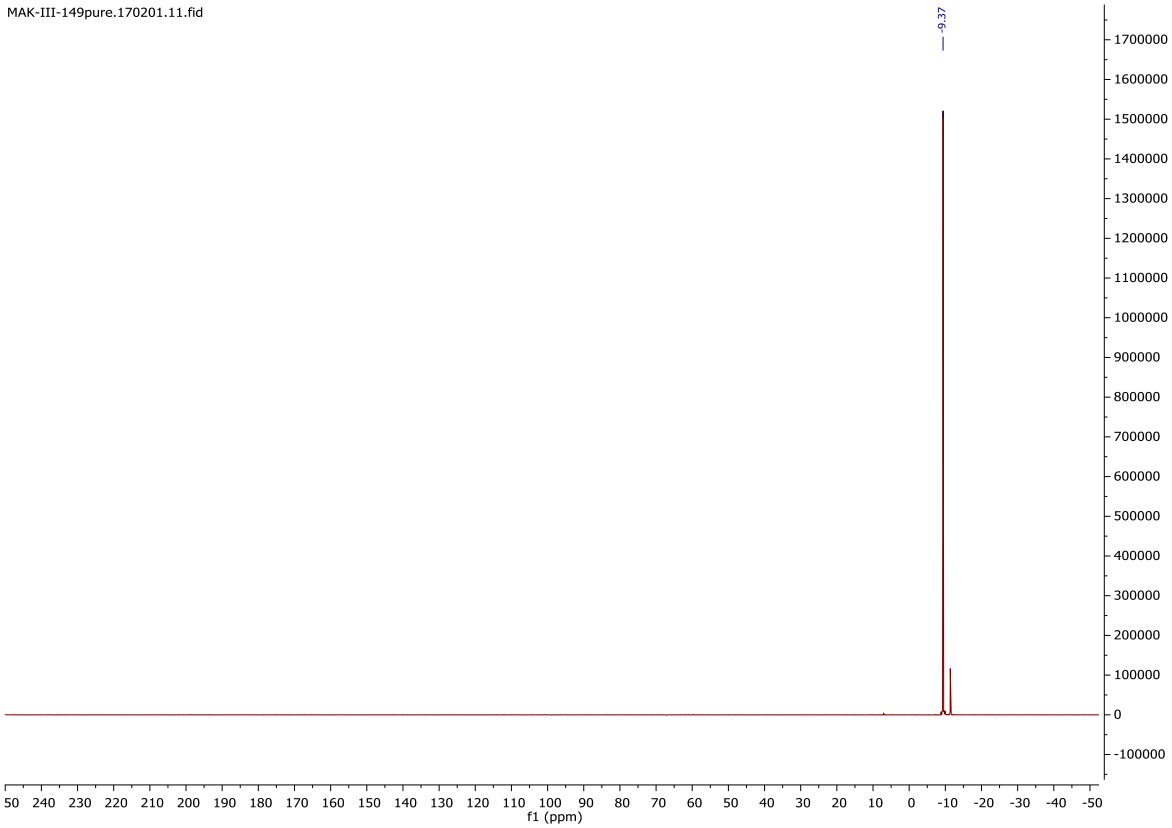

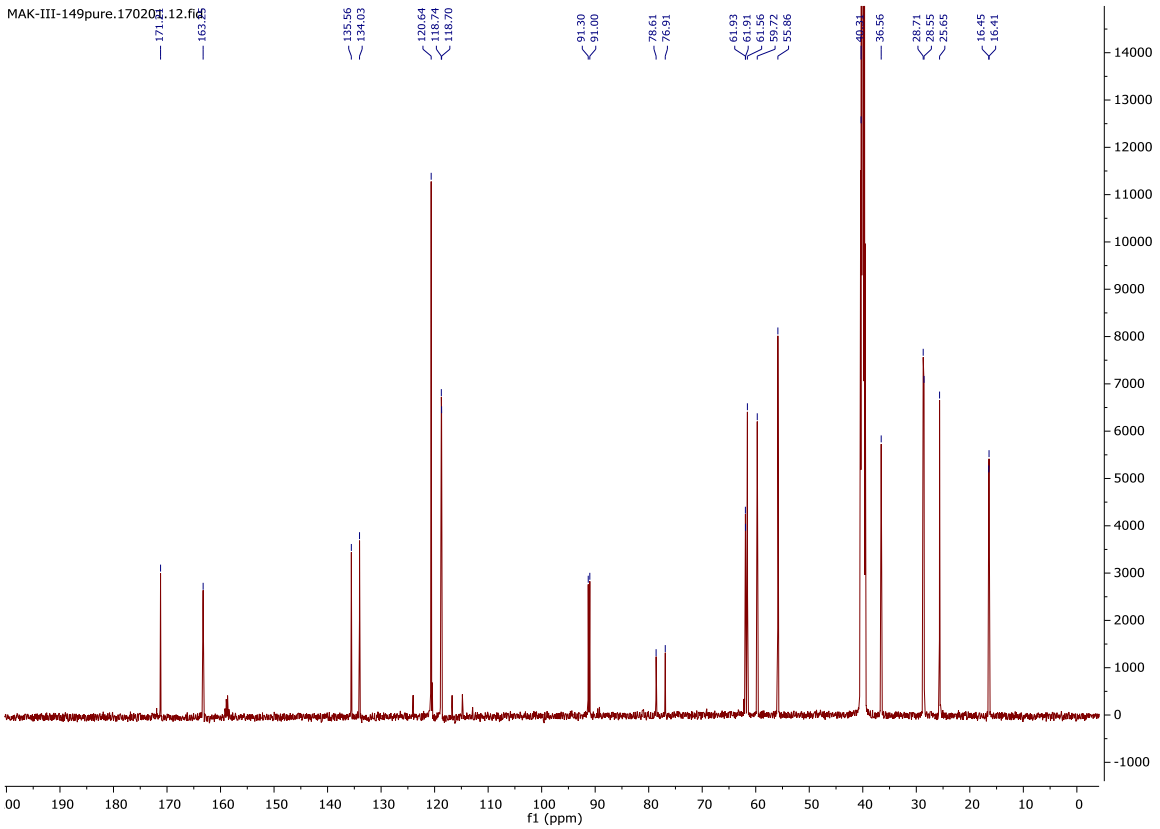

Ethyl-*N*-(3-phenyl-propyl)-*P*-ethynylphosphonamidate (**6**)

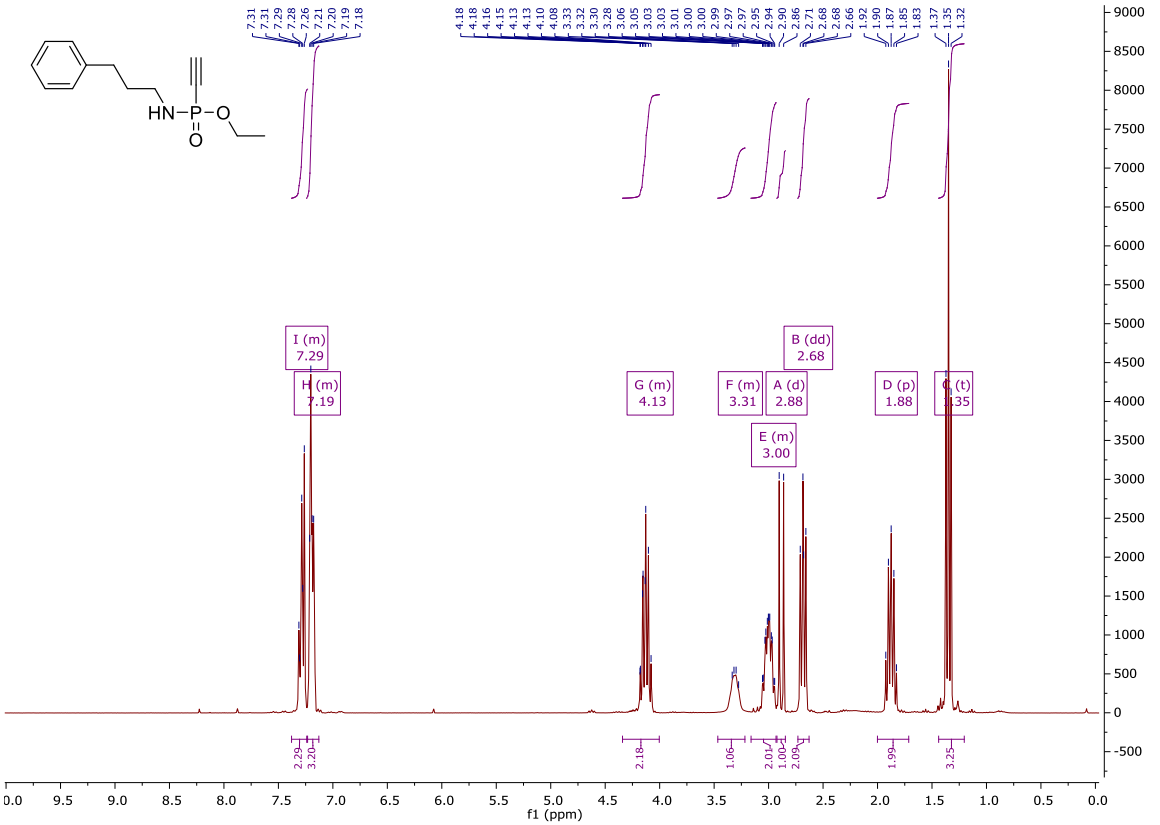

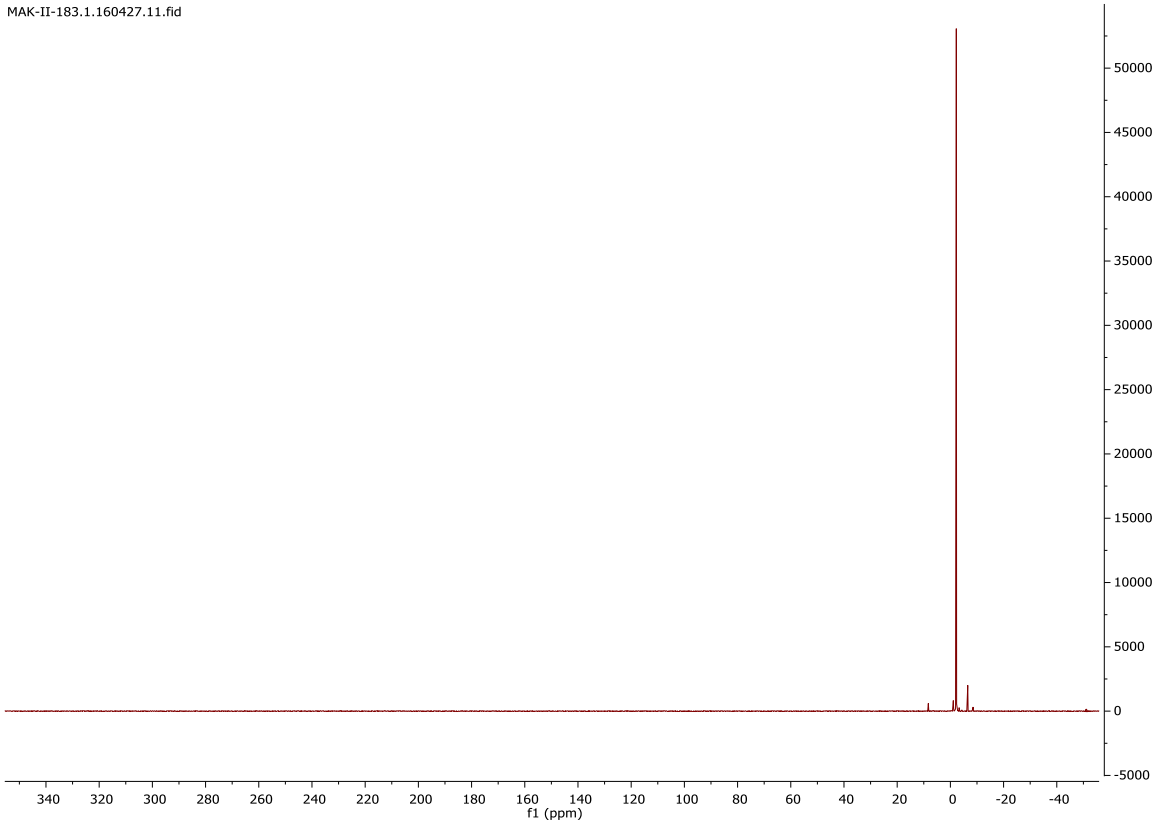
MAK-II-183.1.160427.11.fid
f1 (ppm)

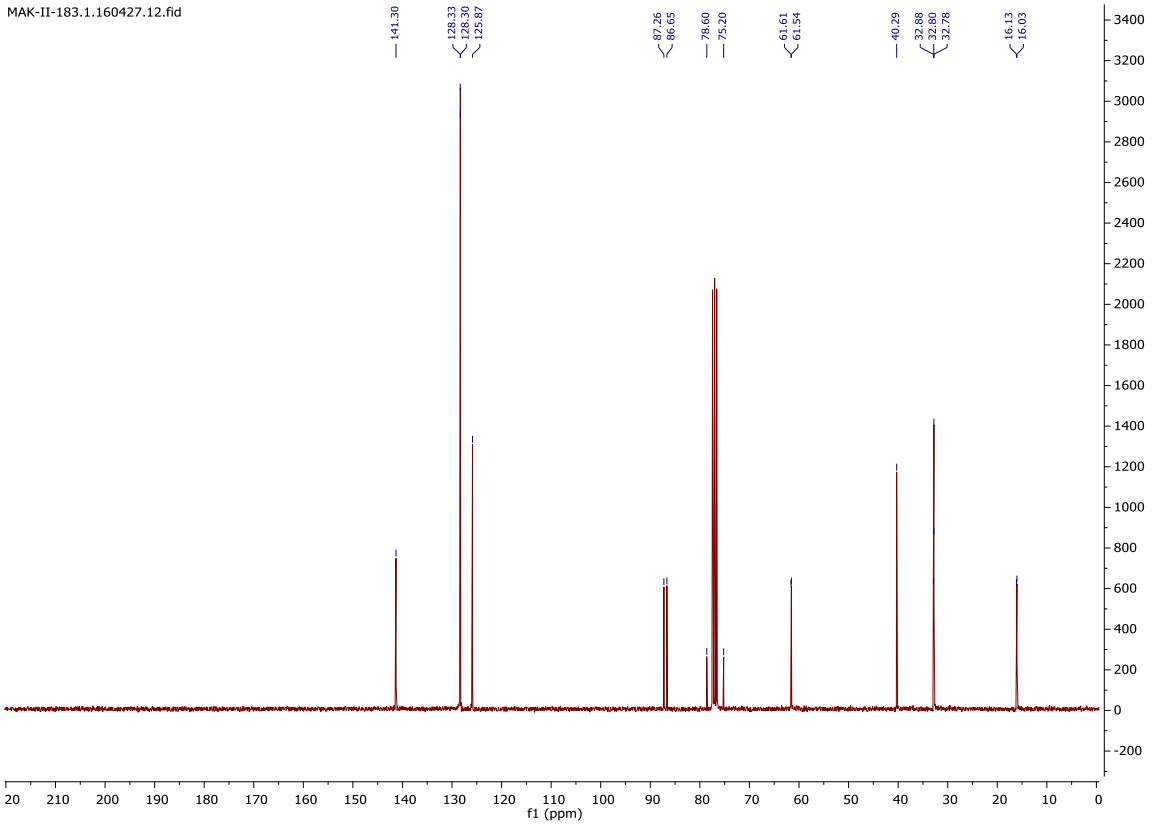
MAK-II-183.1.160427.12.fid
141.30
128.33
128.30
125.87
87.26
86.65
78.60
75.20
61.61
61.54
40.29
32.88
32.80
32.78
16.13
16.03
f1 (ppm)

5-((2-(*O*-Ethyl-*P*-ethynyl-phosphonamidato-*N*-benzoyl)ethyl)amino)naphthalene-1-sulfonic acid (**10**)

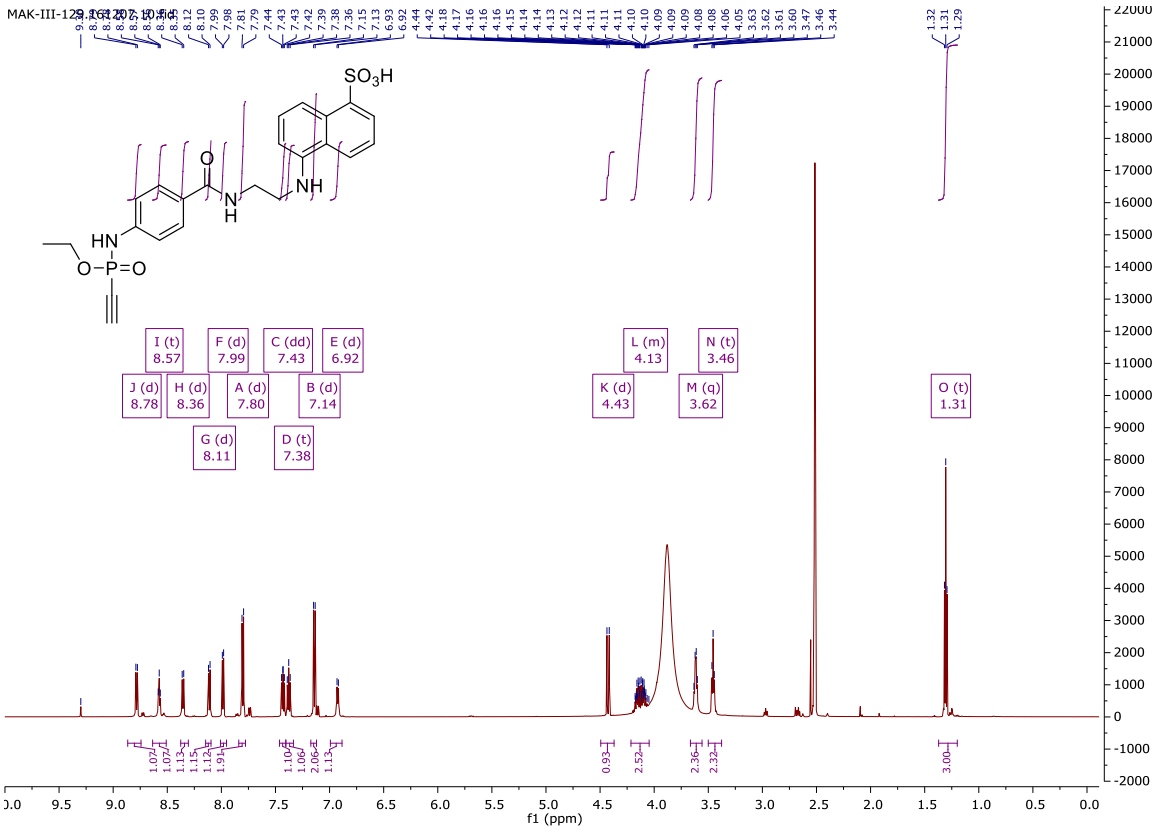

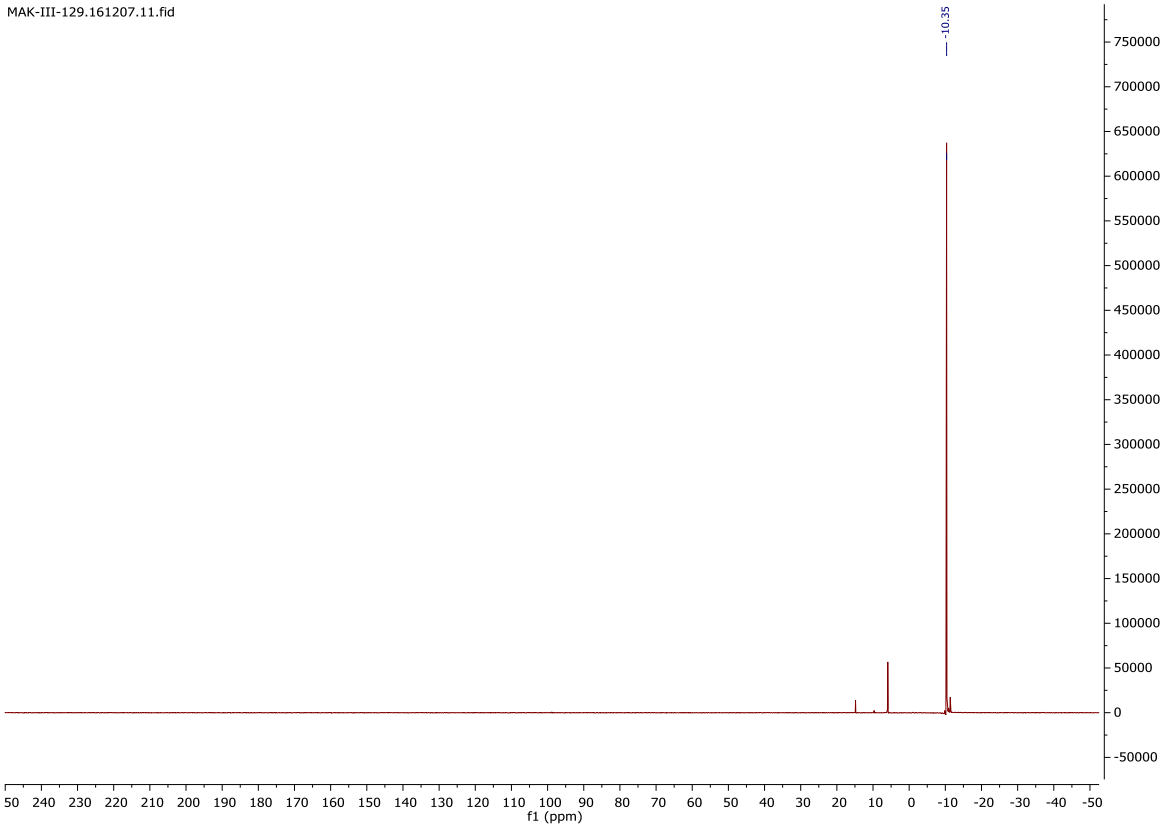

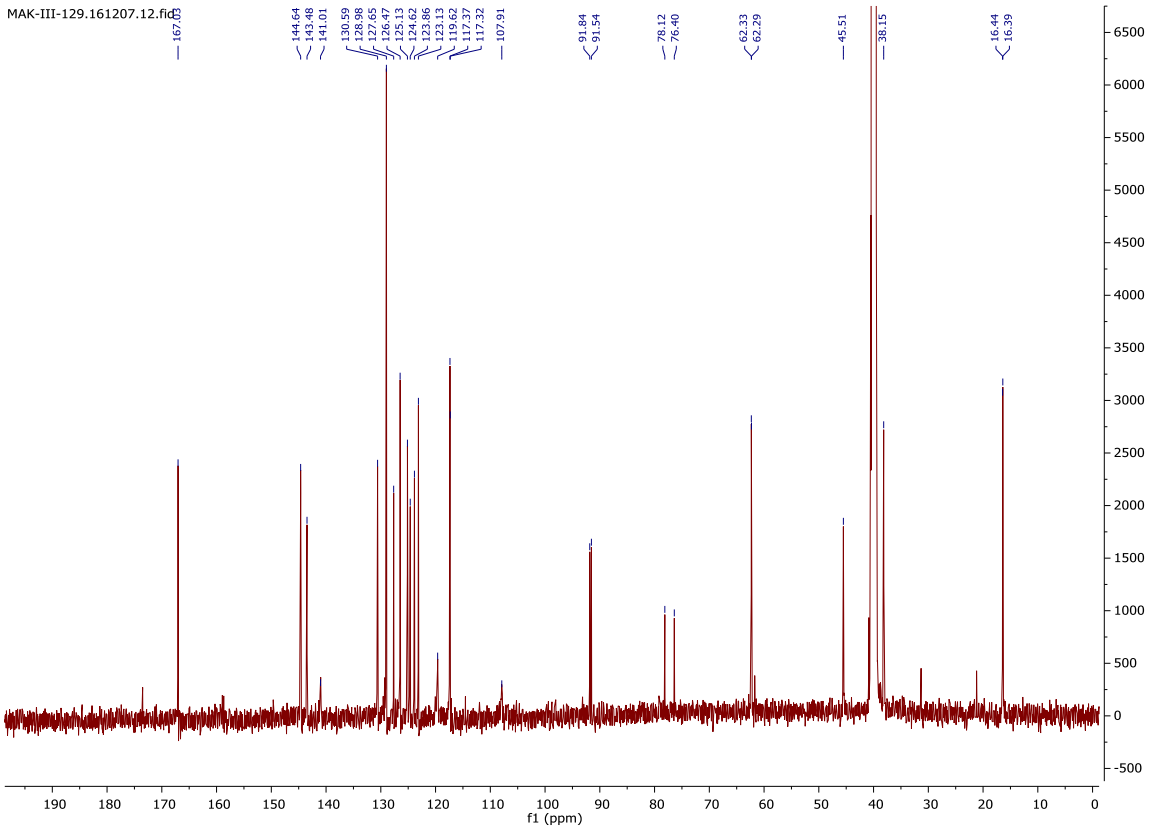

Cy5-*O*-ethyl-*P*-alkynyl-phosphonamidate (**11**)

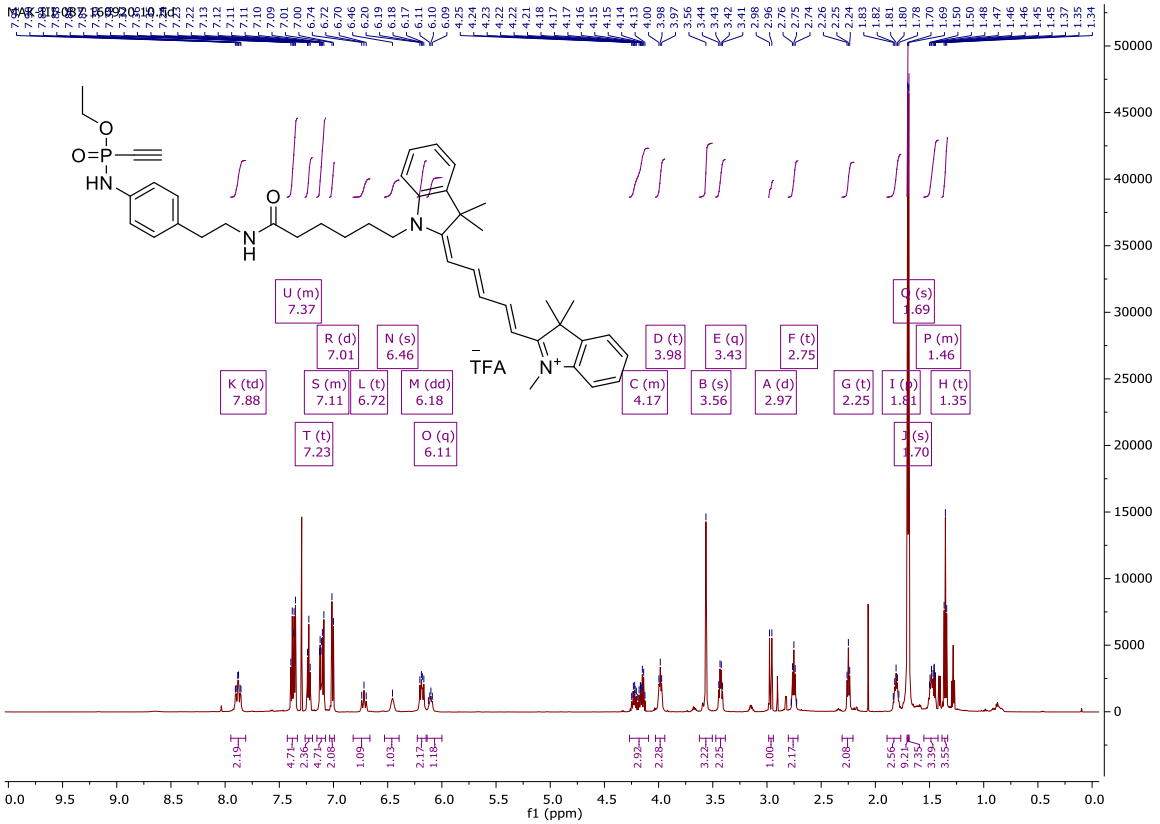

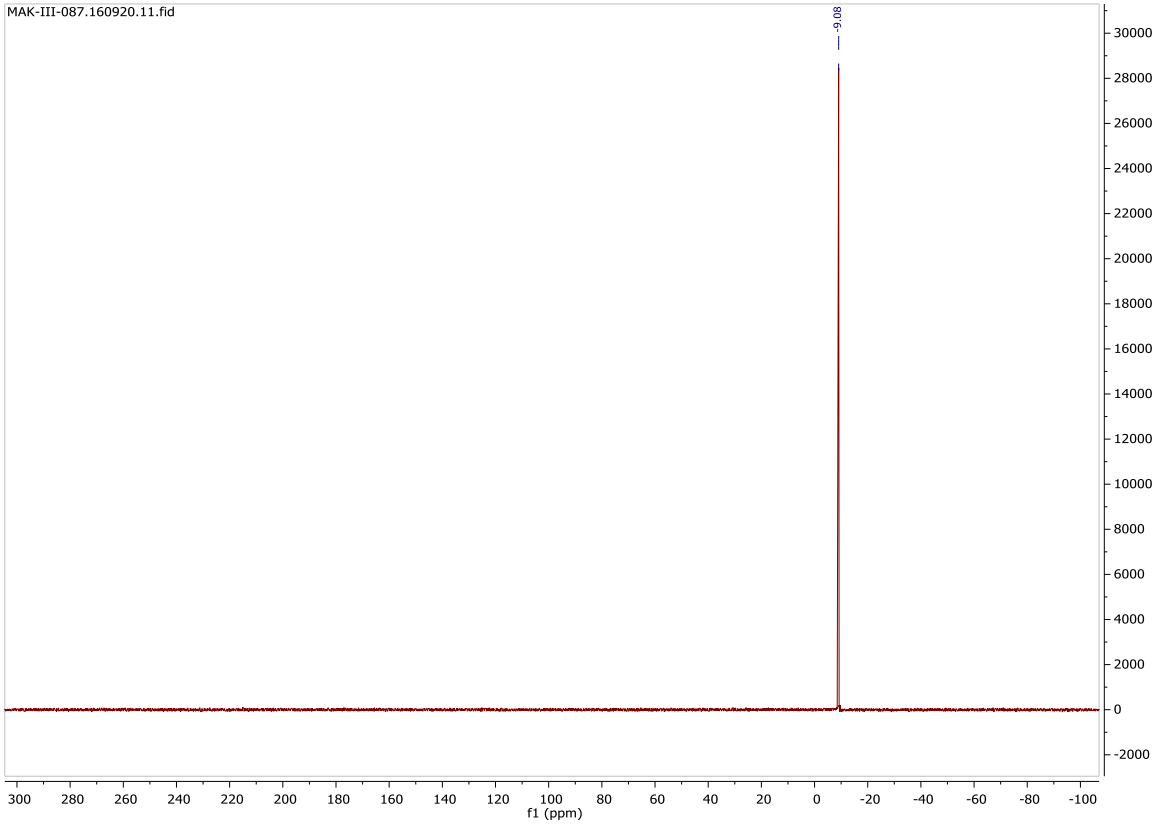
MAK-III-087.160920.11.fid
-9.08
f1 (ppm)

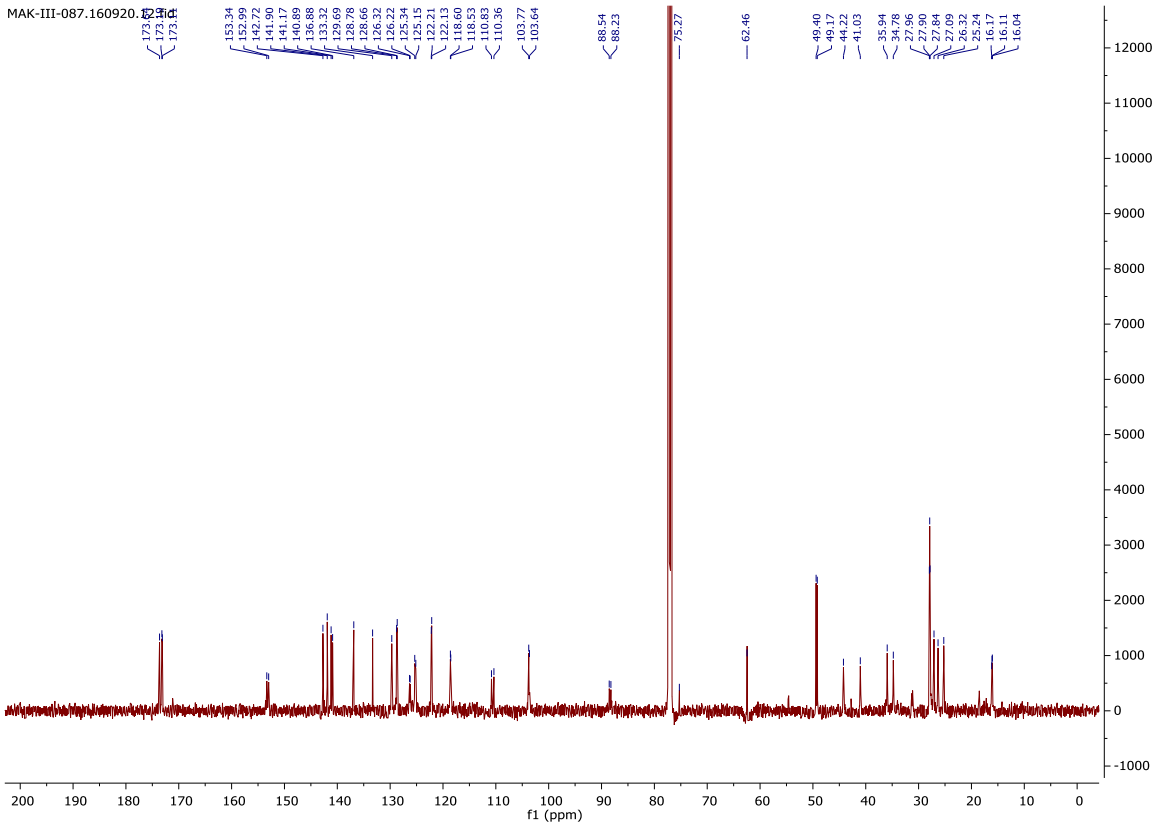
MAK-III-087.160920.12.fid
173.45
173.14
173.11
153.34
152.99
142.72
141.90
141.17
140.89
136.88
133.32
129.69
128.78
128.66
126.32
126.22
125.34
125.15
122.21
122.13
118.60
118.53
110.83
110.36
103.77
103.64
88.54
88.23
75.27
62.46
49.40
49.17
44.22
41.03
35.94
34.78
27.96
27.90
27.84
27.09
26.32
25.24
16.17
16.11
16.04
f1 (ppm)

Ethyl-*N*-phenyl-*P*-(*Z*-ethylthioethenyl) phosphonamidate

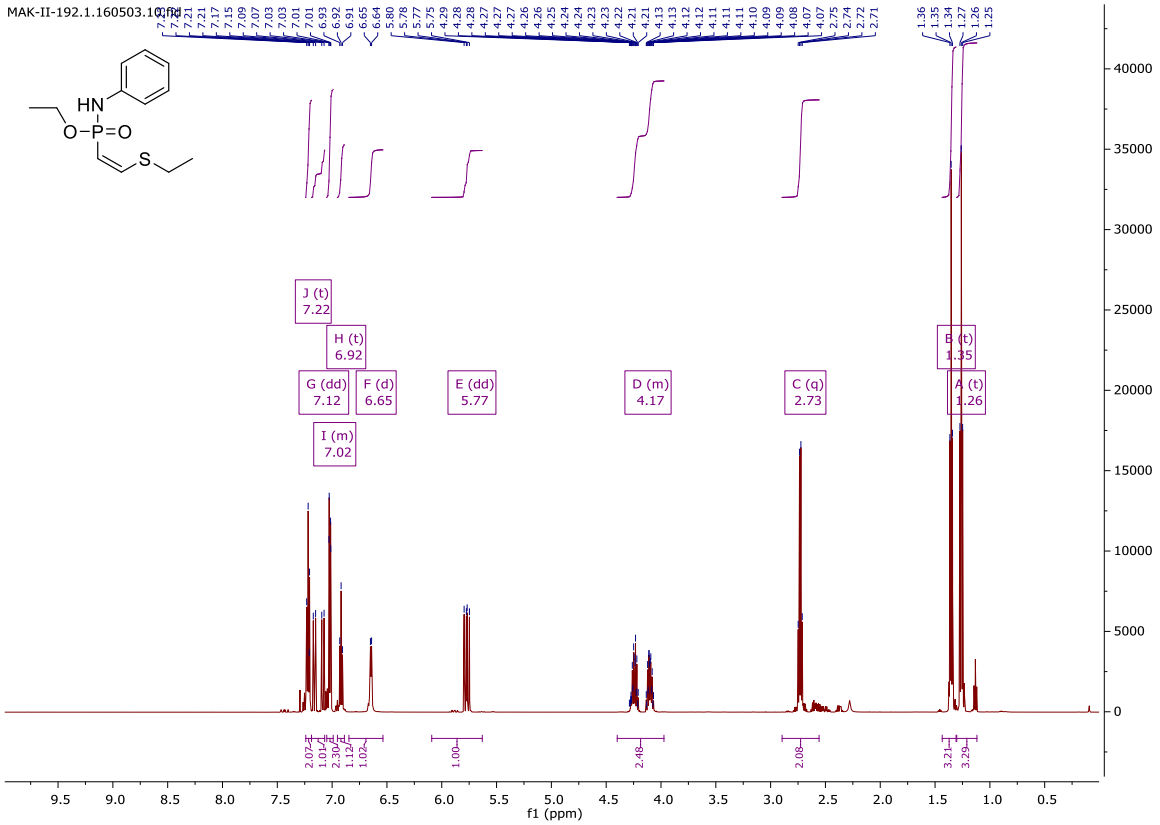

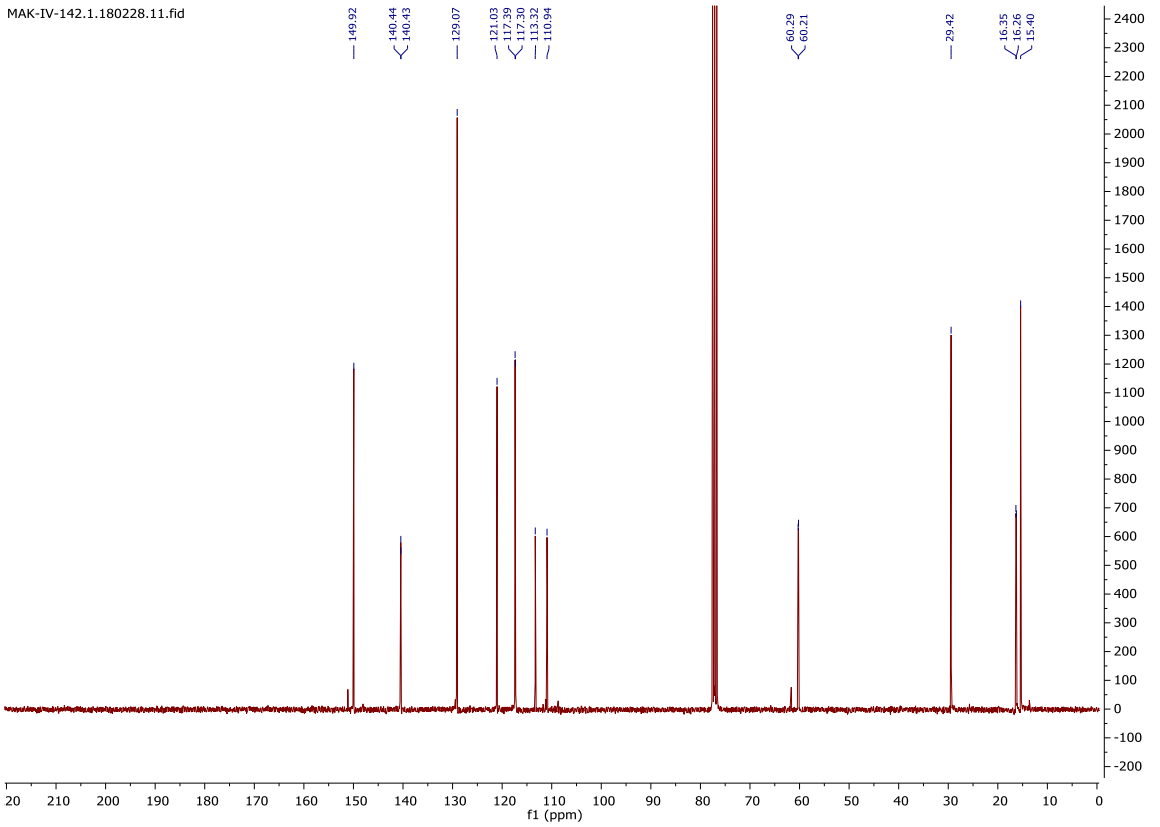

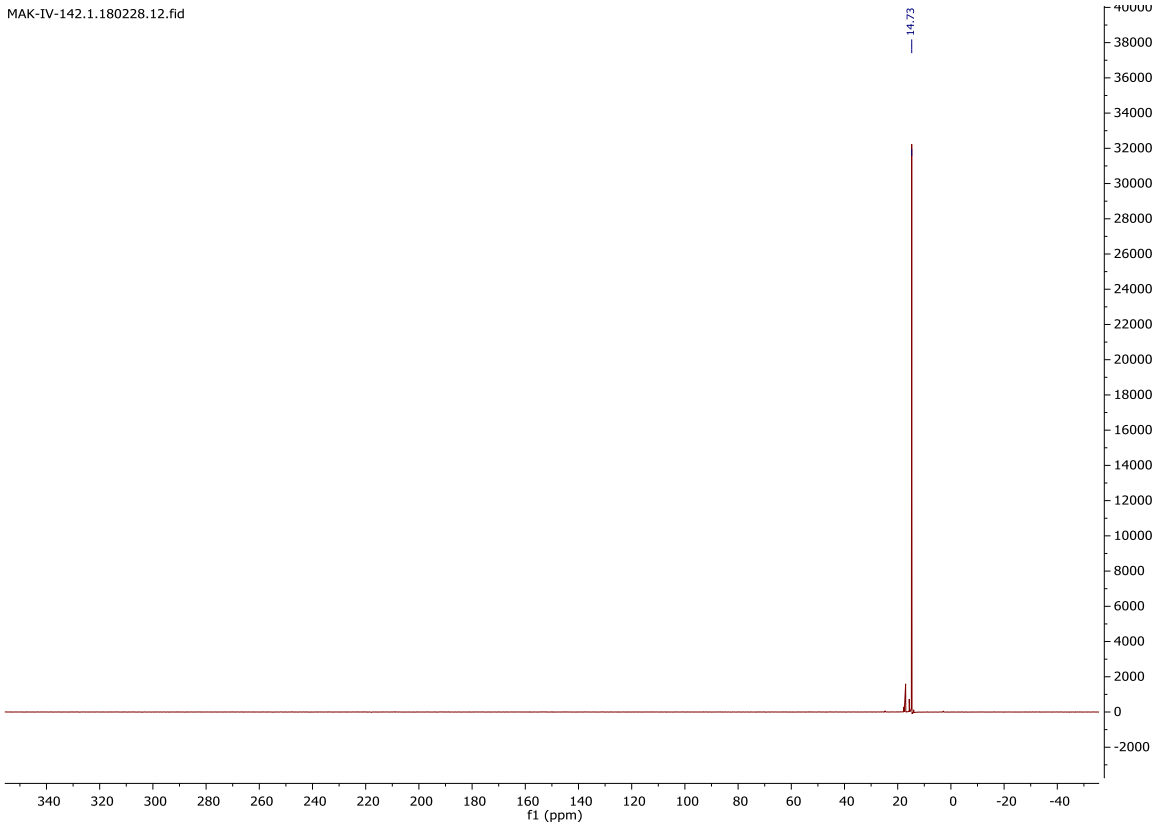

Ethyl-*N*-phenyl-*P*-(*E*-ethylthioethenyl) phosphonamidate

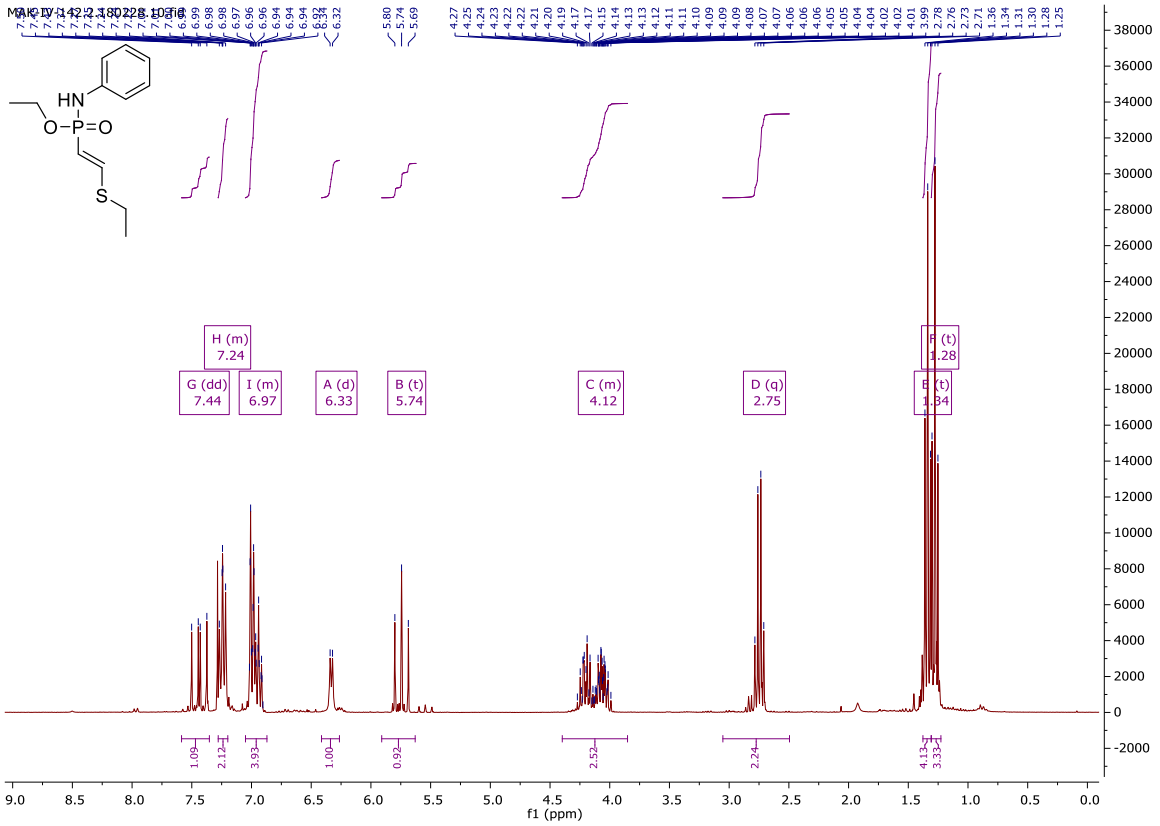

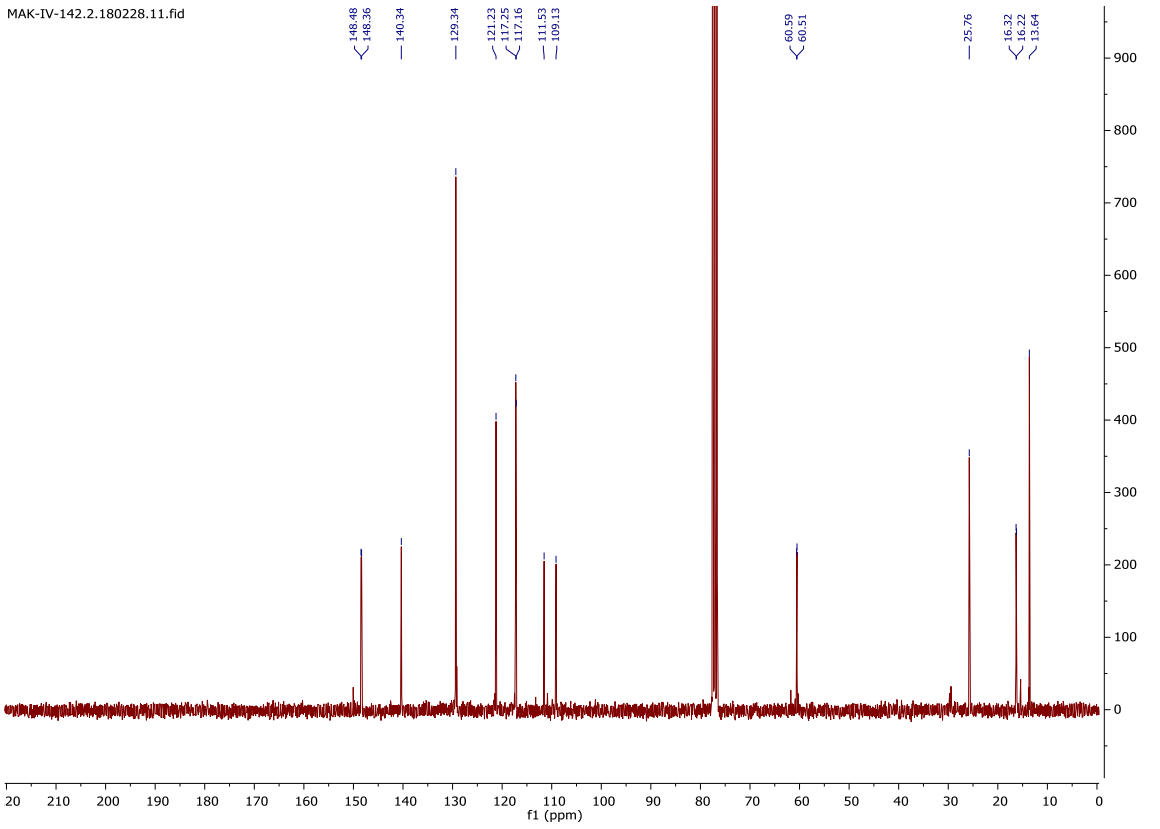
MAK-IV-142.2.180228.11.fid
148.48
148.36
140.34
129.34
121.23
117.25
117.16
111.53
109.13
60.59
60.51
25.76
16.32
16.22
13.64
f1 (ppm)

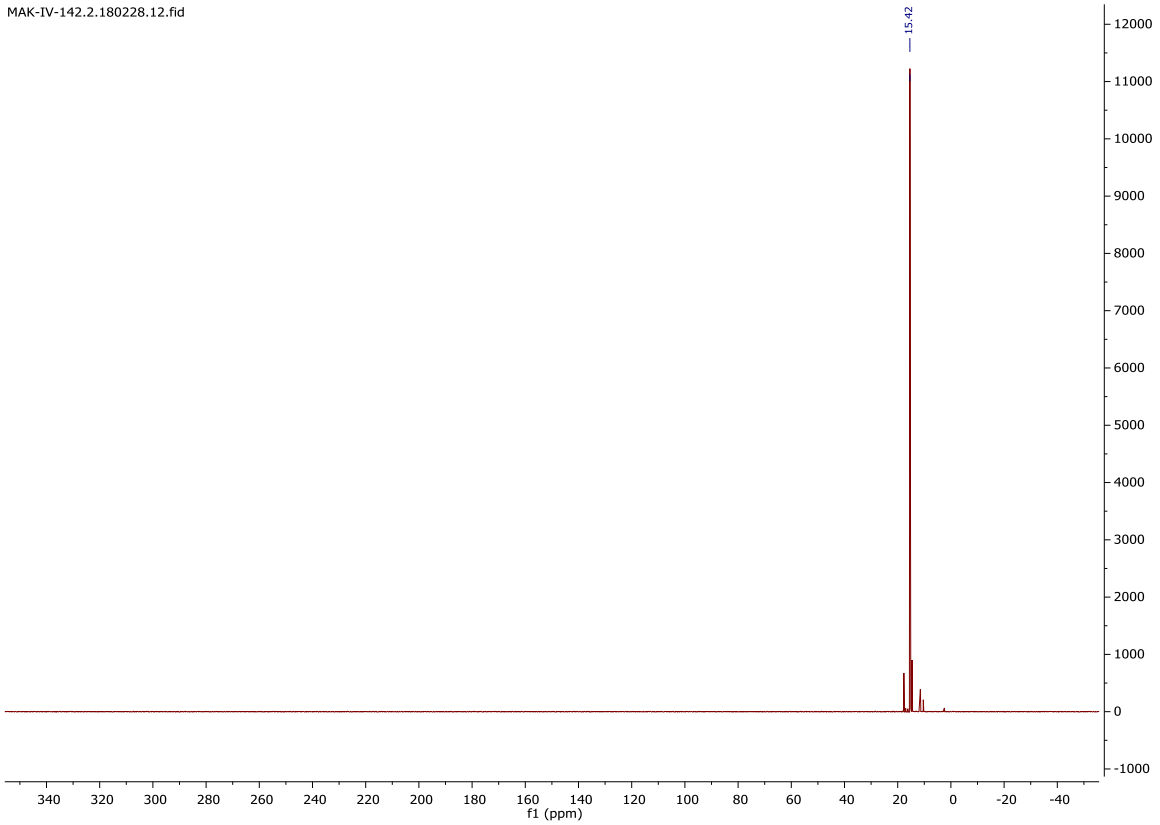
MAK-IV-142.2.180228.12.fid
15.42
f1 (ppm)

6. Computational Details

All DFT calculations were carried out with the *ORCA* program package (Version 3.0.3).[6] The *M06* functional[7] as well as the polarized and minimally augmented *ma-def2-TZVPP*[8] basis set was chosen for geometry optimizations and frequency calculations. This functional performed very well in a comparative study of different functionals for modelling Michael-type additions of thiols to olefins.[9] Minima and transition states were confirmed by frequency calculations, giving no or one imaginary frequency for minima or transition states, respectively. Connectivity of minima and transition states were verified by IRC calculations.

Free enthalpies *G* at 298 K and 1 atm were obtained as follows:

$$G_{298} = H - T \cdot S \quad (1)$$

$$G_{298} = [U + k_B \cdot T] - T \cdot S \quad (2)$$

$$G_{298} = [(E(\text{el}) + E(\text{ZPE}) + E(\text{therm.})) + k_B \cdot T] - T \cdot S \quad (3)$$

with $k_B \cdot T$ = 0.00094421 Eh = 0.59 kcal/mol. Electronic energies *E*(el) were obtained from single-point calculations using the *M06* functional, the *ma-def2-QZVPP* basis set and the COSMO(water) solvent model. Zero point energy *E*(ZPE) and thermal *E*(therm.) corrections to *E*(el) as well as entropy contributions *T·S* were taken from the performed frequency calculations.

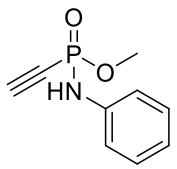

E(el)	-895.458852624575 Eh
E(ZPE)	0.17525247 Eh
E(therm.)	0.01160533 Eh
T·S	0.05031000 Eh

Cartesian Coordinates

P	-0.59808667893139	-0.79193299214631	-1.06157798293773
O	-0.84191595202287	0.20450774235482	-2.09483537170814
N	0.96965046103202	-1.19665078849081	-0.73992993344396
C	1.99671875829470	-0.31544052832699	-0.37033877145969
H	1.14036383293728	-2.17313573738952	-0.55927517552338
C	1.89123801209630	1.05546376836423	-0.58359136071128
C	3.14889631025628	-0.82858616203342	0.21610731821571
C	2.92669060040681	1.88986229494945	-0.20212312754092
C	4.18015324474254	0.01547912488830	0.58365963473391
C	4.07510913902655	1.38144998402923	0.38100548454480
H	3.23330177068336	-1.89685038938847	0.38329533780969
H	1.01060893451755	1.46055785984276	-1.06628035885925
H	2.83278599539945	2.95489222405636	-0.37390872197060
H	5.07181513090782	-0.40034204259692	1.03595841074113

H	4.88134685920472	2.04221125327538	0.67109348259601
O	-1.15697000366242	-2.25036866555863	-1.30763992232812
C	-2.51475846045912	-2.39856369228203	-1.70357045233556
H	-2.65961815297741	-3.44474888140695	-1.95998675137036
H	-2.73201335378030	-1.77390355104223	-2.57057450876158
C	-1.31886812180330	-0.30262653032260	0.46907926519826
C	-1.79617744806682	0.05443290614241	1.51156949293613
H	-2.21899399028480	0.37459086644969	2.43436972006966
H	-3.18410688751695	-2.13096806336774	-0.88296570789472

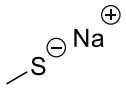

E(el)	-600.465161259222 Eh
E(ZPE)	0.03757793 Eh
E(therm.)	0.00502206 Eh
T·S	0.03488390 Eh

Cartesian Coordinates

H	1.014080	-6.973725	-1.066760
C	0.011793	-6.782643	-1.450494
S	-0.119700	-5.011348	-1.874077
H	-0.137387	-7.422987	-2.320414
Na	-2.417433	-4.527406	-2.723502
H	-0.699582	-7.073231	-0.676803

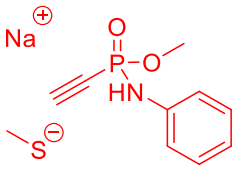

E(el)	-1495.926988297768 Eh
E(ZPE)	0.21416977 Eh
E(therm.)	0.01870608 Eh
T·S	0.06791930 Eh

Cartesian Coordinates

P	-0.15990138938735	-0.42890133226999	1.68066421387234
O	1.28905431940470	-0.55998260868668	1.44642303776843
N	-0.74787526262474	1.10218910608974	1.50582083119721
C	-0.52822641827539	1.78503626389223	0.27743199719787
H	-1.66132340572990	1.24877770195440	1.91111596027621

C	0.76633721846293	2.10196909523885	-0.11765538579724
C	-1.60038884359792	2.12557736147711	-0.53543827557891
C	0.97826992231358	2.74033788382037	-1.32837944090304
C	-1.38004766219673	2.78496999331815	-1.73198549524531
C	-0.09099391207539	3.08638351329645	-2.13706654720796
H	-2.60646344300938	1.85678843069678	-0.23397889204412
H	1.59224452939677	1.86231059178470	0.53967127485290
H	1.98857018908750	2.98144316166376	-1.63438353947903
H	-2.22100737873071	3.04213351296220	-2.36284710454076
H	0.08048729214691	3.58216808562844	-3.08332310574765
O	-0.67085571220736	-0.77331734645779	3.12410918190957
C	-0.36692682120073	-2.05110826576515	3.67686392339406
H	-0.80006172961555	-2.07716500499186	4.67267189974559
H	0.71272288944299	-2.18856873486798	3.74272427469574
C	-0.98868493807023	-1.45840366849309	0.54569293109351
H	-0.80346894473742	-2.84645787195382	3.06917486956848
C	-1.26145146444185	-2.03482879195294	-0.48034991707923
S	0.73169552106387	-1.89499206904874	-3.01729149891012
H	-1.45066474890741	-2.53967157647509	-1.40552983404055
C	-0.09891401953583	-0.31412096883020	-3.40818125130681
H	0.61109376202893	0.42462717350397	-3.78525876785612
H	-0.60339473757962	0.12309476988667	-2.53957185208112
H	-0.85154840840719	-0.47223873416687	-4.18221098601402
Na	1.72387359698248	-1.18076967125357	-0.73155250173993

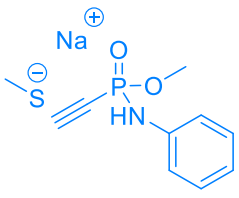

E(el)	-1495.928557055642 Eh
E(ZPE)	0.21391460 Eh
E(therm.)	0.01829736 Eh
T·S	0.06755280 Eh

Cartesian Coordinates

P	-0.36037976685003	0.13355232188078	0.61123685218097
O	1.10235359348308	0.02642981787580	0.46057187745980
N	-0.95877437078580	1.65959785670547	0.72183742296938

C	-0.75197407908927	2.72718413905645	-0.16305004559664
H	-1.60585506357871	1.82193129669133	1.47650460215438
C	0.01723713541010	2.58824521126833	-1.31288993602354
C	-1.33864275829865	3.95638608830814	0.11797571991568
C	0.18949356256277	3.66711486370590	-2.16182508042082
C	-1.15807743273044	5.02739170971521	-0.73649982473076
C	-0.39322013811892	4.89105122844698	-1.88308685914572
H	-1.93739974278876	4.06991078580137	1.01482005029815
H	0.48952203104070	1.64213148843627	-1.54383059140264
H	0.78957899076340	3.54381275378197	-3.05463164392604
H	-1.62027743256610	5.97774827229369	-0.50139049320000
H	-0.25302745117682	5.72980968695513	-2.55187755734917
O	-0.98351571778120	-0.46914587529734	1.91801829236482
C	-0.73167681332266	-1.84193492925137	2.25322153955814
H	-1.42667223794100	-2.10057363121747	3.04678733806946
H	0.29239616168492	-1.95143670560393	2.61028408911116
C	-1.10456297074447	-0.72790637966886	-0.70807884820319
C	-1.44888768891447	-1.53401809800798	-1.53234833648837
H	-0.88265875618574	-2.50016357178798	1.39253193013356
H	0.54192328428941	-6.36834119671117	-0.87890319109539
C	1.28667788503706	-5.57597213453699	-0.95686385438022
S	0.46916664296550	-3.95465138018539	-0.78960212308365
H	2.02881433482387	-5.73691151477983	-0.17444196993379
Na	1.91503910679568	-1.83187459415343	-0.55107612222325
H	1.77994767978370	-5.67348824456517	-1.92436664841333
H	-1.73817798776714	-2.25598926515594	-2.26140658859900

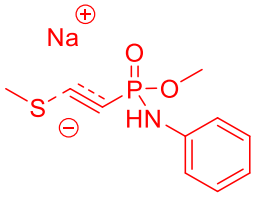

E(el)	-1495.903404154544 Eh
E(ZPE)	0.21390115 Eh
E(therm.)	0.01678484 Eh
T·S	0.06301100 Eh

Cartesian Coordinates

P	0.00432476169549	0.07439378080378	0.03483007911912

O	1.48979535952874	0.11784780285387	0.05205064051289
N	-0.67939745823217	1.60611201619863	0.04828214663593
C	-0.60945443107929	2.38124384695229	-1.12325255303219
H	-1.58117886616957	1.63058322624726	0.50200213429641
C	0.61360622824937	2.59007445787278	-1.75713533565964
C	-1.76173141661530	2.92304785645567	-1.68206632484857
C	0.66683917801570	3.29477411233949	-2.94627840900653
C	-1.69540030100169	3.64486249115244	-2.86070121379741
C	-0.48416662485819	3.82339269203808	-3.50826265088159
H	-2.71687440673611	2.76079990236050	-1.19505440196975
H	1.51362190011937	2.20057594014165	-1.29809859626996
H	1.62286197828597	3.44212827435099	-3.43379068812924
H	-2.60262773972388	4.05759098770230	-3.28387002267648
H	-0.43645805864117	4.37478281746018	-4.43807287728148
O	-0.67986115113054	-0.48578617052310	1.34579071774600
C	-0.36821074667098	-1.79693562996775	1.78523738148224
H	-0.89967750996454	-1.95741435947259	2.72024013978589
H	0.70462159416630	-1.90018077055168	1.95876675060872
C	-0.46684704394486	-0.83690250386103	-1.32368975748261
H	-0.69335476386363	-2.53821695305871	1.05206019661377
C	-0.65045308587053	-0.77389615595494	-2.55662789634114
S	0.57484080092058	-2.15153498080379	-3.99758282840588
H	-1.12272463635685	-0.26894759844267	-3.38904406858779
C	0.39887429035098	-1.08246105636445	-5.44454504796888
H	1.36623393151158	-0.82762080576871	-5.87393774378108
H	-0.09934965201922	-0.14697401098467	-5.16093725008649
H	-0.20435215622752	-1.57063932689784	-6.20876000056083
Na	2.01296002626197	-1.07716988227795	-1.87014252003342

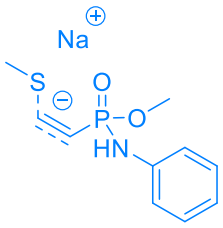

E(el)	-1495.916470890467 Eh
E(ZPE)	0.21408209 Eh
E(therm.)	0.01678282 Eh
T·S	0.06297910 Eh

Cartesian Coordinates

P	0.08297664804403	0.01268079694422	0.22619410842859
O	1.56057219538901	-0.00338119524710	0.37643233521234
N	-0.56131069757442	1.53901847869489	0.16657459276146
C	-0.38205278561491	2.44900896831032	-0.87821970791492
H	-1.37807676278223	1.68115426670683	0.73861484454082
C	0.71168435902738	2.36424981461287	-1.73521917347702
C	-1.31212103575827	3.46635483447016	-1.07089924698579
C	0.85279059993369	3.26938892224779	-2.77142945366212
C	-1.15503187877306	4.37246352691388	-2.10239923438397
C	-0.07514511209937	4.27801349231498	-2.96516596984354
H	-2.16699069977524	3.53872335758424	-0.40766352238659
H	1.45990779365444	1.59917728214409	-1.57382389319361
H	1.70668486306791	3.18578123447073	-3.43245835172661
H	-1.88993671422970	5.15625113648516	-2.23692905018631
H	0.04255052797643	4.98346325688275	-3.77697343661031
O	-0.72996702979485	-0.50343803831498	1.48141929991982
C	-0.54961782805538	-1.85137983206765	1.90346833831624
H	-1.22791876008619	-2.01703308233649	2.73643218877581
H	0.47688815158217	-2.01316906107841	2.23895533356830
C	-0.38491055143777	-0.92171674722083	-1.13745404367154
C	-0.27345422903572	-2.01721683261896	-1.71147087021387
H	-0.77961069471334	-2.54897751532011	1.09459529782401
H	0.50510643116304	-5.79725391568251	-2.20873160404509
C	0.98085515385962	-4.83442500913788	-2.38898907820844
S	1.02831584219300	-3.87211507839207	-0.85882302422860
H	1.97508043723897	-5.00945647481630	-2.79676115252502
Na	2.51917646309879	-1.66806334169796	-0.73028272176178
H	0.39157338639573	-4.30801916887146	-3.14974246849609
H	-0.53108807289377	-2.63278407598016	-2.55630033582618

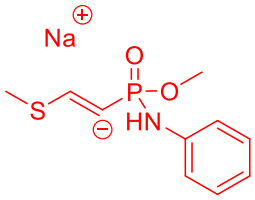

E(el)	-1495.936211350094 Eh
E(ZPE)	0.21581204 Eh
E(therm.)	0.01667476 Eh
T·S	0.06278790 Eh

Cartesian Coordinates

P	0.13190445789879	-0.39544362431027	1.57341806811963
O	1.36785884049088	0.09034133108148	2.26095635068092
N	-0.93135278554734	0.85227434258795	1.17561996490530
C	-0.67872828045422	1.78788077381042	0.17275917567321
H	-1.90385327488597	0.63980157528976	1.33386716151470
C	0.61049718258318	2.26786757669032	-0.05456872676165
C	-1.71749117563628	2.25139721012141	-0.63265842295178
C	0.84888729023589	3.15950796470553	-1.08437854437916
C	-1.46995653888793	3.15342698095931	-1.65055748902673
C	-0.18318994680054	3.60755675202598	-1.89288833332116
H	-2.72318705316351	1.88094155926185	-0.46441044945607
H	1.41374943050895	1.94175802639791	0.59440802495773
H	1.85817552566784	3.51671560494053	-1.25063517369336
H	-2.29146864117551	3.49570346169783	-2.26777009581932
H	0.01109557855656	4.30571687865122	-2.69635952136178
O	-0.86003157005055	-1.14793682555242	2.58076094913618
C	-0.36587481618504	-2.25707682981987	3.30054725818283
H	-1.14901518529915	-2.58235391798314	3.98252489117598
H	0.51628084442688	-1.97937510569729	3.88426003682387
C	0.59077743055756	-1.43843113282618	0.26996702126070
H	-0.11224971395133	-3.08044158849582	2.62773652612117
C	-0.03227714421668	-1.28865458763087	-0.89600355826189
S	0.39512405652662	-2.19890790235265	-2.34438024281346
H	-0.86276963520567	-0.60054862296691	-1.09834472771805
C	-0.55261708171232	-1.29416626908217	-3.58643971354119
H	-0.33667484130893	-1.74869211596690	-4.55119913393233
H	-0.25492070220577	-0.24628406750522	-3.61212847846134
H	-1.62227381905404	-1.36888855869870	-3.39438648209920

Na	2.80115156828766	-1.22266888933307	1.12326366504626

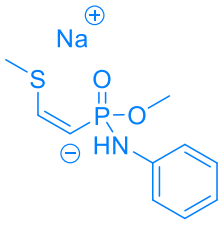

E(el)	-1495.931615683340 Eh
E(ZPE)	0.21522419 Eh
E(therm.)	0.01776208 Eh
T·S	0.06575200 Eh

Cartesian Coordinates

P	-0.18746350698823	-0.31429005717662	-0.55022791305267
O	1.23368130751095	-0.39773105025972	-1.02326320659152
N	-0.98909665388179	1.04344395489395	-1.08088584831332
C	-0.74115610021521	2.38451397898745	-0.80933236204473
H	-1.82740640102437	0.82595786330311	-1.59449350373988
C	0.44200790749066	2.81211498752494	-0.20929217096651
C	-1.69760166578076	3.33640027058733	-1.15854109816395
C	0.64031730345613	4.15600967308731	0.05133453584731
C	-1.48335078238488	4.67738586797046	-0.90431787582489
C	-0.31530095258042	5.09910366240952	-0.29017961091239
H	-2.61823022948042	3.01131792433970	-1.63059286051503
H	1.21054583782706	2.09090878508211	0.03869324231180
H	1.56276585713255	4.47042569490638	0.52450609010491
H	-2.24125186109238	5.39851926183271	-1.18499978047360
H	-0.15073786737756	6.14863916487608	-0.08416827162059
O	-0.22742307789983	-0.07019933209949	1.03166202204200
C	0.79761671524305	-0.55597249009913	1.87173218857205
H	0.54507038199053	-0.26186258882679	2.88892687412815
H	1.76277605441774	-0.12374126356874	1.59906964868359
C	-1.18034267585157	-1.59125524227056	-1.12832951288644
C	-1.12267508952716	-2.89001583208522	-0.95573478213874
H	0.87247015431527	-1.64704554211805	1.83057439639872
H	-1.33721520688497	-5.80489322230161	-0.01107463455198
C	-0.32398567144947	-5.54438060852389	-0.31159147736897
S	0.04483694350864	-3.83415699792097	0.14745026856292
H	0.37674632226972	-6.18749519182302	0.21668753872025

Na	1.37186982811735	-2.39354045190515	-1.88053935040992
H	-0.21142761901564	-5.70278395256589	-1.38368274787106
H	-1.76227925184500	-3.62812726625621	-1.44908979792551

7. References

[1] M. Mikolajczyk, B. Costisella, S. Grzejszczak, *Tetrahedron* **1983**, *39*, 1189-1193.

[2] A. Shevchenko, H. Tomas, J. Havli, J. V. Olsen, M. Mann, *Nat. Protoc.* **2007**, *1*, 2856.

[3] A. Stengl, D. Hörl, H. Leonhardt, J. Helma, *SLAS Discov.* **2017**, *22*, 309-315.

[4] A. J. Pérez, F. Wesche, H. Adihou, H. B. Bode, *Chem. Eur. J.* **2016**, *22*, 639-645.

[5] H. D. Herce, D. Schumacher, A. F. L. Schneider, A. K. Ludwig, F. A. Mann, M. Fillies, M.-A. Kasper, S. Reinke, E. Krause, H. Leonhardt, M. C. Cardoso, C. P. R. Hackenberger, *Nat. Chem.* **2017**.

[6] F. Neese, *Wiley Interdiscip. Rev.-Comput. Mol. Sci.* **2012**, *2*, 73-78.

[7] Y. Zhao, D. G. Truhlar, *Theor. Chem. Acc.* **2008**, *120*, 215-241.

[8] aF. Weigend, R. Ahlrichs, *Phys. Chem. Chem. Phys.* **2005**, *7*, 3297-3305; bJ. Zheng, X. Xu, D. G. Truhlar, *Theor. Chem. Acc.* **2011**, *128*, 295-305.

[9] J. M. Smith, Y. Jami Alahmadi, C. N. Rowley, *J. Chem. Theory Comput.* **2013**, *9*, 4860-4865.

4.4 Ethynylphosphonamidates for the Rapid and Cysteine Selective Generation of Efficacious Antibody-Drug-Conjugates

Ethynylphosphonamidates for the rapid and cysteine selective generation of efficacious Antibody-Drug-Conjugates

Marc-André Kasper,[a][b] Andreas Stengl,[c] Philipp Ochtrop,[a] Marcus Gerlach,[c] Tina Stoschek,[c] Dominik Schumacher,[a][b][c] Jonas Helma,[c] Martin Penkert,[a][b] Eberhard Krause,[b] Heinrich Leonhardt*[c] and Christian P. R. Hackenberger*[a][b]

[a]Chemical Biology Department, Leibniz-Forschungsinstitut für Molekulare Pharmakologie (FMP), Robert-Rössle-Strasse 10, 13125 Berlin (Germany) E-mail: hackenbe@fmp-berlin.de

[b]Department of Chemistry, Humboldt Universität zu Berlin, Brook-Taylor-Str. 2, 12489 Berlin (Germany)

[c]Department of Biology II, and Center for Integrated Protein Science Munich, Ludwig-Maximilians-Universität München, Großhadenerstr. 2, 82152 Martinsried (Germany) E-mail: h.leonhardt@lmu.de

Abstract

Requirements for novel bioconjugation reactions for the synthesis of Antibody-Drug-Conjugates (ADCs) are exceptionally high, since conjugation selectivity as well as stability and hydrophobicity of linkers and payloads drastically influence the performance and safety profile of the final product. Herein we describe Cys-selective ethynylphosphonamidates as new reagents for the rapid generation of efficacious ADCs from native non-engineered monoclonal antibodies, applying a simple one-pot reduction and alkylation protocol. Ethynylphosphonamidates can be easily substituted with hydrophilic residues, giving rise to electrophilic labeling reagents with tunable solubility properties. We demonstrate that ethynylphosphonamidate-linked ADCs have excellent properties for next generation antibody therapeutics in terms of serum stability and *in vivo* antitumor activity.

Introduction

Antibody-conjugates consisting of a drug linked to a tumor selective antibody, so called Antibody Drug Conjugates (ADCs), represent an emerging class of targeted therapeutics.[1] While most of the ADCs in clinical development contain cytotoxic molecules, recent studies also include the treatment of infectious diseases by Antibody Antibiotic Conjugates (AACs).[2] ADCs are particular interesting for the treatment of cancer, since they combine the high potency of cytotoxic molecules with the tumor specificity of monoclonal antibodies. Thus, ADCs have the potential to significantly broaden the therapeutic window compared to standard chemotherapy.[1, 3] Recent progress in clinical development include the approval of inotuzumab ozogamicin (Besponsa™)[4] and the re-approval of gemtuzumab ozogamicin (Mylotarg™).[5] In total, there are four ADCs currently on the market and more than 80 candidates in clinical trials, which clearly underlines the high potential of this compound class.[6] Still, challenges remain especially in improving the linkage between drug and antibody.[7] Commonly used linker systems face problems such as insufficient serum stability and undesired aggregation behavior, limiting the number of drug molecules linked to an antibody and leading to undesired off-target toxicity.[8]

Maleimides have become the prime linker reagents for the generation of ADCs including two approved ADCs – Kadcyla® (trastuzumab emtansine) and Adcetris® (brentuximab vedotin).[6] Maleimides can be applied to either modify native IgG antibodies via interchain-disulfide reduction and alkylation[9] or to engineered antibodies via addition to an additionally incorporated cysteine (Thiomab™).[8a] Nevertheless, one of the biggest drawbacks of maleimide-linkages is their susceptibility towards retro-Michael-additions leading to premature drug cleavage during circulation and reattachment to cysteine containing proteins like albumin.[8a, 10] Even though consequences arising from such payload transfer are not yet fully understood, it is anticipated that the anti-tumor efficacy might be lowered due to a decreased drug delivery to targeted cells. Furthermore toxic side effects might occur.[11] Several compound classes have been developed to overcome this issue, including self-hydrolyzing-maleimides[11] and structurally refined Michael-type acceptors such as carbonyl acrylic derivatives[12] or exocyclic maleimides[13]. All of these methods yield stable sulfhydryl-adducts; however, synthetic incorporation of these electrophiles into functional molecules remains challenging..[14]

Undesired aggregation of ADCs is another challenge, since many drugs used in the context of ADCs are hydrophobic.[15] The addition of organic co-solvents to the conjugation mixture is commonly employed to enable conjugation of hydrophobic drugs, which however may affect the structural integrity of the antibody.[16] Additionally, the hydrophobic nature of drugs increases the formation of High Molecular Weight Species (HMWS) in the final product.[17] Those aggregates impair the pharmacokinetic profile and efficacy[18] of ADCs and often limit the Drug to Antibody Ratio (DAR) to a maximum of 4.[19] To overcome this issue, hydrophilic PEG linkers have been developed that compensate the lipophilic nature of the drug.[20] However, it has recently been shown that PEG can negatively affect pharmacokinetics when incorporated as a linear spacer between antibody and drug.[21] Increasing the solvent exposure of the drug most likely facilitates unspecific hydrophobic interactions. This

unwanted effect was successfully mitigated by side-chain attachment of the solubilizing polymer.[21]

In this study we apply ethynylphosphonamidates as a novel compound class for the generation of stable Cys-linked ADCs. We demonstrate that our previously reported phosphonamidate based labelling protocol[22] is suitable for conjugation of cytotoxic payloads to two model antibodies, brentuximab and trastuzumab which form the basis of two marketed ADCs, facilitating the construction of ADCs that efficiently and selectively kill targeted cells *in vitro*. In addition, we introduce ethynylphosphonamidates, modified with a side-chain ethylene glycol unit promoting improved payload solubility under aqueous conditions without increasing linker length between antibody and drug in the final conjugate. With this, we synthesized a vedotin analog and conjugated it to brentuximab, furnishing a phosphonamidate-linked ADC that is structurally analogous to Adcetris®. Our protocol enables straightforward ADC synthesis, starting from non-engineered native antibodies that can be labelled in a one pot protocol with only minimal reagent excess. In extensive profiling of our ethynylphosphonamidate linked ADC we were able to demonstrate an excellent linkage stability in rat serum and *in vivo* antitumor activity, as investigated in two xenograft mouse model experiments.

Results and Discussion

We initiated our studies by conjugating the antimitotic agent Monomethyl auristatin F (MMAF) [23] to Her2 targeting trastuzumab using a phosphonamidate functionalized cathepsin B cleavable linker 4, which was synthesized based on previously published procedures for Fmoc-protected Val-Cit dipeptides (Figure S1 in the supporting information).[24] In a first proof-of-concept study, we conjugated 4 to trastuzumab following our previously established protocol applying 10 eq. labeling reagent per Cys.[22], giving an average DAR of 4.6 (Figure 1a and S2 in the supporting information). To validate the functionality of trastuzumab-4 it was evaluated in a Her2-based proliferation assay with two Her2-overexpressing cell lines BT474 and SKBR3 as well as a Her2-negative cell line as a control (MDAMB468).[25] Since trastuzumab alone exhibits antiproliferative potency, cell viability was measured via a sensitive, high content assay to asses retained antibody functionality after exposure to the conjugation procedure. Antibody concentrations leading to fifty percent of maximal growth inhibition (IC50) was decreased by 81-fold from 900 to 11 pM for SKBR3 cells (Her2++) with trastuzumab-4 and by 42-fold from 800 to 19 pM for BT474 cells (Her2+). An effect on the proliferation of the control cell line MDAMB468 was only observed at very high ADC concentrations (IC50 > 100 nM). Notably, trastuzumab-4 inhibits the proliferation close to 100% of cell population for SKBR3 cells, while trastuzumab alone only inhibits up to 50%. As an additional control, trastuzumab was treated with 4 without prior disulfide reduction. Those constructs behaved similar to the non-modified antibodies, highlighting the high Cys-selectivity, efficient removal of excessive toxin and gentle reaction conditions of our method (Figure 1b). We additionally validated our measured IC50-values in a standard cell viability assay and obtained similar IC50-growth inhibition constants for trastuzumab-4 (Figure S3 in the supporting information). The mode of action of MMAF is destabilizing microtubules by inhibition of tubulin polymerization.[26] Along this line we observed by fluorescence microscopy a disturbance of tubulin organization in BT474 cells upon treatment with 0.3 nM trastuzumab-4 for 4 days in contrast to proper spindle formation in untreated mitotic control cells (Figure 1c and Figure S4 in the supporting information).

As mentioned above, introducing a polar side chain into a linker-drug molecule was shown to be beneficial compared to adding linear solubilizing units that increase the distance of the drug to the antibody.[21] Ethynylphosphonamidates, bearing O-substituents with increased hydrophilicity might serve as powerful building blocks to increase the polarity of the whole linker system without increasing the overall linker length. Since the Staudinger-phosphonite reaction (SPhR) comprises a very convenient synthetic route to incorporate the ethynylphosphonamidate moiety into a given molecule, we focused on the synthesis of a hydrophilic phosphonite. Following our previous protocols bis(diisopropylamino)chlorophosphine was first treated with ethynylmagnesium bromide followed by the addition of diethylene glycol and tetrazole to yield phosphonite 5 in a one-pot procedure.[27] Subsequent Staudinger-phosphonite reaction was performed with the NHS-modified azide 6 and yielded the desired diethyleneglycol-phosphonamidate 7 in 31% yield (Figure 2a).

To demonstrate the versatility of our method we proceeded with the construction of a second antibody-drug pair. Since we wanted to directly compare our linkage technology

with the maleimide linkage used in Adcetris® we continued our studies with phosphonamidate-linked ADCs, structurally as close to Adcetris® as possible. In addition to the MMAF constructs used in the previous study, two ethynylphosphonamidate MMAE-derivatives were synthesized, one with an ethyl substituent at phosphorous in 9 and one with the diethylene glycol substituent in 10 (Figure 2b). RP-HPLC analysis showed a reduced retention time for compound 10, when compared to 9 or vedotin (Figure 2c). Solubility measurements revealed that the aqueous solubility of 9 is drastically increased by the PEG substituent in 10 from 95 to 298 µM. Aqueous solubility of 10 is also twice as high compared to vedotin (Figure 2d and Figure S5 in the supporting information) Based on these observations we decided to proceed with the hydrophilic compound 10 for subsequent conjugation studies to antibodies. Taken together, we demonstrated that our method enables facile incorporation of hydrophilic substituents to the phosphonamidate via the SPhR, thus improving solubility properties of the linker-payload construct.

Next, we tried to optimize our conjugation protocol to reduce the drug equivalents needed for sufficient conjugation. Since Adcetris® is modified with an average of four vedotin molecules per antibody [28], we started by screening different equivalents of 10 to achieve similar modification and analyzed the DAR by intact protein MS (Figure S6 in the supporting information). We estimated that 16 eq. of 10 per antibody (2 eq. per Cys-residue) are needed to reach a DAR of 4 at 1 mg/ml antibody concentration. We attribute the required excess of phosphonamidate to slower reaction kinetics of ethynylphosphonamidates when compared to maleimides.[22] To compensate for the slower kinetics, we increased the antibody concentration in the conjugation reaction to 5 mg/ml, a concentration that was previously also used for maleimide conjugations.[9] With this, we were able to use as little as 4.5 eq. of 10 per antibody to achieve a DAR of 4.0 (Figure S7 in the supporting information). After this, upscaling of the conjugation reaction to 2.4 mg brentuximab was performed, at 1 or 5 mg/ml followed by a preparative size-exclusion chromatography step to ensure complete removal of the toxin prior to subsequent functional evaluations, yielding 1.6 mg of the desired ADC brentuximab-10 with a DAR of 3.8-4.0. Another approach to achieve control over the number of drug molecules attached to an antibody is partial reduction of the interchain disulfide bonds with few equivalents of TCEP.[29] By screening TCEP equivalents needed to modify brentuximab, we found out that a partial reduction protocol with 3 eq. TCEP, 5 eq. 10 and 5 mg/ml brentuximab, applied in a one pot process, produces an ADC with a DAR of 3.9 without the need for removal of reducing agent prior payload conjugation (Figure S8 in the supporting information). This simplified reduction and alkylation one-pot process can be problematic with other cysteine labeling reagents, since it has been shown that maleimides and vinyl sulfones for instance, irreversibly react with TCEP.[30]

Taking advantage of our ADC synthesis protocols we then evaluated commercially available Adcetris® and our analog brentuximab-10 (Figure 3a) in *in vitro* and *in vivo* experiments. We started with a cell-based viability assay with a CD30-overexpressing cell line Karpas299 and a CD30-negative cell line HL60 as a control. Both ADCs showed similar toxicities of below 1 ng/mL in the antigen positive cell line. Whereas, Adcetris®

slightly affected the antigen negative cell line at high ADC concentrations we observed no such effect for brentuximab-10 (Figure 3b).

As mentioned earlier, stability of the linkage between drug and antibody in serum might improve the properties of ADCs in terms of off-target toxicity and anti-tumor efficacy.[11] It has been shown in recent experiments that maleimidocaproyl linked ADCs significantly lose payloads in rat serum.[31] Although hydrolysis of maleimides was shown to improve conjugate stability and generates ADCs with increased *in vivo* potency,[11, 32] the occurrence of incomplete hydrolysis of many maleimides may limit this approach.[33] In our experiment, we observed that 90% of the phosphonamidate-linked MMAE was still connected to brentuximab after 7 days of incubation in rat serum at 37°C as measured by intact protein MS after pulldown of the ADC from serum. Under the same incubation conditions, Adcetris® lost more than 70% of its payload, already after three days. (Figure 3c). This data is in accordance, with previous observations, that describe a drastic DAR decrease of similar maleimide linked ADCs following 6 days of incubation in serum at 37°C.[31] From the MS-spectra we concluded complete hydrolysis of maleimides to the open ring form at day 3, resulting in no further retro-Michael addition and associated payload loss until day 7 (Figure S9 in the supporting information). Taken together, the stability experiments in serum clearly underlines our previously reported data on excellent phosphonamidate linkage stability [22] in particular when compared to maleimide linked ADCs. Additionally, we performed storage tests with brentuximab-10 to analyze the formation of HMWS, similarly as reported previously.[34] Size-exclusion chromatography revealed less than 9% HMWS formation with respect to the monomeric species after storage at 40°C over two weeks. No significant increase of HMWS was observed after two weeks of storage at 4°C (Figure S10 in the supporting information).

Finally, brentuximab-10 was evaluated *in vivo* in a Karpas 299 derived tumor xenograft model in immune-deficient female CB17-SCID mice similar as previously reported.[35] In a first study, four mice were treated with brentuximab-10 twice, at day 7 and day 10, with 1 mg ADC per kg bodyweight. In addition, we used commercially available Adcetris® as a reference to compare the performance of brentuximab-10 in this *in vivo* model. Mice in the control group were treated with PBS only. All 4 mice treated with brentuximab-10 or Adcetris® showed an excellent response to the treatment. Treated mice were in tumor remission already a few days after ADC injection and no relapse was observed over the whole observation period of 58 days, while the untreated control showed an uncontrolled tumor growth and had to be sacrificed within three weeks after tumor transplantation (Figure 3d and S10 in the supporting information). It was previously reported, that an ADC with an average of four MMAE molecules connected to brentuximab via maleimides is significantly less efficacious in a tumor xenograft model when the dosing is lowered from 1 to 0.5 mg/kg.[35] From our serum stability studies (Figure 3c), we anticipated that phosphonamidate linked ADCs might still be active at lower doses due to a prolonged drug delivery in circulation. Therefore, we initiated a second *in vivo* study with eight mice, treated with either 0.5 mg/kg brentuximab-10 or Adcetris® twice at day 8 and day 12. As expected, we observed decreased antitumor activity for both constructs when compared to the first study, leading to tumor remission in two mice for brentuximab-10 and only one for Adcetris®.

However, five out of eight mice did not show any observable response to the treatment with Adcetris®. Here, the tumor growth was as fast as in the PBS treated control group. In contrast, this was only observed in two mice treated with brentuximab-10 (Figure 3f and S10 in the supporting information). Hence, we were able to show a drastic increase in median survival from 21 days for commercial Adcetris® to 48 days for brentuximab-10 (Figure 3g). We strongly believe that this increase by a factor of 2.3 in comparison to Adcetris® indicates a promising antitumor activity of our novel phosphonamidate-linked ADCs. It should be noted that all of the mice, treated with both constructs did not significantly change in bodyweight over the whole observation period (Figure S10 in the supporting information).

In summary, we present ethynylphosphonamidates as cysteine reactive handles for the construction of next generation cancer therapeutics. We obtained a new modular hydrophilic ethynylphosphonamidate building block for the synthesis of hydrophilic, Cys-selective linker systems for the conjugation of unpolar payloads. With this, we synthesized an ADC from brentuximab and MMAE, and demonstrated appropriate linkage stability combined with beneficial *in vivo* antitumor activity, resulting in an increased median survival from 21 days for Adcetris® to 48 days for the phosphonamidate linkage. The conjugation protocol is straightforward, using only minimal drug excesses and facilitates a one-pot synthesis of an ADC starting from native antibodies. Taken together, we believe that ethynylphosphonamidates described herein facilitate the straightforward construction of ADCs for cancer therapeutics with great promise for other pharmacological targets.

Acknowledgements and Funding

We thank K. K. Hassanin for excellent technical assistance. This work was supported by grants from the Deutsche Forschungsgemeinschaft (DFG) (SPP1623) to C.P.R.H. and (HA 4468/9-1), (LE 721/13-2) and (SFB1243/A01) to H.L., the Einstein Foundation Berlin (Leibniz-Humboldt Professorship), the Boehringer-Ingelheim Foundation (Plus 3 award) and the Fonds der Chemischen Industrie to C.P.R.H, by the Leibniz Association with the Leibniz Wettbewerb to C.P.R.H and H.L., by the German Federal Ministry for Economic Affairs and Energy and the European Social Fund with grants to D.S. and J.H. (EXIST FT I) and by the Bavarian Ministry of Economic Affairs, Regional Development and Energy with grants to D.S., J.H., H.L. and C.P.R.H. (m4-Award). A.S. was trained and supported by the graduate school RTG1721 of the DFG.

Figures

Scheme 1. Synthesis of a phosphonamidate modified, cathepsin B cleavable MMAF **4**.

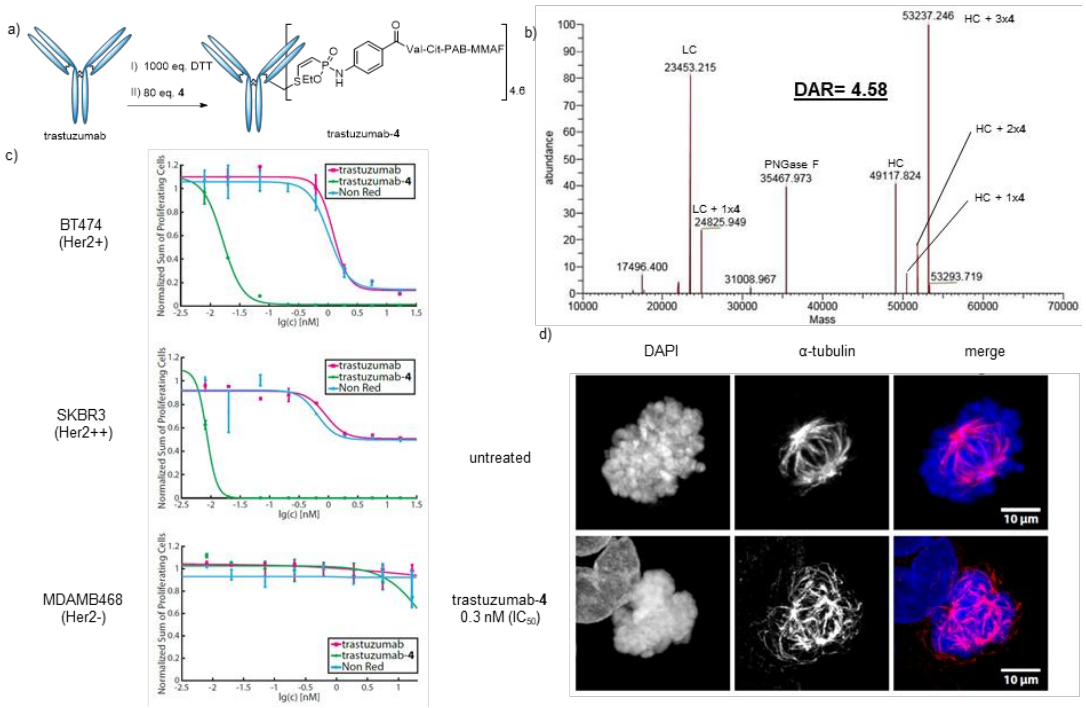

Figure 1. a) Synthetic scheme for the attachment of 4 to trastuzumab b) Deconvoluted spectrum of deglycosylated and reduced trastuzumab-4. LC: Light chain, HC: Heavy Chain. DAR: Drug to Antibody Ratio c) Antiproliferative potency of trastuzumab-4 on two Her2 overexpressing cell lines (SKBR3, BT474) and a control (MDAMB468). Plots depict the number of proliferating cells after 4 days of antibody treatment in dependency of the antibody concentration. Trastuzumab alone (magenta), trastuzumab-4 (green) and trastuzumab without disulfide reduction prior incubation with 4 (cyan). d) Effect of trastuzumab-4 treatment on mitotic tubulin organization in BT474 (Her2+) cells. Shown are representative images of mitotic BT474 cells after 4 days of treatment with 0.3 nM trastuzumab-4 and untreated.

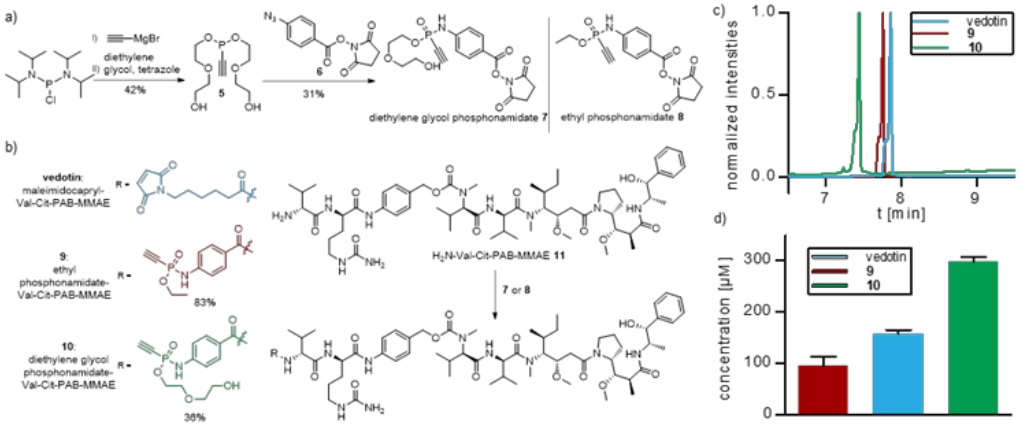

Figure 2. a) Synthesis of an ethylene glycol substituted ethynylphosphonamidate NHS-ester containing building block **7** and structural comparison to the corresponding ethyl substitute **8**.[22] b) Structure of vedotin and synthesis of ethyl- and diethylene glycol phosphonamidate-based vedotin analogs. c) RP-HPLC analysis of vedotin (cyan) and the analogs **9** (red) and **10** (green). Shown are normalized absorption spectra at 254 nm. d) Solubility in PBS with 5% DMSO of vedotin (cyan) and the analogs **9** (red) and **10** (green) in µM. Error bars originate from three independent measurements.

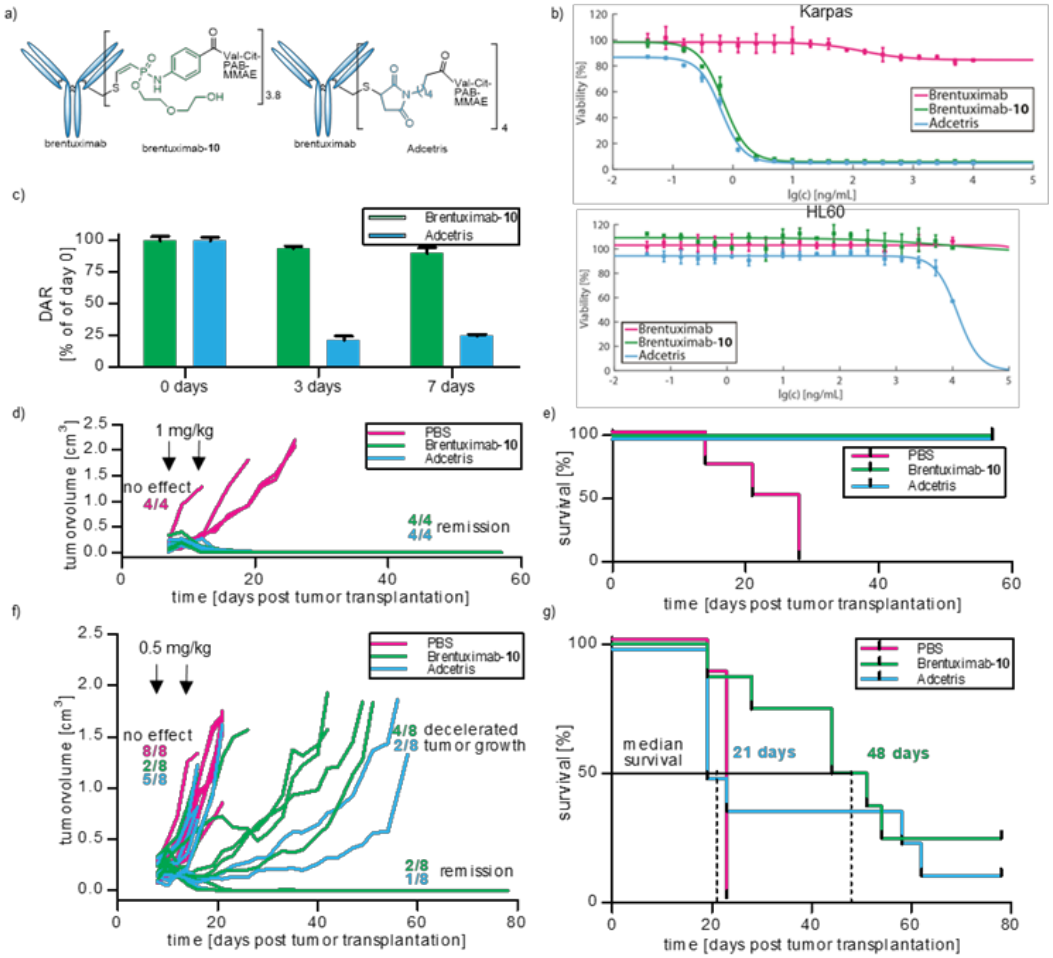

Figure 3. a) Structural comparison of Adcetris® with brentuximab-**10** b) Cell viability assays with a CD30 overexpressing cell line (Karpas299, top) and a control (HL60, bottom) for brentuximab-**10** (green) and Adcetris® (cyan) and brentuximab alone (magenta) c) Linkage-stability studies in rat serum. ADCs were incubated in rat serum for 0, 3 and 7 days at 37 °C and analyzed by MS after pulldown, deglycosylation and reduction. Shown is the DAR relative to the average DAR of day 0 for brentuximab-**10** (green) and Adcetris® (cyan). d) Antitumor activity of brentuximab-**10** (green) and Adcetris® (cyan) and a PBS control (magenta) in a Karpas 299 tumor xenograft model in SCID mice. Treatment of 1 mg/kg was administered twice at day 7 and day 10 after tumor transplantation Shown are tumor volumes of four mice per group separately. e) Kaplan-Meier survival analysis of the study described in d. f) Antitumor activity of brentuximab-**10** (green) and Adcetris® (cyan) and a PBS control (magenta) in a Karpas 299 tumor xenograft model in SCID mice. Treatment of 0.5 mg/kg was administered twice at day 8 and day 12 after tumor transplantation Shown are tumor volumes of eight mice per group separately. g) Kaplan-Meier survival analysis of the study described in f. Median survival is 21 days for Adcetris® and 48 days for brentuximab-**10**.

References

[1] V. Chudasama, A. Maruani, S. Caddick, Nat. Chem. 2016, 8, 114-119.

[2] S. Mariathasan, M.-W. Tan, Trends Mol. Med. 2017, 23, 135-149.

[3] D. Schumacher, C. P. R. Hackenberger, H. Leonhardt, J. Helma, Journal of Clinical Immunology 2016, 36, 100-107.

[4] N. Uy, M. Nadeau, M. Stahl, A. M. Zeidan, J. Blood Med. 2018, 9, 67-74.

[5] F. R. Appelbaum, I. D. Bernstein, Blood 2017.

[6] A. Beck, L. Goetsch, C. Dumontet, N. Corvaïa, Nature Reviews Drug Discovery 2017, 16, 315.

[7] P. Agarwal, C. R. Bertozzi, Bioconjugate chemistry 2015, 26, 176-192.

[8] aB.-Q. Shen, K. Xu, L. Liu, H. Raab, S. Bhakta, M. Kenrick, K. L. Parsons-Reponte, J. Tien, S.-F. Yu, E. Mai, D. Li, J. Tibbitts, J. Baudys, O. M. Saad, S. J. Scales, P. J. McDonald, P. E. Hass, C. Eigenbrot, T. Nguyen, W. A. Solis, R. N. Fuji, K. M. Flagella, D. Patel, S. D. Spencer, L. A. Khawli, A. Ebens, W. L. Wong, R. Vandlen, S. Kaur, M. X. Sliwkowski, R. H. Scheller, P. Polakis, J. R. Junutula, Nat. Biotechnol. 2012, 30, 184-189; bP. J. Burke, J. Z. Hamilton, S. C. Jeffrey, J. H. Hunter, S. O. Doronina, N. M. Okeley, J. B. Miyamoto, M. E. Anderson, I. J. Stone, M. L. Ulrich, J. K. Simmons, E. E. McKinney, P. D. Senter, R. P. Lyon, Mol. Cancer Ther. 2017, 16, 116.

[9] S. O. Doronina, B. E. Toki, M. Y. Torgov, B. A. Mendelsohn, C. G. Cerveny, D. F. Chace, R. L. DeBlanc, R. P. Gearing, T. D. Bovee, C. B. Siegall, J. A. Francisco, A. F. Wahl, D. L. Meyer, P. D. Senter, Nat. Biotechnol. 2003, 21, 778-784.

[10] J. F. Ponte, X. Sun, N. C. Yoder, N. Fishkin, R. Laleau, J. Coccia, L. Lanieri, M. Bogalhas, L. Wang, S. Wilhelm, W. Widdison, J. Pinkas, T. A. Keating, R. Chari, H. K. Erickson, J. M. Lambert, Bioconjugate Chem. 2016, 27, 1588-1598.

[11] R. P. Lyon, J. R. Setter, T. D. Bovee, S. O. Doronina, J. H. Hunter, M. E. Anderson, C. L. Balasubramanian, S. M. Duniho, C. I. Leiske, F. Li, P. D. Senter, Nat. Biotechnol. 2014, 32, 1059.

[12] B. Bernardim, P. M. S. D. Cal, M. J. Matos, B. L. Oliveira, N. Martínez-Sáez, I. S. Albuquerque, E. Perkins, F. Corzana, A. C. B. Burtoloso, G. Jiménez-Osés, G. J. L. Bernardes, Nat. Commun. 2016, 7, 13128.

[13] D. Kalia, P. V. Malekar, M. Parthasarathy, Angew. Chem. Int. Ed. 2016, 55, 1432-1435.

[14] O. Koniev, A. Wagner, Chem. Soc. Rev. 2015, 44, 5495-5551.

[15] C. D. Medley, J. Kay, Y. Li, J. Gruenhagen, P. Yehl, N. P. Chetwyn, Anal. Chim. Acta 2014, 850, 92-96.

[16] J. R. McCombs, S. C. Owen, The AAPS journal 2015, 17, 339-351.

[17] aI. Hollander, A. Kunz, P. R. Hamann, Bioconjugate Chem. 2008, 19, 358-361; bA. Wakankar, Y. Chen, Y. Gokarn, F. S. Jacobson, mAbs 2011, 3, 161-172.

[18] A. Saluja, D. S. Kalonia, Int. J. Pharm. 2008, 358, 1-15.

[19] A. Mullard, Nat. Rev. Drug Discov. 2013, 12, 329.

[20] R. Y. Zhao, S. D. Wilhelm, C. Audette, G. Jones, B. A. Leece, A. C. Lazar, V. S. Goldmacher, R. Singh, Y. Kovtun, W. C. Widdison, J. M. Lambert, R. V. J. Chari, J. Med. Chem. 2011, 54, 3606-3623.

[21] R. P. Lyon, T. D. Bovee, S. O. Doronina, P. J. Burke, J. H. Hunter, H. D. Neff-LaFord, M. Jonas, M. E. Anderson, J. R. Setter, P. D. Senter, Nat. Biotechnol. 2015, 33, 733.

[22] M.-A. Kasper, M. Glanz, A. Stengl, M. Penkert, S. Klenk, T. Sauer, D. Schumacher, J. Helma, E. Krause, M. C. Cardoso, H. Leonhardt, C. P. R. Hackenberger, Angew. Chem. Int. Ed., Manuscript submitted.

[23] S. O. Doronina, B. A. Mendelsohn, T. D. Bovee, C. G. Cerveny, S. C. Alley, D. L. Meyer, E. Oflazoglu, B. E. Toki, R. J. Sanderson, R. F. Zabinski, A. F. Wahl, P. D. Senter, Bioconjugate Chem. 2006, 17, 114-124.

[24] aI. Rillat, M. Perez, L. Goetsch, M. Broussas, C. Beau-Larvor, J.-F. Haeuw, Vol. WO2015162293, WO2015162293 (A1) ed., 2015; bL. Liang, S.-W. Lin, W. Dai, J.-K. Lu, T.-Y. Yang, Y. Xiang, Y. Zhang, R.-T. Li, Q. Zhang, J. Control. Release 2012, 160, 618-629.

[25] A. Stengl, D. Hörl, H. Leonhardt, J. Helma, SLAS Discov. 2017, 22, 309-315.

[26] A. B. Waight, K. Bargsten, S. Doronina, M. O. Steinmetz, D. Sussman, A. E. Prota, PLoS One 2016, 11, e0160890.

[27] aM. R. J. Vallée, P. Majkut, I. Wilkening, C. Weise, G. Müller, C. P. R. Hackenberger, Organic Letters 2011, 13, 5440-5443; bK. D. Siebertz, C. P. R. Hackenberger, Chem. Commun. 2018, 54, 763-766.

[28] S. M. Ansell, Blood 2014, 124, 3197-3200.

[29] C. Bahou, E. A. Love, S. Leonard, R. J. Spears, A. Maruani, K. Armour, J. R. Baker, V. Chudasama, Bioconjugate Chem. 2019.

[30] T. Kantner, A. G. Watts, Bioconjugate Chem. 2016, 27, 2400-2406.

[31] C. Wei, G. Zhang, T. Clark, F. Barletta, L. N. Tumey, B. Rago, S. Hansel, X. Han, Anal. Chem. 2016, 88, 4979-4986.

[32] L. N. Tumey, M. Charati, T. He, E. Sousa, D. Ma, X. Han, T. Clark, J. Casavant, F. Loganzo, F. Barletta, J. Lucas, E. I. Graziani, Bioconjugate Chem. 2014, 25, 1871-1880.

[33] S. D. Fontaine, R. Reid, L. Robinson, G. W. Ashley, D. V. Santi, Bioconjugate Chem. 2015, 26, 145-152.

[34] N. S. Beckley, K. P. Lazzareschi, H.-W. Chih, V. K. Sharma, H. L. Flores, Bioconjugate Chem. 2013, 24, 1674-1683.

[35] K. J. Hamblett, P. D. Senter, D. F. Chace, M. M. C. Sun, J. Lenox, C. G. Cerveny, K. M. Kissler, S. X. Bernhardt, A. K. Kopcha, R. F. Zabinski, D. L. Meyer, J. A. Francisco, Clin. Cancer Res. 2004, 10, 7063-7070.

Ethynylphosphonamidates for the rapid and cysteine selective generation of efficacious Antibody-Drug-Conjugates

Marc-André Kasper, Andreas Stengl, Philipp Ochtrop, Marcus Gerlach, Tina Stoschek, Dominik Schumacher, Jonas Helma, Martin Penkert, Eberhard Krause, Heinrich Leonhardt and Christian P. R. Hackenberger

Supplementary Information

Ethynylphosphonamidates for the rapid and cysteine selective generation of efficacious Antibody-Drug-Conjugates

Marc-André Kasper[1,2], Andreas Stengl[3], Philipp Ochtrop[1], Marcus Gerlach[3], Tina Stoschek[3], Dominik Schumacher[1,2,3], Jonas Helma[3], Martin Penkert[1,2], Eberhard Krause[1], Heinrich Leonhardt[3]* and Christian P. R. Hackenberger[1,2,]*

[1]Leibniz-Forschungsinstitut für Molekulare Pharmakologie (FMP), Chemical Biology Department, Robert-Rössle-Strasse 10, 13125 Berlin (Germany)

[2]Humboldt Universität zu Berlin, Department of Chemistry, Brook-Taylor-Str. 2, 12489 Berlin (Germany)

[3]Ludwig-Maximilians-Universität München, Department of Biology II, and Center for Integrated Protein Science Munich, Großhadenerstr. 2, 82152 Martinsried (Germany)

*e-mail: hackenbe@fmp-berlin.de, h.leonhardt@lmu.de

Supporting Information

Table of contents

1. Supplementary Figures

1.1. Figure S1

Synthetic route to compound **1**

1.2. Figure S2

Increased cytotoxicity of MMAF linked trastuzumab on a Her2 overexpressing cell line (SKBR3) and a control (MDAMB468), demonstrated in a Resazurin assay. Plots depict cell viability after antibody treatment in dependency of the antibody concentration. Trastuzumab alone (pink) and trastuzumab-**4** (green). (See chapter 3.4 for details)

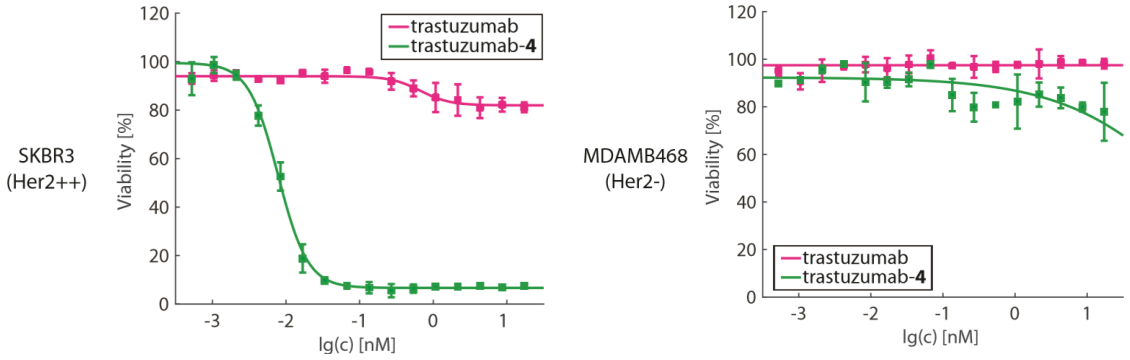

1.3. Figure S3

Effect of trastuzumab-**4** treatment on mitotic tubulin organization in BT474 (Her2+) cells. Shown are three representative images of mitotic BT474 cells after 4 days of treatment with 0.3 nM trastuzumab-**4** (a) and untreated (b). DAPI stain visualizes DNA condensation. Anti α-tubulin immunostaining visualizes spindle organization in untreated mitotic cells. Cells treated with trastuzumab-**4** show DNA condensation but a strongly altered and distorted α-tubulin pattern.

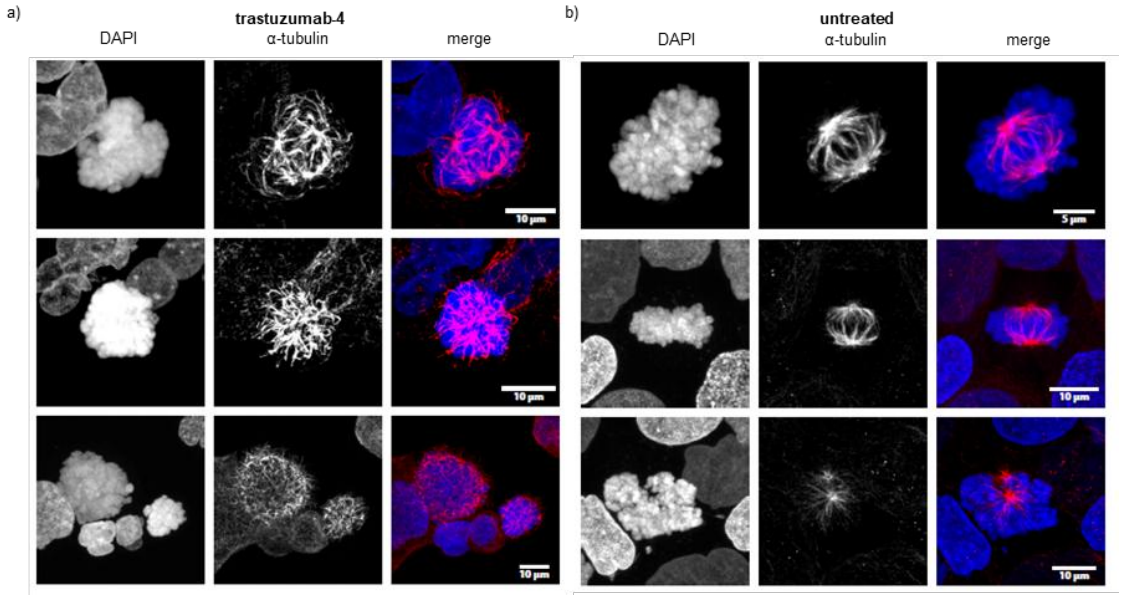

1.4. Figure S4

Solubility measurements of **9** (red), **10** (green) and vedotin (cyan) in PBS with 5% DMSO and Inosine as an internal standard. (See chapter 3.5 for details) a) Calibration curves of different analyte concentrations (5, 10, 50, 100 and 200 µM) were recorded by UPLC/UV by peak integration of the analyte in relation to Inosin as an internal standard. Shown are error bars from three independent measurements (black) and a linear fit. Values that were out of the concentration range and therefore not in the linear region were excluded from the fit (grey). b) Three independent measurements of saturated solutions and concentration calculation with the linear equation, estimated in a.

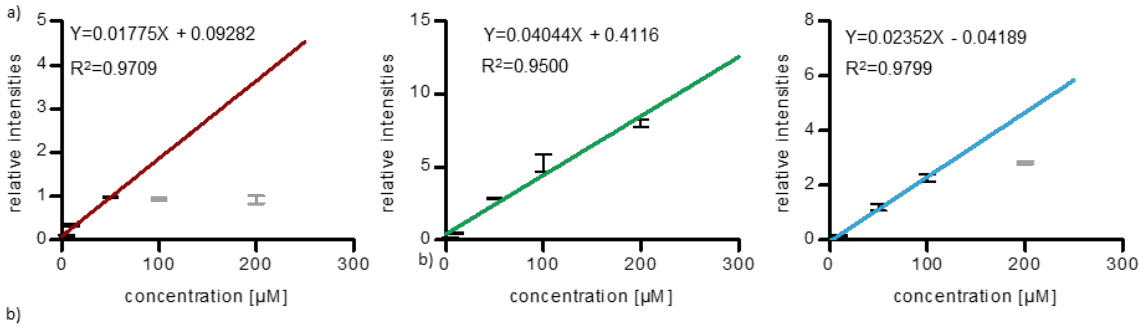

b)

relative intensities	concentration [µM]	relative intensities	concentration [µM]	relative intensities	concentration [µM]
1.47054541	78	12.19842	291	3.57240427	154
1.75660984	93	12.9149908	309	3.87751283	167
2.10353633	113	12.2324009	292	3.53587418	152

1.5. Figure S5

Modification of brentuximab at **1 mg/ml** with varying equivalents of the vedotin analog **10** delivers ADCs with different DARs. (See chapter 3.7 for details) a) SDS-PAGE and DAR-analysis of brentuximab, reduced with 1000 eq. DTT and alkylated with **10**. Modification was carried out under the same conditions for every reaction: 1 mg/ml antibody, 50 mM tris-buffer, 1 mM EDTA pH 8.5 and 5% DMSO; reaction over-night at 14°C as described in chapter 3.6. DAR-analysis was carried as described in chapter 3.9. b) Exemplary MS-spectrum and calculated DAR of sample in lane 5 (modification carried out with 10 eq. **10**). HC: heavy chain, LC: light chain. *deconvolution artefacts (half mass of HC species and double mass of LC species) c) Plot of phosphonamidate equivalents against the measured DAR. Shown are results of 20 independent experiments (dots) and an exponential fit (solid line, R^2= 0.9540). Red line marks the theoretical equivalents (16 in this case) to reach a DAR of 4.

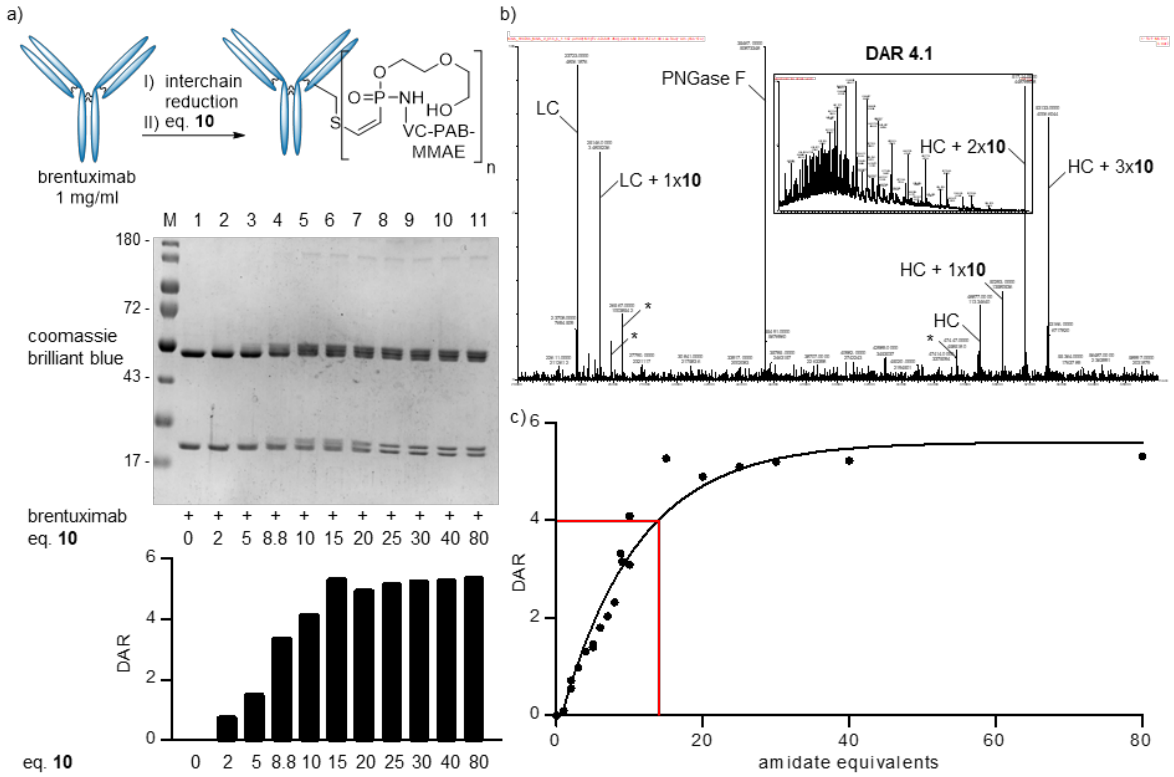

1.6. Figure S6

Increased conjugation efficiency can be observed at **5 mg/ml** brentuximab. (See chapter 3.8 for details) a) DAR-analysis of brentuximab, reduced with 200 eq. of DTT and alkylated with **10**. Modification was carried out under the same conditions for every reaction: 5 mg/ml antibody, 50 mM tris-buffer, 1 mM EDTA pH 8.5 and 5% DMSO; reaction over-night at 14°C as described in chapter 3.7. DAR-analysis was carried as described in chapter 3.9. b) Exemplary MS-spectrum and calculated DAR of sample in lane 2 (modification carried out with 6 eq. **10**). HC: heavy chain, LC: light chain.

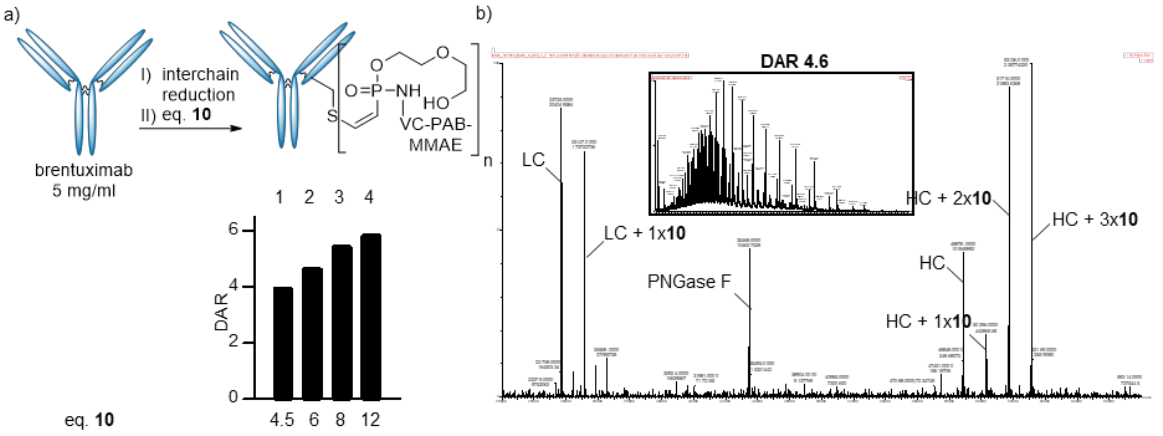

1.7. Figure S7

Partial reduction of the interchain disulfides with small excess of TCEP yields ADCs with a high conjugation effiency in a one-step procedure. (See chapter 3.9 for details) a) DAR-analysis of brentuximab, reduced and alkylated with **10**. Modification was carried out under the same conditions for every reaction with varying equivalents of TCEP: 5 mg/ml antibody, 50 mM tris-buffer, 100 mM NaCl, 1 mM EDTA pH 8.5, 167 µM **10** (5.0 eq.) and 5% DMSO; reaction over-night at 14°C as described in chapter 3.8. DAR-analysis was carried as described in chapter 3.9. b) Exemplary MS-spectrum and calculated DAR of sample in lane 3 (modification carried out with 3 eq. TCEP). HC: heavy chain, LC: light chain.

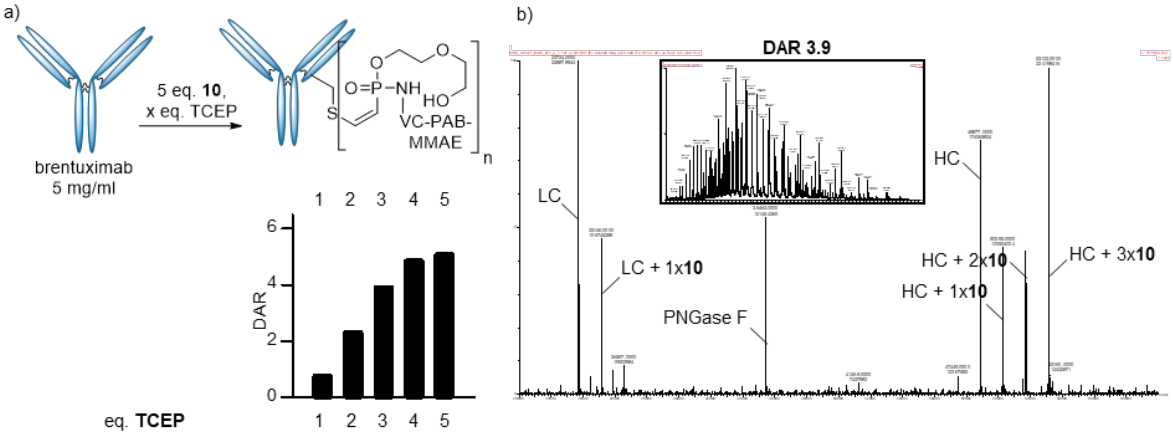

1.8. Figure S8

DAR analysis of brentuximab-**10** (a, green) and Adcetris® (b, cyan) after incubation in rat serum for 0, 3 and 7 days as described in chapter 3.12. Shown are values from three independent measurements for each time point. We measured a DAR of 3.05 (mean of three measurements) for Adcetris at Day 0, even though, Adcetris is known to be modified with an average of 4 drug molecules.[1] We attribute this to a loss of modification during the analysis process of pulldown, deglycosylation, reduction and MS-analysis. Since this sample-preparation was conducted in the same way for day 0, 3 and 7, this should not influence the relative values, given in the main manuscript. c) MS analysis of two Adcetris® measurements (day 0 top and day 3 bottom) indicating hydrolysis of the vedotin molecules that are still attached to the antibody.

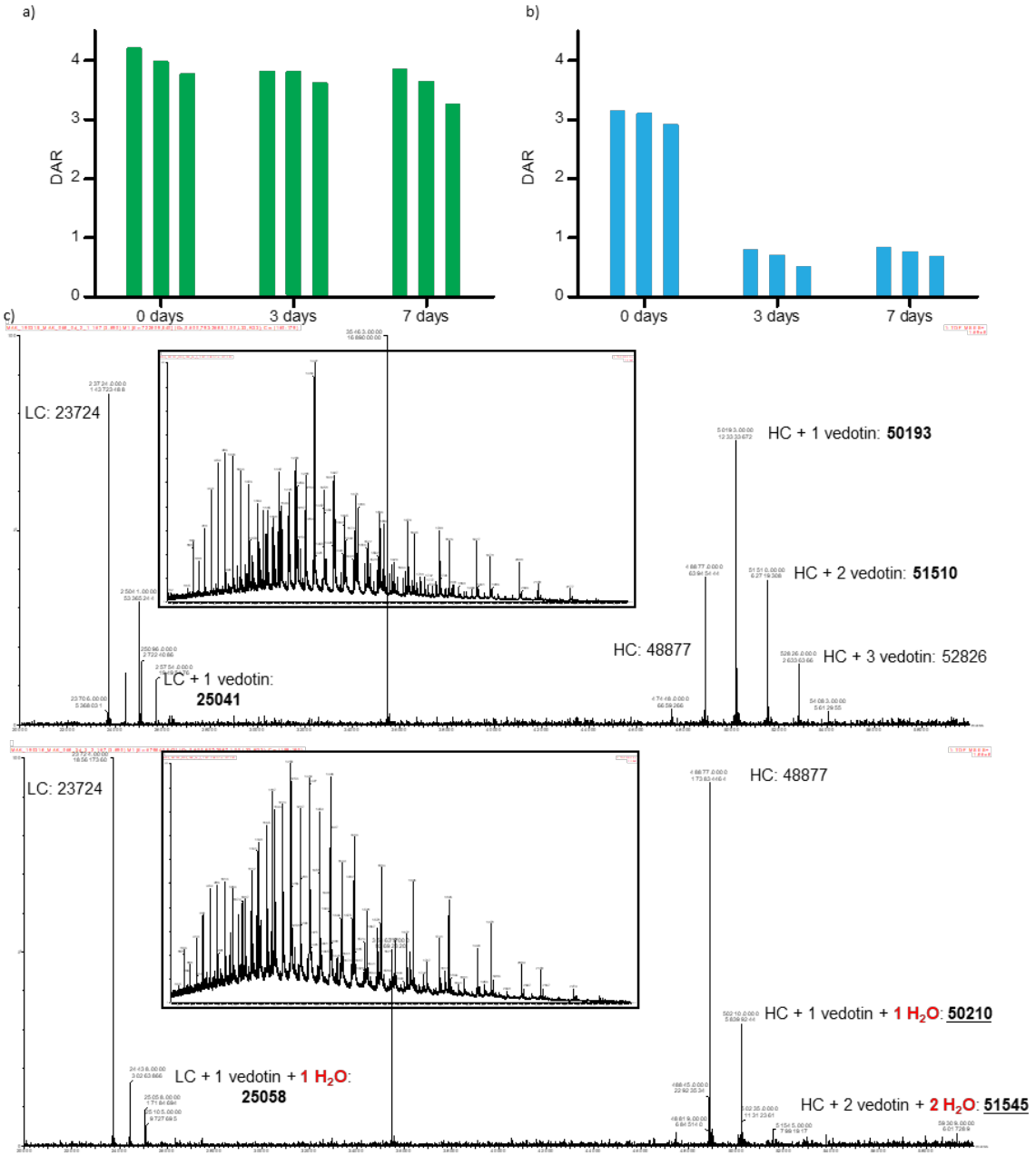

1.9. Figure S9

Size-exclusion HPLC analysis of Brentuximab-**10** after storage at different temperatures in PBS. Chromatograms were recorded after 0, 7 and 14 days. Chromatograms are normalized to the maximal intensity. (See chapter 3.13 for details)

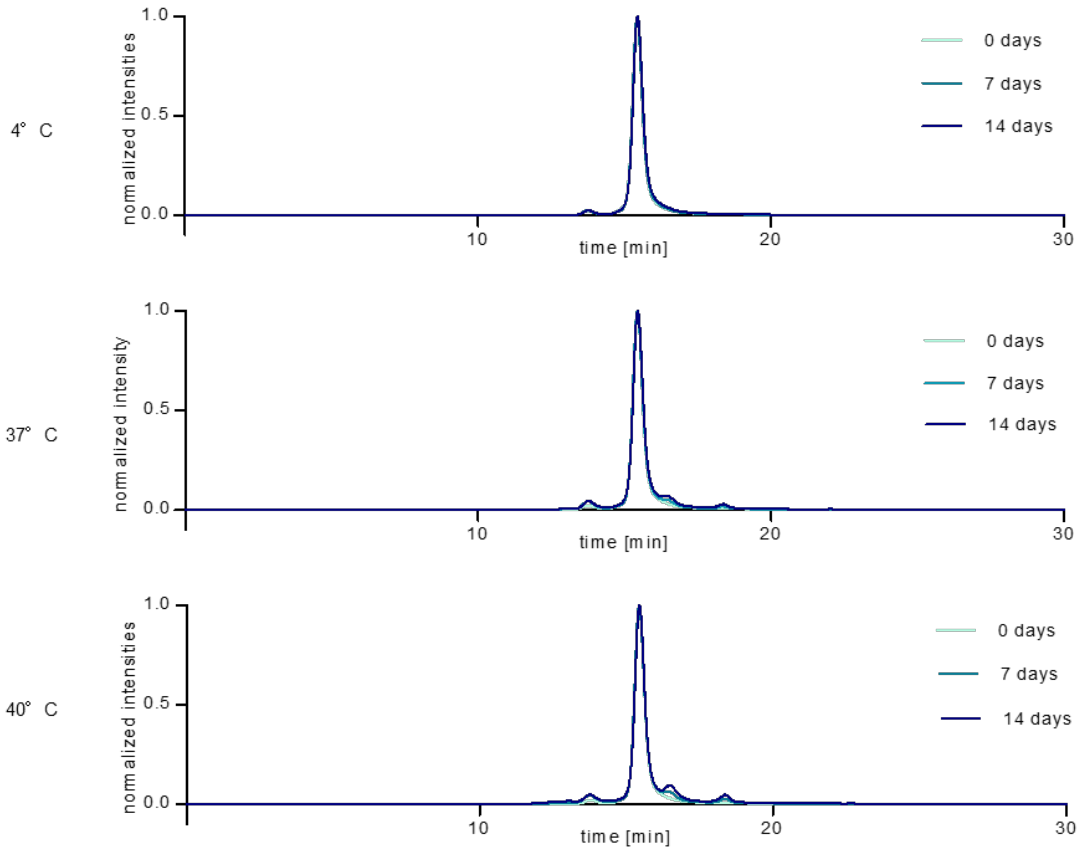

1.10. Figure S10

Changes in bodyweight and tumorvolumes of SCID mice with a Karpas 299 tumor xenograft after treatment with PBS (magenta), Brentuximab-**10** (blue) or PBS (green). Shown are tumor volumes of eight mice per group separately. a) 1. Study: Shown are tumor volumes of four mice per group separately treated at day 7 and 10 with 1 mg/kg ADC. b) 2. Study: Shown are tumor volumes of eight mice per group separately treated at day 8 and 11 with 0.5 mg/kg ADC. (See chapter 3.14 for details)

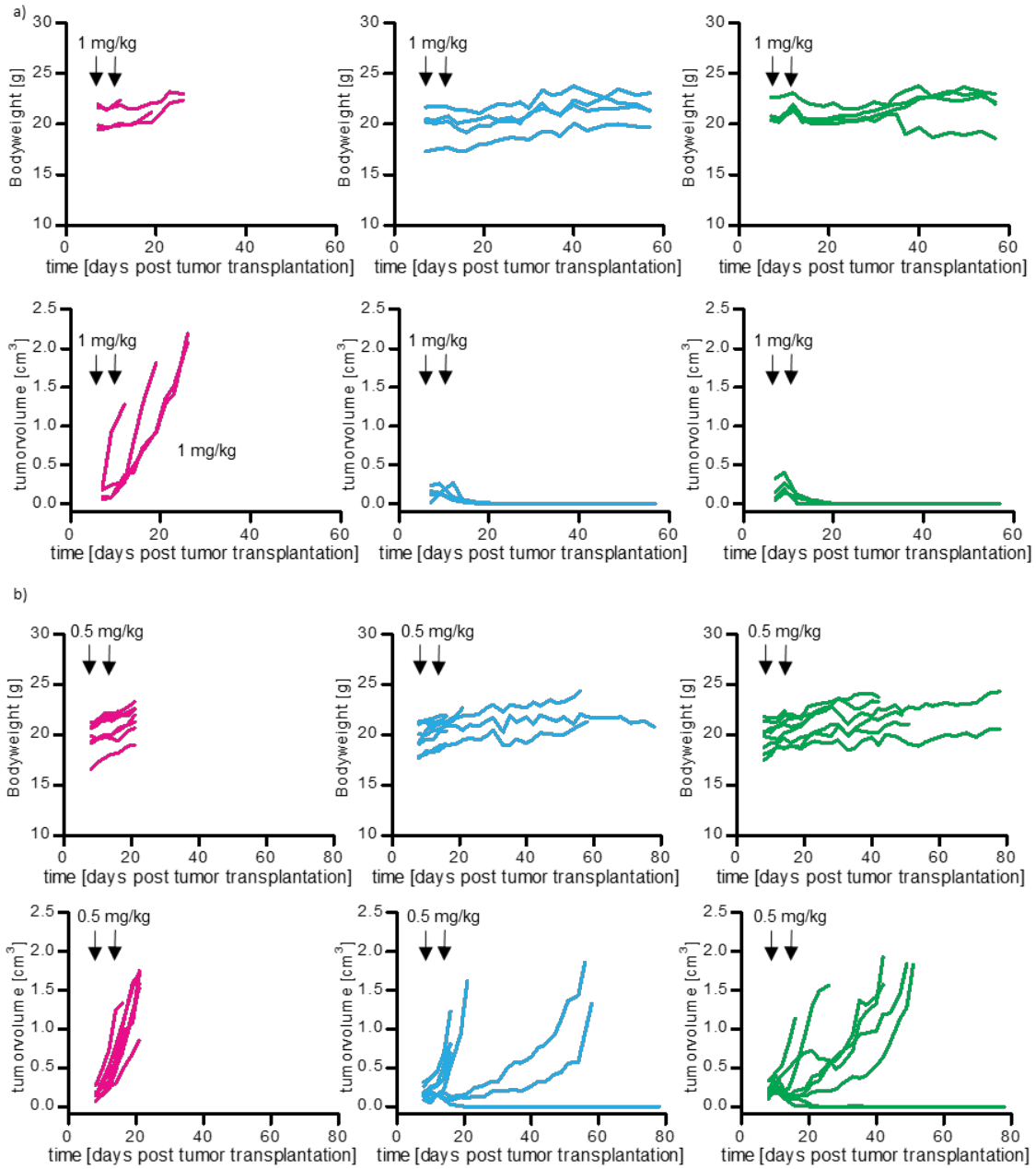

2. General Information

2.1. Chemicals and solvents

Chemicals and solvents were purchased from Merck (Merck group, Germany), TCI (Tokyo chemical industry CO., LTD., Japan) and Acros Organics (Thermo Fisher scientific, USA) and used without further purification. Dry solvents were purchased from Acros Organics (Thermo Fisher scientific, USA).

2.2. Flash- and thin layer chromatography

Flash column chromatography was performed, using NORMASIL 60® silica gel 40-63 µm (VWR international, USA). Glass TLC plates, silica gel 60 W coated with fluorescent indicator F254s were purchased from Merck (Merck Group, Germany). Spots were visualized by fluorescence depletion with a 254 nm lamp or manganese staining (10 g K_2CO_3, 1.5 g $KMnO_4$, 0.1 g NaOH in 200 ml H_2O), followed by heating.

2.3. Preparative HPLC

Preparative HPLC was performed on a Gilson PLC 2020 system (Gilson Inc, WI, Middleton, USA) using a VP 250/32 Macherey-Nagel Nucleodur C18 HTec Spum column (Macherey-Nagel GmbH & Co. Kg, Germany). The following gradients were used: Method C: (A = H_2O + 0.1% TFA (trifluoroacetic acid), B = MeCN (acetonitrile) + 0.1% TFA, flow rate 30 ml/min, 5% B 0-5 min, 5-90% B 5-60 min, 90% B 60-65 min. Method D: (A = H_2O + 0.1% TFA, B = MeCN + +0.1% TFA), flow rate 30 ml/min, 5% B 0-5 min, 5-25% B 5-10 min, 25%-45% B 10-50 min, 45-90% 50-60 min, 90% B 60-65 min. Method E: 0.1% TFA, flow rate 18 ml/min, 5% B 0-5 min, 5-90% B 5-60 min, 90% B 60-65 min, using a VP 250/21 Macherey-Nagel Nucleodur C18 HTec Spum column (Macherey-Nagel GmbH & Co. Kg, Germany)

2.4. Semi-preparative HPLC

Semi-preparative HPLC was performed on a Shimadzu prominence HPLC system (Shimadzu Corp., Japan) with a CBM20A communication bus module, a FRC-10A fraction collector, 2 pumps LC-20AP, and a SPD-20A UV/VIS detector, using a VP250/10 Macherey-Nagel Nucleodur C18 HTec Spum column (Macherey-Nagel GmbH & Co. Kg, Germany). The following gradients were used: Method F: (A = H_2O + 0.1% TFA, B = MeCN + +0.1% TFA), flow rate 5 ml/min, 30% B 0-5 min, 30-99% B 5-65 min, 99% B 65-75 min.

2.5. NMR

NMR spectra were recorded with a Bruker Ultrashield 300 MHz spectrometer and a Bruker Avance III 600 MHz spectrometer (Bruker Corp., USA) at ambient temperature. Chemical shifts δ are reported in ppm relative to residual solvent peak ($CDCl_3$: 7.26 [ppm]; DMSO-d6: 2.50 [ppm] for ^{1}H-spectra and $CDCl_3$: 77.16 [ppm]; DMSO-d6: 39.52 [ppm] for ^{13}C-spectra . Coupling constants *J* are stated in Hz. Signal multiplicities are abbreviated as follows: s: singlet; d: doublet; t: triplet; q: quartet; m: multiplet.

2.6. HR-MS

High resolution ESI-MS spectra were recorded on a Waters H-class instrument equipped with a quaternary solvent manager, a Waters sample manager-FTN, a Waters PDA detector and a Waters column manager with an Acquity UPLC protein BEH C18 column (1.7 µm, 2.1 mm x 50 mm). Samples were eluted with a flow rate of 0.3 mL/min. The following gradient was used: A: 0.01% FA in H_2O; B: 0.01% FA in MeCN. 5% B: 0-1 min; 5 to 95% B: 1-7min; 95% B: 7 to 8.5 min. Mass analysis was conducted with a Waters XEVO G2-XS QTof analyzer.

2.7. UPLC-UV/MS

UPLC-UV/MS traces were recorded on a Waters H-class instrument equipped with a quaternary solvent manager, a Waters autosampler, a Waters TUV detector and a Waters Acquity QDa detector with an Acquity UPLC BEH C18 1.7 µm, 2.1 x 50 mm RP column with a flow rate of 0.6 mL/min (Waters Corp., USA). The following gradient was used for purity analyses: A: 0.1% TFA in H_2O; B: 0.1% TFA in MeCN. 5% B 0 - 1.5 min, 5-95% B 1.5-11 min, 95% B 11-13 min, 5% B 13-15 min. The following gradient was used in the solubility assay: A: 0.1% TFA in H_2O; B: 0.1% TFA in MeCN. 5% B 0 - 0.5 min, 5-95% B 0.5-3 min, 95% B 3-3.9 min, 5% B 3.9-5 min.

2.8. Intact protein MS (trastuzumab conjugates only)

Reduced antibody subunits were analyzed using a reversed-phase liquid chromatography system (Dionex Ultimate 3000 NCS-3500RS Nano, Thermo Scientific) connected to an Orbitrap Fusion mass spectrometer (Thermo Scientific). Chromatographic separation was performed with an Acquity UPLC protein BEH C4 column (300 Å, 1.7 µm, 2.1 mm x 50 mm). Component A of the mobile phase was 0.01% formic acid in water and component B consist of Acetonitrile with 0.01% formic acid. Separation was performed with a flow rate of 300 µL/min within 7.5 min linear gradient starting with 0% and ending with 40% of component B, followed by a flushing step until 80% of component B. Proteins were ionized in positive ion mode applying a spray voltage of 4.5 kV, using sheath gas (75 Arb), aux gas (12 Arb), sweep gas (1 Arb) and a vaporizer temperature of 300°C. Ionized proteins were analyzed in intact protein mode with a resolution of 15000 (FWHM), 10 microscans and a scan range of m/z 500-3000. The maximum injection time was set to 100 ms to reach an AGC-Target value of 5e5.

Raw data were analyzed with ProteinDeconvolut version 3.0 (Thermo Scientific), considering a m/z range of 800-3000 and charge states ranging from 10-100. 30000 was used as a targeted mass and the intact protein model was chosen. The output mass range was 10000-70000.

2.9. Intact protein MS (all brentuximab conjugates)

Intact proteins were analyzed using a Waters H-class instrument equipped with a quaternary solvent manager, a Waters sample manager-FTN, a Waters PDA detector and a Waters column manager with an Acquity UPLC protein BEH C4 column (300 Å, 1.7 µm, 2.1 mm x 50 mm). Proteins were eluted with a flow rate of 0.3 mL/min. The following gradient was used: A: 0.01% FA in H_2O; B: 0.01% FA in MeCN. 5-95% B 0-6 min. Mass analysis was conducted with a Waters XEVO G2-XS QTof analyzer. Proteins were ionized in positive ion mode applying a cone voltage of 40 kV. Raw data was analyzed with MaxEnt 1.

2.10. Preparative size-exclusion chromatography

Protein purification by size-exclusion chromatography was conducted with an ÄKTA FPLC system (GE Healthcare, United States) equipped with a P-920 pump system, a UPC-900 detector and a FRAC-950 fraction collector.

2.11. Analytical size-exclusion chromatography

Analytical size-exclusion chromatography (A-SEC) of the ADCs was conducted on a Vanquish Flex UHPLC System with a DAD detector, Split Sampler FT (4°C), Column Compartment H (25°C) and binary pump F (Thermo Fisher Scientific, USA) using a MAbPac SEC-1 300 Å, 4 x 300 mm column (Thermo Fisher Scientific, USA) with a flow rate of 0.15 mL/min. Separation of different ADC/mAb populations have been achieved during a 30 minute isocratic gradient using a phosphate buffer at pH 7 (20 mM Na_2HPO_4/NaH_2PO_4,

300 mM NaCl, 5% v/v isopropyl alcohol as a mobile phase. 8 µg ADC/mAb where loaded onto the column for A-SEC analysis. UV chromatograms were recorded at 220 and 280 nm. Quantification of monomer and HMWS was achieved after integration of the peak area at 220 nm.

3. Experimental procedures

3.1. Trastuzumab production

Trastuzumab expression and purification was executed as previously published with an additional final purification by gel filtration on a Superdex 200 Increase 10/300 from GE (GE life sciences, USA) with PBS and flow rate of 0.75 ml/min.[2]

3.2. Synthesis and analysis of trastuzumab-MMAF conjugates

Trastuzumab modification was carried out by incubating freshly expressed antibody (0.5 mg/ml, 3.33 µM) with 1000 eq. of DTT in a buffer containing 50 mM sodium borate in PBS (pH 8.0) with a total volume of 80 µl at 37 °C for 40 min. Excess DTT removal and buffer exchange to a solution containing 50 mM NH_4HCO_3 and 1mM EDTA (pH 8.5) was conducted afterwards using 0.5 mL Zeba™ Spin Desalting Columns with 7K MWCO (Thermo Fisher Scientific, USA). 4 µl of *O*-Ethyl-*P*-ethynyl-phosphonamidate-VC-PAB-MMAF **4**, dissolved in DMSO (5.33 mM) were added quickly to reach a final DMSO content of 5% and 80 eq. phoshonamidate with respect to the antibody. The mixture was shaken at 850 rpm and 14 °C for 16 hours. Excess reagent was again removed by buffer exchange to sterile PBS using 0.5 mL Zeba™ Spin Desalting Columns with 7K MWCO.

For SDS-page-analysis, 2 µl of the crude reaction mixture were mixed with 10 µl of ultrapure water and 4 µl Laemmli sample buffer (Bio-Rad Laboratories, USA) containing 0.4 µl 2-mercaptoethanol. Samples were heated to 95 °C for 15 minutes and completely loaded to the SDS-PAGE gel.

For MS analysis: The modified antibody was rebuffered to 100 mM NH_4HCO_3 and 500 mM NaCl using 75 µL Zeba™ Spin Desalting Columns with 7K MWCO (Thermo Fisher Scientific, USA). 8 µl of this solution were treated with 1 µl RapiGest™ (Waters Corp., USA) solution (1% in H_2O) and heated to 60 °C for 30 min. The solution was allowed to cool to room temperature, 1 µl PNGase-F solution (Pomega, Germany, Recombinant, cloned from Elizabethkingia miricola 10 u/µl) was added and the solution was incubated at 37 °C over night. Remaining disulfide bridges were reduced by addition of 1 µl DTT solution (50 mM in H_2O) and incubation at 37°C for 30 min. Samples were diluted with 1% HCl subjected to MS analysis with the Orbitrap Fusion system. (See chapter 2.8)

MS spectrum shows the ion series, which was deconvoluted to obtain the spectrum in Figure 1b.

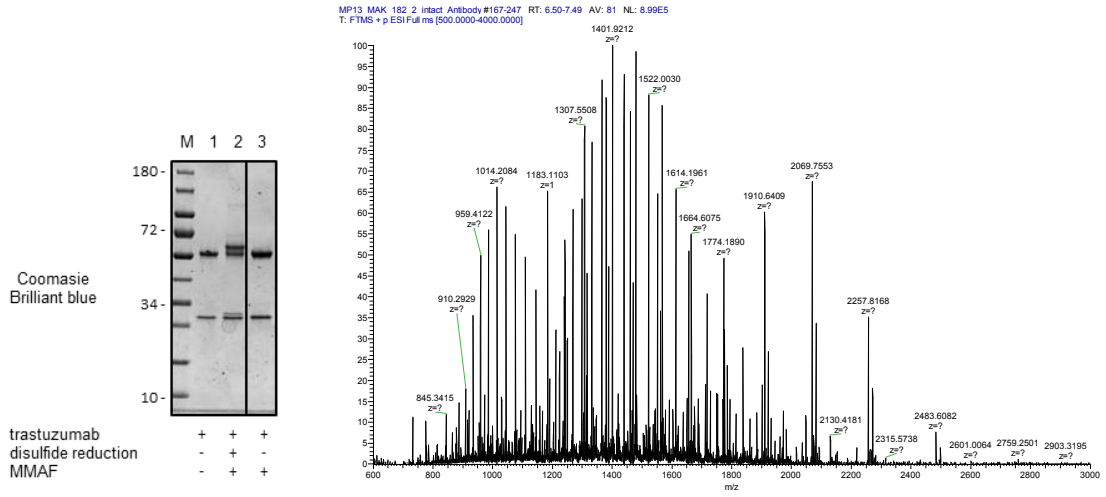

3.3. Cell based antiproliferation assays

Antiproliferation assays were conducted as previously reported[2] with the following minor changes:

- For MDAMB468 cells, a reduced amount of $2*10^3$ cells were seeded in each well of a 96-well optical cell culture plate supplemented with 100 µL culture media.
- Images were acquired with an Operetta High-Content Imaging system (PerkinElmer, Waltham, MA, USA) equipped with a 20× high NA objective.
- Cell counts were calculated from duplicates

3.4. Resazurin assay

HL60 and Karpas cell lines were cultured in RPMI-1640 supplemented with 10% FCS and 0.5% Penicillin-Streptomycin. SKBR3 and MDAMB468 cell lines were cultured in DMEM/F12 supplemented with 10% FCS and 0.5% Penicillin-Streptomycin. Cells were seeded at a density of 5*10^3 cells/well (SKBR3, HL60 and Karpas) or 1*10^3 cells/well (MDAMB468) in 96-well cell culture microplate. 1:4 serial dilutions of ADCs or antibodies were performed in cell culture medium starting at 3 µg/mL final concentration and transferred in duplicates to respective wells on the microplate. Plates were incubated for 96 h at 37°C 5 % CO_2. Subsequently, resazurin was added to a final concentration of 50 µM followed by incubation for 3 – 4 h at 37°C, 5% CO_2. Metabolic conversion of resazurin to resorufin is quantified by the fluorescent signal of resorufin (λ_{EX} = 560 nm and λ_{EM} = 590 nm) on a Tecan Infinite M1000 micro plate reader. Mean and standard deviation was calculated from duplicates, normalized to untreated control and plotted against antibody concentration. Data analysis was performed with MatLab R2016 software.

3.5. Solubility assay

The aqueous solubility of compounds **9**, **10** and vedotin was determined using a shake flask solubility assay. Saturated solutions of the compounds in 5% DMSO/PBS at pH 7.4 were prepared in triplicates by adding 2 µL of compound (40 mM in DMSO) to 38 µL PBS, pH 7.4 containing 50 µM inosine as internal standard. The samples were incubated at 25°C for 2h and subsequently subjected to high-speed centrifugation (10 minutes, 16873 rcf). The supernatant was analyzed by UPLC/UV and the concentration was determined using a standard curve. For the standard curves, serial dilutions in 5% DMSO/PBS at pH 7.4 containing 50 µM Inosine were prepared in triplicates with final compound concentrations of 5 µM, 10 µM, 50 µM, 100 µM and 200 µM. The samples were incubated at 25°C for 2 h and subsequently subjected to high-speed centrifugation (10 minutes, 16873 rcf). The supernatant was analyzed by UPLC/UV and the peak area of compound and internal

standard were integrated. The normalized peak areas (integrated area compound divided by integrated area standard) were plotted against the concentration and a linear fit was applied within the respective solubility range.

3.6. Brentuximab production

Brentuximab expression and purification was executed in analogy to trastuzumab with final purification by gel filtration on a Superdex 200 Increase 10/300 from GE (GE life sciences, USA) with PBS and flow rate of 0.75 ml/min.

3.7. Procedure for the modification of brentuximab (1mg/ml) with different equivalents of 10

35 µl of a 70 mM solution of DTT in 50 mM sodium borate in PBS (pH 8.0) was added to 350 µl of a brentuximab solution of 1.0 mg/ml in 50 mM sodium borate in PBS (pH 8.0) and the mixture was incubated at 37 °C for 40 min. Excess DTT removal and exchange to the conjugation buffer (50 mM Tris, 1 mM EDTA, 100 mM NaCl, pH 8.5 at 14°C) was conducted afterwards using 2 mL Zeba™ Spin Desalting Columns with 7K MWCO (Thermo Fisher Scientific, USA). 50 µl of the reduced antibody solution (0.91 mg/ml, 6.07 µM antibody) were mixed quickly afterwards with the desired amount of *O*-2-(2-Hydroxyethoxy)ethyl-*P*-ethynyl-phosphonamidate-VC-PAB-MMAE **10** dissolved in DMSO to give a final amount of 5% DMSO. The mixture was shaken at 850 rpm and 14 °C for 16 hours. For SDS-page-analysis, 2 µl of the crude reaction mixture were mixed with 10 µl of ultrapure water and 4 µl Laemmli sample buffer (Bio-Rad Laboratories, USA) containing 0.4 µl 2-mercaptoethanol. Samples were heated to 95 °C for 15 minutes and completely loaded to the SDS-PAGE gel.

3.8. Procedure for the modification of brentuximab (5.0 mg/ml) with different equivalents of 10

5 µl of a 70 mM solution of DTT in 50 mM sodium borate in PBS (pH 8.0) was added to 50 µl of a brentuximab solution of 5.0 mg/ml in 50 mM sodium borate in PBS (pH 8.0) and the mixture was incubated at 37 °C for 40 min. Excess DTT removal and exchange to the conjugation buffer (50 mM Tris, 1 mM EDTA, 100 mM NaCl, pH 8.5 at 14°C) was conducted afterwards using 0.5 mL Zeba™ Spin Desalting Columns with 7K MWCO (Thermo Fisher Scientific, USA). 50 µl of the reduced antibody solution (4.55 mg/ml, 30.30 µM antibody) were mixed quickly afterwards with desired amount of *O*-2-(2-Hydroxyethoxy)ethyl-*P*-ethynyl-phosphonamidate-VC-PAB-MMAE **10** dissolved in DMSO to give a final amount of 5% DMSO. The mixture was shaken at 850 rpm and 14 °C for 16 hours.

3.9. Procedure for the partial reduction of brentuximabs interchain disulfide bonds with TCEP

50 µl of a brentuximab solution of 5.0 mg/ml in conjugation buffer (50 mM Tris, 1 mM EDTA, 100 mM NaCl, pH 8.5 at 14°C) were mixed with 5 µl of a TCEP solution in conjugation buffer containing the appropriate amount of TCEP. Directly afterwards, 2.75 µl of a 3.03 mM solution of *O*-2-(2-Hydroxyethoxy)ethyl-*P*-ethynyl-phosphonamidate-VC-PAB-MMAE **10** (5.0 eq. with respect to the antibody) dissolved in DMSO were added to give a final amount of 5% DMSO. The mixture was shaken at 850 rpm and 14 °C for 16 hours.

3.10. Procedure for DAR determination of brentuximab conjugates by intact protein MS

a)

40 µl of the crude antibody modification mixture were purified by size-exclusion chromatography with a 5 ml HiTrap® desalting column and a flow of 1.5 ml/min eluting with 100 mM $NaHCO_3$ and 500 mM NaCl over two column volumes. An exemplary chromatogram is shown below.

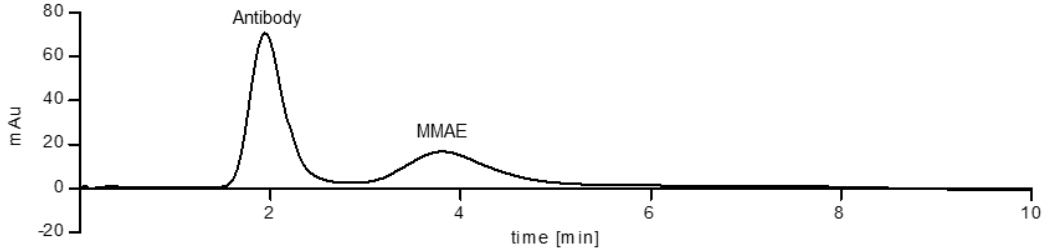

The antibody containing fractions were pooled and concentrated by spin-filtration to 40 µl (MWCO: 10 kDa, 0.5 ml, Sartorius, Germany).

b)

2 µl RapiGest™ solution (1% in H_2O) (Waters Corp., USA) were added and the solution was heated to 60 °C for 30 min. The solution was allowed to cool to room temperature, 1 µl PNGase-F solution (Pomega, Germany, Recombinant, cloned from Elizabethkingia miricola 10 u/µl) was added and the solution was incubated at 37 °C for at least 2 hours. Disulfide bridges were reduced by addition of 2 µl DTT solution (70 mM in H_2O) and incubation at 37°C for 30 min. Samples were diluted with 120 µl 1% HCl and subjected to intact protein MS (see chapter 2.9), injecting 5 µl for each sample.

c) For Adcetris pulldown samples from serum, 1 µl PNGase-F solution (Pomega, Germany, Recombinant, cloned from Elizabethkingia miricola 10 u/µl) was added to 20 µl of Adcetris in PBS and the solution was incubated at 37 °C for at least 2 hours. Disulfide bridges were reduced by addition of 2 µl DTT solution (70 mM in H_2O) and incubation at 37°C for 30 min. 10 µl of the samples were diluted with 190 µl of pure water and subjected to intact protein MS (see chapter 2.9), injecting 3 µl for each sample.

After deconvolution of the crude spectra, the DAR was determined with the following formula, were **I** corresponds to the mass intensities of the respective species.

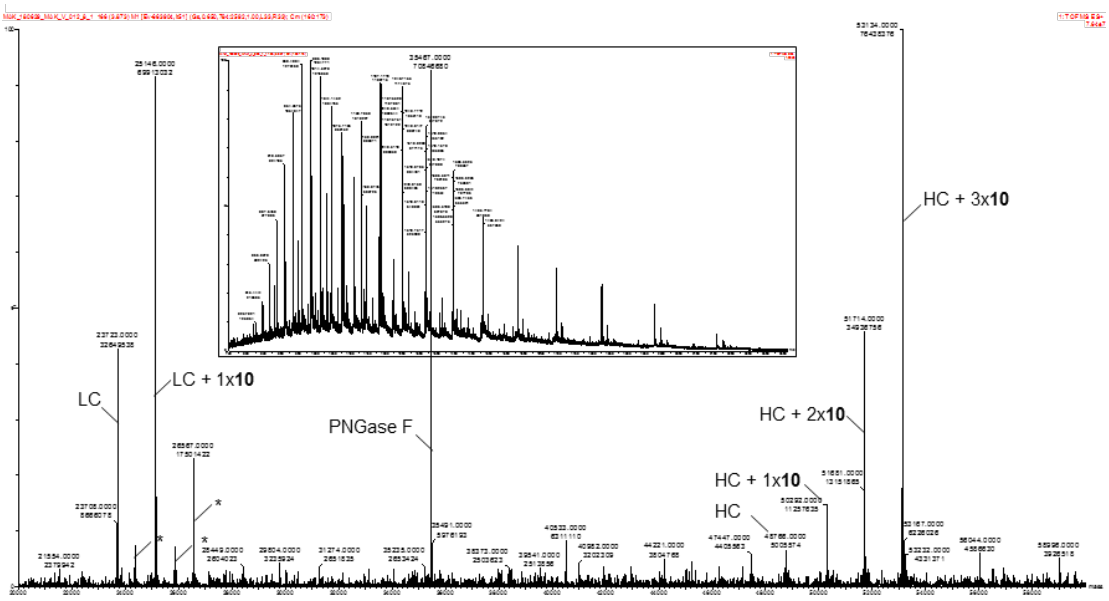

$$\mathrm{DAR} = 2 \times \frac{\mathrm{I}(LC{+}1x\mathbf{10})}{\mathrm{I}(LC){+}\mathrm{I}(LC{+}1x\mathbf{10})} + 2 \times \frac{\mathrm{I}(HC{+}1x\mathbf{10}){+}2{\times}\mathrm{I}(HC{+}2x\mathbf{10}){+}3{\times}\mathrm{I}(HC{+}3x\mathbf{10})}{\mathrm{I}(HC){+}\mathrm{I}(HC{+}1x\mathbf{10}){+}\mathrm{I}(HC{+}2x\mathbf{10}){+}\mathrm{I}(HC{+}3x\mathbf{10})}$$

3.11. Synthesis and purification of an ADC from brentuximab and 10.

240 µl of a 70 mM solution of DTT in 50 mM sodium borate in PBS (pH 8.0) were added to 2.4 ml of a brentuximab solution of 1.0 mg/ml in 50 mM sodium borate in PBS (pH 8.0) and the mixture was incubated at 37 °C for 40 min. Excess DTT removal and exchange to the conjugation buffer was conducted afterwards using 10 mL Zeba™ Spin Desalting Columns with 7K MWCO (Thermo Fisher Scientific, USA). The reduced antibody solution (0.91 mg/ml, 6.07 µM) was mixed quickly afterwards with 132 µl of a 1.94 mM solution of *O*-2-(2-Hydroxyethoxy)ethyl-*P*-ethynyl-phosphonamidate-VC-PAB-MMAE **10** dissolved in DMSO to give a final amount of 5% DMSO and 16 eq. phosphonamidate. The solution was shaken at 850 rpm and 14 °C for 16 hours. Afterwards, the mixture was concentrated to 900 µl by spin-filtration (MWCO: 10 kDa, 0.5 ml, Sartorius, Germany)

Alternatively, 48 µl of a 70 mM solution of DTT in 50 mM sodium borate in PBS (pH 8.0) was added to 480 µl of a brentuximab solution of 5.0 mg/ml in 50 mM sodium borate in PBS (pH 8.0) and the mixture was incubated at 37 °C for 40 min. Excess DTT removal and exchange to the conjugation buffer was conducted afterwards using 2 mL Zeba™ Spin Desalting Columns with 7K MWCO (Thermo Fisher Scientific, USA). The reduced antibody solution (4.55 mg/ml, 30.35 µM) was mixed quickly afterwards with 27.5 µl of a 2.73 mM solution of *O*-2-(2-Hydroxyethoxy)ethyl-*P*-ethynyl-phosphonamidate-VC-PAB-MMAE **10** dissolved in DMSO to give a final amount of 5% DMSO and 4. eq. phosphonamidate. The solution was shaken at 850 rpm and 14 °C for 16 hours.

The reaction mixtures were purified in two portions by size-exclusion chromatography with a 25 ml Superose™ 6 Increase 10/300GL (GE healthcare, United States) and a flow of 0.8 ml/min eluting with sterile PBS (Merck, Germany). The antibody containing fractions were pooled and concentrated by spin-filtration (MWCO: 10 kDa, 6 ml, Sartorius, Germany). For DAR analysis, 10 µl of this sample were mixed with 30 µl of a buffer containing 500 mM NaCl and 100 mM $NaHCO_3$and the sample was processed further as described under 3.9b. The final concentration was determined in a 96-well plate with a Pierce™ Rapid Gold BCA Protein Assay Kit (Thermo Fisher Scientific, USA) and a Bradford reagent B6916 (Merck, Germany) with pre-diluted protein assay standards of bovine gamma globulin (Thermo Fisher Scientific, USA). Results of both Assays were arithmetically averaged.

The ADC was analyzed by analytical size exclusion chromatography (a) and intact protein MS (b) before subsequent experiments. HC: heavy chain, LC: light chain. *deconvolution artefacts (half mass of HC species and double mass of LC species). It should be noted that no species was detected in the MS that could be assigned to any form of unconjugated MMAE.

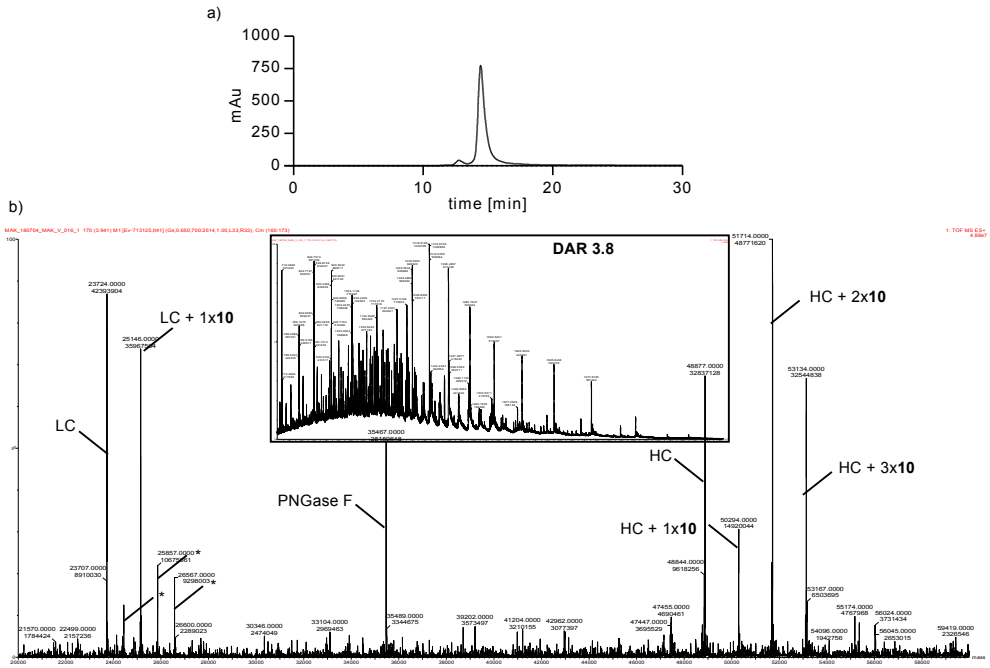

3.12. Stability studies in rat serum: ADC incubation serum and analysis of the DAR after antibody pulldown

In an Eppendorf-tube, 200 µl rat serum (Sigma Aldrich, United States) were mixed with 50 µl Brentuximab-**10** (2.0 mg/ml) or Adcetris® for each sample individually to give a final solution of 0.4 mg/ml ADC in 80% rat serum. Samples were sterile filtered with UFC30GV0S centrifugal filter units (Merck, Germany) and incubated at 37°C for 3 and 7 days. Samples for day 0 were directly processed further.

The supernatant of 50 µl anti human igG (Fc-Specific) agarose slurry (Sigma Aldrich, United States) was removed by centrifugation and the remaining resin washed three times with 200 µl PBS. The resin was incubated with 240 µl of the serum-ADC mix for 30 min at room temperature. Afterwards, the supernatant was removed and the resin washed 5 times with 200 µl PBS. Following by incubation for 5 minutes with 200 µl IgG elution buffer (Thermo-Fisher, United States) at room temperature. Now the supernatant was transferred into a Spin filter (MWCO: 10 kDa, 0.5 ml, Sartorius, Germany), rebuffered to a buffer containing 500 mM NaCl and 100 mM $NaHCO_3$, concentrated to 40 µl and processed further as described under 3.9b for the Brentuximab-**10** samples. Since we observed decomposition of the maleimide linkage in Adcetris® under our standard deglycosylation conditions, all Adcetris® samples were rebuffered to PBS, concentrated to 100 µl and processed further as described under 3.9c. All measurements were performed in triplicates (n=3). MS Spectra that were obtained after 0, 3 and 7 days are shown below. HC: heavy chain, LC: light chain.

0 days of incubation of brentuximab-**10** in rat serum at 37°C:

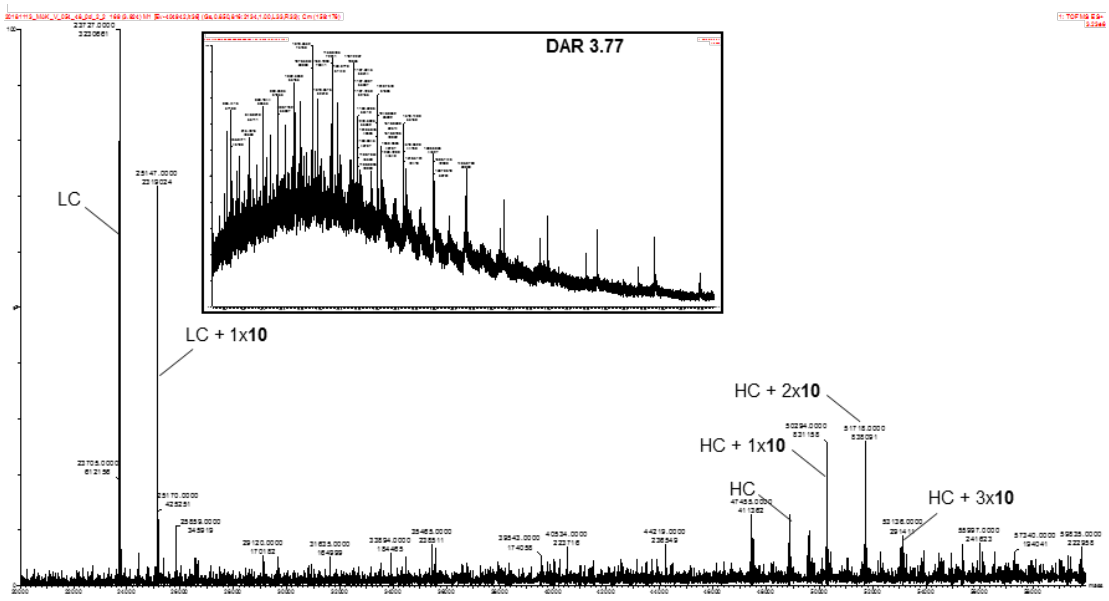

3 days of incubation of brentuximab-**10** in rat serum at 37°C:

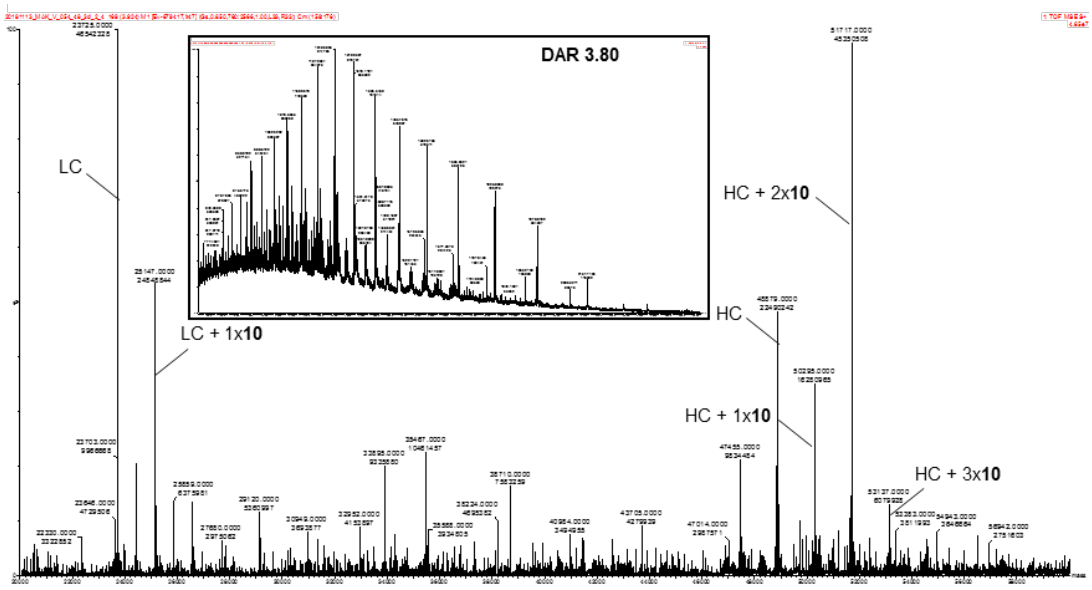

7 days of incubation of brentuximab-**10** in rat serum at 37°C:

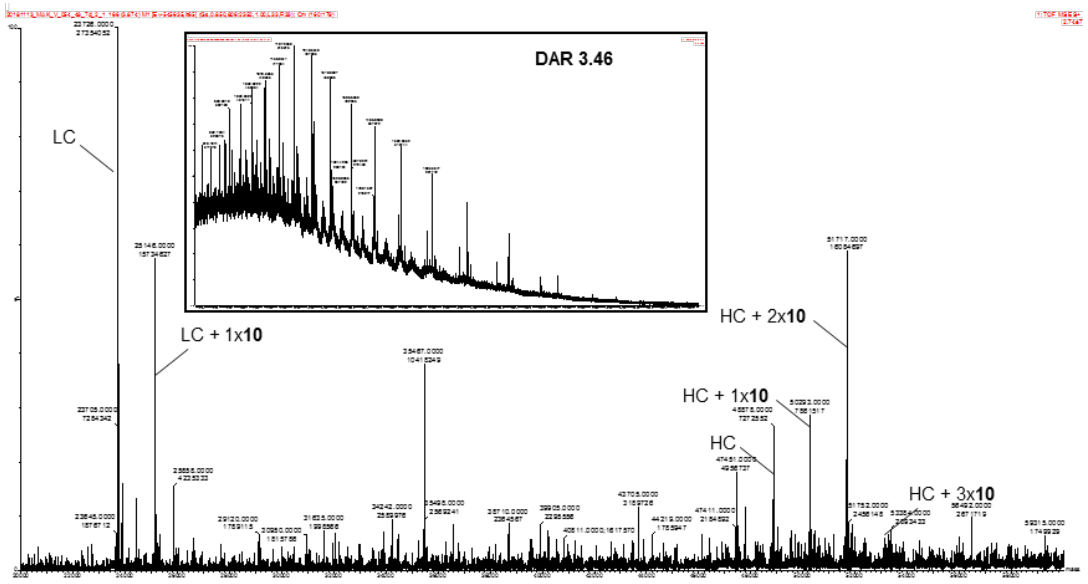

0 days of incubation of Adcetris® in rat serum at 37°C:

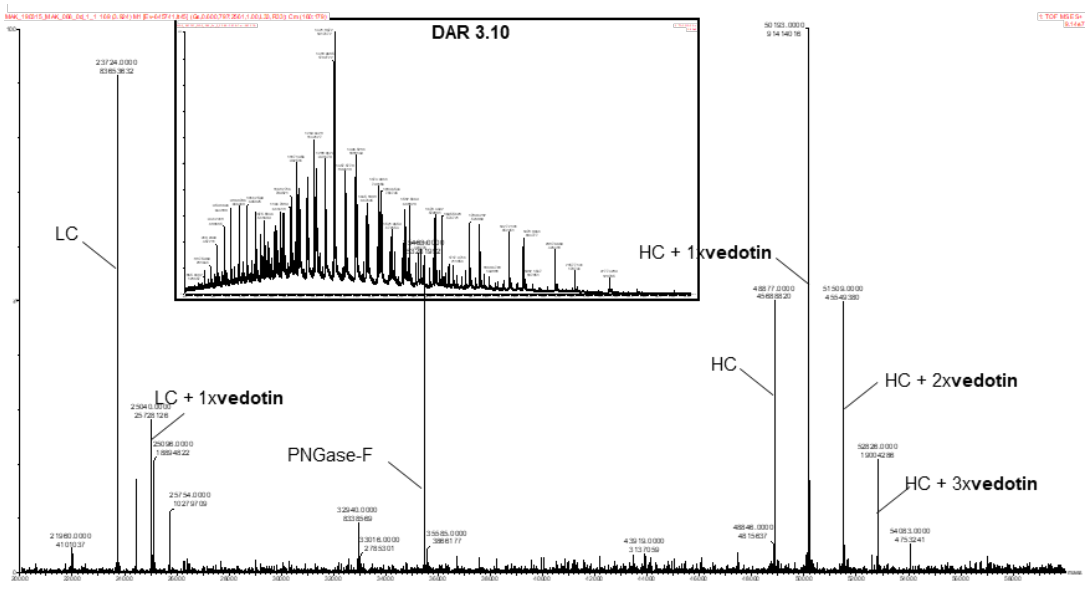

3 days of incubation of Adcetris® in rat serum at 37°C:

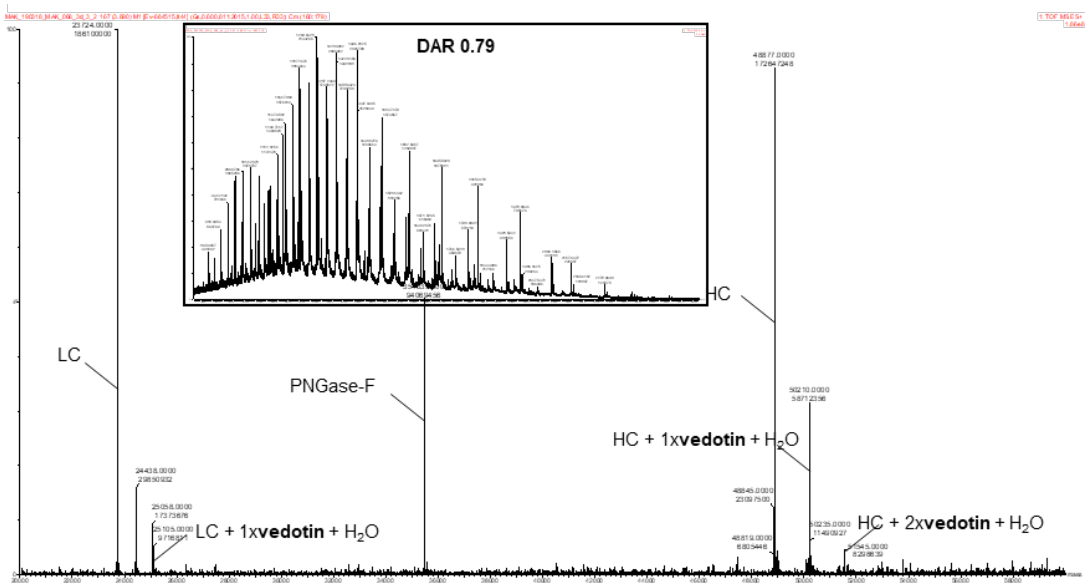

7 days of incubation of Adcetris® in rat serum at 37°C:

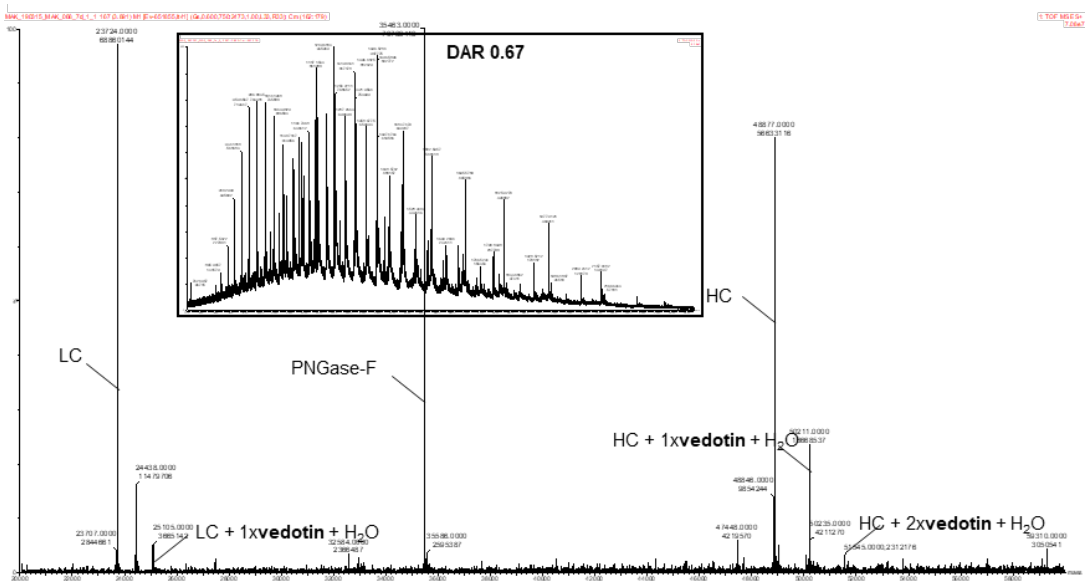

3.13. Stability assessment of ADCs with A-SEC

Brentuximab-**10** was adjusted to a protein concentration of 1 mg/mL in PBS (Dulbeccos Phospahte Bufferd Saline, Sigma-Aldrich Merck KGaA) and filtered sterile (Ultrafree-MC Centrifugal filter units, Merck Millipore). Samples were stored at 4-8°C, 37°C and 40°C for up to 14 days. For samples stored at elevated temperatures, it was ensured that no condensate was formed. Before analysis via A-SEC the samples where centrifuged at 4°C, 4000 x g for 4 minutes.

3.14. In vivo xenograft model

The *in vivo* evaluations were performed at EPO GmbH. All animal experiments were conducted in accordance with German animal welfare law and approved by local authorities. In brief, $1x10^7$ Karpas 299 cells were subcutaneously injected to CB17-Scid mice at day 0. Treatment was initiated when tumors reached a mean tumor volume of 0.136±0.087 cm^3 at

day 7 (study 1) and day 8 (study 2). Following randomization of mice into treatment and control groups, 1 mg/kg of brentuximab-**10** or Adcetris as well as vehicle (PBS) were administered as intravenous injection on days 7 and 10 for the first study and 0.5 mg/kg of brentuximab-**10** or Adcetris as well as vehicle (PBS) on days 8 and 12 for the second study. Tumor volumes, body weights and general health conditions were recorded throughout the whole study.

4. Organic synthesis

4.1. *N*-(4-azidobenzoyl)-*L*-valine

A 50-ml Schlenk-flask was charged with 1.00 g of 4-azidobenzoic acid (6.13 mmol, 1.00 eq.) and suspended in 8.5 ml of dry CH_2Cl_2 together with a drop of DMF under argon. 630 µl of oxalylchloride were added drop-wise at 0 °C and the reaction mixture was stirred at room temperature for 2 h until the solution became clear. All volatiles were removed under reduced pressure and the corresponding solid was redissolved in 4 ml of DMF. The corresponding solution was added drop-wise at 0 °C to a solution of 720 mg *L*-valin (6.13 mmol, 1.00 eq.) and 612 mg sodium hydroxide (15.33 mmol, 2.50 eq.) in 8 ml water and stirred for 2 more hours. The solution was acidified with 1 N HCl and extracted three times with diethylether. The organic fractions were pooled, dried ($MgSO_4$) and the solvents were removed under reduced pressure. Pure product was obtained by flash column chromatography on silicagel (30% EtOAc, 0.5% formic acid in *n*-hexane) as colourless fume. (954 mg, 4.96 mmol, 80.9%)

^{1}H NMR (600 MHz, Chloroform-*d*) δ = 10.12 (s, 1H), 7.79 (d, *J*=8.6, 2H), 7.05 (d, *J*=8.6, 2H), 6.79 (d, *J*=8.5, 1H), 4.76 (dd, *J*=8.5, 4.9, 1H), 2.33 (pd, *J*=6.9, 4.9, 1H), 1.03 (d, *J*=6.9, 3H), 1.01 (d, *J*=6.9, 3H). ^{13}C NMR (151 MHz, $CDCl_3$) δ = 175.82, 167.28, 144.03, 130.17, 129.13, 119.20, 77.16, 57.79, 31.40, 19.16, 17.99. HR-MS for $C_{12}H_{15}N_4O_3^+$ $[M+H]^+$ calcd.: 263.1139, found 263.1151.

4.2. *N*-(4-azidobenzoyl)-*L*-valine-anhydride

In a 100-ml round-bottom flask, 954 mg *N*-(4-azidobenzoyl)-*L*-valine (3.64 mmol, 1.00 eq.), 750 mg dicyclohexylcarbodiimide (3.64 mmol, 1.00 eq.), 418 mg *N*-hydroxysuccinimide (3.64 mmol, 1.00 eq.) and 9 mg 4-(dimethylamino)-pyridine (0.07 mmol, 0.02 eq.) were dissolved in 25 ml of THF and stirred over night at room temperature. The reaction mixture was filtered, the solids were washed several times with THF, the solvent was removed under reduced pressure and the crude product was purified by flash column chromatography on silicagel (20 to 40% EtOAc in *n*-hexane). The compound was isolated as white powder (513 mg, 1.01 mmol, 55.7%)

^{1}H NMR (600 MHz, Chloroform-*d*) δ = 8.01 (d, *J*=8.7, 2H), 7.13 (d, *J*=8.7, 2H), 4.29 (d, *J*=4.6, 1H), 2.39 (heptd, *J*=6.9, 4.6, 1H), 1.16 (d, *J*=6.9, 3H), 1.03 (d, *J*=6.9, 3H). ^{13}C NMR (151 MHz, $CDCl_3$) δ = 177.52, 160.90, 144.51, 129.60, 122.43, 119.30, 70.68, 31.28, 18.76, 17.57.

4.3. *N*-(4-azidobenzoyl)-*L*-valine-*L*-citrulline

In a 50-ml round-bottom flask, 380 mg *N*-(4-azidobenzoyl)-*L*-valine-anhydride (0.75 mmol, 1.00 eq.) were dissolved in 2 ml of 1,2-Dimethoxyethane and cooled to 0 °C. A solution of 351 mg *L*-citrulline (1.50 mmol, 2.00 eq.) and 144 mg sodium hydrogencarbonate (2.25 mmol, 3.00 eq.) in 4 ml H_2O and 2 ml THF was added dropwise and stirred over night at room temperature. All volatiles were removed under reduced pressure and the crude product was purified by flash column chromatography on silicagel (10% MeOH, 0.5% formic acid in CH_2Cl_2). The compound was isolated as colourless oil (312 mg, 0.74 mmol, 99.0%).

^{1}H NMR (600 MHz, DMSO-d_6) δ = 8.31 (d, *J*=8.8, 1H), 8.27 – 8.21 (m, 1H), 7.96 (d, *J*=8.6, 2H), 7.20 (d, *J*=8.6, 2H), 6.05 (t, *J*=5.5, 1H), 5.47 (s, 2H), 4.37 (t, *J*=8.3, 1H), 4.18 (td, *J*=8.1, 5.1, 1H), 2.98 (q, *J*=6.4, 2H), 2.15 (dq, *J*=13.6, 6.8, 1H), 1.78 – 1.68 (m, 1H), 1.68 – 1.56 (m, 1H), 1.51 – 1.35 (m, 2H), 0.96 (d, *J*=6.8, 3H), 0.94 (d, *J*=6.8, 3H). ^{13}C NMR (151 MHz, DMSO) δ = 174.09, 171.54, 165.99, 159.40, 142.77, 131.36, 129.93, 119.23, 59.31, 52.57, 49.07, 30.77, 29.01, 27.07, 19.75, 19.28. HR-MS for $C_{18}H_{26}N_7O_5^+$ $[M+H]^+$ calcd.: 420.1990, found 420.1990.

4.4. *N*-(4-azidobenzoyl)-*L*-valine-*L*-citrulline-4-aminobenzyl alcohol (1)

In a 50-ml round-bottom flask, 330 mg *N*-(4-azidobenzoyl)-*L*-vaine-*L*-citrulline (0.787 mmol, 1.0 eq.) and 107 mg 4-aminobenzyl alcohol (0.866 mmol, 1.10 eq.) were dissolved in 8 ml CH_2Cl_2 and 4 ml MeOH under an argon atmosphere and cooled to 0 °C. 390 mg N-Ethoxycarbonyl-2-ethoxy-1,2-dihydroquinoline (1.574 mmol, 2.00 eq.) were added portion-wise and the resulting solution was allowed to warm to room temperature overnight. All volatiles were removed under reduced pressure and the crude product was isolated by flash column chromatography on silicagel (10% to 15% MeOH in CH_2Cl_2) and obtained as white solid (164 mg, 0.313 mmol, 39.8%). Enantiomeric pure compound was isolated by preparative HPLC (Method D) and obtained as a white solid after lyophilisation.

^{1}H NMR (600 MHz, DMSO-d_6) δ = 9.93 (s, 1H), 8.32 (d, *J*=8.4, 1H), 8.21 (d, *J*=7.6, 1H), 7.96 (d, *J*=8.6, 2H), 7.55 (d, *J*=8.6, 2H), 7.24 (d, *J*=8.6, 2H), 7.21 (d, *J*=8.6, 2H), 6.12 (bs, 2H), 4.44 (s, 2H), 4.46 – 4.40 (m, 1H), 4.36 (t, *J*=8.1, 1H), 3.09 – 2.93 (m, 2H), 2.24 – 2.04 (m, *J*=6.7, 1H), 1.84 – 1.58 (m, 2H), 1.55 – 1.34 (m, 2H), 0.95 (d, *J*=6.7, 3H), 0.94 (d, *J*=6.7, 3H). ^{13}C NMR (151 MHz, DMSO) δ = 171.62, 170.79, 166.15, 159.46, 142.83, 137.95, 137.91, 131.29, 129.96, 127.38, 119.34, 119.26, 63.07, 59.56, 53.64, 39.20, 30.61, 29.88, 27.16, 19.79, 19.37. HR-MS for $C_{25}H_{33}N_8O_5^+$ $[M+H]^+$ calcd.: 525.2568, found 525.2563. $[\alpha]_D^{24}$ = –49.6 (c = 0.81; MeOH)

4.5. *N*-(4-(*O*-Ethyl-*P*-ethynyl-phosphonamidato-*N*-benzoyl)-*L*-valine-*L*-citrulline-4-aminobenzyl-4-nitrophenyl carbonate (2)

A 5-ml round-bottom flask was charged with 31 mg *N*-(4-(*O*-Ethyl-*P*-ethynyl-phosphonamidato-*N*-benzoyl)-*L*-valine-*L*-citrulline-4-aminobenzyl alcohol (**1**) (0.050 mmol, 1.00 eq.) and 31 mg Bis(4-nitrophenyl) carbonate (0.101 mmol, 2.00 eq.). The solids were dissolved in 140 µl of DMF and 17.4 µl DIPEA (0.101 mmol, 2.00 eq.) were added. The yellow solution was stirred for 1 h at room temperature and the solution was added to 30 ml of ice-cold diethyl ether. The precipitate was collected by centrifugation, redissolved in DMF and again precipitated with ether. The procedure was conducted three times in total and finally the solid was dried under high vacuum conditions. The compound was isolated in quantitative yields and sufficiently pure for the next step. Analytical pure material was purified by preparative HPLC using method C.

^{1}H NMR (600 MHz, DMSO-d_6) δ = 10.10 (s, 1H), 8.79 (d, *J*=8.5, 1H), 8.32 (d, *J*=9.1, 1H), 8.23 (d, *J*=7.4, 1H), 8.07 (dd, *J*=8.5, 2.2, 1H), 7.81 (d, *J*=8.7, 2H), 7.66 (d, *J*=8.5, 2H), 7.57 (d, *J*=9.1, 1H), 7.42 (d, *J*=8.5, 2H), 7.13 (d, *J*=8.7, 2H), 5.25 (s, 2H), 4.47 – 4.40 (m, 2H), 4.34 (t, *J*=8.0, 1H), 4.20 – 4.05 (m, 2H), 3.01 (ddt, *J*=47.1, 13.4, 6.8, 2H), 2.20 – 2.09 (m, *J*=6.8, 1H), 1.80 – 1.59 (m, 2H), 1.55 – 1.35 (m, 2H), 1.30 (t, *J*=7.0, 3H), 0.95 (d, *J*=6.7, 3H), 0.93 (d, *J*=6.7, 3H). ^{13}C NMR (151 MHz, DMSO-d_6) δ = 171.79, 171.17, 166.58, 159.44, 155.75, 152.42, 145.63, 143.50, 139.83, 129.95, 129.77, 129.30, 127.59, 125.86, 123.08, 119.51, 117.24 (d, *J*=7.8), 91.67 (d, *J*=45.6), 77.26 (d, *J*=261.0), 70.71, 62.26 (d, *J*=5.0), 59.31, 53.68, 39.14, 30.71, 29.76, 27.19, 19.80, 19.30, 16.41 (d, *J*=6.9). ^{31}P NMR (243 MHz, DMSO) δ = -10.39, -10.44. HR-MS for $C_{36}H_{43}N_7O_{11}P^+$ $[M+H]^+$ calcd.: 780.2753, found 780.2744.

4.6. *N*-(4-(*O*-Ethyl-*P*-ethynyl-phosphonamidato-*N*-benzoyl)-L-valine-L-citrulline-4-aminobenzyl-4-nitrophenyl carbonate (3)

A 5-ml round-bottom flask was charged with 31 mg *N*-(4-(*O*-Ethyl-*P*-ethynyl-phosphonamidato-*N*-benzoyl)-*L*-valine-*L*-citrulline-4-aminobenzyl alcohol (**2**) (0.050 mmol, 1.00 eq.) and 31 mg Bis(4-nitrophenyl) carbonate (0.101 mmol, 2.00 eq.). The solids were dissolved in 140 µl of DMF and 17.4 µl DIPEA (0.101 mmol, 2.00 eq.) were added. The yellow solution was stirred for 1 h at room temperature and the solution was added to 30 ml of ice-cold diethyl ether. The precipitate was collected by centrifugation, redissolved in DMF and again precipitated with ether. The procedure was conducted three times in total and finally the solid was dried under high vacuum conditions. The compound was isolated in

quantitative yields and sufficiently pure for the next step. Analytical pure material was purified by preparative HPLC using method C.

^{1}H NMR (600 MHz, DMSO-d_6) δ = 10.10 (s, 1H), 8.79 (d, *J*=8.5, 1H), 8.32 (d, *J*=9.1, 1H), 8.23 (d, *J*=7.4, 1H), 8.07 (dd, *J*=8.5, 2.2, 1H), 7.81 (d, *J*=8.7, 2H), 7.66 (d, *J*=8.5, 2H), 7.57 (d, *J*=9.1, 1H), 7.42 (d, *J*=8.5, 2H), 7.13 (d, *J*=8.7, 2H), 5.25 (s, 2H), 4.47 – 4.40 (m, 2H), 4.34 (t, *J*=8.0, 1H), 4.20 – 4.05 (m, 2H), 3.01 (ddt, *J*=47.1, 13.4, 6.8, 2H), 2.20 – 2.09 (m, *J*=6.8, 1H), 1.80 – 1.59 (m, 2H), 1.55 – 1.35 (m, 2H), 1.30 (t, *J*=7.0, 3H), 0.95 (d, *J*=6.7, 3H), 0.93 (d, *J*=6.7, 3H). ^{13}C NMR (151 MHz, DMSO-d_6) δ = 171.79, 171.17, 166.58, 159.44, 155.75, 152.42, 145.63, 143.50, 139.83, 129.95, 129.77, 129.30, 127.59, 125.86, 123.08, 119.51, 117.24 (d, *J*=7.8), 91.67 (d, *J*=45.6), 77.26 (d, *J*=261.0), 70.71, 62.26 (d, *J*=5.0), 59.31, 53.68, 39.14, 30.71, 29.76, 27.19, 19.80, 19.30, 16.41 (d, *J*=6.9). ^{31}P NMR (243 MHz, DMSO) δ = -10.39, -10.44. HR-MS for $C_{36}H_{43}N_7O_{11}P^+$ $[M+H]^+$ calcd.: 780.2753, found 780.2744.

4.7. *O*-Ethyl-*P*-ethynyl-phosphonamidate-VC-PAB-MMAF 4

A screw-cap vial was charged with 14.35 mg *N*-(4-(*O*-Ethyl-*P*-ethynyl-phosphonamidato-*N*-benzoyl)-*L*-valine-*L*-citrulline-4-aminobenzyl-4-nitrophenyl carbonate (**3)** (0.0184 mmol, 1.00 eq.), 0.50 mg 1-Hydroxybenzotriazol (0.0037 mmol, 0.20 eq.) and 13.15 mg MMAF (0.0184 mmol, 1.00 eq.). The solids were dissolved in 250 µl dry DMF and 25 µl pyridine and heated to 60 °C over-night. All volatiles were removed under reduced pressure, the crude product was purified by preparative HPLC using method E and the desired compound obtained as a white solid after lyophilization. (4.84 mg, 0.0035 mmol, 19.2 %). HR-MS for $C_{69}H_{104}N_{11}O_{16}P^{2+}$ $[M+2H]^{2+}$ calcd.: 686.8695, found 686.8694.

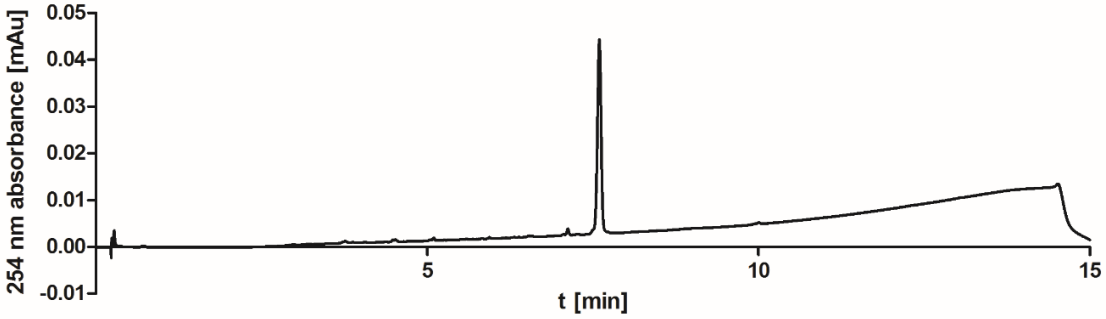

4.8. Di-(2-(2-Hydroxyethoxy)ethyl) ethynylphosphonite (5)

A 25-ml Schlenk flask was charged with 267 mg bis(diisopropylamino)chlorophosphine (1.00 mmol, 1.00 eq.) under an argon atmosphere, cooled to 0 °C and 2.20 ml ethynylmagnesium bromide solution (0.5 M in THF, 1.10 mmol, 1.10 eq.) was added drop wise. The yellowish solution was allowed to warm to room temperature and stirred for further 30 minutes. 1.06 g diethylene glycol (10.00 mmol, 10.00 eq.), dissolved in 5.56 ml 1H-tetrazole solution (0.45 M

in MeCN, 2.50 mmol, 2.50 eq.) were added and the white suspension was stirred over night at room temperature. The reaction mixture was directly placed on a silica gel flash column for purification (5% MeOH in CH_2Cl_2). The desired compound was obtained as a yellowish oil. (112 mg, 0.421 mmol, 42.1%).

^{1}H NMR (300 MHz, Chloroform-*d*) δ = 4.14 – 3.98 (m, 4H), 3.65 – 3.59 (m, 4H), 3.58 – 3.49 (m, 8H), 3.15 (d, *J*=2.4, 1H) ^{13}C NMR (75 MHz, Chloroform-*d*) δ = 92.51 (d, *J*=1.4), 84.30 (d, *J*=46.8), 72.60, 70.72 (d, *J*=4.0), 67.20 (d, *J*=6.0), 61.44. ^{31}P NMR (122 MHz, $CDCl_3$) δ = 131.97.

4.9. 2-(2-Hydroxyethoxy)ethyl-*N*-(4-benzoic-acid-*N*-hydroxysuccinimideester)-*P*-ethynyl phosphonamidate (8)

In a 5 ml round-bottom-flask, 93 mg Di-(2-(2-Hydroxyethoxy)ethyl) ethynylphosphonite (**5**) (0.192 mmol, 1.00 eq.) and 91 mg 4-azidobenzoic-acid-*N*-hydroxysuccinimide ester (**6**) (0.192 mmol, 1.00 eq.) were dissolved in 1 ml of DMF and the solution was stirred overnight. All volatiles were removed under reduced pressure and the residue purified by column chromatographie on silicagel (100% EtOAc). The compound was obtained as colourless oil. (45 mg, 0.109 mmol, 31.4%).

^{1}H NMR (300 MHz, Chloroform-*d*) δ 8.02 (d, *J* = 8.7 Hz, 2H), 7.79 (d, *J* = 7.6 Hz, 1H), 7.21 (d, *J* = 8.8 Hz, 2H), 4.30 (dp, *J* = 13.6, 4.5 Hz, 2H), 3.89 – 3.67 (m, 6H), 3.09 (d, *J* = 13.3 Hz, 1H), 2.89 (s, 4H). ^{13}C NMR (75 MHz, Chloroform-*d*) δ 169.67, 161.45, 145.78 (d, *J* = 1.6 Hz), 132.32, 118.04, 117.66 (d, *J* = 8.1 Hz), 89.29 (d, *J* = 50.1 Hz), 75.34 (d, *J* = 294.4 Hz), 72.59, 69.44 (d, *J* = 5.1 Hz), 66.19 (d, *J* = 5.9 Hz), 61.35, 25.68. ^{31}P NMR (122 MHz, $CDCl_3$) δ -9.66. HRMS for $C_{17}H_{20}N_2O_8P^+$ $[M+H]^+$ calcd.: 411.0952, found: 411.0951.

4.10. *O*-ethyl-*P*-ethynyl-phosphonamidate-VC-PAB-MMAE 9

In a screw-cap-vial equipped with a stirring bar, 5 mg of H_2N-Val-Cit-PAB-MMAE **11** (4.452 µmol, 1.00 eq.) and 3.12 mg 2-ethyl-*N*-(4-benzoic-acid-*N*-hydroxysuccinimideester)-*P*-ethynyl phosphonamidate (**7**) (8.904 µmol, 2.00 eq.) were dissolved in 50 µl DMF. 3.1 µl DIPEA (17.808 µmol, 4.00 eq.) were added and the solution was stirred overnight at room temperature. The solution was diluted with 4 ml 30% MeCN in H_2O and subjected to semi-preparative HPLC purification using method F and the desired compound obtained as a white solid after lyophilization. (5.00 mg, 3.681 µmol, 82.7%). HR-MS for $C_{69}H_{105}N_{11}O_{15}P^+$ $[M+H]^+$ calcd.: 1358.7524, found 1358.7518.

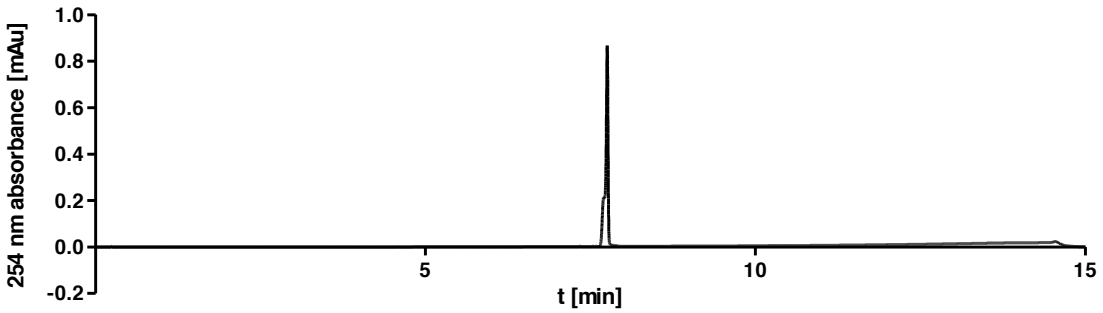

4.11. *O*-2-(2-Hydroxyethoxy)ethyl-*P*-ethynyl-phosphonamidate-VC-PAB-MMAE 10

In a screw-cap-vial equipped with a stirring bar, 5 mg of H_2N-Val-Cit-PAB-MMAE **11** (4.452 µmol, 1.00 eq.) and 3.65 mg 2-(2-Hydroxyethoxy)ethyl-*N*-(4-benzoic-acid-*N*-hydroxysuccinimideester)-*P*-ethynyl phosphonamidate (**8**) (8.904 µmol, 2.00 eq.) were dissolved in 50 µl DMF. 3.1 µl DIPEA (17.808 µmol, 4.00 eq.) were added and the solution was stirred overnight at room temperature. The solution was diluted with 4 ml 30% MeCN in H_2O and subjected to semi-preparative HPLC purification using method F and the desired compound obtained as a white solid after lyophilization. (2.73 mg, 1.589 µmol, 35.7%). HR-MS for $C_{71}H_{109}N_{11}O_{17}P^+$ $[M+H]^+$ calcd.: 1418.7735, found 1418.7729.

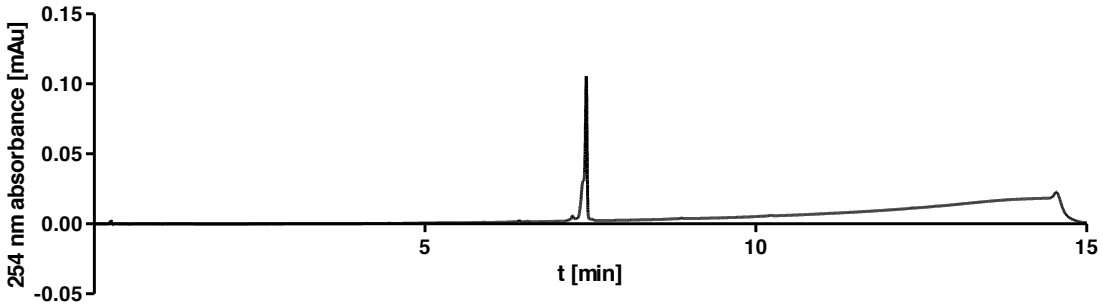

5. NMR spectra

N-(4-azidobenzoyl)-*L*-valine

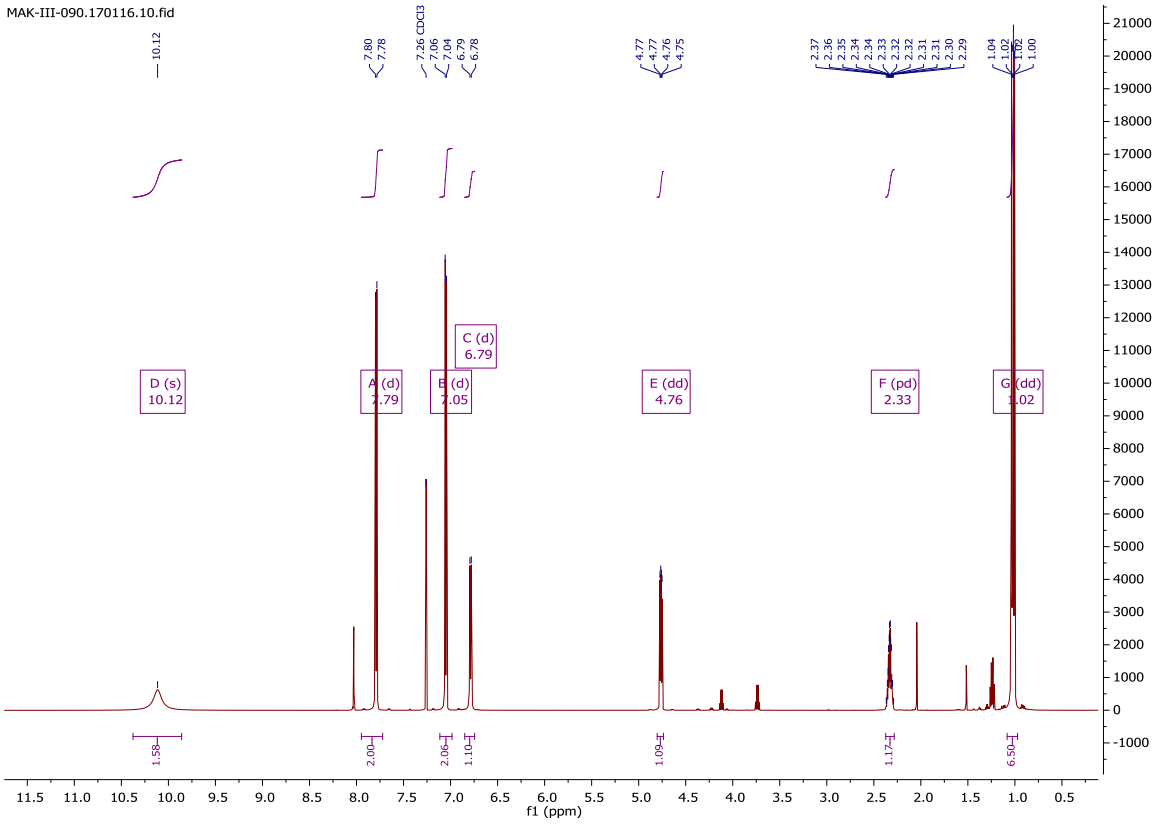

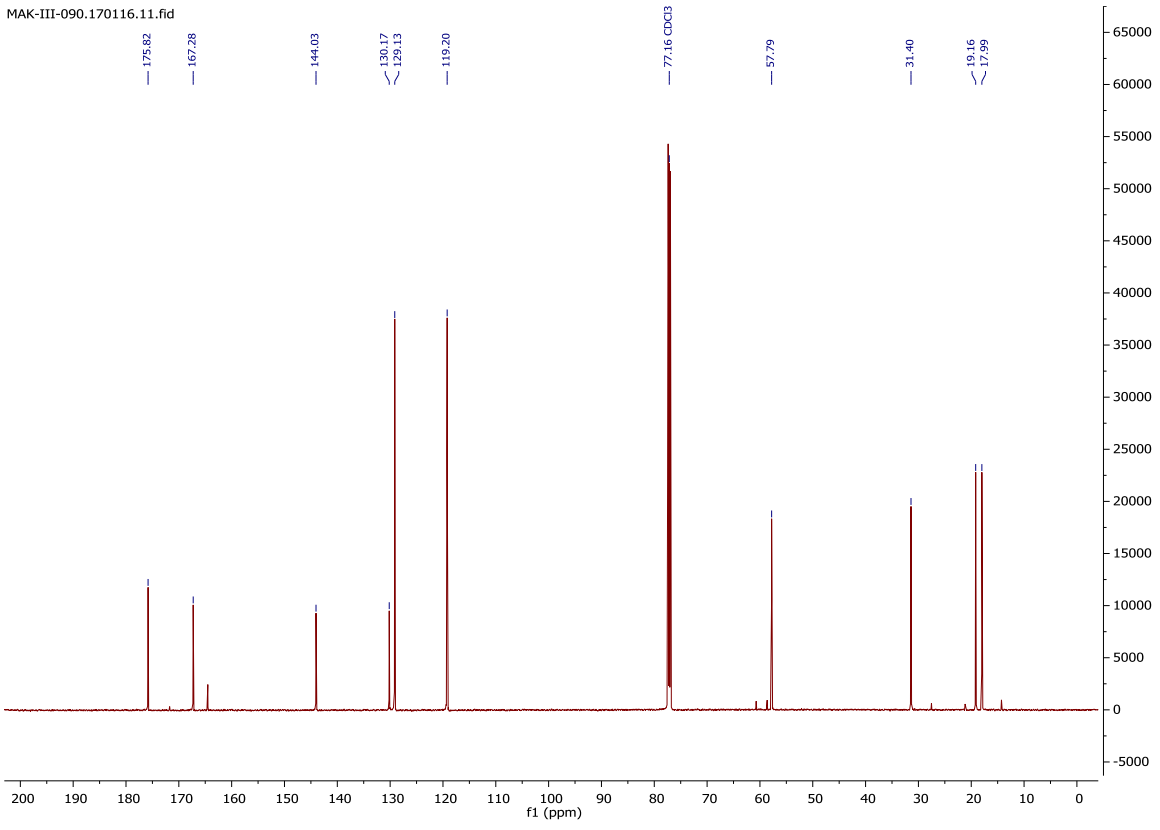

N-(4-azidobenzoyl)-*L*-valine-anhydride

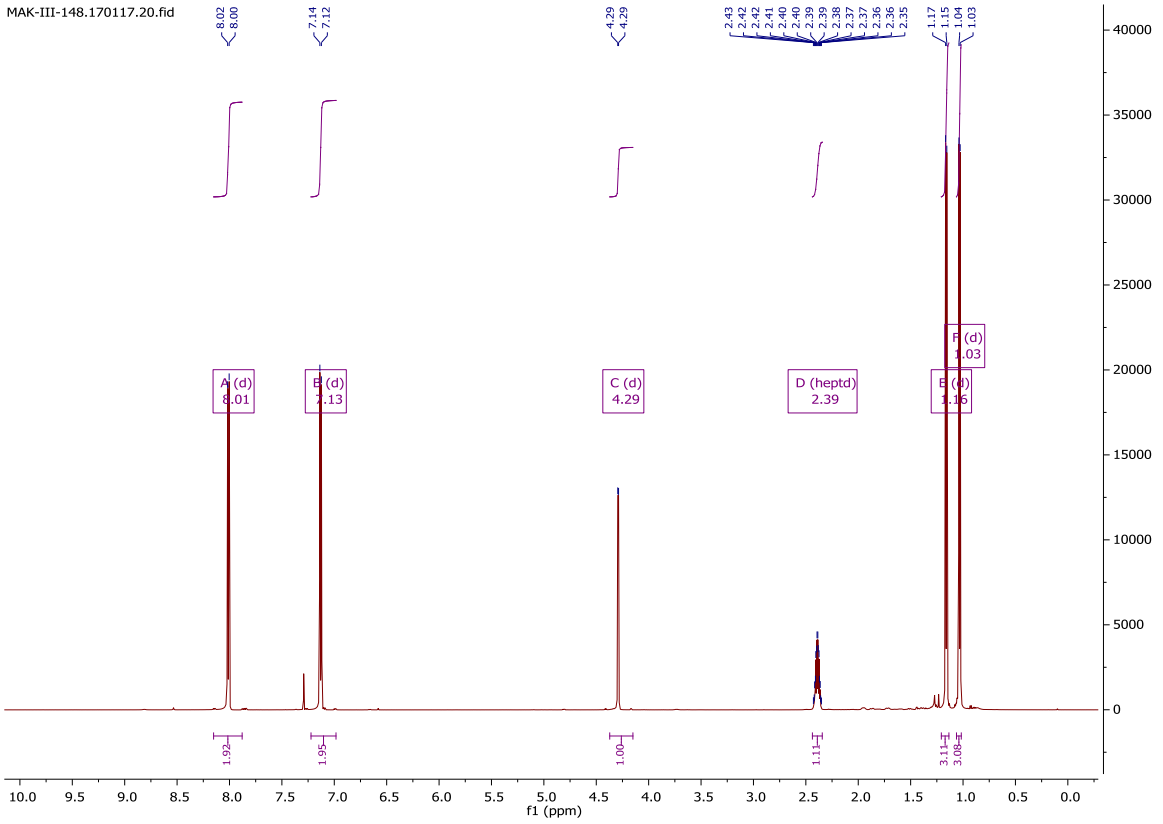

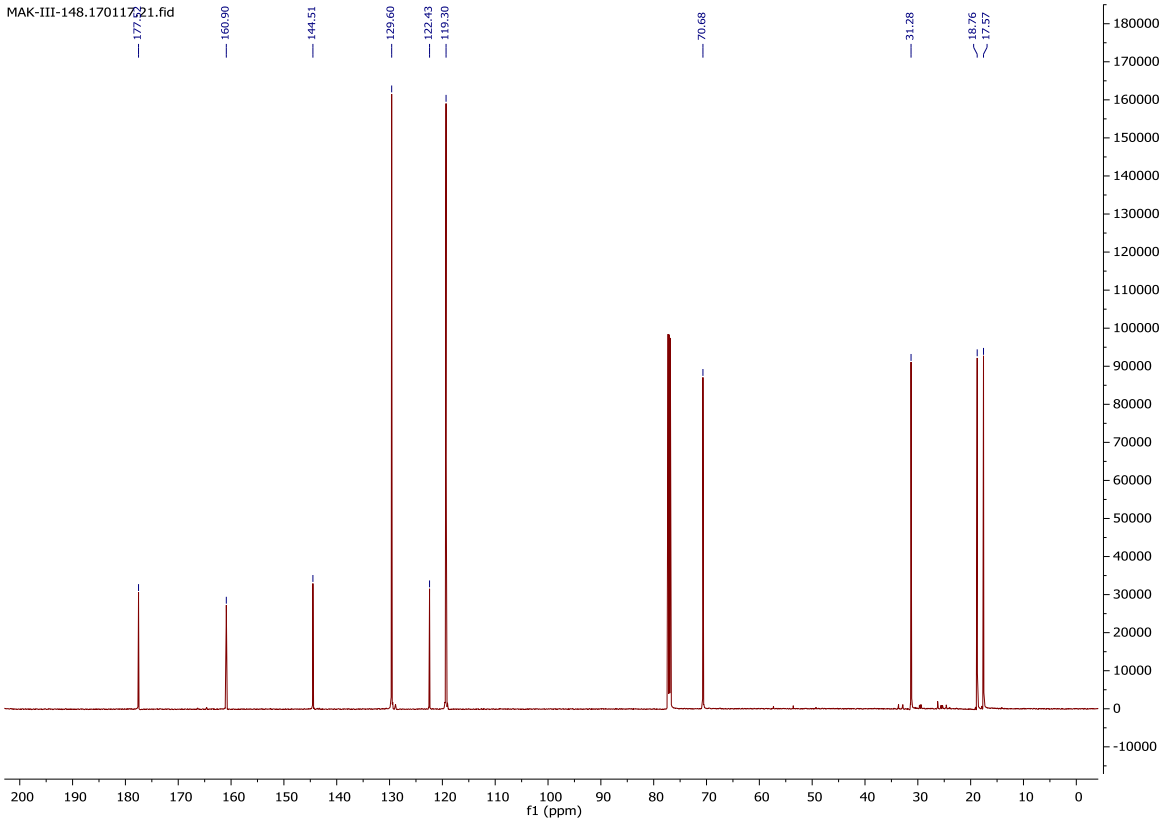

N-(4-azidobenzoyl)-*L*-valine-*L*-citrulline

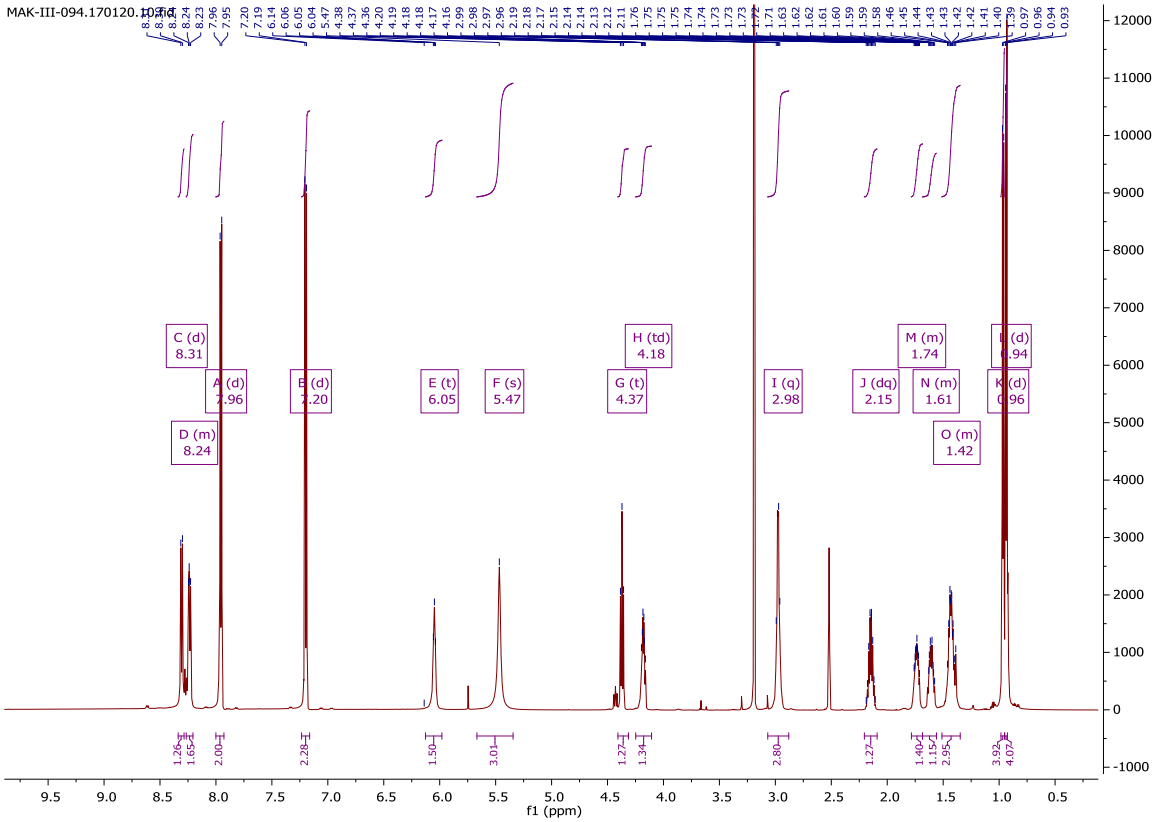

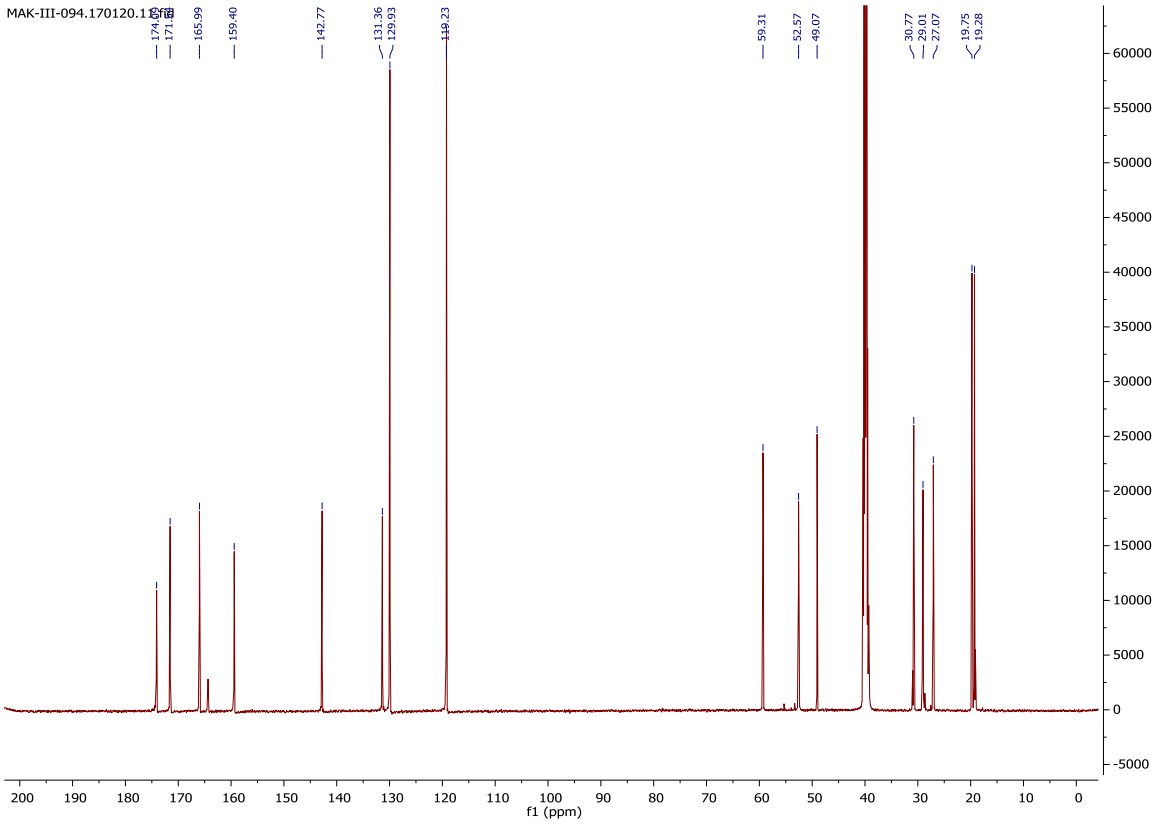

N-(4-azidobenzoyl)-*L*-valine-*L*-citrulline-4-aminobenzyl alcohol **(2)**

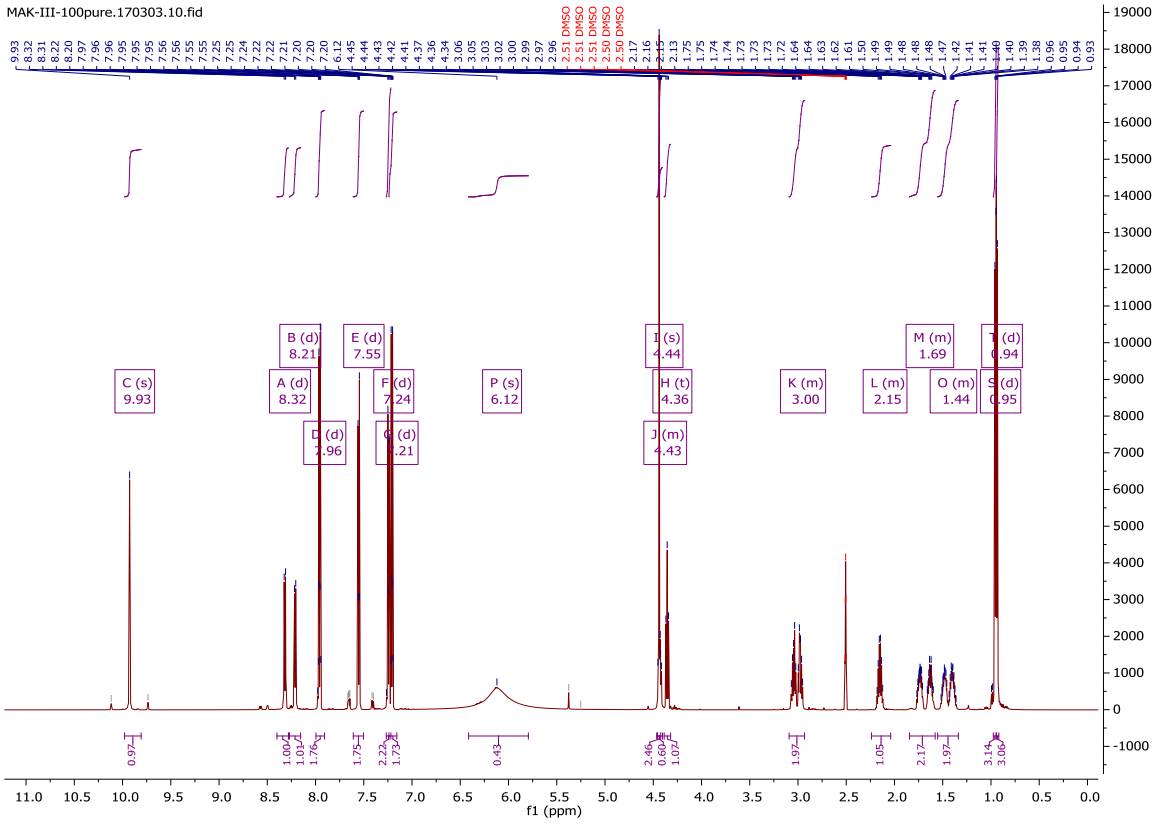

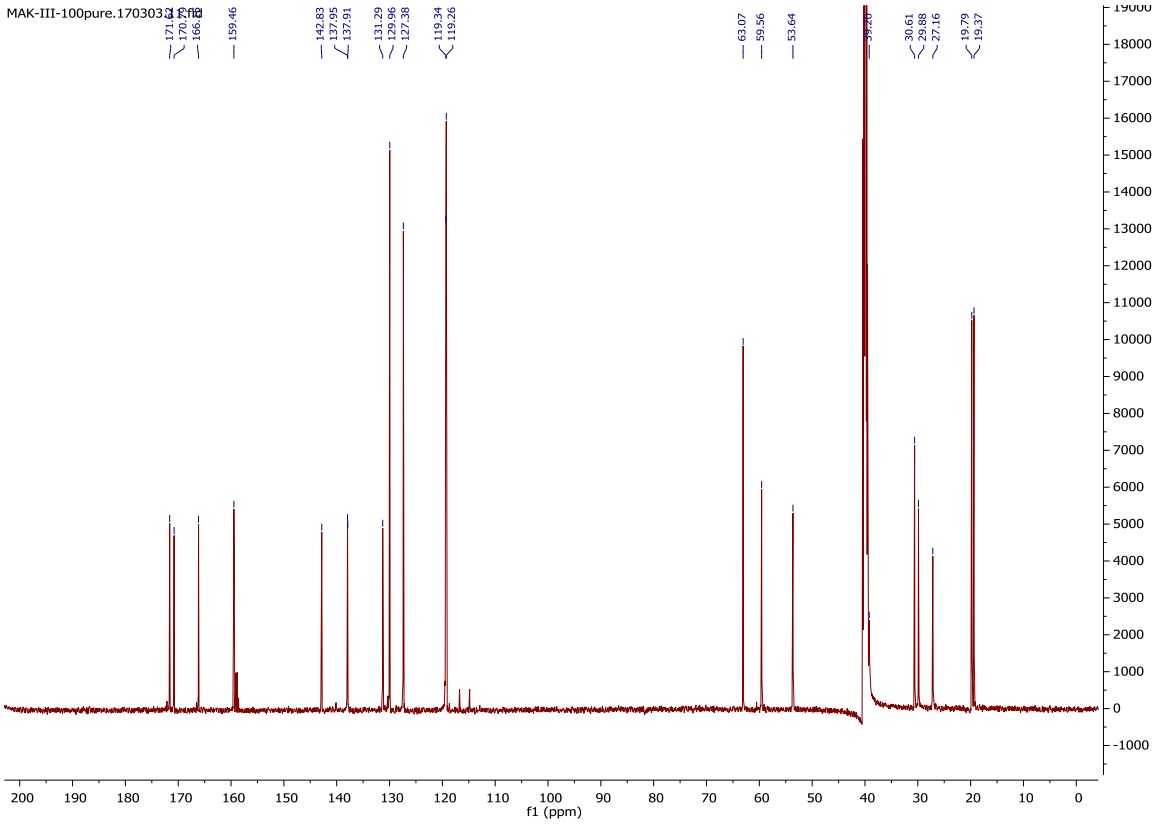

N-(4-(*O*-Ethyl-*P*-ethynyl-phosphonamidato-*N*-benzoyl)-*L*-valine-*L*-citrulline-4-aminobenzyl alcohol **(2)**

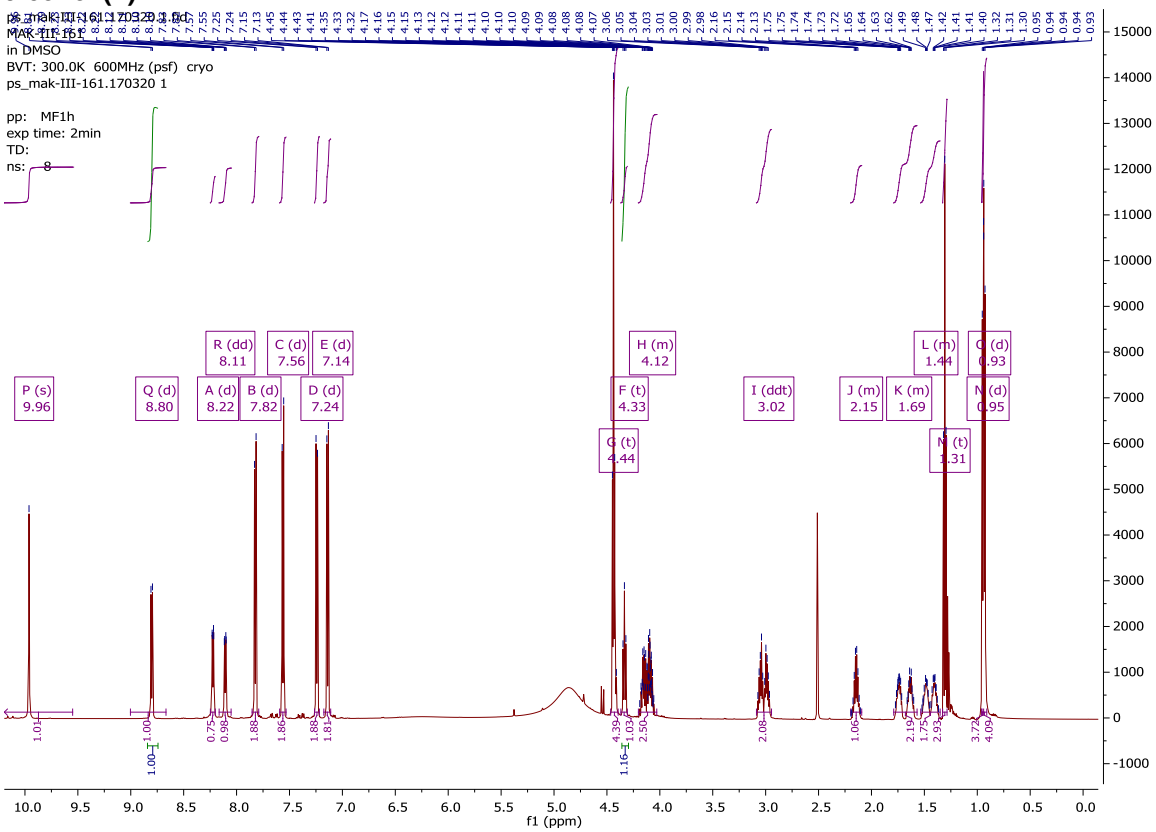

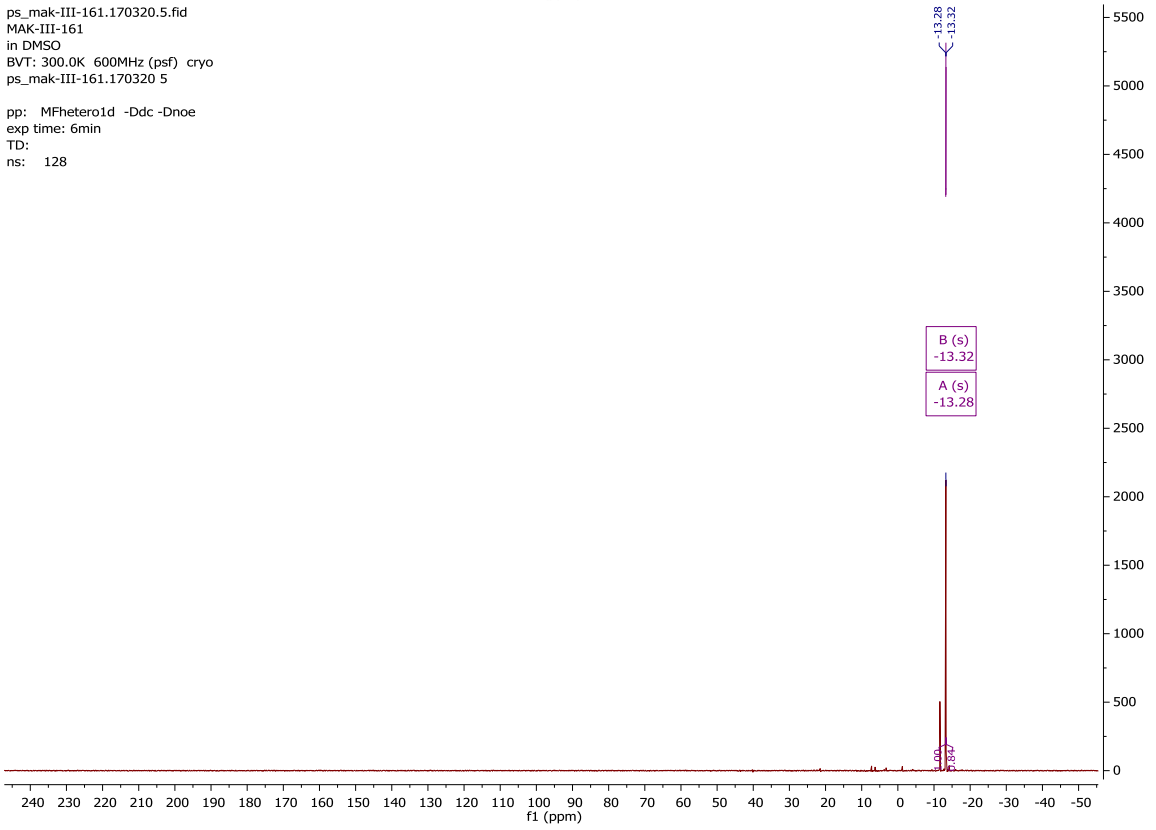

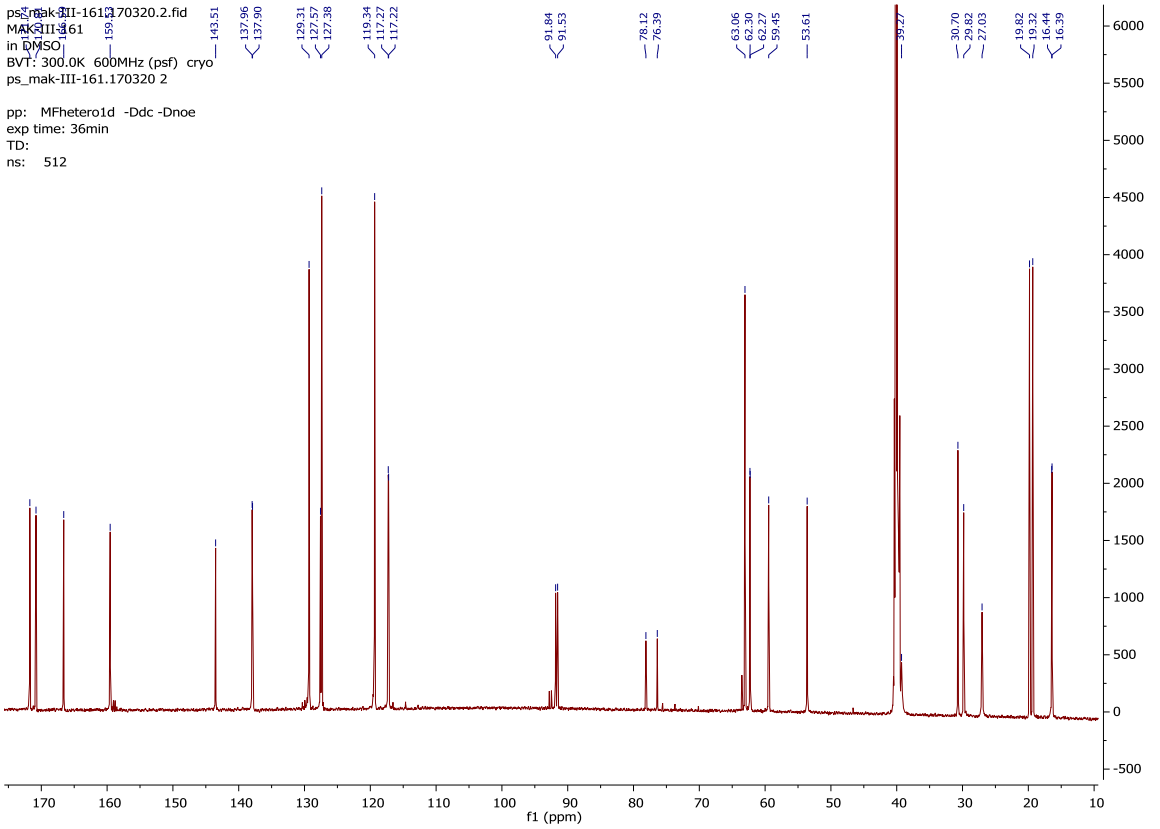

N-(4-(*O*-Ethyl-*P*-ethynyl-phosphonamidato-*N*-benzoyl)-*L*-valine-*L*-citrulline-4-aminobenzyl-4-nitrophenyl carbonate **(3)**

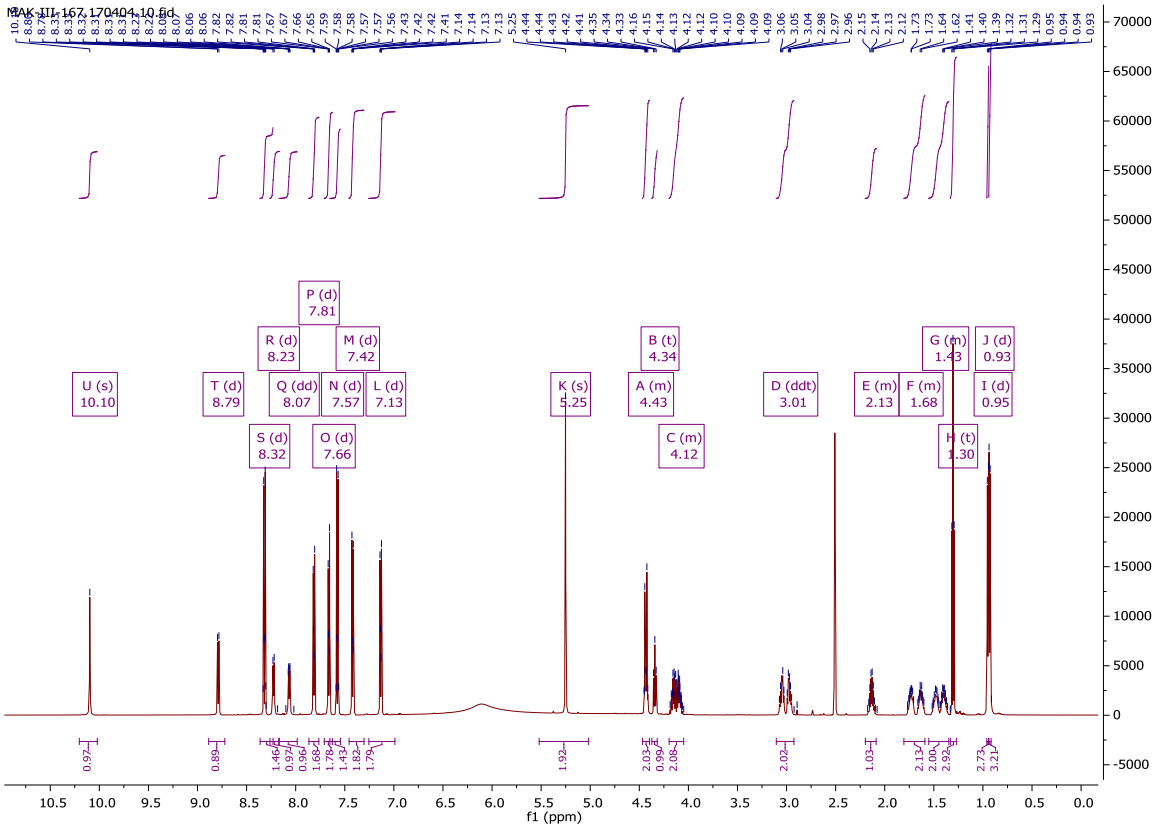

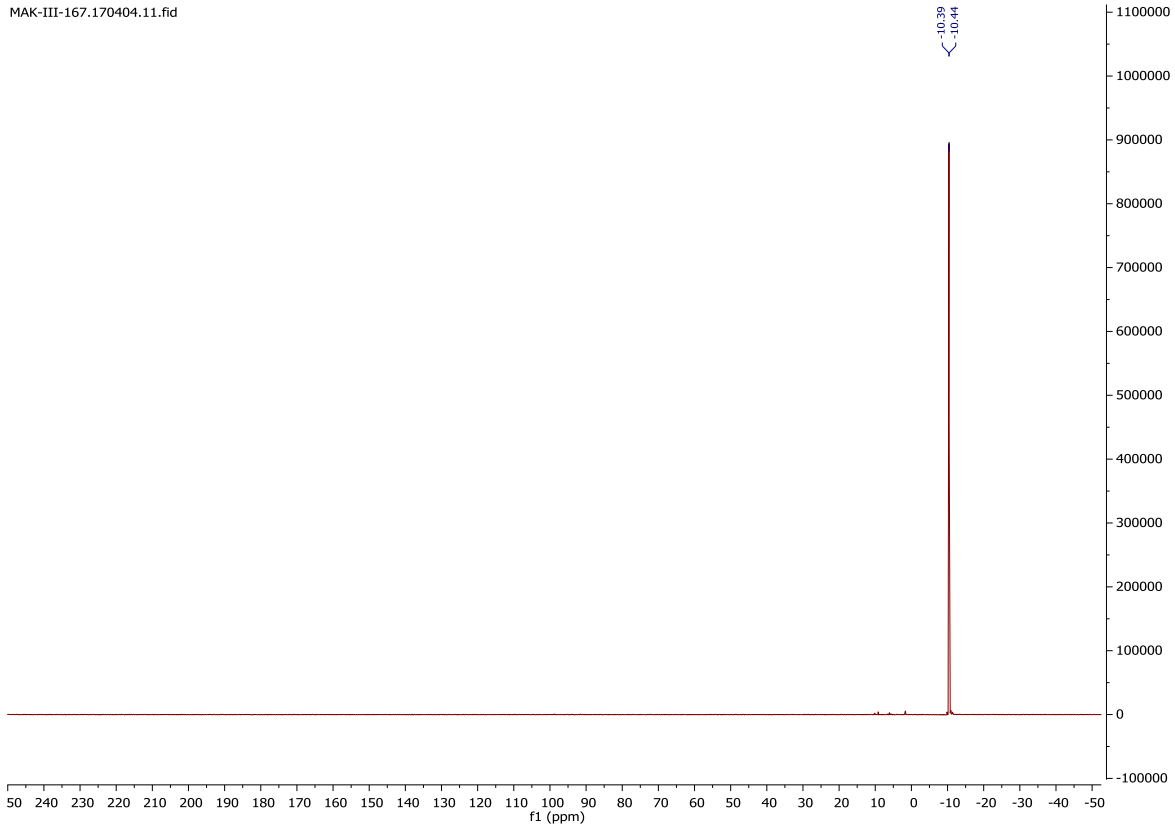
MAK-III-167.170404.11.fid
-10.39
-10.44
f1 (ppm)

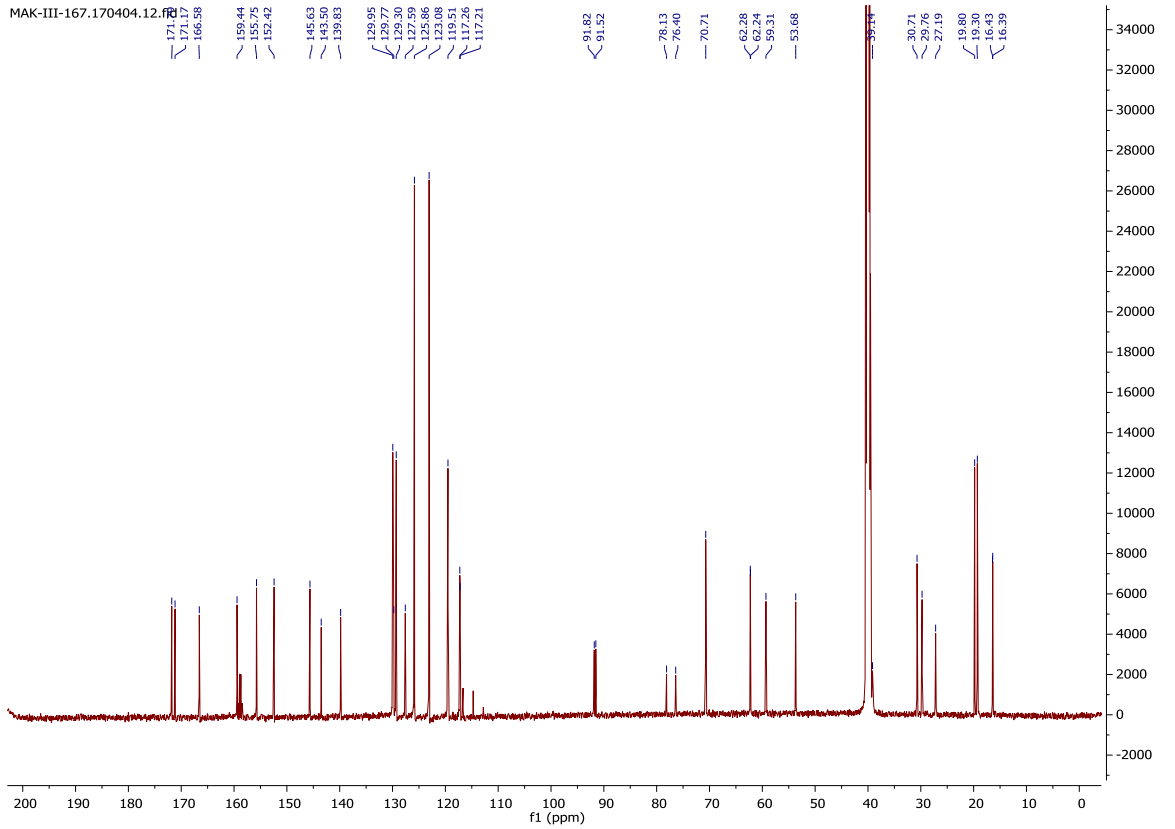
MAK-III-167.170404.12.fid
171.75
171.17
166.58
159.44
155.75
152.42
145.63
143.50
139.83
129.95
129.77
129.30
127.59
125.86
123.08
119.51
117.26
117.21
91.82
91.52
78.13
76.40
70.71
62.28
62.24
59.31
53.68
39.14
30.71
29.76
27.19
19.80
19.30
16.43
16.39
f1 (ppm)

Di-(2-(2-Hydroxyethoxy)ethyl) ethynylphosphonite (**5**)

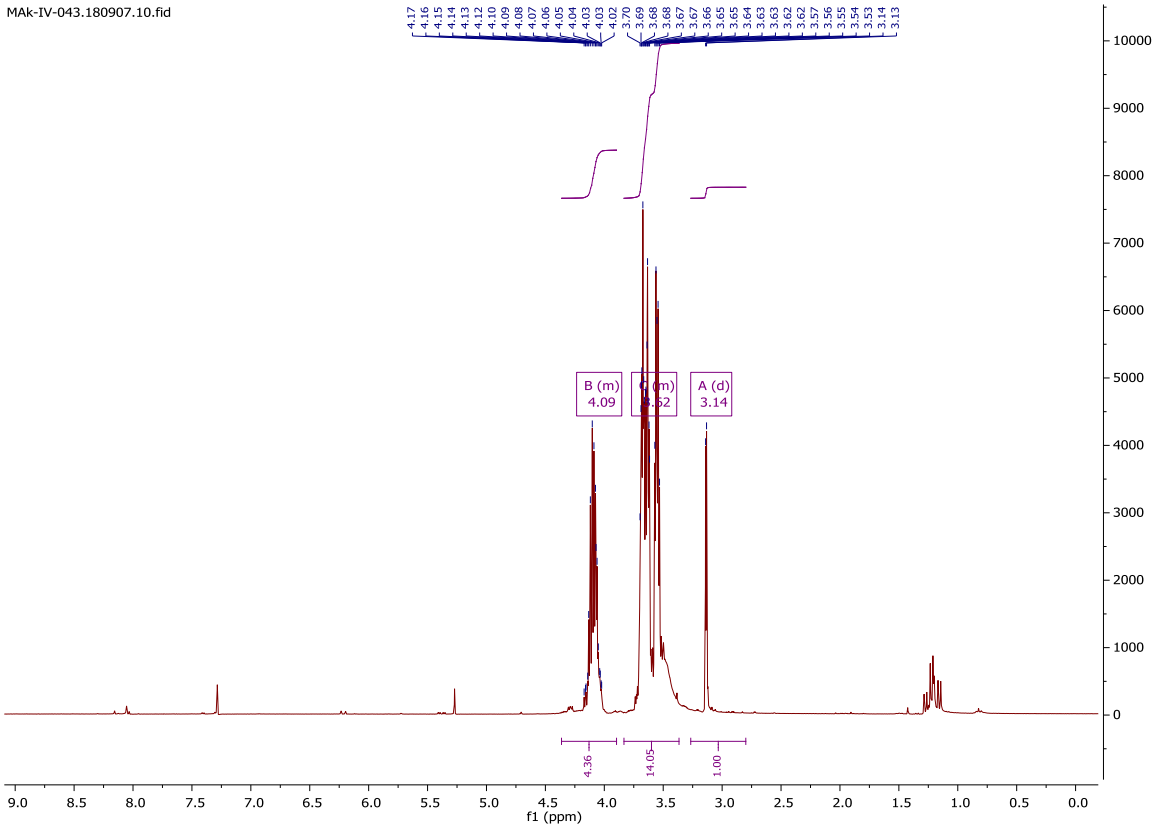

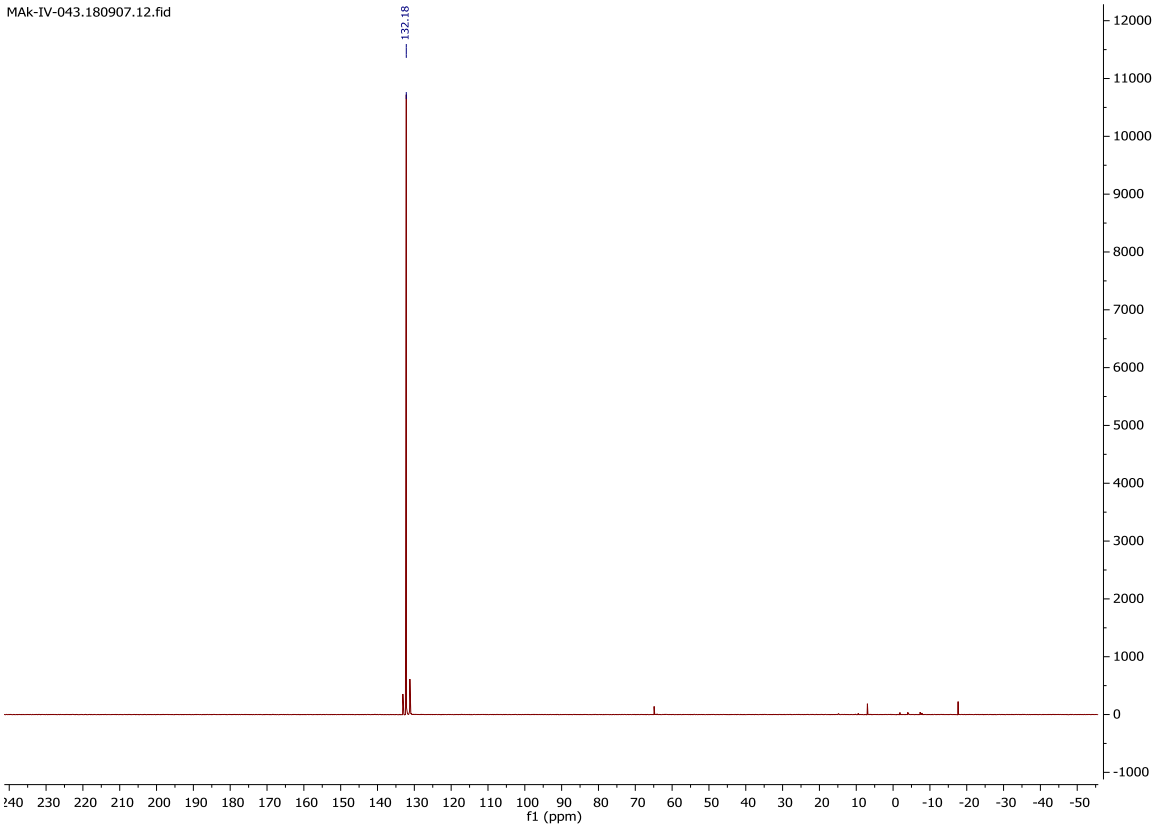

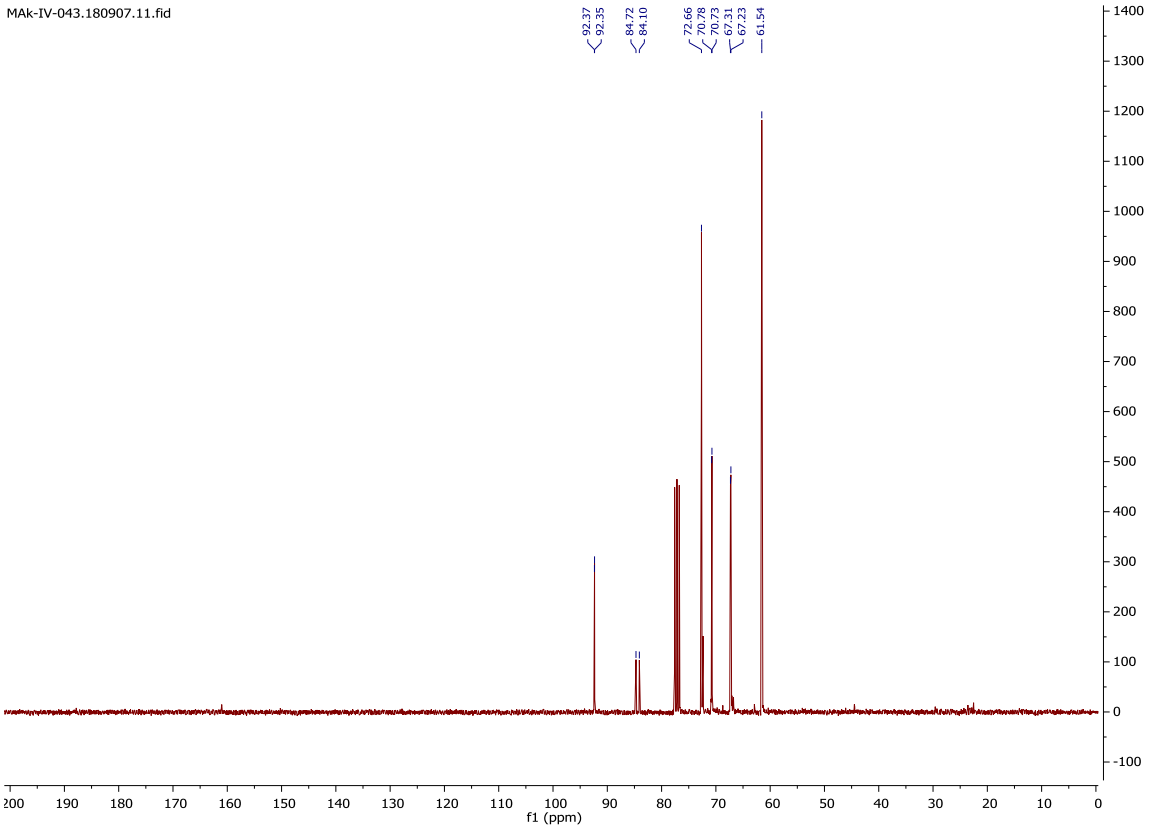

Di-(2-(2-Hydroxyethoxy)ethyl)-*N*-(4-benzoic-acid-*N*-hydroxysuccinimideester)-*P*-ethynyl phosphonamidate (**8**)

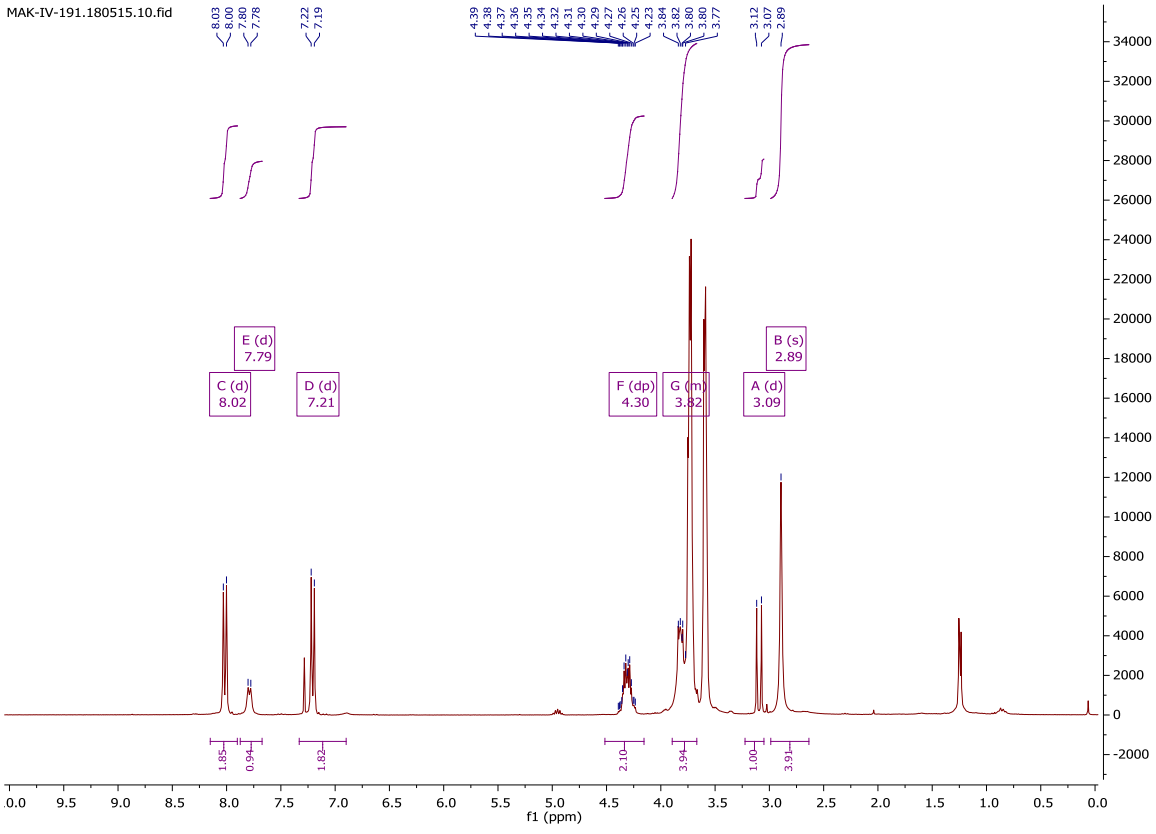

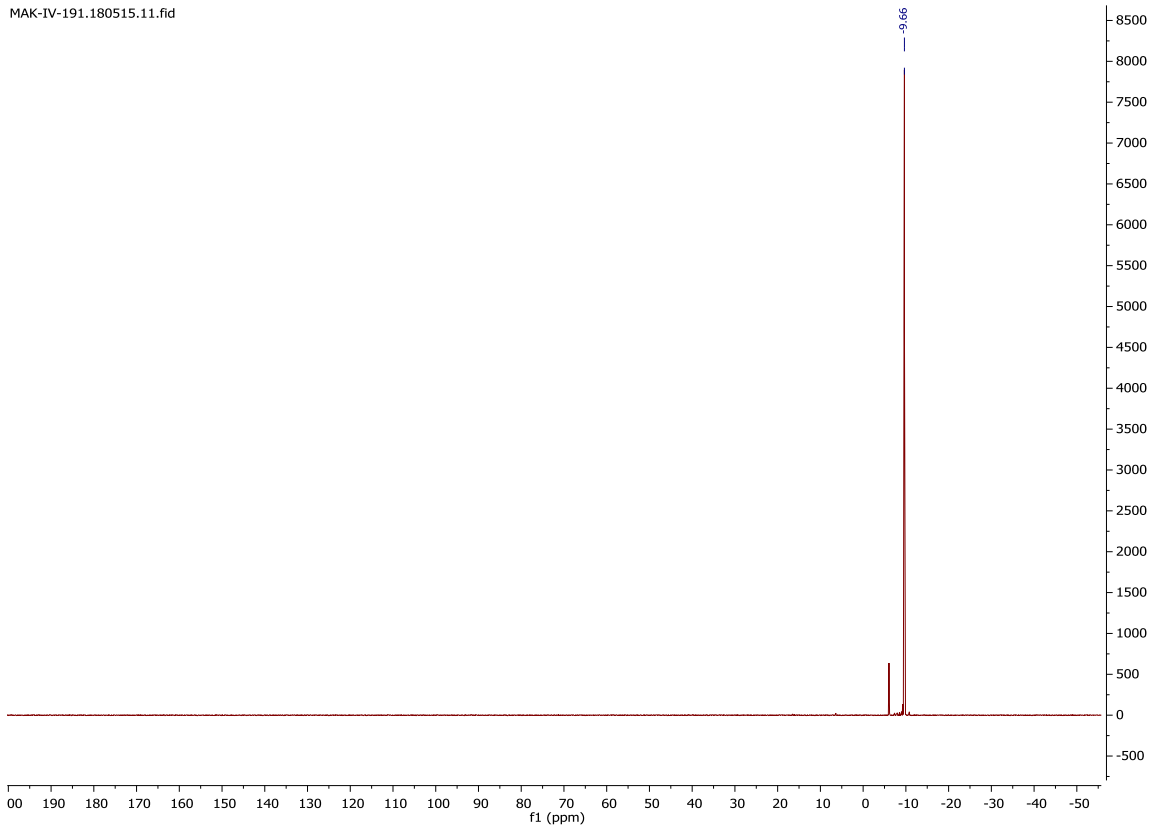
MAK-IV-191.180515.11.fid
-9.66
f1 (ppm)

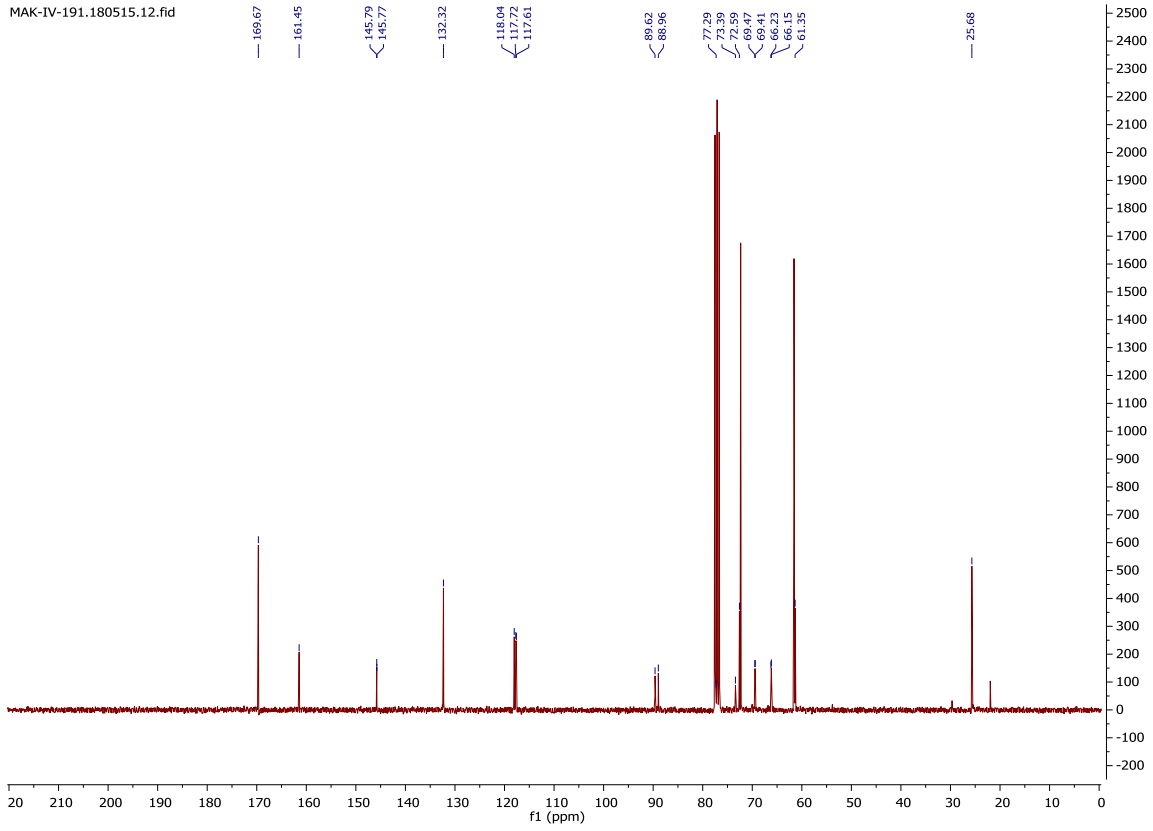
MAK-IV-191.180515.12.fid
169.67
161.45
145.79
145.77
132.32
118.04
117.72
117.61
89.62
88.96
77.29
73.39
72.59
69.47
69.41
66.23
66.15
61.35
25.68
f1 (ppm)

References

[1] S. M. Ansell, *Blood* **2014**, *124*, 3197-3200.

[2] A. Stengl, D. Hörl, H. Leonhardt, J. Helma, *SLAS Discov.* **2017**, *22*, 309-315.

4.5 FLEXAMERS: A DOUBLE-TAG FOR UNIVERSAL GENERATION OF VERSATILE PMHC MULTIMERS

The Journal of Immunology

FLEXamers: A Double Tag for Universal Generation of Versatile Peptide-MHC Multimers

Manuel Effenberger, Andreas Stengl, Kilian Schober, Maria Gerget, Maximilian Kampick, Thomas R. Müller, Dominik Schumacher, Jonas Helma, Heinrich Leonhardt and Dirk H. Busch

J Immunol 2019; 202:2164-2171; Prepublished online 13 February 2019;
doi: 10.4049/jimmunol.1801435
http://www.jimmunol.org/content/202/7/2164

The Journal of Immunology is published twice each month by
The American Association of Immunologists, Inc.,
1451 Rockville Pike, Suite 650, Rockville, MD 20852

Print ISSN: 0022-1767 Online ISSN: 1550-6606.

FLEXamers: A Double Tag for Universal Generation of Versatile Peptide-MHC Multimers

Manuel Effenberger,*[,1] Andreas Stengl,[†,1] Kilian Schober,*[,1] Maria Gerget,* Maximilian Kampick,* Thomas R. Müller,*[,‡] Dominik Schumacher,[†] Jonas Helma,[†] Heinrich Leonhardt,[†] and Dirk H. Busch*[,‡,§]

Peptide-MHC (pMHC) multimers have become a valuable tool for immunological research, clinical immune monitoring, and immunotherapeutic applications. Biotinylated tetramers, reversible Streptamers, or dye-conjugated pMHC multimers are distinct pMHC reagents tailored for T cell identification, traceless T cell isolation, or TCR characterization, respectively. The specific applicability of each pMHC-based reagent is made possible either through conjugation of probes or reversible multimerization in separate production processes, which is laborious, time-consuming, and prone to variability between the different types of pMHC reagents. This prohibits broad implementation of different types of pMHC reagents as a standard toolbox in routine clinical immune monitoring and immunotherapy. In this article, we describe a novel method for fast and standardized generation of any pMHC multimer reagent from a single precursor ("FLEXamer"). FLEXamers unite reversible multimerization and versatile probe conjugation through a novel double tag (Strep-tag for reversibility and Tub-tag for versatile probe conjugation). We demonstrate that FLEXamers can substitute conventional pMHC reagents in all state-of-the-art applications, considerably accelerating and standardizing production without sacrificing functional performance. Although FLEXamers significantly aid the applicability of pMHC-based reagents in routine workflows, the double tag also provides a universal tool for the investigation of transient molecular interactions in general. ***The Journal of Immunology*****, 2019, 202: 2164–2171.**

A T cell's function is determined largely through the affinity of the TCR to Ags presented on the MHC (peptide-MHC [pMHC]) of cells. Analyses of TCR:pMHC interactions have been challenging as the affinity of monomeric pMHC molecules is not strong enough for stable binding. Scaffolds allowing multimerization enable analyses of weak and transient interactions of molecules through a gain in avidity through multivalent binding. Soluble pMHC monomers (biotinylated, e.g., via an Avi-tag) can be multimerized on a dye-conjugated streptavidin backbone ("tetramer") (1). This enables sensitive identification and isolation of Ag-specific T cells and has opened up new avenues for in-depth T cell analysis in basic research and immune monitoring in a clinical setting (2).

*Institute for Medical Microbiology, Immunology, and Hygiene, Technical University of Munich, 81675 Munich, Germany; [†]Department of Biology II, Ludwig Maximilian University of Munich, 82152 Planegg-Martinsried, Germany; [‡]National Center for Infection Research, 85748 Munich, Germany; and [§]Clinical Cell Processing and Purification Focus Group, Institute for Advanced Study, Technical University of Munich, 81675 Munich, Germany

[1]M.E., A.S., and K.S. contributed equally to this work.

ORCIDs: 0000-0001-9323-9472 (K.S.); 0000-0003-3487-1341 (M.K.); 0000-0001-7095-6858 (D.S.); 0000-0002-5086-6449 (H.L.); 0000-0001-8713-093X (D.H.B.).

Received for publication October 25, 2018. Accepted for publication January 25, 2019.

This work was supported by the graduate school of the Deutsche Forschungsgemeinschaft (DFG) (GRK1721 to A.S.). This work was further supported by the DFG with grants to H.L. (SFB1243/A01 and SPP1623) and by the German Federal Ministry for Economic Affairs and Energy with grants to D.S. and J.H. (EXIST FT I).

Address correspondence and reprint requests to Prof. Dirk H. Busch, Institute for Medical Microbiology, Immunology and Hygiene, Technical University of Munich, Trogerstraße 30, 81675 Munich, Germany. E-mail address: dirk.busch@tum.de

The online version of this article contains supplemental material.

Abbreviations used in this article: HC, H chain; pMHC, peptide-MHC; SrtA, sortase A; TTL, tubulin tyrosine ligase.

www.jimmunol.org/cgi/doi/10.4049/jimmunol.1801435

However, stable binding of pMHC tetramers can also deteriorate T cell functionality in vivo (3, 4). The fact that pMHC ligand binding to the TCR is stable in its multivalent form but can be reversed upon monomerization has been exploited for the development of clinical cell selection and processing technologies (5–8) and is further used for in-depth characterization of TCR:pMHC interactions. Reversible pMHC multimer reagents, such as "Streptamers," allow traceless isolation of cell products with no functional difference compared with cells that have never bound pMHC multimers (5–9). When reversible pMHC monomers themselves are labeled with a fluorophore, their dissociation from TCRs on living T cells can be tracked over time (10, 11). Through this, absolute and reproducible measurements of TCR:pMHC dissociation (k_{off}) rates can be achieved in a relatively easy and high-throughput compatible manner. TCR-ligand k_{off} rates indicate TCR avidity and are predictive of T cell functionality (10).

Until now, the versatility of pMHC multimer reagents comes at the cost of distinct generation processes for each application (Supplemental Fig. 1). Separate recombinant protein expression, in vitro refolding, and pMHC purification processes make the synthesis of pMHC-based reagents laborious, time-consuming, and prone to batch-to-batch variability. The cumbersome and expensive effort to generate distinct pMHC constructs for each application has so far prevented many laboratories to make broad use of the versatility of pMHC multimer reagents. Ideally, the three distinct constructs should emerge from one common pMHC precursor, thus streamlining the production process while simultaneously providing full flexibility to generate all other pMHC multimer types. Flexibility can be achieved by enzymatic functionalization tags (12, 13). In addition, Strep- and His-tags can be used to generate reversible pMHC multimer reagents (14). So far, however, no approach has provided an all-in-one solution to produce versatile pMHC-based reagents within a simple generation process. In this article, to our knowledge, we

present a novel approach to generate distinct pMHC multimer reagents from a single, highly functional, double-tagged pMHC precursor protein ("FLEXamer"). FLEXamers can be used without further modification for traceless isolation of T cells but can also be conjugated 1) with biotin for stable identification of Ag-specific T cells, 2) with fluorescent dyes to track dissociation of monomeric pMHC molecules for TCR avidity measurement, or 3) with any probe of interest.

Materials and Methods

Tubulin tyrosine ligase expression and purification

Tubulin tyrosine ligase (TTL) was expressed and purified as follows, according to a published protocol (15). The TTL (*Canis lupus*) coding sequence was amplified from a mammalian expression vector (16), cloned into a pET28-SUMO3 (EMBL-Heidelberg, Protein Expression Facility), and expressed in *Escherichia coli* BL21(DE3) as a Sumo-TTL fusion protein with an N-terminal His-tag. Expression was induced with 0.5 mM isopropyl β-D-thiogalactoside and incubated at 18°C for 18 h. Lysis was performed in the presence of lysozyme (100 μg/ml), DNAse (25 μg/ml), and PMSF (2 mM), followed by sonication (Branson Sonifier; five times, 7 × 8 s, 40% amplitude) and debris centrifugation at 20,000 × *g* for 30 min. His-Sumo-TTL was purified using a 5 ml HisTrap (GE Healthcare). Purified protein was desalted on a PD10 column (GE Healthcare); buffer was exchanged to MES/K (pH 7.0; 20 mM MES, 100 mM KCl, 10 mM $MgCl_2$) supplemented with 3 mM 2-ME, 50 mM L-glutamate, and 50 mM L-arginine. Protein aliquots were shock frozen and stored at −80°C.

Cloning of Tub- and sortase A tag into Streptamer expression vector

pET3a expression vectors containing the coding sequence of Strep-tagged HLA allotypes, including murine H2-K^b, served as parental plasmid to insert the Tub-tag or sortase A (SrtA)-tag sequence seamlessly downstream of Strep-tag. All insertions were performed using the Q5 Site-Directed Mutagenesis Kit (New England BioLabs) following manufacturer's protocol. Insertion primers (Sigma-Aldrich) contained 18 bp of plasmid binding sequence flanking the integration site and encoded one-half of the Tub- or SrtA-tag sequence.

Generation of pMHC monomers

All pMHC monomers described in this report, including the double-tagged pMHC molecules, were generated as previously described (2, 5). In brief, recombinantly expressed and purified human as well as murine MHC H chain (HC) and β2 microglobulin were denatured in urea and subsequently refolded into the heterotrimeric pMHC complex in the presence of an excess of peptides (synthetic peptides purchased by Peptides and Elephants). Correctly folded pMHC monomers were purified using size exclusion chromatography, concentrated, and stored at −80°C or in liquid nitrogen. All conventional dye-conjugated Streptamers used for k_{off} rate measurements were generated by Maleimide chemistry using a solvent-exposed artificial cysteine residue as described (10, 17).

TTL reaction on Tub-tagged FLEXamers

TTL-catalyzed ligation of 3-azido-L-tyrosine (Watanabe Chemical Industries) to Tub-tagged FLEXamers was performed in 25–100 μl consisting of 20 μM FLEXamer, 5 μM TTL, and 1 mM 3-azido-L-tyrosine in TTL-reaction buffer (20 mM MES, 100 mM KCl, 10 mM $MgCl_2$, 2.5 mM ATP, and 5 mM reduced glutathione) at 25°C for 3 h followed by buffer exchange to 20 mM Tris HCl and 50 mM NaCl (pH 8) by size-exclusion chromatography (Zeba Spin desalting columns, 7K MWCO; Thermo Scientific). Azido-FLEXamers were stored at 4°C or directly used for click functionalization.

Click functionalization of azido-FLEXamers

Azido-FLEXamers were functionalized by incubation of 20 μM azido-FLEXamer with either 400 μM DBCO-PEG_4-Biotin, 400 μM DBCO-sulfoCy5, or 200 μM DBCO-PEG_4-Atto488 (Jena Bioscience) for 18 h at 16°C followed by buffer exchange to 20 mM Tris, 50 mM NaCl (pH 8), and storage at −80°C. Conjugation was analyzed by reducing SDS-PAGE and Coomassie staining. Conjugation efficacies were assessed from scanned Coomassie-stained SDS-PAGE gels. For this, the Gel Analyzer plugin of the Fiji software was used to quantify band intensities of unconjugated and conjugated HC. The efficiency was calculated using the following equation: intensity-labeled HC/(intensity-labeled HC + intensity-unlabeled HC). To confirm the identity of the attached functional groups, biotinylated FLEXamers were plotted on a nitrocellulose membrane, stained with a streptavidin-Alexa Fluor 594 (Dianova) conjugate, and detected on an Amersham Imager 600 system (GE Healthcare). In-gel fluorescence of fluorophore-labeled FLEXamers was directly detected using the same instrumentation.

Functionalization of SrtA-tagged FLEXamers

A total of 10 μM SrtA-tagged FLEXamer was incubated with 1 mM Gly_5-FITC or 1 mM Gly_5-biotin peptide (JPT Peptide Technologies GmbH) and 30 μM SrtA (kindly provided as purified enzyme derived from *Staphylococcus aureus* by Dr. H. Meyer; Technical University of Munich) in 20 mM HEPES and 5 mM $CaCl_2$ (pH 7.5) at 25°C for 18 h. Ni-NTA Agarose–based pulldown (Quiagen) in PBS and 20 mM imidazole (pH 8) at 4°C for 30 min was used to remove His-tagged SrtA and SrtA-tagged FLEXamer educts still carrying the His-tag. Purified functionalized SrtA-tagged FLEXamers were buffer exchanged after functionalization to 20 mM Tris and 50 mM NaCl (pH 8). Conjugation and purification were analyzed by SDS-PAGE, followed by detection of in-gel fluorescence and Coomassie staining.

CMV-reactive primary T cells and T cell clones

CMV-reactive T cell clones were generated and cultured as described previously (10). Primary T cells reactive for CMV were derived from healthy CMV-seropositive donors. Written informed consent was obtained from the donors, and usage of the blood samples was approved according to national law by the local Institutional Review Board (Ethikkommission der Medizinischen Fakultät der Technischen Universität München). Blood was diluted 1:1 with sterile PBS and PBMCs isolated by density gradient centrifugation using Leucosep tubes (Greiner Bio-One) following manufacturer's protocol.

pMHC multimer and Ab staining

All reversible pMHC monomers (with and without dye) were multimerized on Strep-Tactin APC or Strep-Tactin PE (IBA) by incubating 1 μg of reversible pMHC monomer and 1 μl of Strep-Tactin APC or PE in a total volume of 50 μl of FACS buffer for 30 min on ice in the dark. Conventionally biotinylated pMHC monomers for generation of nonreversible multimers were generated as described (2). Subsequently, all biotin functionalized pMHC monomers described in this report were multimerized by incubation of 0.4 μg of biotinylated pMHC monomers with 0.1 μg of streptavidin-BV421 (BioLegend), 0.25 μg of streptavidin-PE (eBioscience), or 0.1 μg of streptavidin-APC (BioLegend) in a total volume of 50 μl of FACS buffer for 30 min on ice in the dark. For k_{off} rate measurements, up to 5 × 10^6 cells were incubated with dye-conjugated reversible pMHC multimers for 45 min on ice in the dark. Ab staining (CD8 eF450 eBioscience, Thermo Scientific) was added after 25 min, and cells were incubated for an additional 20 min. If combinatorial staining with nonreversible pMHC multimers was performed, cells were washed and incubated for 10 min with nonreversible pMHC multimers on ice in the dark. For live/dead discrimination, cells were washed in propidium iodide solution. When solely performing pMHC multimer staining with a combination of nonreversible pMHC multimers, staining was incubated for 30 min on ice in the dark. We routinely stain the pMHC multimer conjugated to the smaller dye first. After incubation, cells were washed and stained with the second pMHC multimer for 30 min. Ab staining was added after 10 min, and cells were incubated for an additional 20 min. When cells were stained with reversible pMHC multimers for traceless cell isolation, samples were incubated for 45 min with the multimer regent. After 25 min, Ab staining was added, and cells were incubated for an additional 20 min. All FACS data were analyzed with FlowJo software (FlowJo).

FACS analysis and flow sorting

Acquisition of FACS samples was done on a CyAn ADP Px9 color flow cytometer (Beckman Coulter). Flow sorting was conducted on a MoFlo legacy (Beckman Coulter). k_{off} rate measurements were performed as described (18). In brief, samples were transferred into precooled FACS tubes containing a total volume of 1 ml of FACS buffer and placed into a Peltier cooler (qutools GmbH) set to 5.5°C. After 30 s acquisition, 1 ml of cold 2 mM D-biotin was added into the ongoing measurement. Dissociation kinetics were measured for 15 min. For analysis of k_{off} rate data, fluorescence data of Ag-specific cells were exported from FlowJo to PRISM (GraphPad Software). The $t_{1/2}$ was determined by fitting a one-phase exponential decay curve.

Results

A double tag enables generation of both reversible and functionalizable pMHC monomers from one precursor construct

We hypothesized that combining a site-specific functionalization tag with a reversible multimerization tag to a double-tagged FLEXamer will unite reversibility with the opportunity to equip the pMHC with any desired additional functionality (Fig. 1, Supplemental Fig. 1). For site-specific conjugation, we first chose a new chemoenzymatic system, termed Tub-tag (15), which is based on a short hydrophilic, unstructured sequence recognized by TTL (19). TTL-catalyzed attachment of tyrosine derivatives, such as 3-azido-*L*-tyrosine, allows subsequent addition of a variety of functional groups, such as biotin or dyes, by highly efficient and mild click chemistry (15). Similar to other chemoenzymatic approaches, the TTL reaction is not reversible; however, the product does not suffer from hydrolysis, and the substrate tyrosine derivatives represent compounds that are easy to synthesize (15) or commercially available (see *Materials and Methods*).

We performed proof-of-concept experiments to test if we could use this strategy to conjugate biotin or dyes to Strep- and Tub-tagged FLEXamers. We generated two different FLEXamers for the HLA class I HC B*07:02 and B*08:01, which present CMV pp65 and IE1, respectively (Fig. 2A). Enzymatic activation of the common precursor FLEXamer and subsequent conjugation with biotin, Atto488, or sulfo-cyanine5 was highly efficient, with conversion rates >95% based on Coomassie-stained SDS-PAGE gel band intensities (Fig. 2B; see *Materials and Methods*).

FLEXamers are highly functional pMHC reagents

We then tested whether the nonreversible biotinylated FLEXamer, the reversible dye-conjugated FLEXamer, and their reversible FLEXamer precursor could fulfill their distinct functions. Biotinylated FLEXamers stained B*07:02/pp65$_{417–426}$–specific T cells from peripheral blood of a CMV-seropositive donor with high sensitivity and no difference to conventionally biotinylated tetramers (Fig. 3). An irrelevant epitope/MHC combination (A*02:01/Her2neu$_{369–377}$) served as control for unspecific staining (Fig. 3).

To test for possible interference of the functionalization tag with reversibility, we stained and flow sorted B*07:02/pp65$_{417–426}$–specific CD8$^+$ T cells from peripheral blood of a CMV-seropositive donor either with conventional Streptamers or FLEXamers (Fig. 4). FLEXamers could stain B*07:02/pp65$_{417–426}$-specific T cells and allowed high purity flow cytometric sorting like conventional Streptamers (Fig. 4B). Upon addition of D-biotin, the pMHC label could be detached. Complete removal of pMHC monomers from the cells is demonstrated by the inability to restain the cells by solely adding the Strep-Tactin backbone, whereas addition of the multimerized FLEXamer resulted in efficient restaining (Fig. 4B).

Conjugation of dyes to Streptamer pMHCs allows direct tracing of pMHC monomer dissociation kinetics after addition of D-biotin, to measure TCR:pMHC k_{off} rates for TCR structural avidity estimation (10, 18) (Fig. 5). When a B*07:02/pp65$_{417–426}$ T cell clone was stained with dye-conjugated Streptamers or

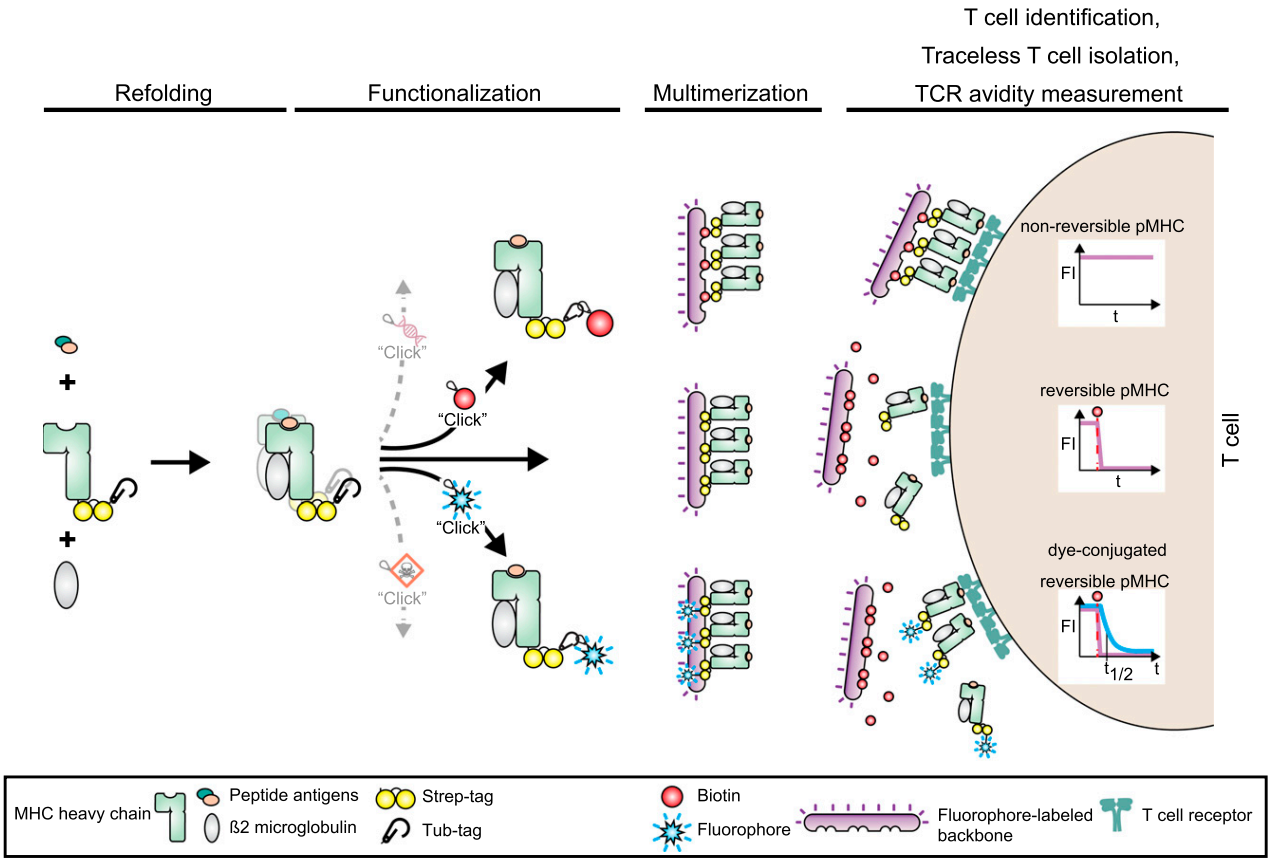

FIGURE 1. Double-tagged pMHC FLEXamers streamline generation process of distinct pMHC reagents. Schematic depiction of pMHC generation from "FLEXamers" and their respective application in T cell immunology. pMHC FLEXamer complexes are assembled from combinations of double-tagged HC, peptide Ags, and β2 microglobulin. The double tag consists of a Strep-tag for reversible multimerization and a Tub-tag for site-specific functionalization. This allows functionalization and multimerization of nonreversible, reversible, or dye-conjugated reversible pMHCs from the same precursor molecule for T cell identification, traceless T cell isolation, or TCR avidity measurement respectively.

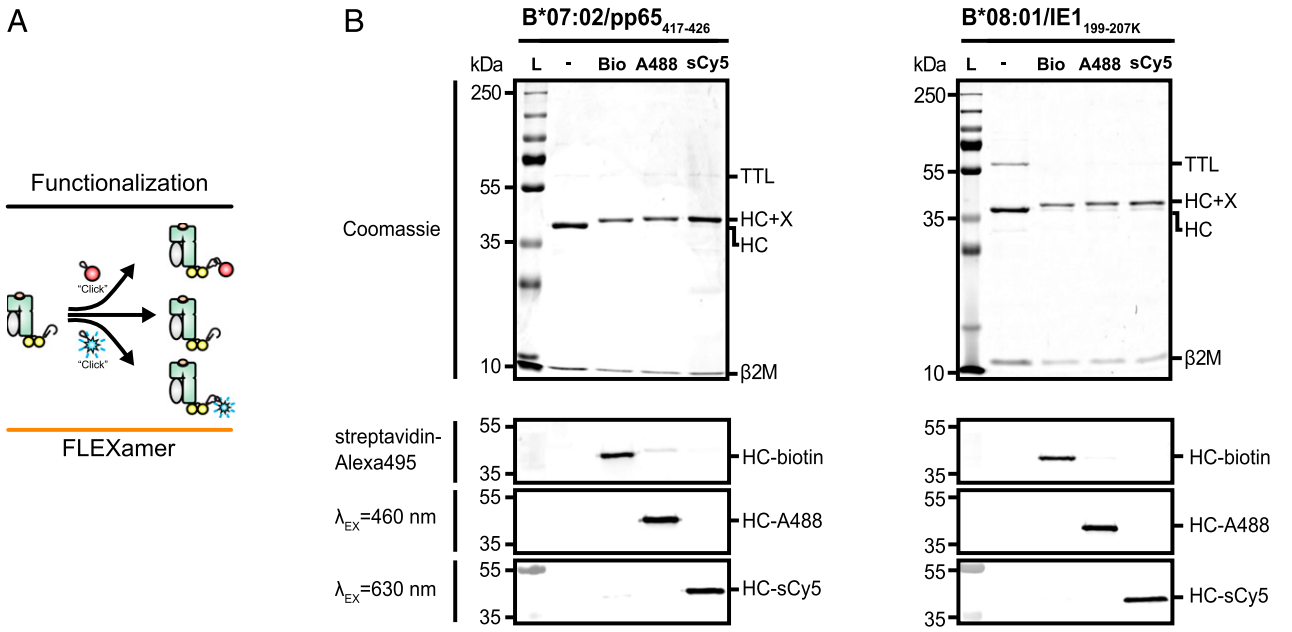

FIGURE 2. Efficient functionalization of double-tagged FLEXamers with biotin or fluorophores. (**A**) Schematic depiction of FLEXamer-mediated functionalization into distinct pMHC reagents. (**B**) SDS-PAGE, followed by Coomassie and Western blot analysis of site-specific labeling of B*07:02/pp65(417–426) and B*08:01/IE1(199–207K) HC by TTL-mediated incorporation of 3-azido-L-tyrosine (lane "-") and subsequent click conjugation of DBCO-PEG4-biotin (Bio), DBCO-PEG4-Atto488 (A488), or DBCO-sulfoCy5 (sCy5). HC+X indicates the m.w. after conjugation of HC. Presence of the respective functional group is shown by streptavidin-Alexa495–based detection of Bio or in-gel fluorescence of A488 and sCy5. Lane "L" represents the m.w. marker.

FLEXamers, the dye-conjugated pMHC molecules showed monomeric pMHC dissociation after initial dye dequenching, as previously described (10) (Fig. 5B). The k_{off} rates determined by fitting of exponential decay curves were identical for dye-conjugated Streptamers and FLEXamers (Fig. 5D). We next tested the functionality of murine FLEXamers and therefore generated FLEXamers for H2-K^b/$OVA_{257–264}$. We measured k_{off} rates of OT-I transgenic T cells, which were as fast as expected (20) and did not differ between conventionally generated dye-conjugated Streptamers and dye-conjugated FLEXamers (Supplemental Fig. 2A).

Using double staining with a nonreversible biotinylated pMHC multimer and a reversible dye-conjugated pMHC Streptamer, dissociation kinetics can be tracked without previous purification on a flow cytometer through continuous gating on the nonreversible pMHC multimer$^+$ T cell population (18). This emphasizes that not only the different pMHC constructs themselves but also their

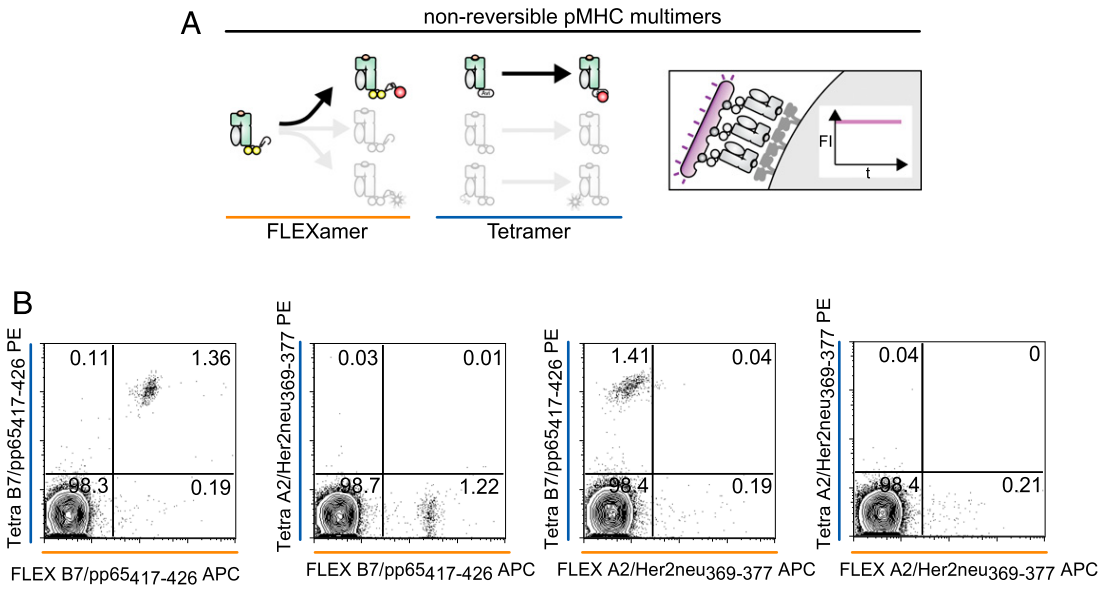

FIGURE 3. T cell identification: comparing nonreversible biotinylated double-tagged FLEXamers versus conventional tetramers. (**A**) Schematic depiction comparing generation of nonreversible pMHC monomers using FLEXamer or BirA technique. (**B**) pMHC multimer staining of B7/pp65(417–426)-specific CD8$^+$ T cells from peripheral blood of a CMV-seropositive donor. pMHCs were conventionally biotinylated (Tetra) and multimerized on streptavidin-PE or biotinylated via Tub-tag technique (FLEX) and multimerized on streptavidin-APC. Relevant epitope: B7/pp65(417–426); irrelevant control epitope: A2/Her2neu(369–377). Pregated on single, living CD8$^+$ T cells.

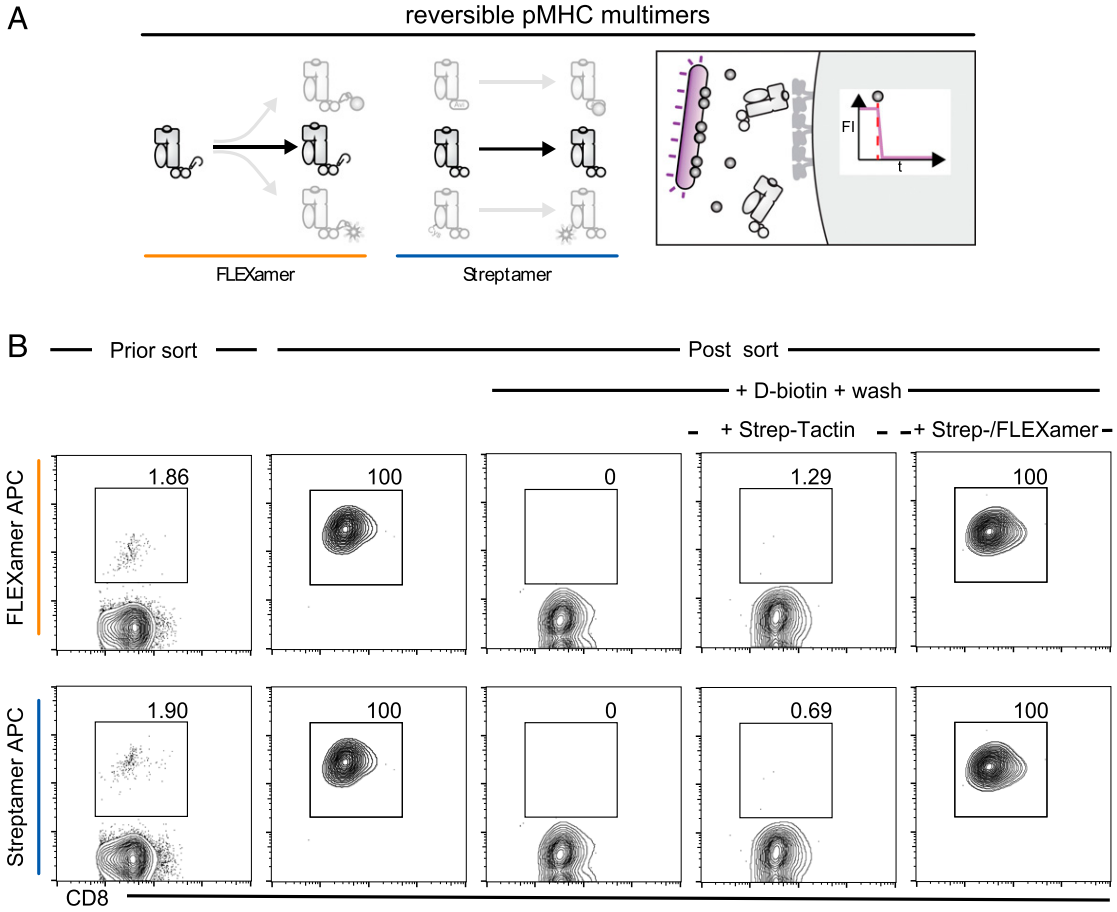

FIGURE 4. Traceless T cell isolation: comparing unmodified reversible double-tagged FLEXamers versus Streptamers. (**A**) Schematic depiction comparing generation of reversible pMHC monomers using FLEXamer or Streptamer technique. (**B**) Flow sort purification and restaining of B7/pp65 (417–426)-specific $CD8^+$ T cells from peripheral blood of a CMV-seropositive donor with FLEXamers or conventional Streptamers. Pregated on single, living lymphocytes.

combinatorial use enable in-depth T cell characterization. We costained a heterogeneous B*07:02/$pp65_{417–426}$–specific T cell population directly ex vivo with both nonreversible pMHC conjugated to biotin and reversible pMHC conjugated to Atto488 (Fig. 5C). Nonreversible pMHC multimers allowed continuous gating on the Ag-specific T cell population after the addition of D-biotin (Supplemental Fig. 2B), whereas the reversible fluorophore-conjugated pMHC monomers dissociated over time (Fig. 5C, Supplemental Fig. 2E). The heterogeneous T cell populations specific for B*07:02/$pp65_{417–426}$ entailed two distinct kinetics (Fig. 5C, Supplemental Fig. 2D). We retrieved T cell clones from both kinetics and stained them with dye-conjugated Streptamers and FLEXamers. Again, we obtained highly comparable dissociation rates resembling those of the parental T cell population (Supplemental Fig. 2D). After 60 min of D-biotin addition, both kinetics reached baseline, validating that both populations represented true dissociation kinetics (Supplemental Fig. 2C). The combinatorial use of pMHC reagents therefore allows visualization of subpopulations with different dissociation kinetics from a common native heterogeneous T cell population directly ex vivo. FLEXamers enable universal generation of these different pMHC constructs from a common precursor protein.

FLEXamers can be generated with different functionalization tags

Next, we set out to test the general applicability of our double-tag approach. Therefore, we cloned and refolded an HLA-A*02:01 FLEXamer harboring a SrtA recognition tag for versatile protein conjugation via transpeptidation (13). This construct is additionally equipped with a His-tag for fast and efficient protein purification after transpeptidation (Supplemental Fig. 3A). We stained PBMCs with a transgenic TCR specific for A*02:01/$pp65_{495–503}$ with Tub-tag– or SrtA-biotinylated tetramers (Supplemental Fig. 3B) and also tested reversibility of the SrtA-tag carrying FLEXamer precursor (Supplemental Fig. 3C). Furthermore, Tub- or SrtA-tag dye-conjugated reversible FLEXamers were tested for characterization of TCR:pMHC k_{off} rates (Supplemental Fig. 3D, 3E). In each case, SrtA FLEXamers, Tub-tag FLEXamers, and their biotin- or dye-conjugated downstream pMHC products performed equally well (Supplemental Fig. 3B–E) independent of the respective functionalization strategy. However, compared with Tub-tag, SrtA-mediated pMHC functionalization is less efficient overall, which had to be compensated by significantly increased educt consumption. We therefore focused on Tub-tag technology to generate FLEXamers.

Double-tagging of pMHC monomers allows highly efficient and flexible functionalization independent of HLA allotype and Ag peptide

Encouraged by the much simpler generation process of different pMHC multimer reagents from a single double-tagged FLEXamer precursor, we also generated FLEXamers for other epitope–HLA combinations. For B*08:01 presenting $IE1_{199–207K}$, we validated the equal functionality of nonreversible, reversible, and

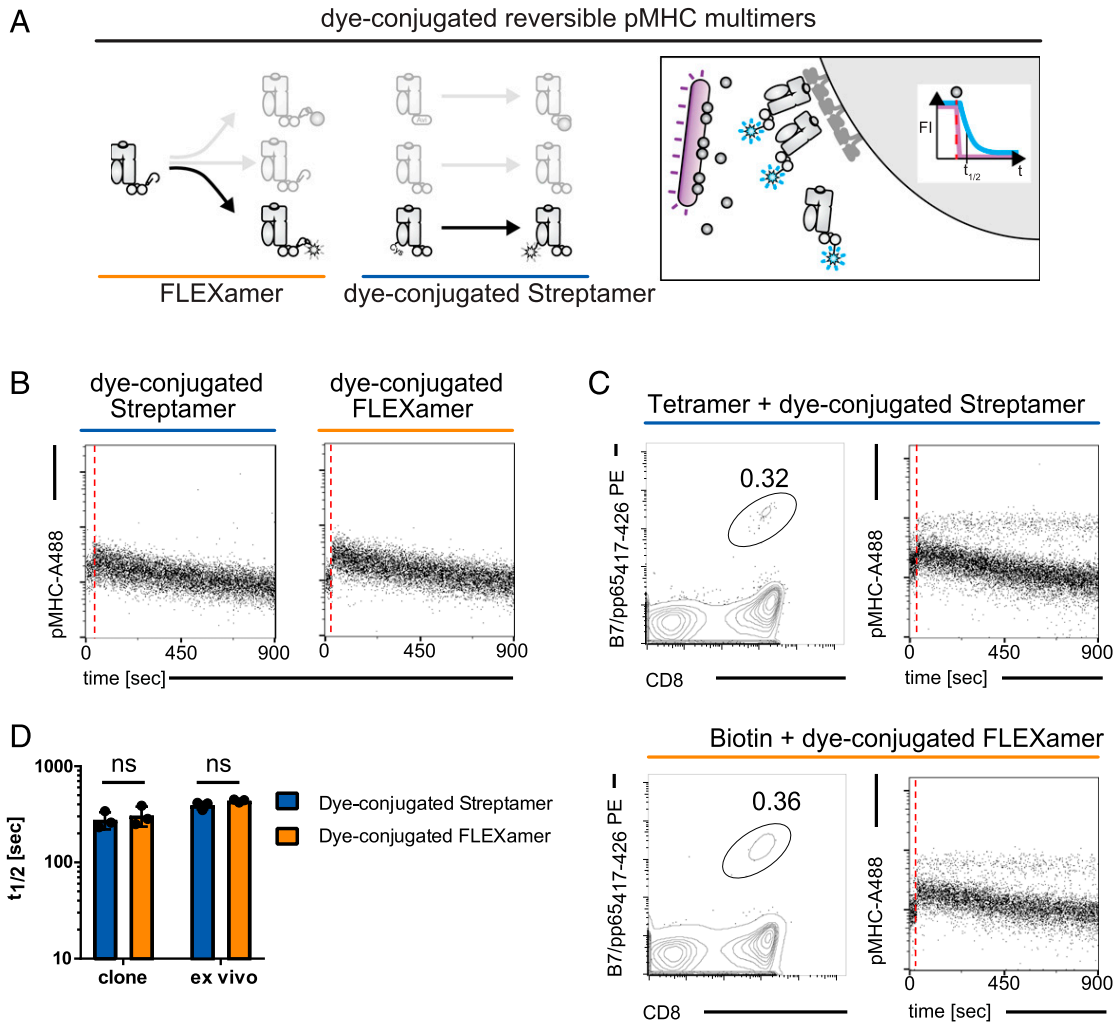

FIGURE 5. TCR avidity measurement: comparing dye-conjugated double-tagged FLEXamers versus dye-conjugated Streptamers. (**A**) Schematic depiction comparing generation of dye-conjugated reversible pMHC monomers using FLEXamer technique or maleimide dye chemistry on Streptamers. (**B**) Dissociation kinetics of a B7/pp65(417–426)-specific $CD8^+$ T cell clone measured with dye-conjugated Streptamers or dye-conjugated FLEXamers. Red dotted line indicates D-biotin addition. (**C**) Dissociation kinetics of B7/pp65(417–426)-specific $CD8^+$ T cells from peripheral blood of a CMV-seropositive donor, stained with a combination of nonreversible biotinylated pMHCs and reversible dye-conjugated pMHCs. Nonreversible pMHC multimer$^+$ $CD8^+$ T cells are gated for dissociation kinetics of dye-coupled pMHCs after D-biotin addition (red dotted line). (**D**) Quantification of technical triplicates of representative experiment shown in (B) and (C). One symbol represents one dissociation. Unpaired, non parametric Kolmogorov-Smirnov test. Pregated on single, living $CD8^+$ T cells in (B) and pregated on single, living lymphocytes in (C).

fluorophore-conjugated FLEXamers (Supplemental Fig. 4). To even further extend the set of available FLEXamers, we folded 26 FLEXamers in total, covering nine HLA class I HC as well as the murine HC H2-K^b (Fig. 6A). The conjugation efficacy with fluorophore or biotin was consistently high for all FLEXamers (Fig. 6B). Because of the skewed frequency distribution of HLA class I alleles, the nine human HLA HC together cover 76.5% of the European Caucasian population (Fig. 6C, 6D) and also entail two allotypes (A*24:02 and A*11:01), which are highly prevalent in Asian populations. This set of FLEXamers can serve as precursors for any kind of pMHC reagent.

Discussion

The heterogeneity of infectious agents and cancers is met by the adaptive immune system's ability to present and recognize many different targets. The total epitope repertoire has been estimated to be between 10^6 and 10^{11} in mice (21) and is likely similarly, if not even more diverse in humans. More than 13,000 HLA class I alleles have now been described for humans (22), and the total human TCR repertoire encompasses more than 10^8 unique clonotypes (23). Customized monitoring of Ag-specific immune responses and individualized immunotherapy therefore require streamlined methods that allow flexible adaptation for each patient and disease in terms of target-specific epitopes as well as patient-specific HLA (24). The versatile applicability of pMHC multimer reagents (for T cell identification, traceless isolation, or TCR avidity measurement) makes them particularly valuable tools for the investigation and therapeutic use of T cells (25) but consequently adds even a third level of complexity as so far as the specific reagents needed to be produced separately.

To be compatible with the extreme diversity of epitopes, UV exchange (26) or dipeptide (27) technologies have been developed that can be used to load HLA class I with any epitope of interest. In addition, combinatorial pMHC staining (28, 29) and DNA barcoding (30) have massively enhanced the throughput of screening Ag-specific T cell populations and their respective TCR repertoires. Despite this progress, difficulties to generate distinct pMHC multimer reagents appropriate for each individual

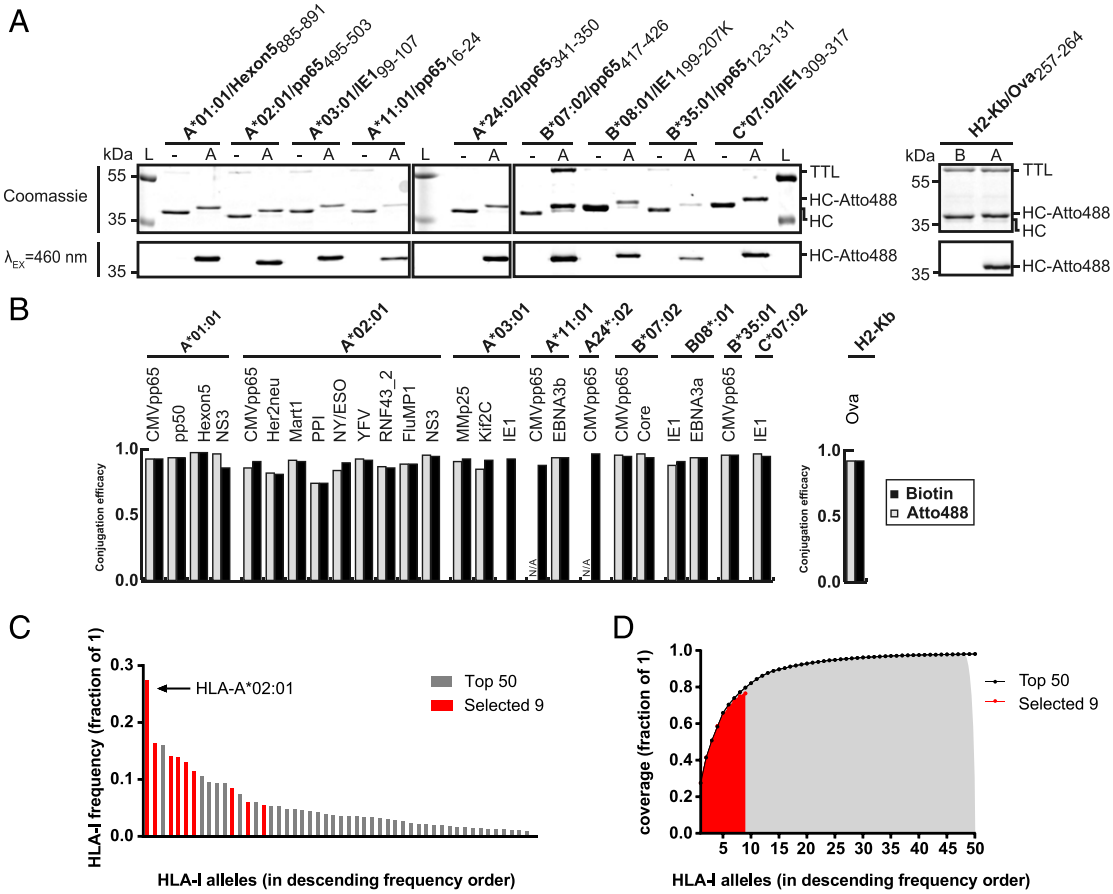

FIGURE 6. Double-tagged FLEXamers allow highly efficient functionalization irrespective of HLA allotype and presented peptide epitope and can also be transferred to murine MHC. (**A**) SDS-PAGE analysis of site-specific labeling of HLA and MHC monomers by TTL. Incorporation of 3-azido-L-tyrosine (-) and subsequent click conjugation of DBCO-PEG4-Atto488. HC-Atto488 indicates the m.w. after conjugation of HC. Presence of Atto488 was proven by in-gel fluorescence. L indicates the m.w. marker. (**B**) Conjugation efficacy of all 26 HLA-FLEXamers and murine FLEXamer H2-Kb/OVA coupled to Biotin or Atto488. (**C**) Fifty most frequent HLA class I alleles of European Caucasian population in descending order, with HC used for FLEXamer generation, shown in red. (**D**) Cumulative coverage of 50 most frequent HLA class I alleles (area under the curve in gray) or selected nine FLEXamer H chains.

setting in a fast and reliable manner remain a significant challenge to personalized cell therapy and T cell–based diagnostics. Importantly, for broad applicability of pMHC multimer reagents, the production process of different kinds of pMHC multimer reagents needs to also be feasible for many different HLA class I HC.

FLEXamers combine the provision of versatility through distinct pMHC constructs with a simple generation process from a single precursor protein (Fig. 1). FLEXamers are highly functional while being produced in a faster and more standardized manner compared with conventionally generated pMHC reagents. A core feature of FLEXamers is a novel double tag that allows reversible multimerization as well as functionalization with any probe of interest. In this study, we provide proof of concept to generate biotinylated tetramers, reversible Streptamers, or reversible dye-conjugated pMHC multimer reagents from a common FLEXamer precursor protein. Notably, the use of FLEXamers is not limited to these specific reagents as the functionalization tag also allows conjugation, for example, of DNA oligonucleotide sequences, toxins (Fig. 1), and many more entities. Furthermore, FLEXamers can be readily combined with epitope exchange technologies (27, 31). Because of the combination of a simple generation process with versatile application, FLEXamers facilitate implementation of different types of pMHC reagents in routine clinical immune monitoring and immunotherapy.

The effort and costs needed to generate distinct pMHC multimer reagents for each application has so far been a key obstacle for laboratories to fully exploit the versatility of pMHC-based reagents. Double-tagged pMHC FLEXamers can be easily generated and applied. Furthermore, although the double tag is a general concept readily compatible with the use of alternative functionalization tags (e.g., SrtA-tag). Notable advantages of Tub-tag technology are mild reaction conditions combined with high conjugation efficiencies using click chemistry, whereas functionalization via artificial solvent-exposed cysteine residues generates the risk of dimer formation via disulfide bridges and changes in tertiary structure because of the introduction of a polar amino acid. Finally, we used Tub-tag technology to generate a comprehensive set of versatile pMHC FLEXamers for nine different human HLA as well as murine H2-K^b.

Multivalent binding can serve as an “on switch” to stabilize otherwise transient binding of weak interaction partners. In turn, receptor–ligand binding can be switched off via disruption of the multimeric complex, which requires that the multimerization is reversible. Versatile functionalization thereby allows further stabilization of the interaction or tracking via fluorescent dyes. The field of T cell immunology has made extensive use of this trick through multimerization of pMHC monomers. Our double-tag approach enables universal generation of different pMHC constructs, but also constitutes a flexible

tool for investigation of transient protein–protein interactions in general.

Acknowledgments

We thank I. Andrä, L. Henkel, and all members of the TU Munich Flow Core Facility for cell sorting; I. Andrä for technical support in flow cytometry and J. Groffmann and J. Schwach for excellent practical support in FACS experiments; P. Lückemeier for development of k_{off} rate analysis software; F. Mohr for critical discussions and helpful advice in experimental design; F. Graml and A. Hochholzer for excellent technical support in the generation of pMHC monomers; and V. R. Buchholz, F. Mohr, J. Baldwin, J. Leube, and J. Schütz for critical reading of the manuscript.

Disclosures

The Tub-tag technology is part of a patent application filed by D.S., J.H., and H.L. and is subject to the spin-off project Tubulis. M.E., A.S, D.H.B., and L.H. applied for a patent covering the double tag. D.H.B. invented the Streptamer technology. The other authors have no financial conflicts of interest.

References

1. Altman, J. D., P. A. Moss, P. J. Goulder, D. H. Barouch, M. G. McHeyzer-Williams, J. I. Bell, A. J. McMichael, and M. M. Davis. 1996. Phenotypic analysis of antigen-specific T lymphocytes. [Published erratum appears in 1998 *Science* 280: 1821.] *Science* 274: 94–96.
2. Busch, D. H., and E. G. Pamer. 1998. MHC class I/peptide stability: implications for immunodominance, in vitro proliferation, and diversity of responding CTL. *J. Immunol.* 160: 4441–4448.
3. O'Herrin, S. M., J. E. Slansky, Q. Tang, M. A. Markiewicz, T. F. Gajewski, D. M. Pardoll, J. P. Schneck, and J. A. Bluestone. 2001. Antigen-specific blockade of T cells in vivo using dimeric MHC peptide. *J. Immunol.* 167: 2555–2560.
4. Maile, R., B. Wang, W. Schooler, A. Meyer, E. J. Collins, and J. A. Frelinger. 2001. Antigen-specific modulation of an immune response by in vivo administration of soluble MHC class I tetramers. *J. Immunol.* 167: 3708–3714.
5. Knabel, M., T. J. Franz, M. Schiemann, A. Wulf, B. Villmow, B. Schmidt, H. Bernhard, H. Wagner, and D. H. Busch. 2002. Reversible MHC multimer staining for functional isolation of T-cell populations and effective adoptive transfer. *Nat. Med.* 8: 631–637.
6. Cobbold, M., N. Khan, B. Pourgheysari, S. Tauro, D. McDonald, H. Osman, M. Assenmacher, L. Billingham, C. Steward, C. Crawley, et al. 2005. Adoptive transfer of cytomegalovirus-specific CTL to stem cell transplant patients after selection by HLA-peptide tetramers. *J. Exp. Med.* 202: 379–386.
7. Stemberger, C., S. Dreher, C. Tschulik, C. Piossek, J. Bet, T. N. Yamamoto, M. Schiemann, M. Neuenhahn, K. Martin, M. Schlapschy, et al. 2012. Novel serial positive enrichment technology enables clinical multiparameter cell sorting. *PLoS One* 7: e35798.
8. Neuenhahn, M., J. Albrecht, M. Odendahl, F. Schlott, G. Dössinger, M. Schiemann, S. Lakshmipathi, K. Martin, D. Bunjes, S. Harsdorf, et al. 2017. Transfer of minimally manipulated CMV-specific T cells from stem cell or third-party donors to treat CMV infection after allo-HSCT. *Leukemia* 31: 2161–2171.
9. Mohr, F., J. C. Fischer, M. Nikolaus, C. Stemberger, S. Dreher, A. Verschoor, T. Haas, H. Poeck, and D. H. Busch. 2017. Minimally manipulated murine regulatory T cells purified by reversible Fab Multimers are potent suppressors for adoptive T-cell therapy. *Eur. J. Immunol.* 47: 2153–2162.
10. Nauerth, M., B. Weißbrich, R. Knall, T. Franz, G. Dössinger, J. Bet, P. J. Paszkiewicz, L. Pfeifer, M. Bunse, W. Uckert, et al. 2013. TCR-ligand koff rate correlates with the protective capacity of antigen-specific CD8+ T cells for adoptive transfer. *Sci. Transl. Med.* 5: 192ra87.
11. Hebeisen, M., J. Schmidt, P. Guillaume, P. Baumgaertner, D. E. Speiser, I. Luescher, and N. Rufer. 2015. Identification of rare high avidity, tumor reactive CD8+ T cells by monomeric TCR-ligand off-rates measurements on living cells. *Cancer Res.* 75: 1983–1991.
12. Chen, I., M. Howarth, W. Lin, and A. Y. Ting. 2005. Site-specific labeling of cell surface proteins with biophysical probes using biotin ligase. *Nat. Methods* 2: 99–104.
13. Popp, M. W., J. M. Antos, G. M. Grotenbreg, E. Spooner, and H. L. Ploegh. 2007. Sortagging: a versatile method for protein labeling. *Nat. Chem. Biol.* 3: 707–708.
14. Schmidt, J., P. Guillaume, M. Irving, P. Baumgaertner, D. Speiser, and I. F. Luescher. 2011. Reversible major histocompatibility complex I-peptide multimers containing Ni(2+)-nitrilotriacetic acid peptides and histidine tags improve analysis and sorting of CD8(+) T cells. *J. Biol. Chem.* 286: 41723–41735.
15. Schumacher, D., J. Helma, F. A. Mann, G. Pichler, F. Natale, E. Krause, M. C. Cardoso, C. P. R. Hackenberger, and H. Leonhardt. 2015. Versatile and efficient site-specific protein functionalization by tubulin tyrosine ligase. *Angew. Chem. Int. Ed. Engl.* 54: 13787–13791.
16. Zink, S., L. Grosse, A. Freikamp, S. Bänfer, F. Müksch, and R. Jacob. 2012. Tubulin detyrosination promotes monolayer formation and apical trafficking in epithelial cells. *J. Cell Sci.* 125: 5998–6008.
17. Davis, D. M., H. T. Reyburn, L. Pazmany, I. Chiu, O. Mandelboim, and J. L. Strominger. 1997. Impaired spontaneous endocytosis of HLA-G. *Eur. J. Immunol.* 27: 2714–2719.
18. Nauerth, M., C. Stemberger, F. Mohr, B. Weißbrich, M. Schiemann, L. Germeroth, and D. H. Busch. 2016. Flow cytometry-based TCR-ligand Koff -rate assay for fast avidity screening of even very small antigen-specific T cell populations ex vivo. *Cytometry A* 89: 816–825.
19. Prota, A. E., M. M. Magiera, M. Kuijpers, K. Bargsten, D. Frey, M. Wieser, R. Jaussi, C. C. Hoogenraad, R. A. Kammerer, C. Janke, and M. O. Steinmetz. 2013. Structural basis of tubulin tyrosination by tubulin tyrosine ligase. *J. Cell Biol.* 200: 259–270.
20. Rosette, C., G. Werlen, M. A. Daniels, P. O. Holman, S. M. Alam, P. J. Travers, N. R. J. Gascoigne, E. Palmer, and S. C. Jameson. 2001. The impact of duration versus extent of TCR occupancy on T cell activation: a revision of the kinetic proofreading model. *Immunity* 15: 59–70.
21. Cohn, M. 2016. Dissecting the two models of TCR structure-function relationships. *Immunol. Res.* 64: 795–803.
22. Robinson, J., J. A. Halliwell, J. D. Hayhurst, P. Flicek, P. Parham, and S. G. E. Marsh. 2015. The IPD and IMGT/HLA database: allele variant databases. *Nucleic Acids Res.* 43: D423–D431.
23. Qi, Q., Y. Liu, Y. Cheng, J. Glanville, D. Zhang, J.-Y. Lee, R. A. Olshen, C. M. Weyand, S. D. Boyd, and J. J. Goronzy. 2014. Diversity and clonal selection in the human T-cell repertoire. *Proc. Natl. Acad. Sci. USA* 111: 13139–13144.
24. Schumacher, T. N., and R. D. Schreiber. 2015. Neoantigens in cancer immunotherapy. *Science* 348: 69–74.
25. Davis, M. M., J. D. Altman, and E. W. Newell. 2011. Interrogating the repertoire: broadening the scope of peptide-MHC multimer analysis. *Nat. Rev. Immunol.* 11: 551–558.
26. Toebes, M., M. Coccoris, A. Bins, B. Rodenko, R. Gomez, N. J. Nieuwkoop, W. van de Kasteele, G. F. Rimmelzwaan, J. B. A. G. Haanen, H. Ovaa, and T. N. M. Schumacher. 2006. Design and use of conditional MHC class I ligands. *Nat. Med.* 12: 246–251.
27. Saini, S. K., H. Schuster, V. R. Ramnarayan, H.-G. Rammensee, S. Stevanović, and S. Springer. 2015. Dipeptides catalyze rapid peptide exchange on MHC class I molecules. *Proc. Natl. Acad. Sci. USA* 112: 202–207.
28. Hadrup, S. R., A. H. Bakker, C. J. Shu, R. S. Andersen, J. van Veluw, P. Hombrink, E. Castermans, P. Thor Straten, C. Blank, J. B. Haanen, et al. 2009. Parallel detection of antigen-specific T-cell responses by multidimensional encoding of MHC multimers. *Nat. Methods* 6: 520–526.
29. Newell, E. W., L. O. Klein, W. Yu, and M. M. Davis. 2009. Simultaneous detection of many T-cell specificities using combinatorial tetramer staining. *Nat. Methods* 6: 497–499.
30. Bentzen, A. K., A. M. Marquard, R. Lyngaa, S. K. Saini, S. Ramskov, M. Donia, L. Such, A. J. S. Furness, N. McGranahan, R. Rosenthal, et al. 2016. Large-scale detection of antigen-specific T cells using peptide-MHC-I multimers labeled with DNA barcodes. *Nat. Biotechnol.* 34: 1037–1045.
31. Rodenko, B., M. Toebes, S. R. Hadrup, W. J. E. van Esch, A. M. Molenaar, T. N. M. Schumacher, and H. Ovaa. 2006. Generation of peptide-MHC class I complexes through UV-mediated ligand exchange. *Nat. Protoc.* 1: 1120–1132.

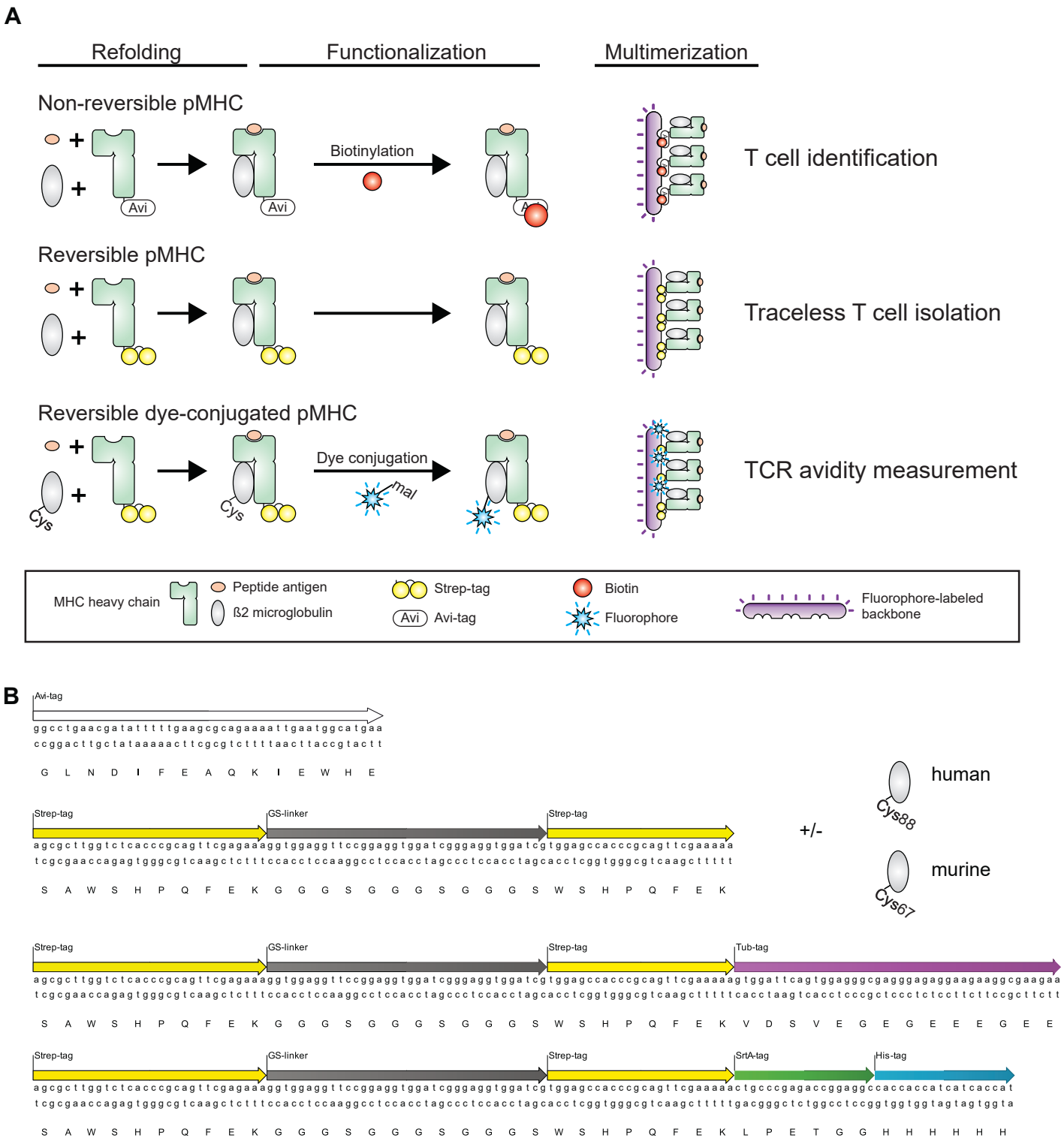

Figure S1. Generation of conventional pMHC reagents and corresponding tags for functionalization. **A**) Non-reversible pMHC reagents ('tetramers') are generated by refolding of pMHC molecules harboring an Avi-tag at the C-terminus of the heavy chain for biotinylation. Biotinylated pMHC monomers can be non- reversibly multimerized on streptavidin. Reversible pMHCs carry an affinity-tag, e.g. a Strep-tag at the C- terminus of the heavy chain, that allows stable multimerization on Strep-Tactin, which can be reversed upon addition of higher affine competitor molecules. Reversible dye-conjugated pMHC reagents can be generated through the introduction of an artificial solvent-exposed cysteine in the pMHC (e.g. mβ2m Y67C or hβ2m S88C), which allows dye coupling via maleimide chemistry after folding. **B**) Tags used for pMHC functionalization.

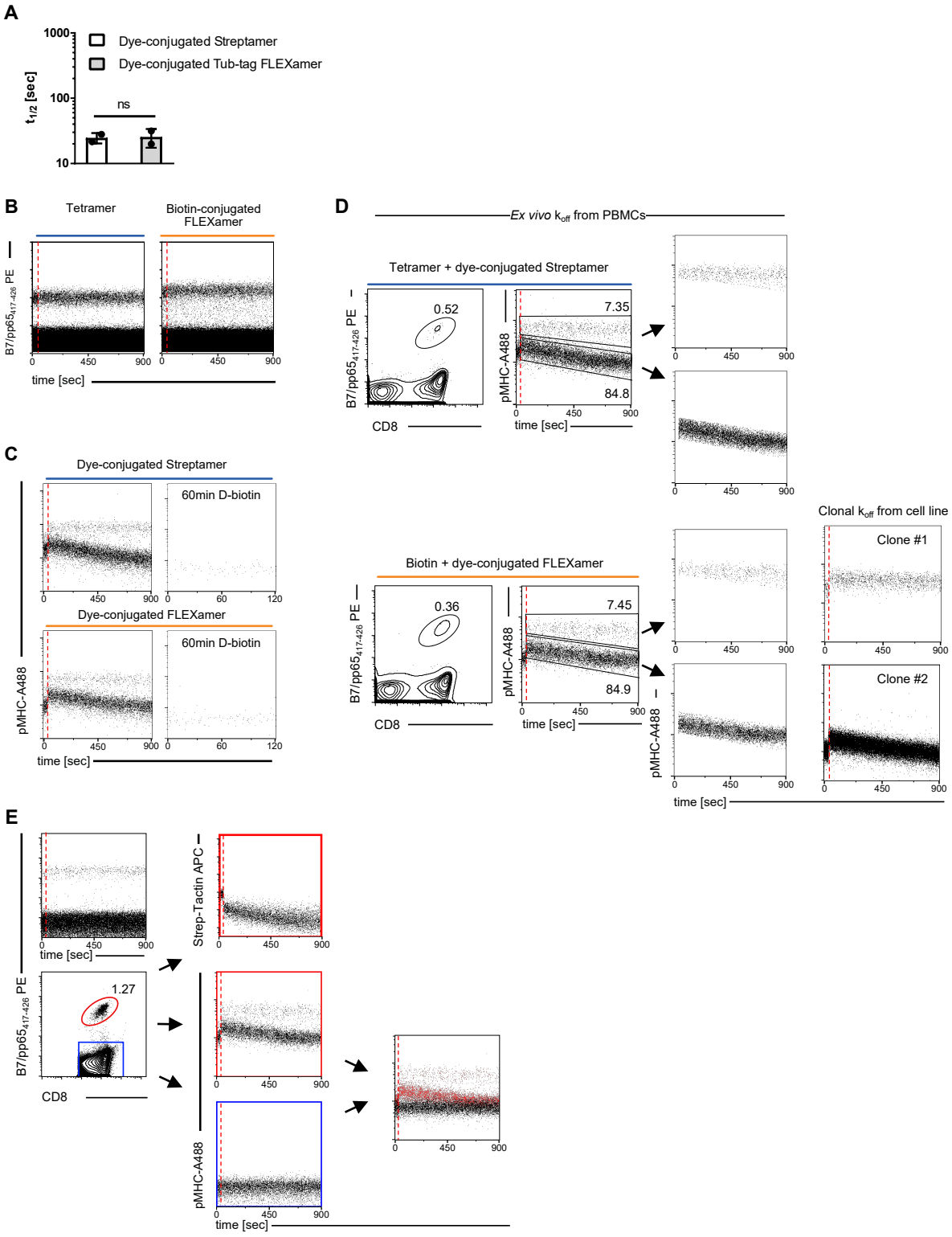

Figure S2. Conventional tetramers and biotinylated FLEXamers allow continuous gating on antigen-specific CD8+ T cells over time also after addition of D-biotin, while dye-conjugated conventional Streptamers and dye-conjugated FLEXamers allow discrimination of antigen-specific CD8+ populations with distinct structural avidities. (**A**) Quantification of dissociation kinetics measured with OT-I T cells of a representativ experiment. One symbol represents one dissociation. Unpaired, non-parametric Kolmogorov-Smirnov test. (**B**) Conventionally biotinylated pMHCs (tetramers upon multimerization) or biotin-functionalized FLEXamer pMHCs were multimerized on streptavidin- PE and used to stain B7/pp65(417-426)-specific CD8+ T cells from peripheral blood of a CMV-seropositive donor. The pMHC multimer signal is gated over time. Red dotted line indicates injection of D-biotin. (**C**) Dissociation kinetic of B7/pp65(417-426)-specific CD8+ T cells from peripheral blood of a CMV-seropositive donor. PBMCs were stained with reversible dye-conjugated pMHCs either conventionally generated via maleimide chemistry or using Tub-tag technique. Decay influorescence intensity directly after D-biotin incubation for 15 min and after 60 min for 2 min. Pre-gated on single, living, CD8+ non-reversible pMHC+ T cells. (**D**) Dissociation kinetic of B7/pp65(417-426)-specific CD8+ T cells from peripheral blood of a CMV-seropositive donor shown in Figure 5C. Manual gating on the population with the slower (upper) dissociation kinetic and the population with the faster (lower) kinetic. Subsequent gating on the kinetics is compared to dissociation kinetics derived from T cell clones generated from the upper and lower population. (**E**) B7/pp65(417-426)-specific CD8+ T cells shown in B/C/D with varying gating strategy. Plots illustrate non-reversibility of biotinylated pMHC-PE and dissociation kinetics of reversible of pMHC-A88 monomers versus StrepTactin APC backbone. Only pre-gating on non-rev-pMHC-PE+ CD8+ T cells allows gating on complete pMHC-A488 dissociation over time. Pre-gated on single, living CD19- T cells followed by indicated gating strategy.

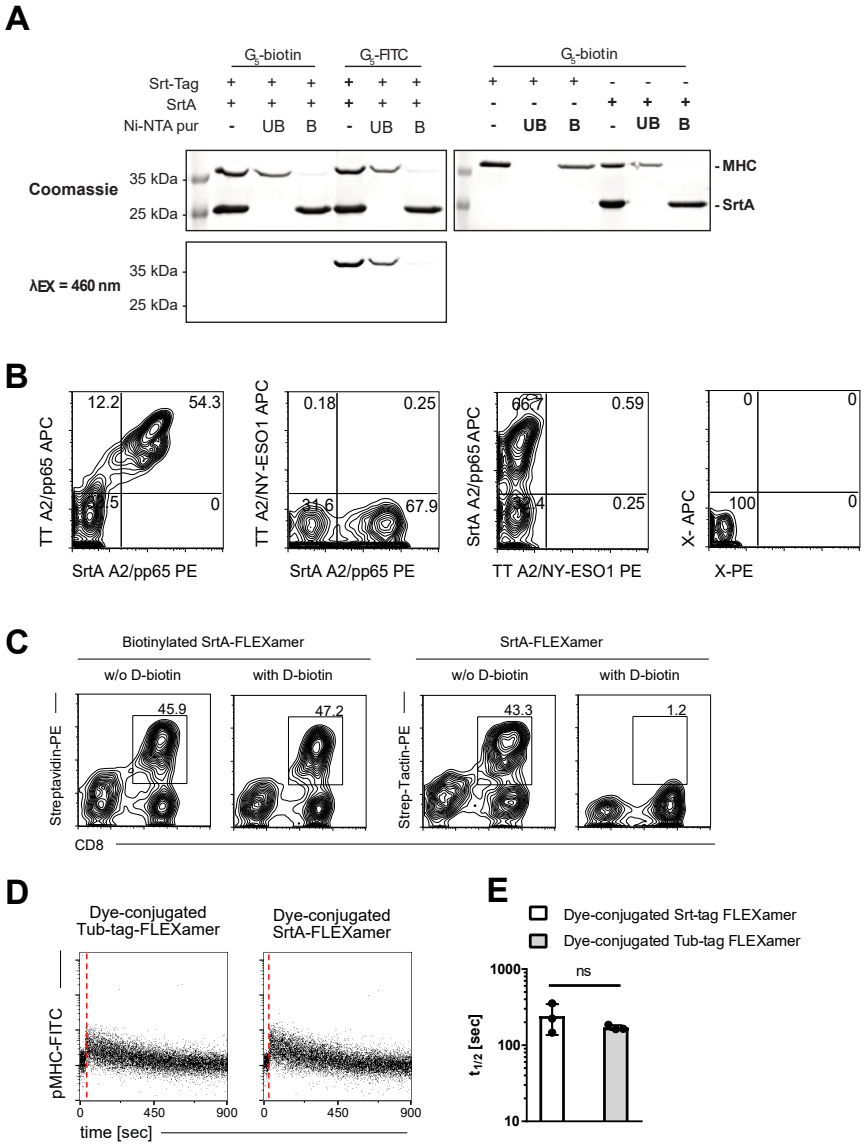

Figure S3. Poly-functionality of double-tagged pMHCs can also be achieved by transpeptidation using SrtA-tag. (**A**) SDS-PAGE of SrtA-mediated functionalization of Srt-tagged FLEXamer (MHC) with biotin or FITC. Transpeptidase reaction components are shown before (-) and after Ni-NTA purification (UB and B). The FLEXamers C-terminal His-tag is replaced with either G5-biotin or G5-FITC by the transpeptidation reaction. Labeled FLEXamers remain unbound to Ni-NTA-sepharose beads (UB) wherase the His-tagged SrtA is efficiently captured on the beads (B). Absence of FLEXamer in the bound fraction indicates efficient transpeptidation. Conjugation of FITC is further validated by in-gel fluorescence. Control reactions omitting either SrtA or the Srt-tag show no unspecific coupling. (**B**) Staining of PBMCs transduced with an A2/pp65(495-503)-specific TCR. pMHC reagents were multimerized from pMHC monomers either biotin-functionalized via Tub-tag technique or via SrtA-tag. Staining was performed with a combination of both pMHC reagents. Control stainings were performed with an irrelevant peptide epitope (A2/NY-ESO(157-165)). (**C**) PBMCs transduced with an A2/pp65(495-503)-specific TCR were stained with either biotin-functionalized SrtA FLEXamers multimerized on streptavidin-PE or with their reversible SrtA FLEXamer precursor multimerized on Strep-Tactin-PE. Samples were incubated with or without D-biotin before acquisition. (**D**) Dissociation kinetic of PBMCs transduced with an A2/pp65(495-503)-specific TCR. Dye-conjugated pMHCs were generated either via Tub-tag technique or via SrtA-tag. Red dotted line indicates injection of D-biotin. (**E**) Quantification of technical triplicates of representative experiment shown in (D). One symbol represents one dissociation. Unpaired, non-parametric Kolmogorov-Smirnov test. Pre-gated on single, living CD8+ T cells in (B), pre-gated on single, living T cells in (D) and pre-gated on single, living CD8+ mTrbc+ T cells in (D).

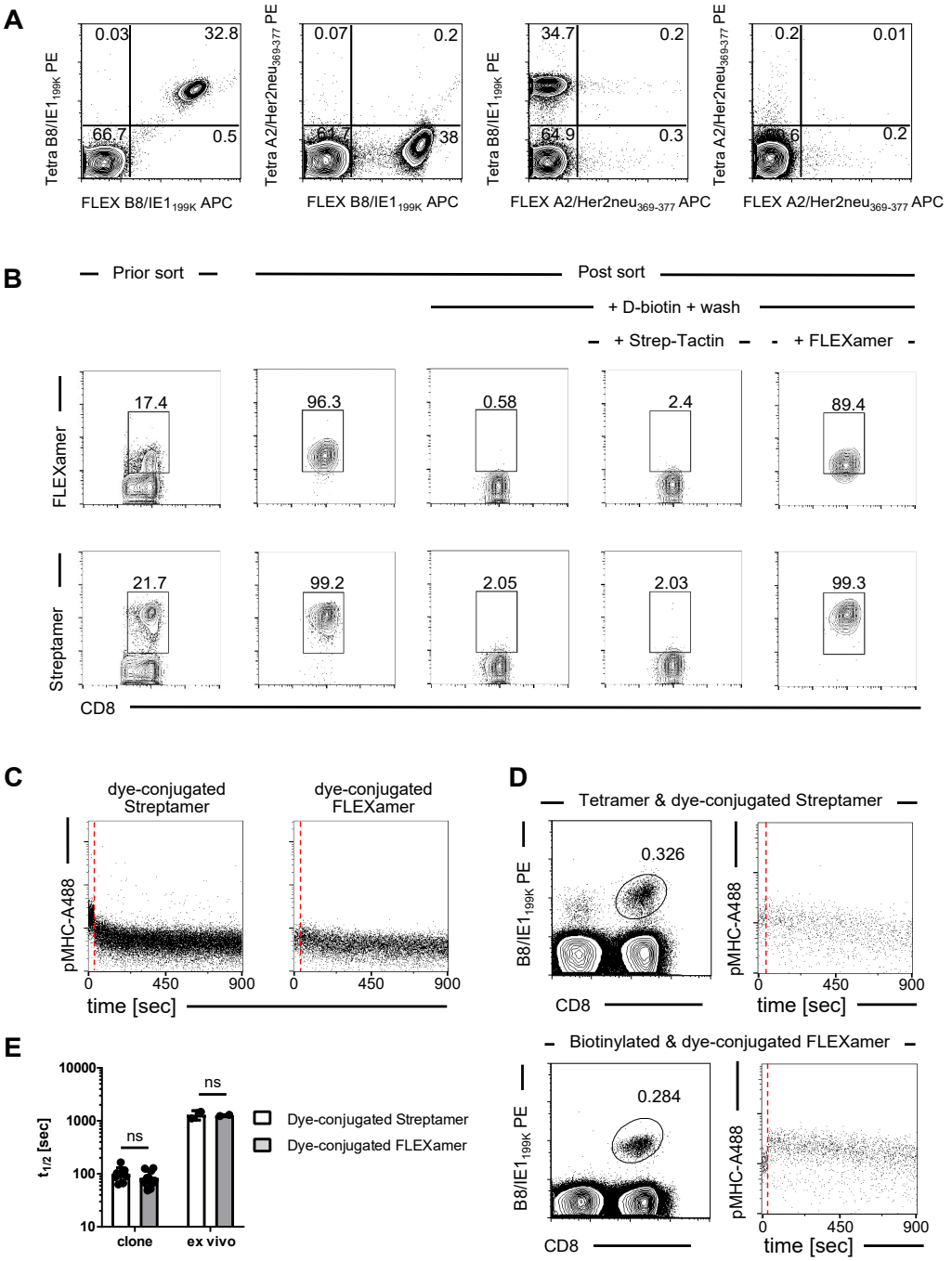

Figure S4. Double-tagged FLEXamer for distinct HLA epitope combination. (**A**) B8/IE1(199-207K)-specific CD8+ T cells from peripheral blood of a CMV-seropositive donor were stained with non-reversible pMHC multimers. pMHCs were either conventionally biotinylated (Tetra) and multimerized on streptavidin-PE or biotinylated via Tub-tag technique (FLEX) and multimerized on streptavidin APC. Cells were stained with either a combination of both reagents presenting the relevant epitope (B8/IE1(199-207K)), with combinations of relevant and irrelevant (A2/Her2neu(369-377)) epitope for each reagent, or with a combination of both reagents presenting the irrelevant epitope. (**B**) Flow cytometric sorting of B8/IE1(199-207K)-specific CD8+ T cells from peripheral blood of a CMV-seropositive donor using FLEXamers and Streptamers. FLEXamers and Streptamers were multimerized on Strep-Tactin-APC. Sort-purified population was subsequently split and either analyzed as purity control or incubated with D-biotin, with D-biotin and Strep-Tactin backbone only, or D-biotin and reversible pMHCs multimerized on Strep-Tactin backbone. (**C**) Dissociation kinetic of a B8/IE1(199-207K)-specific CD8+ T cell clone measured with either dye-conjugated Streptamers or dye-conjugated FLEXamers. Red dotted line indicates time point of D-biotin addition. (**D**) Dissociation kinetic of B8/IE1(199-207K)-specific T cells in peripheral blood of a CMV-seropositive donor. PBMCs were stained with a combination of non-reversible biotinylated pMHCs and reversible dye-conjugated pMHCs. Reagents were generated either conventionally via BirA-mediated biotinylation and maleimid chemistry mediated dye coupling or using Tub-tag technique conjugating biotin or a dye. Non-reversible pMHC multimer+ CD8+ population is gated for dissociation kinetic of dye-coupled pMHCs after addition of D-biotin (red dotted line) over time. (**E**) Quantification of technical replicates of representative experiments shown in (C) and (D). One symbol represents one dissociation. Unpaired, non-parametric Kolmogorov-Smirnov test. Pre-gated on single, living CD8+ T cells in (A) and (C), pre-gated on single, living lymphocytes in (B) and (D).

5 DISCUSSION

Therapeutic drugs have undergone constant development since the dawn of modern medicine. Some changes were incremental improvements of contemporary concepts, others were radical shifts to revolutionary approaches. Common goals of all developments were, on the one hand, more effective and safer therapy and, on the other hand, treatment of previously incurable diseases. Cancer has become apparent as a particularly challenging disease due to its inherent heterogeneity, evolutionary adaption mechanisms of cancer cells and the intricate similarity of cancerous and healthy cells. These challenges stringently require sophisticated drugs, hence, have moved cancer in the spotlight of applied pharmaceutical as well as basic biomedical research. This attention established cancer as a role model for the development of novel classes of therapeutics. Namely, therapeutic antibody formats and cell therapy concepts have recently gained strong momentum. In this context, the present work addresses assays for comprehensive analysis, of anti-proliferative antibodies, methods for the generation of antibody-drug conjugates, bispecific antibodies and protein conjugates in general as well as reagents for the identification and characterization of therapeutic T cells.

5.1 QUANTIFICATION OF REPLICATING CELLS AND DNA CONTENT AS SENSITIVE MEASURES OF ANTI-PROLIFERATIVE ANTIBODY ACTIVITY

Monoclonal antibodies (mAbs) have become a central class of therapeutic agents, in particular as anti-proliferative compounds. Their often complex modes of action require sensitive assays already during early, functional characterization. Current cell-based proliferation assays often detect metabolites that are indicative of metabolic activity, but do not directly account for cell proliferation. Measuring DNA replication by incorporation of base analogues fills this analytical gap but was previously restricted to bulk effect characterization in ELISA formats. DNA replication can be visualized by the incorporation of 5-ethynyl-2′-deoxyuridine (EdU) and subsequent conjugation of flourophores by click chemistry. Single-cell high-content-analysis (HCA) offers the possibility of quantifying EdU incorporation of individual cells in an automated, high throughput manner. This allows the analysis of thousands of cells per well and hundreds of wells in a multi-well format. Thus, the combination of EdU incorporation with high content imaging is suitable for sensitive but convenient quantification of replicating cells, hence, can provide a sensitive measure for anti-proliferative mAb activity. Furthermore, parallel quantification of single cell DNA content by DAPI staining allows additional insight into cell cycle distributions in a single experiment. Using trastuzumab, an anti-proliferative therapeutic antibody interfering with HER2 signaling, this strategy demonstrated increased signal to background ratios compared to merely counting surviving cells and, additionally, revealed a shift in cell cycle profiles indicating antibody induced cell cycle arrest (see chapter 4.1). Increased signal to background ratio has recently also been demonstrated with a DELFIA-BrdU assay (X. Lu & Bergelson, 2014). However, EdU incorporation, subsequent staining by click chemistry and microscopy based evaluation i) is more sensitive and mild, ii) provides the possibility for

multiplexed readout of various parameters and iii) increases the assay resolution by the detection of single cells instead of averaging over a bulk population. Microscopic detection of the proliferative state of individual cells might also allow assessment of an antibodie's penetrance in multi-cell aggregates. Additionally, antibody uptake could be visualized for each cell of a multi-cell aggregate in the same experiment. Furthermore, the fate of individual cells can be assessed and their individual microenvironment can be taken into account. Along this line, additional cell types like stromal cells or immune cells could be cocultured to simulate tumor environments or asses the role of ADCC or CDC in an antibodie's mode of action. EdU based labeling of proliferating cells with subsequent automated imaging and analysis combined with DAPI based cell cycle profiling is a simple and sensitive way for parallel investigation of anti-proliferative potency and mode of action of therapeutic antibodies. The described assay is simple, cost-effective and sensitive, hence, might provide a cell-based format for preclinical characterization of therapeutic mAbs.

5.2 Modular Assembly of Bispecific Antibodies by Site-specific Protein Ligation

Bispecific antibodies have recently emerged as highly promising therapeutic antibody format. The combination of two (or more) binding units in a single molecule opens up the possibilities for completely new modes of action. The bispecific format can, for example, increase specificity by simultaneously targeting two individual markers on a target cell. Furthermore, bispecific constructs can also act as a sort of heterobifunctional crosslinker. For example, two different cell types can be linked with a bispecific targeting two antigens of either one of the two cells. In a therapeutic setting such linker molecules can serve as adaptors for the recruitment of immune cells to malignant cells. Especially for the treatment of cancer, such immune cell redirection emerges as a promising strategy. For example, it allows the recruitment of immune cells to the immunesuppressive microenvironment of tumors. Although the combinatorial possibilities for bi- and multispecific antibodies and resulting novel modes of action are tremendous, it is crucial but not trivial how one connects the individual antibodies. Chemical crosslinking of IgGs was one of the first methods applied for the construction of bispecific antibodies since it does not require recombinant protein techniques and is compatible with early on antibody production methods like hybridoma technology. Amine or thiol reactive crosslinking reagents can readily be used as adaptors to covalently link antibodies, however, resulting heterogeneity in conjugation stoichiometry and site can be detrimental to antibodies' function. Alternatively, chains of two antibodies can be shuffled by reduction and reoxidation of interchain disulfides to create an asymmetric IgG with two different binding units. However, random shuffling of chains also yields unwanted pairings and reduces the yield of functional bispecific antibodies. The correct pairing can be fostered by the introduction of asymmetric mutations (e.g.: knob-into-hole), CH1-CL domain exchange or common light chains. These approaches have the advantage of retaining the natural IgG architecture, however, are limited to two binding domains and consequently restricted to monovalent binding of a maximum of two antigens. The expansion of valency and

number of different paratopes can be achieved by appending the natural IgG structure with additional binding units. In this regard predominantly antibody fragments and single domain antibody mimetics have proven suitable for genetic fusion to either end of heavy or light chains. Even though genetic fusions are straightforward to construct, this approach comes with limitations such as strict C- to N-terminal linkage or the necessity of a mutual expression and purification strategy for both fusion partners. To circumvent these limitations alternative strategies like chemical ligation methods have been described for *in vitro* conjugation. Yet, just like genetic fusions, they are also limited to N- to C-terminal linkage. This structural constraint can influence conjugation efficiency and functional activity since the orientation of the fusion partners and their flexibility. Alternative connections, such as N-to-N or C-to-C fusions became available by the development of several site-specific, bioorthogonal conjugation methods. For example, peptide-tag based systems have been applied for protein-protein-ligation and have the advantage that they do not require engineered expression systems and generally allow flexible incorporation of bioorthogonal handles after protein production. Along this line we developed Tub-tag mediated C-terminal protein-protein-ligation (TuPPL) as a modular site-specific conjugation approach for the C-terminal ligation of proteins post expression. The modularity of TuPPL allows parallel functionalization of antibody fragments with bioorthogonal handles as well as straightforward conjugation of proteins that are produced in different expression systems. TTL catalyzed incorporation of 3-azido-*L*- and O-propargyl-*L*-tyrosine in combination with CuAAC chemistry enables the convenient generation of homodimeric and heterodimeric antibody-fragments (see chapter 0). Prominent examples of the later are Bispecific T cell Engagers (BiTEs). They combine two different antigen binding domains in a genetically fused tandem scFv to redirect immune cells to tumor cells. Especially in such cases where the combination product might not be sufficiently described by the characteristics of the individual binding units but rather by the novel synergistic effects it is crucial to screen early on in the final bispecific format. The great advantage of conjugating the individually expressed units lies in the convenient generation of combinatorial libraries. For example, multiple alternative tumor antigen binder can be criss-cross ligated to multiple alternative immune marker binder to find the most suitable combination. Since, contemporary antibody development strategies are mainly focused on the characterization of monospecific antibodies a modular ligation platform might prove as a useful complement. Moreover, especially for antibodies the C-to-C linkage generated by TuPPL can be beneficial since N-terminal fusion, as generated by standard genetic fusion or EPL, can impair antigen binding due to steric obstruction of the paratope. The relative orientation of binding sites in a multimeric complex has been shown to influence binding properties, hence, fusion proteins in general might benefit from the C-to-C-terminal linkage generated by TuPPL. In addition, TuPPL may readily be combined with other site-specific protein modification techniques due to the use of universal bioorthogonal handles. Moreover, the use of TuPPL can be expanded to many more proteins such as full length antibodies, enzymes or proteinaceous toxins. In this case, sets of pre-functionalized proteins could be used as building blocks for a modular and scalable protein ligation platform in which TuPPL serves as a central conjugation hub (Stengl et al., 2019).

5.3 Ethynylphosphonamidates for Advanced Thiol-selective Bioconjugation and Generation of Antibody-Drug Conjugates

Site-specific modification of proteins has drawn great attention in recent years and put forth a set of novel functionalization strategies. Thiols have ever since been very attractive due to their strong nucleophilic character and the low abundance of cysteines on protein surfaces. Especially proteins with natural cysteines can thus be fairly specifically modified without the need for sequence manipulation or recombinant production. Alternatively, thiols can also be introduced recombinantly as a relatively compact handle for site-specific modification. As a proteinogenic amino acid, cysteine is readily inserted at a desired position in a protein sequence by standard molecular cloning and protein expression techniques. Both strategies have their benefits and either one might be more suitable depending on the specific application. Both strategies have been used successfully for the modification of antibodies, however, the conjugation to reduced interchain disulfide bridges allows very convenient yet relatively site-specific modification of non-recombinant antibodies, e.g. isolated from hybridoma clones, animals or humans. Although recombinant screening platforms are on the rise, immunization of animals and subsequent isolation of antibodies or antibody producing plasma cells is still widely used for antibody production. For those cases, the antibody sequences are not readily accessible or editable. Thus, cysteine conjugation is a convenient method to modify those antibodies for early on functional screening of conjugated antibody clones. For example, antibodies developed for the use in antibody-drug conjugates can readily be tested for cytotoxic activity, potency and specificity. Several cysteine-selective modification techniques applying various compound classes have been employed. Maleimides still remain the most widely used method for chemical modification on cysteine residues (Gunnoo & Madder, 2016) mostly due to their rapid kinetics in the reaction with sulfhydryl groups. However, one of the biggest drawbacks of maleimide-conjugates is their instability caused by a retro Michael-addition in the presence of external thiols (Shen et al., 2012). Recently developed alternatives including self-hydrolyzing-maleimides (Shen et al., 2012; Szijj, Bahou, & Chudasama, 2018a) yield stable sulfhydryl-adducts; however, challenges remain, since stereo- or regioisomers are formed and their incorporation into functional molecules usually requires protecting group manipulations.

Phosphonites and phosphonamidates are known as reactive groups for the modification of azide containing proteins. On the one hand, borane-protected ethynyl-phosphonites can react sequentially with two different azide containing entities by CuAAC coupling to their alkyne group and subsequent Staudinger-phosphonite reaction (SPhR) with the second azide. Using unprotected ethynyl-phosphonites, the conjugation of azides via SPhR turns the electron-rich ethynyl triple bond into a thiol-reactive electron-poor triple bond in the resulting phosphonamidate. Along this line, we used ethynyl-phosphonamidates to chemoselectively incorporate functionalities such as biotin, fluorophores, and peptides with highly selective toward cysteine residues of proteins (see chapter 0). The generated cysteine adducts show superior stability compared to maleimides. Proof of concept experiments confirmed stable linkage and successful

conjugation of fluorophores to native antibody interchain cysteines and a cyclic cell penetrating peptide (cCPP) to an engineered cysteine on the surface of eGFP. The concept was further applied for the generation of antibody-drug conjugates (see chapter 4.4). The conjugates also displayed superior stability properties in blood serum. Linkage stability is crucial for ADCs since drug loss on the one hand reduces the drug load of the ADC and thus its potency, on the other hand, free toxin can lead to off-target effects. In addition, phosphonamidate conjugated ADCs also proved efficacious *in vitro* as well as *in vivo*. Furthermore, the described conjugation strategy allows the introduction of hydrophilic moieties like polyethylene glycol (PEG) units together with the toxin. However, the PEG group is not attached as a linear spacer between antibody and toxin but rather attached as a second functional group to the phosphonamidate. This architecture allows counteracting the hydrophobicity introduced by the toxin but does not space the toxin farther from the antibody. The latter increases the solvent exposure of the drug and can negatively impact pharmacokinetic properties of an ADC. Cysteine-selective protein modification by phosphonamidates is a valuable alternative to maleimide conjugation and might prove as an elegant strategy for the generation of antibody-drug conjugates in early-on screening of antibody candidates. Apart from antibody modification, it could also serve as a more stable alternative to maleimide conjugation for a large variety of proteins equipped with engineered cysteines.

5.4 Site-specific Bioconjugation in Combination with Reversible Multimerization for the Characterization of Weak Ligand-Receptor Interactions

Novel bioconjugation strategies commonly use bioorthogonal reactions and unite characteristics such as robustness, outstanding specificity, fast reaction kinetics, tolerance of complex solvents, high linkage stability in biological systems and compatibility with a great range of proteins and functional groups. Advanced thiol-reactive reagents like ethynylphosphonamidates discussed in chapter 5.3 can readily be used to improve conjugate quality for already established cysteine conjugation pipelines. This can be beneficial if a large reagent set with engineered cysteines already exists or the protein to be modified contains targetable endogenous cysteines. Site-specific (chemo)enzymatic approaches are conceptually different in that they mostly require sequence manipulation, but allow convenient use of novel bioorthogonal reactions like click chemistry. However, these methods come with benefits such as mild reaction conditions, stable linkage and a defined number of attached functional groups. The former two can increase the overall quality of reagents generated by bioconjugation. The latter yields homogeneous reagents with defined properties. For example, fluorophores can be attached to affinity reagents in a defined number presumably resulting in a quantitative relation between fluorescent signal and bound antigen for each individual molecule. Advanced detection reagents may prove useful in the study of biomolecular interactions in general and the quantification of interaction stoichiometry and affinity in particular. Biomolecular interactions can be categorized by their binding strength. Binding affinity can range from low picomolar to millimolar values and a relative distinction between low affinity and high affinity biomolecular interactions can be made. Although one cannot define a clear cut-off value to discriminate the two groups, the associated molecular and cellular functions are different. High affinity binding is predominantly found in processes that require stable interaction between two or more molecules over an extended period of time or such that need to withstand physical forces. For example, structural complexes like actin and myosin filaments in muscle cells necessarily require strong protein-protein interaction. Another well known example is the binding of an antibody to its antigen. Antibodies can fulfill their immunological function by sequestration of harmful substances or tagging of pathogens. Hence, the stable attachment of such tags is desirable and requires high binding affinity. Notably, in the case of antibodies, interaction strength is further increased by the avidity effect generated by the presence of two binding units in close proximity in a single molecule. Avidity is a general concept found in many biomolecular interactions. Multiprotein complexes can be very stable although the individual interactions of the subunits are rather weak. In this case, the simultaneous interaction of all entities results in high avidity. Low affinity binding is generally less stable over time and is associated with transient contact of molecules. This short lived interaction can be found in processes that transmit information such as the binding of ligands to cell surface receptors or in dynamic cellular processes like motion. Furthermore, transient cell-cell contact can be mediated by low affinity interaction of proteins that are present in multiple copies on each cell. In this case, the cell surface serves as a backbone for the receptors resulting in

a stabilizing avidity effect. Intensity and duration of cell-cell contacts can thus be regulated on a molecular level by the affinity of the individual receptor-receptor interaction or by the number of receptor molecules. An example for this would be the interaction of T cell with target cell via TCR-MHC interaction. The recombinant production and manipulation of one interaction partner, generally the MHC complex, allows the investigation of the other interaction partner in its natural context. To mimic multivalent display on cell surfaces, recombinant ligands can be equipped with multimerization sequences or handles. In this setting, individual ligand molecules are assembled on a scaffold protein to form so called multimers. Multimers equipped with reversible multimerization sequences allow the triggered release of the backbone, thus, the dissociation of the individual molecules. Labeled with traceable markers such as fluorophores, this procedure can be used to follow dissociation over time and measurement of k_{off} rates, a characteristic for interaction strength. Combining reversibility with versatile, facile and gentle site-specific bioconjugation in a universal double-tag, yields a very handy tool for the characterization of weak biomolecular interactions.

5.5 FLEXAMERS: A DOUBLE-TAG FOR UNIVERSAL GENERATION OF VERSATILE PMHC MULTIMERS

The interaction between T cell and antigen presenting cell is a prominent example for transient cell-cell contact mediated by weak receptor-ligand interactions discussed in chapter 5.4. A variety of pMHC reagents has been designed for T cell and TCR characterization to cope, firstly, with the enormous number of peptide-MHC complexes and, secondly, with the diversity of applications. The former becomes evident when looking at the total epitope repertoire that has been estimated between 10^6 and 10^{11} in mice (Cohn, 2016) and is likely similar, if not even more diverse in humans. Furthermore, 13.000 HLA class I alleles have now been described for humans (Cohn, 2016). To handle this extreme diversity of epitopes, UV exchange or di-peptide technologies have been developed to load primed recombinant MHCs with any epitope of interest. Just as diverse as the presented epitopes are, so numerous are the TCR variants. The total human TCR repertoire encompasses more than 10^8 unique clonotypes (Qi et al., 2014). To analyze diverse T cell populations, combinatorial pMHC staining and DNA barcoding have massively enhanced throughput in screening T cell populations and their respective TCR repertoires. Identification of antigen specific TCRs from large repertoires is a common strategy for isolation of therapeutic TCR candidates. In this regard, pMHC multimer reagents have been developed for T cell identification, traceless isolation or TCR avidity measurement. The applicability of pMHCs for all those different tasks underscores their versatile applicability. pMHCs for the individual applications have been developed sequentially. This development entailed the use of different technologies to produce, functionalize and multimerize the individual reagents. Uniting different variants of the same functionality (e.g. multimerization or conjugation method), reducing the architecture to the essential elements and using versatile elements, could result in a generic pMHC molecule that can be conveniently modified for the desired application.

Within this scope, FLEXamers represent universal pMHC multimer constructs that combine versatility with simple generation from a single precursor protein. FLEXamers maintain high functionality although produced in a more standardized manner compared to conventionally generated pMHC reagents (see chapter 4.5). The essential features of various conventional multimers are condensed in a novel double-tag that allows reversible multimerization as well as stable and versatile functionalization. Starting with a common FLEXamer precursor, we produced biotinylated tetramers, reversible Streptamers and reversible dye-conjugated pMHC multimer reagents to generate a comprehensive set of versatile pMHC FLEXamers for 9 different human HLAs as well as murine H2-K^b (see chapter 5.5). Since novel bioorthogonal conjugation methods like Tub-tag labeling, sortagging and click chemistry are used, FLEXamers can readily be conjugated with other entities such as DNA oligonucleotides or toxins. Since FLEXamers are structurally based on conventional MHCs, they can additionally be combined with further extensions such as epitope exchange technologies. Customized monitoring of antigen-specific immune responses and individualized immunotherapy require streamlined methods that allow flexible adaptation for each patient and disease in terms of first, target-specific epitopes, and second, patient-specific HLAs. Difficulties

to generate distinct pMHC multimer reagents for each setting in a fast and reliable manner remain a significant challenge to personalized cell therapy and T cell-based diagnostics. FLEXamers for instance could become a condensed multimer platform that implements different types of pMHC reagents for use in routine clinical immune monitoring and immunotherapy. Additionally, they might reduce effort and costs associated with generating distinct pMHC multimer reagents for each application that has so far been an impediment to fully exploit the versatility of pMHC based reagents. Furthermore, the double tag is a general concept that can also be realized with alternative functionalization or multimerization tags.

The combination of multimerization and versatile functionalization might also prove useful for the study of many other receptor-ligand pairs. Especially in the case of weak interactions, multivalent binding can serve as an 'on-switch' to stabilize the transient binding. Reversible multimerization allows triggered switching off of the interaction by disruption of the multimeric complex. Versatile functionalization, on the other hand, allows further stabilization of the interaction, or tracking via fluorescent dyes. In T cell immunology, this mechanism has found widespread use and the described double-tag approach enables universal generation of different pMHC reagents, but might more generally also serve as a flexible tool for the investigation of transient protein-protein interactions (Effenberger et al., 2019).

6 REFERENCES

Abel, C. A., Spiegelberg, H. L., & Grey, H. M. (1968). Carbohydrate content of fragments and polypeptide chains of human .gamma.G-myeloma proteins of different heavy-chain subclasses. *Biochemistry, 7*(4), 1271-1278.

Agard, N. J., Prescher, J. A., & Bertozzi, C. R. (2004). A Strain-Promoted [3 + 2] Azide–Alkyne Cycloaddition for Covalent Modification of Biomolecules in Living Systems. *Journal of the American Chemical Society, 126*(46), 15046-15047.

Agarwal, P., & Bertozzi, C. R. (2015a). Site-specific antibody-drug conjugates: the nexus of bioorthogonal chemistry, protein engineering, and drug development. *Bioconjugate chemistry, 26*(2), 176-192.

Agarwal, P., & Bertozzi, C. R. (2015b). Site-Specific Antibody–Drug Conjugates: The Nexus of Bioorthogonal Chemistry, Protein Engineering, and Drug Development. *Bioconjugate Chemistry, 26*(2), 176-192.

Alanio, C., Lemaitre, F., Law, H. K., Hasan, M., & Albert, M. L. (2010). Enumeration of human antigen-specific naive CD8+ T cells reveals conserved precursor frequencies. *Blood, 115*(18), 3718-3725.

Alizadeh, A. A., Aranda, V., Bardelli, A., Blanpain, C., Bock, C., Borowski, C., et al. (2015). Toward understanding and exploiting tumor heterogeneity. [Perspective]. *Nature Medicine, 21*, 846.

Almagro, J. C., Daniels-Wells, T. R., Perez-Tapia, S. M., & Penichet, M. L. (2018). Progress and Challenges in the Design and Clinical Development of Antibodies for Cancer Therapy. [Review]. *Frontiers in Immunology, 8*(1751).

Altman, J. D., Moss, P. A., Goulder, P. J., Barouch, D. H., McHeyzer-Williams, M. G., Bell, J. I., et al. (1996). Phenotypic analysis of antigen-specific T lymphocytes. *Science, 274*(5284), 94-96.

Andersen, R., Donia, M., Ellebaek, E., Borch, T. H., Kongsted, P., Iversen, T. Z., et al. (2016). Long-Lasting Complete Responses in Patients with Metastatic Melanoma after Adoptive Cell Therapy with Tumor-Infiltrating Lymphocytes and an Attenuated IL2 Regimen. *Clin Cancer Res, 22*(15), 3734-3745.

Andreev, J., Thambi, N., Perez Bay, A. E., Delfino, F., Martin, J., Kelly, M. P., et al. (2017). Bispecific Antibodies and Antibody-Drug Conjugates (ADCs) Bridging HER2 and Prolactin Receptor Improve Efficacy of HER2 ADCs. *Mol Cancer Ther, 16*(4), 681-693.

Antos, J. M., Truttmann, M. C., & Ploegh, H. L. (2016). Recent advances in sortase-catalyzed ligation methodology. *Current Opinion in Structural Biology, 38*, 111-118.

Arruebo, M., Vilaboa, N., Sáez-Gutierrez, B., Lambea, J., Tres, A., Valladares, M., et al. (2011). Assessment of the evolution of cancer treatment therapies. *Cancers, 3*(3), 3279-3330.

Axup, J. Y., Bajjuri, K. M., Ritland, M., Hutchins, B. M., Kim, C. H., Kazane, S. A., et al. (2012). Synthesis of site-specific antibody-drug conjugates using unnatural amino acids. *Proc Natl Acad Sci U S A, 109*(40), 16101-16106.

Aysun, A., Yağmur, K., & Yusuf, B. (2016). Cell Proliferation and Cytotoxicity Assays. *Current Pharmaceutical Biotechnology, 17*(14), 1213-1221.

Banting, F. G., & Best, C. H. (1990). Pancreatic extracts. 1922. *J Lab Clin Med, 115*(2), 254-272.

Beckett, D., Kovaleva, E., & Schatz, P. J. (1999). A minimal peptide substrate in biotin holoenzyme synthetase-catalyzed biotinylation. *Protein Sci, 8*(4), 921-929.

Beerli, R. R., Hell, T., Merkel, A. S., & Grawunder, U. (2015). Sortase Enzyme-Mediated Generation of Site-Specifically Conjugated Antibody Drug Conjugates with High In Vitro and In Vivo Potency. *PLoS One, 10*(7), e0131177.

Bertozzi, C. R. (2011). A decade of bioorthogonal chemistry. *Accounts of chemical research, 44*(9), 651-653.

Bhakta, S., Raab, H., & Junutula, J. R. (2013). Engineering THIOMABs for site-specific conjugation of thiol-reactive linkers. *Methods Mol Biol, 1045*, 189-203.

Bjorkman, P. J., Saper, M. A., Samraoui, B., Bennett, W. S., Strominger, J. L., & Wiley, D. C. (1987). Structure of the human class I histocompatibility antigen, HLA-A2. *Nature, 329*(6139), 506-512.

Blackman, M. L., Royzen, M., & Fox, J. M. (2008). Tetrazine Ligation: Fast Bioconjugation Based on Inverse-Electron-Demand Diels–Alder Reactivity. *Journal of the American Chemical Society, 130*(41), 13518-13519.

Brinkmann, U., & Kontermann, R. E. (2017). The making of bispecific antibodies. *MAbs, 9*(2), 182-212.

Browne, B. C., O'Brien, N., Duffy, M. J., Crown, J., & O'Donovan, N. (2009). HER-2 signaling and inhibition in breast cancer. *Curr Cancer Drug Targets, 9*(3), 419-438.

Brunker, P., Wartha, K., Friess, T., Grau-Richards, S., Waldhauer, I., Koller, C. F., et al. (2016). RG7386, a Novel Tetravalent FAP-DR5 Antibody, Effectively Triggers FAP-Dependent, Avidity-Driven DR5 Hyperclustering and Tumor Cell Apoptosis. *Mol Cancer Ther, 15*(5), 946-957.

Carell, T., & Vrabel, M. (2016). Bioorthogonal Chemistry—Introduction and Overview. [journal article]. *Topics in Current Chemistry, 374*(1), 9.

Carrico, I. S., Carlson, B. L., & Bertozzi, C. R. (2007). Introducing genetically encoded aldehydes into proteins. *Nat Chem Biol, 3*(6), 321-322.

Carrico, I. S., Carlson, B. L., & Bertozzi, C. R. (2007). Introducing genetically encoded aldehydes into proteins. *Nature Chemical Biology, 3*, 321.

Chabner, B. A., & Roberts Jr, T. G. (2005). Chemotherapy and the war on cancer. [Perspective]. *Nature Reviews Cancer, 5*, 65.

Chalker, J. M., Bernardes, G. J., Lin, Y. A., & Davis, B. G. (2009). Chemical modification of proteins at cysteine: opportunities in chemistry and biology. *Chem Asian J, 4*(5), 630-640.

Chalker, J. M., Bernardes, G. J. L., Lin, Y. A., & Davis, B. G. (2009). Chemical Modification of Proteins at Cysteine: Opportunities in Chemistry and Biology. *Chemistry – An Asian Journal, 4*(5), 630-640.

Chames, P., Van Regenmortel, M., Weiss, E., & Baty, D. (2009). Therapeutic antibodies: successes, limitations and hopes for the future. *British journal of pharmacology, 157*(2), 220-233.

Chatterjee, N., & Bivona, T. G. (2019). Polytherapy and Targeted Cancer Drug Resistance. *Trends Cancer, 5*(3), 170-182.

Chen, I., Howarth, M., Lin, W., & Ting, A. Y. (2005). Site-specific labeling of cell surface proteins with biophysical probes using biotin ligase. *Nat Methods, 2*(2), 99-104.

Chen, W., Wang, D., Dai, C., Hamelberg, D., & Wang, B. (2012). Clicking 1,2,4,5-tetrazine and cyclooctynes with tunable reaction rates. [10.1039/C2CC16716F]. *Chemical Communications, 48*(12), 1736-1738.

Chin, J. W. (2017). Expanding and reprogramming the genetic code. [Review Article]. *Nature, 550*, 53.

Cohn, M. (2016). Dissecting the two models of TCR structure-function relationships. *Immunol Res, 64*(4), 795-803.

Corse, E., Gottschalk, R. A., & Allison, J. P. (2011). Strength of TCR–Peptide/MHC Interactions and In Vivo T Cell Responses. *The Journal of Immunology, 186*(9), 5039-5045.

Dahlén, E., Veitonmäki, N., & Norlén, P. (2018). Bispecific antibodies in cancer immunotherapy. *Therapeutic advances in vaccines and immunotherapy, 6*(1), 3-17.

Dan, N., Setua, S., Kashyap, V. K., Khan, S., Jaggi, M., Yallapu, M. M., et al. (2018). Antibody-Drug Conjugates for Cancer Therapy: Chemistry to Clinical Implications. *Pharmaceuticals (Basel, Switzerland), 11*(2), 32.

Davies, D. M., & Maher, J. (2016). Gated chimeric antigen receptor T-cells: the next logical step in reducing toxicity? *Translational Cancer Research*, S61-S65.

Dennler, P., Chiotellis, A., Fischer, E., Bregeon, D., Belmant, C., Gauthier, L., et al. (2014). Transglutaminase-based chemo-enzymatic conjugation approach yields homogeneous antibody-drug conjugates. *Bioconjug Chem, 25*(3), 569-578.

Devaraj, N. K., Weissleder, R., & Hilderbrand, S. A. (2008). Tetrazine-Based Cycloadditions: Application to Pretargeted Live Cell Imaging. *Bioconjugate Chemistry, 19*(12), 2297-2299.

DeVita, V. T., & Rosenberg, S. A. (2012). Two Hundred Years of Cancer Research. *New England Journal of Medicine, 366*(23), 2207-2214.

Diamantis, N., & Banerji, U. (2016). Antibody-drug conjugates—an emerging class of cancer treatment. [Minireview]. *British Journal Of Cancer, 114*, 362.

Dierks, T., Dickmanns, A., Preusser-Kunze, A., Schmidt, B., Mariappan, M., von Figura, K., et al. (2005). Molecular basis for multiple sulfatase deficiency and mechanism for formylglycine generation of the human formylglycine-generating enzyme. *Cell, 121*(4), 541-552.

Dotti, G., Gottschalk, S., Savoldo, B., & Brenner, M. K. (2014). Design and development of therapies using chimeric antigen receptor-expressing T cells. *Immunological reviews, 257*(1), 107-126.

Drake, P. M., Albers, A. E., Baker, J., Banas, S., Barfield, R. M., Bhat, A. S., et al. (2014). Aldehyde tag coupled with HIPS chemistry enables the production of ADCs conjugated site-specifically to different antibody regions with distinct in vivo efficacy and PK outcomes. *Bioconjug Chem, 25*(7), 1331-1341.

Dreier, T., Lorenczewski, G., Brandl, C., Hoffmann, P., Syring, U., Hanakam, F., et al. (2002). Extremely potent, rapid and costimulation-independent cytotoxic T-cell response against lymphoma cells catalyzed by a single-chain bispecific antibody. *Int J Cancer, 100*(6), 690-697.

Du, J., Meledeo, M. A., Wang, Z., Khanna, H. S., Paruchuri, V. D. P., & Yarema, K. J. (2009). Metabolic glycoengineering: Sialic acid and beyond. *Glycobiology, 19*(12), 1382-1401.

Dudley, M. E., Yang, J. C., Sherry, R., Hughes, M. S., Royal, R., Kammula, U., et al. (2008). Adoptive cell therapy for patients with metastatic melanoma: evaluation of intensive myeloablative chemoradiation preparative regimens. *J Clin Oncol, 26*(32), 5233-5239.

Dustin, M. L. (2003). Coordination of T cell activation and migration through formation of the immunological synapse. *Ann N Y Acad Sci, 987*, 51-59.

Ecker, D. M., Jones, S. D., & Levine, H. L. (2014). The therapeutic monoclonal antibody market. *mAbs, 7*(1), 9-14.

Effenberger, M., Stengl, A., Schober, K., Gerget, M., Kampick, M., Müller, T. R., et al. (2019). FLEXamers: A Double Tag for Universal Generation of Versatile Peptide-MHC Multimers. *The Journal of Immunology*, ji1801435.

Fairhead, M., & Howarth, M. (2015). Site-specific biotinylation of purified proteins using BirA. *Methods in molecular biology (Clifton, N.J.), 1266*, 171-184.

Falzone, L., Salomone, S., & Libra, M. (2018). Evolution of Cancer Pharmacological Treatments at the Turn of the Third Millennium. [Review]. *Frontiers in Pharmacology, 9*(1300).

Ferlay, J., Colombet, M., Soerjomataram, I., Mathers, C., Parkin, D. M., Piñeros, M., et al. (2019). Estimating the global cancer incidence and mortality in 2018: GLOBOCAN sources and methods. *International Journal of Cancer, 144*(8), 1941-1953.

Ferlay J, E. M., Lam F, Colombet M, Mery L, Piñeros M, Znaor A, Soerjomataram I, Bray F. (2018, Sep 2018). Global Cancer Observatory: Cancer Tomorrow. Lyon, France: International Agency for Research on Cancer. Retrieved 29.04.2019, 2019, from https://gco.iarc.fr/tomorrow

Foillard, S., Rasmussen, M. O., Razkin, J., Boturyn, D., & Dumy, P. (2008). 1-Ethoxyethylidene, a new group for the stepwise SPPS of aminooxyacetic acid containing peptides. *J Org Chem, 73*(3), 983-991.

Gantke, T., Weichel, M., Herbrecht, C., Reusch, U., Ellwanger, K., Fucek, I., et al. (2017). Trispecific antibodies for CD16A-directed NK cell engagement and dual-targeting of tumor cells. *Protein Eng Des Sel, 30*(9), 673-684.

Garcia, K. C., Degano, M., Stanfield, R. L., Brunmark, A., Jackson, M. R., Peterson, P. A., et al. (1996). An αβ T Cell Receptor Structure at 2.5 Å and Its Orientation in the TCR-MHC Complex. *Science, 274*(5285), 209-219.

Gillies, R. J., Verduzco, D., & Gatenby, R. A. (2012). Evolutionary dynamics of carcinogenesis and why targeted therapy does not work. *Nat Rev Cancer, 12*(7), 487-493.

Greaves, M., & Maley, C. C. (2012). Clonal evolution in cancer. *Nature, 481*(7381), 306-313.

Greaves, M., & Maley, C. C. (2012). Clonal evolution in cancer. *Nature, 481*, 306.

Gunnarsen, K. S., Høydahl, L. S., Neumann, R. S., Bjerregaard-Andersen, K., Nilssen, N. R., Sollid, L. M., et al. (2018). Soluble T-cell receptor design influences functional yield in an E. coli chaperone-assisted expression system. *PLOS ONE, 13*(4), e0195868.

Gunnoo, S. B., & Madder, A. (2016). Chemical Protein Modification through Cysteine. *ChemBioChem, 17*(7), 529-553.

Halenius, A., Gerke, C., & Hengel, H. (2014). Classical and non-classical MHC I molecule manipulation by human cytomegalovirus: so many targets—but how many arrows in the quiver? [Review]. *Cellular And Molecular Immunology, 12*, 139.

Hamann, P. R., Hinman, L. M., Hollander, I., Beyer, C. F., Lindh, D., Holcomb, R., et al. (2002). Gemtuzumab ozogamicin, a potent and selective anti-CD33 antibody-calicheamicin conjugate for treatment of acute myeloid leukemia. *Bioconjug Chem, 13*(1), 47-58.

Hanahan, D., & Weinberg, Robert A. (2011). Hallmarks of Cancer: The Next Generation. *Cell, 144*(5), 646-674.

Haraya, K., Tachibana, T., & Igawa, T. (2019). Improvement of pharmacokinetic properties of therapeutic antibodies by antibody engineering. *Drug Metab Pharmacokinet, 34*(1), 25-41.

Hein, J. E., & Fokin, V. V. (2010). Copper-catalyzed azide–alkyne cycloaddition (CuAAC) and beyond: new reactivity of copper(i) acetylides. [10.1039/B904091A]. *Chemical Society Reviews, 39*(4), 1302-1315.

Hermanson, G. T. (2013a). Chapter 2 - Functional Targets for Bioconjugation. In G. T. Hermanson (Ed.), *Bioconjugate Techniques (Third Edition)* (pp. 127-228). Boston: Academic Press.

Hermanson, G. T. (2013b). Chapter 3 - The Reactions of Bioconjugation. In G. T. Hermanson (Ed.), *Bioconjugate Techniques (Third Edition)* (pp. 229-258). Boston: Academic Press.

Heron, M. P. (2018). Deaths : leading causes for 2016. [Journal Issue].

Herrera, A. F., & Molina, A. (2018). Investigational Antibody–Drug Conjugates for Treatment of B-lineage Malignancies. *Clinical Lymphoma Myeloma and Leukemia, 18*(7), 452-468.e454.

Hewitt, E. W. (2003). The MHC class I antigen presentation pathway: strategies for viral immune evasion. *Immunology, 110*(2), 163-169.

Higel, F., Seidl, A., Sörgel, F., & Friess, W. (2016). N-glycosylation heterogeneity and the influence on structure, function and pharmacokinetics of monoclonal antibodies and Fc fusion proteins. *European Journal of Pharmaceutics and Biopharmaceutics, 100*, 94-100.

Hoffmann, P., Hofmeister, R., Brischwein, K., Brandl, C., Crommer, S., Bargou, R., et al. (2005). Serial killing of tumor cells by cytotoxic T cells redirected with a CD19-/CD3-bispecific single-chain antibody construct. *Int J Cancer, 115*(1), 98-104.

Hoffmann, R. M., Coumbe, B. G. T., Josephs, D. H., Mele, S., Ilieva, K. M., Cheung, A., et al. (2017). Antibody structure and engineering considerations for the design and function of Antibody Drug Conjugates (ADCs). *Oncoimmunology, 7*(3), e1395127-e1395127.

Holling, T. M., Schooten, E., & van Den Elsen, P. J. (2004). Function and regulation of MHC class II molecules in T-lymphocytes: of mice and men. *Hum Immunol, 65*(4), 282-290.

Hong, V., Presolski, S. I., Ma, C., & Finn, M. G. (2009). Analysis and optimization of copper-catalyzed azide-alkyne cycloaddition for bioconjugation. *Angew Chem Int Ed Engl, 48*(52), 9879-9883.

Hornig, N., & Farber-Schwarz, A. (2012). Production of bispecific antibodies: diabodies and tandem scFv. *Methods Mol Biol, 907*, 713-727.

Hudis, C. A. (2007). Trastuzumab — Mechanism of Action and Use in Clinical Practice. *New England Journal of Medicine, 357*(1), 39-51.

Hudson, P. J., & Souriau, C. (2003). Engineered antibodies. [Review Article]. *Nature Medicine, 9*, 129.

Huehls, A. M., Coupet, T. A., & Sentman, C. L. (2015). Bispecific T-cell engagers for cancer immunotherapy. *Immunology and cell biology, 93*(3), 290-296.

Huisgen, R. (1963). 1,3-Dipolar Cycloadditions. Past and Future. *Angewandte Chemie International Edition in English, 2*(10), 565-598.

Husain, B., & Ellerman, D. (2018). Expanding the Boundaries of Biotherapeutics with Bispecific Antibodies. [journal article]. *BioDrugs, 32*(5), 441-464.

Inozume, T., Hanada, K., Wang, Q. J., Ahmadzadeh, M., Wunderlich, J. R., Rosenberg, S. A., et al. (2010). Selection of CD8+PD-1+ lymphocytes in fresh human melanomas enriches for tumor-reactive T cells. *J Immunother, 33*(9), 956-964.

Ioannidou, K., Baumgaertner, P., Gannon, P. O., Speiser, M. F., Allard, M., Hebeisen, M., et al. (2017). Heterogeneity assessment of functional T cell avidity. [Article]. *Scientific Reports, 7*, 44320.

Iwamoto, F. M., Abrey, L. E., Beal, K., Gutin, P. H., Rosenblum, M. K., Reuter, V. E., et al. (2009). Patterns of relapse and prognosis after bevacizumab failure in recurrent glioblastoma. *Neurology, 73*(15), 1200-1206.

Janiszewska, M., & Polyak, K. (2015). Clonal Evolution in Cancer: A Tale of Twisted Twines. *Cell Stem Cell, 16*(1), 11-12.

Janke, C. (2014). The tubulin code: molecular components, readout mechanisms, and functions. *J Cell Biol, 206*(4), 461-472.

Jeger, S., Zimmermann, K., Blanc, A., Grunberg, J., Honer, M., Hunziker, P., et al. (2010). Site-specific and stoichiometric modification of antibodies by bacterial transglutaminase. *Angew Chem Int Ed Engl, 49*(51), 9995-9997.

Jones, A. W. (2011). Early drug discovery and the rise of pharmaceutical chemistry. *Drug Test Anal, 3*(6), 337-344.

June, C. H., Riddell, S. R., & Schumacher, T. N. (2015). Adoptive cellular therapy: a race to the finish line. *Sci Transl Med, 7*(280), 280ps287.

Junutula, J. R., Raab, H., Clark, S., Bhakta, S., Leipold, D. D., Weir, S., et al. (2008). Site-specific conjugation of a cytotoxic drug to an antibody improves the therapeutic index. *Nat Biotechnol, 26*(8), 925-932.

Kalos, M., Levine, B. L., Porter, D. L., Katz, S., Grupp, S. A., Bagg, A., et al. (2011). T cells with chimeric antigen receptors have potent antitumor effects and can establish memory in patients with advanced leukemia. *Sci Transl Med, 3*(95), 95ra73.

Karamitsos, D. T. (2011). The story of insulin discovery. *Diabetes Research and Clinical Practice, 93*, S2-S8.

Kelderman, S., Heemskerk, B., Fanchi, L., Philips, D., Toebes, M., Kvistborg, P., et al. (2016). Antigen-specific TIL therapy for melanoma: A flexible platform for personalized cancer immunotherapy. *Eur J Immunol, 46*(6), 1351-1360.

Kellner, C., Peipp, M., & Valerius, T. (2011). Effector Cell Recruitment by Bispecific Antibodies. In R. E. Kontermann (Ed.), *Bispecific Antibodies* (pp. 217-241). Berlin, Heidelberg: Springer Berlin Heidelberg.

Kennedy, D. C., McKay, C. S., Legault, M. C., Danielson, D. C., Blake, J. A., Pegoraro, A. F., et al. (2011). Cellular consequences of copper complexes used to catalyze bioorthogonal click reactions. *J Am Chem Soc, 133*(44), 17993-18001.

Klein, J., & Sato, A. (2000). The HLA System. *New England Journal of Medicine, 343*(10), 702-709.

Klein, L., Kyewski, B., Allen, P. M., & Hogquist, K. A. (2014). Positive and negative selection of the T cell repertoire: what thymocytes see (and don't see). *Nature reviews. Immunology, 14*(6), 377-391.

Knabel, M., Franz, T. J., Schiemann, M., Wulf, A., Villmow, B., Schmidt, B., et al. (2002). Reversible MHC multimer staining for functional isolation of T-cell populations and effective adoptive transfer. *Nature Medicine, 8*(6), 631-637.

Knudson, K. M., Gameiro, S. R., Lo, K.-M., & Schlom, J. (2017). Abstract 594: Dual targeting of TGFb and PD-L1 promotes potent anti-tumor efficacy in multiple murine models of solid carcinomas. *Cancer Research, 77*(13 Supplement), 594-594.

Kochenderfer, J. N., Wilson, W. H., Janik, J. E., Dudley, M. E., Stetler-Stevenson, M., Feldman, S. A., et al. (2010). Eradication of B-lineage cells and regression of lymphoma in a patient treated with autologous T cells genetically engineered to recognize CD19. *Blood, 116*(20), 4099-4102.

Kölmel, D. K., & Kool, E. T. (2017). Oximes and Hydrazones in Bioconjugation: Mechanism and Catalysis. *Chemical Reviews, 117*(15), 10358-10376.

Kunert, A., Obenaus, M., Lamers, C. H. J., Blankenstein, T., & Debets, R. (2017). T-cell Receptors for Clinical Therapy: In Vitro Assessment of Toxicity Risk. *Clin Cancer Res, 23*(20), 6012-6020.

Labrecque, N., Whitfield, L. S., Obst, R., Waltzinger, C., Benoist, C., & Mathis, D. (2001). How much TCR does a T cell need? *Immunity, 15*(1), 71-82.

Lallemand, C., Liang, F., Staub, F., Simansour, M., Vallette, B., Huang, L., et al. (2017). A Novel System for the Quantification of the ADCC Activity of Therapeutic Antibodies. *Journal of immunology research, 2017*, 3908289-3908289.

Lang, K., & Chin, J. W. (2014). Cellular Incorporation of Unnatural Amino Acids and Bioorthogonal Labeling of Proteins. *Chemical Reviews, 114*(9), 4764-4806.

Lang, K., & Chin, J. W. (2014). Cellular incorporation of unnatural amino acids and bioorthogonal labeling of proteins. *Chem Rev, 114*(9), 4764-4806.

Lang, K., Davis, L., Torres-Kolbus, J., Chou, C., Deiters, A., & Chin, J. W. (2012). Genetically encoded norbornene directs site-specific cellular protein labelling via a rapid bioorthogonal reaction. *Nature chemistry, 4*(4), 298-304.

Lang, K., Davis, L., Wallace, S., Mahesh, M., Cox, D. J., Blackman, M. L., et al. (2012). Genetic Encoding of Bicyclononynes and trans-Cyclooctenes for Site-Specific Protein Labeling in Vitro and in Live Mammalian Cells via Rapid Fluorogenic Diels–Alder Reactions. *Journal of the American Chemical Society, 134*(25), 10317-10320.

Lanzavecchia, A., Iezzi, G., & Viola, A. (1999). From TCR Engagement to T Cell Activation: A Kinetic View of T Cell Behavior. *Cell, 96*(1), 1-4.

Lee, N. K., Zhang, Y., Su, Y., Bidlingmaier, S., Sherbenou, D. W., Ha, K. D., et al. (2018). Cell-type specific potent Wnt signaling blockade by bispecific antibody. *Sci Rep, 8*(1), 766.

Lee, S., & Margolin, K. (2012). Tumor-infiltrating lymphocytes in melanoma. *Current oncology reports, 14*(5), 468-474.

Levary, D. A., Parthasarathy, R., Boder, E. T., & Ackerman, M. E. (2011). Protein-Protein Fusion Catalyzed by Sortase A. *PLOS ONE, 6*(4), e18342.

Lewis, P. (2002). Recombinant protein drugs. *British Journal of Clinical Pharmacology, 53*(4), 411-411.

Lewis Phillips, G. D., Li, G., Dugger, D. L., Crocker, L. M., Parsons, K. L., Mai, E., et al. (2008). Targeting HER2-positive breast cancer with trastuzumab-DM1, an antibody-cytotoxic drug conjugate. *Cancer Res, 68*(22), 9280-9290.

Li, H., & d'Anjou, M. (2009). Pharmacological significance of glycosylation in therapeutic proteins. *Current Opinion in Biotechnology, 20*(6), 678-684.

Li, J. Y., Perry, S. R., Muniz-Medina, V., Wang, X., Wetzel, L. K., Rebelatto, M. C., et al. (2016). A Biparatopic HER2-Targeting Antibody-Drug Conjugate Induces Tumor Regression in Primary Models Refractory to or Ineligible for HER2-Targeted Therapy. *Cancer Cell, 29*(1), 117-129.

Li, L., & Zhang, Z. (2016). Development and Applications of the Copper-Catalyzed Azide-Alkyne Cycloaddition (CuAAC) as a Bioorthogonal Reaction. *Molecules, 21*(10).

Lin, C.-W., & Ting, A. Y. (2006). Transglutaminase-catalyzed site-specific conjugation of small-molecule probes to proteins in vitro and on the surface of living cells. *Journal of the American Chemical Society, 128*(14), 4542-4543.

Liu, C. C., & Schultz, P. G. (2010). Adding New Chemistries to the Genetic Code. *Annual Review of Biochemistry, 79*(1), 413-444.

Liu, W., Brock, A., Chen, S., Chen, S., & Schultz, P. G. (2007). Genetic incorporation of unnatural amino acids into proteins in mammalian cells. *Nat Methods, 4*(3), 239-244.

Liu, X., Jiang, S., Fang, C., Yang, S., Olalere, D., Pequignot, E. C., et al. (2015). Affinity-Tuned ErbB2 or EGFR Chimeric Antigen Receptor T Cells Exhibit an Increased Therapeutic Index against Tumors in Mice. *Cancer research, 75*(17), 3596-3607.

Loffler, A., Kufer, P., Lutterbuse, R., Zettl, F., Daniel, P. T., Schwenkenbecher, J. M., et al. (2000). A recombinant bispecific single-chain antibody, CD19 x CD3, induces rapid and high lymphoma-directed cytotoxicity by unstimulated T lymphocytes. *Blood, 95*(6), 2098-2103.

Lotze, J., Reinhardt, U., Seitz, O., & Beck-Sickinger, A. G. (2016). Peptide-tags for site-specific protein labelling in vitro and in vivo. [10.1039/C6MB00023A]. *Molecular BioSystems, 12*(6), 1731-1745.

Lu, L. L., Suscovich, T. J., Fortune, S. M., & Alter, G. (2017). Beyond binding: antibody effector functions in infectious diseases. [Review Article]. *Nature Reviews Immunology, 18*, 46.

Lu, X., & Bergelson, S. (2014). Development of a sensitive potency assay to measure the anti-proliferation effect of an anti-HER2 antibody. *J Immunol Methods, 415*, 80-85.

Lyon, R. P., Bovee, T. D., Doronina, S. O., Burke, P. J., Hunter, J. H., Neff-LaFord, H. D., et al. (2015). Reducing hydrophobicity of homogeneous antibody-drug conjugates improves pharmacokinetics and therapeutic index. *Nat Biotechnol, 33*(7), 733-735.

Mao, H., Hart, S. A., Schink, A., & Pollok, B. A. (2004). Sortase-mediated protein ligation: a new method for protein engineering. *J Am Chem Soc, 126*(9), 2670-2671.

Marrocco, I., Romaniello, D., & Yarden, Y. (2019). Cancer Immunotherapy: The Dawn of Antibody Cocktails. In M. Steinitz (Ed.), *Human Monoclonal Antibodies: Methods and Protocols* (pp. 11-51). New York, NY: Springer New York.

Masuda, H., Zhang, D., Bartholomeusz, C., Doihara, H., Hortobagyi, G. N., & Ueno, N. T. (2012). Role of epidermal growth factor receptor in breast cancer. *Breast cancer research and treatment, 136*(2), 331-345.

Matos, M. J., Oliveira, B. L., Martinez-Saez, N., Guerreiro, A., Cal, P., Bertoldo, J., et al. (2018). Chemo- and Regioselective Lysine Modification on Native Proteins. *J Am Chem Soc, 140*(11), 4004-4017.

Maude, S. L., Laetsch, T. W., Buechner, J., Rives, S., Boyer, M., Bittencourt, H., et al. (2018). Tisagenlecleucel in Children and Young Adults with B-Cell Lymphoblastic Leukemia. *New England Journal of Medicine, 378*(5), 439-448.

Maxwell, M. B., & Maher, K. E. (1992). Chemotherapy-induced myelosuppression. *Semin Oncol Nurs, 8*(2), 113-123.

Mayer, S., & Lang, K. (2017). Tetrazines in Inverse-Electron-Demand Diels–Alder Cycloadditions and Their Use in Biology. *Synthesis, 49*(04), 830-848.

McDonagh, C. F., Huhalov, A., Harms, B. D., Adams, S., Paragas, V., Oyama, S., et al. (2012). Antitumor activity of a novel bispecific antibody that targets the ErbB2/ErbB3 oncogenic unit and inhibits heregulin-induced activation of ErbB3. *Mol Cancer Ther, 11*(3), 582-593.

McGaraughty, S., Davis-Taber, R. A., Zhu, C. Z., Cole, T. B., Nikkel, A. L., Chhaya, M., et al. (2017). Targeting Anti-TGF-beta Therapy to Fibrotic Kidneys with a Dual Specificity Antibody Approach. *J Am Soc Nephrol, 28*(12), 3616-3626.

McGranahan, N., & Swanton, C. (2017). Clonal Heterogeneity and Tumor Evolution: Past, Present, and the Future. *Cell, 168*(4), 613-628.

Mensah, G. A., Wei, G. S., Sorlie, P. D., Fine, L. J., Rosenberg, Y., Kaufmann, P. G., et al. (2017). Decline in Cardiovascular Mortality: Possible Causes and Implications. *Circulation research, 120*(2), 366-380.

Miceli, M. C., & Parnes, J. R. (1991). The roles of CD4 and CD8 in T cell activation. *Semin Immunol, 3*(3), 133-141.

Nauerth, M., Weissbrich, B., Knall, R., Franz, T., Dossinger, G., Bet, J., et al. (2013). TCR-ligand koff rate correlates with the protective capacity of antigen-specific CD8+ T cells for adoptive transfer. *Sci Transl Med, 5*(192), 192ra187.

O'Leary, M. C., Lu, X., Huang, Y., Lin, X., Mahmood, I., Przepiorka, D., et al. (2019). FDA Approval Summary: Tisagenlecleucel for Treatment of Patients with Relapsed or Refractory B-cell Precursor Acute Lymphoblastic Leukemia. *Clin Cancer Res, 25*(4), 1142-1146.

Ohtsubo, K., & Marth, J. D. (2006). Glycosylation in Cellular Mechanisms of Health and Disease. *Cell, 126*(5), 855-867.

Oller-Salvia, B., Kym, G., & Chin, J. W. (2018). Rapid and Efficient Generation of Stable Antibody-Drug Conjugates via an Encoded Cyclopropene and an Inverse-

Electron-Demand Diels-Alder Reaction. *Angewandte Chemie (International ed. in English), 57*(11), 2831-2834.

Patterson, D. M., Nazarova, L. A., Xie, B., Kamber, D. N., & Prescher, J. A. (2012). Functionalized Cyclopropenes As Bioorthogonal Chemical Reporters. *Journal of the American Chemical Society, 134*(45), 18638-18643.

Perica, K., Varela, J. C., Oelke, M., & Schneck, J. (2015). Adoptive T cell immunotherapy for cancer. *Rambam Maimonides medical journal, 6*(1), e0004-e0004.

Pickens, C. J., Johnson, S. N., Pressnall, M. M., Leon, M. A., & Berkland, C. J. (2018). Practical Considerations, Challenges, and Limitations of Bioconjugation via Azide-Alkyne Cycloaddition. *Bioconjug Chem, 29*(3), 686-701.

Plass, T., Milles, S., Koehler, C., Szymański, J., Mueller, R., Wießler, M., et al. (2012). Amino Acids for Diels–Alder Reactions in Living Cells. *Angewandte Chemie International Edition, 51*(17), 4166-4170.

Ponte, J. F., Sun, X., Yoder, N. C., Fishkin, N., Laleau, R., Coccia, J., et al. (2016). Understanding How the Stability of the Thiol-Maleimide Linkage Impacts the Pharmacokinetics of Lysine-Linked Antibody-Maytansinoid Conjugates. *Bioconjug Chem, 27*(7), 1588-1598.

Prescher, J. A., & Bertozzi, C. R. (2005). Chemistry in living systems. *Nature Chemical Biology, 1*(1), 13-21.

Presta, L. G. (2008). Molecular engineering and design of therapeutic antibodies. *Current Opinion in Immunology, 20*(4), 460-470.

Prota, A. E., Magiera, M. M., Kuijpers, M., Bargsten, K., Frey, D., Wieser, M., et al. (2013). Structural basis of tubulin tyrosination by tubulin tyrosine ligase. *J Cell Biol, 200*(3), 259-270.

Przepiorka, D., Ko, C. W., Deisseroth, A., Yancey, C. L., Candau-Chacon, R., Chiu, H. J., et al. (2015). FDA Approval: Blinatumomab. *Clin Cancer Res, 21*(18), 4035-4039.

Qasba, P. K. (2015). Glycans of Antibodies as a Specific Site for Drug Conjugation Using Glycosyltransferases. *Bioconjugate Chemistry, 26*(11), 2170-2175.

Qi, Q., Liu, Y., Cheng, Y., Glanville, J., Zhang, D., Lee, J. Y., et al. (2014). Diversity and clonal selection in the human T-cell repertoire. *Proc Natl Acad Sci U S A, 111*(36), 13139-13144.

Radvanyi, L. G., Bernatchez, C., Zhang, M., Fox, P. S., Miller, P., Chacon, J., et al. (2012). Specific lymphocyte subsets predict response to adoptive cell therapy using expanded autologous tumor-infiltrating lymphocytes in metastatic melanoma patients. *Clin Cancer Res, 18*(24), 6758-6770.

Ramil, C. P., & Lin, Q. (2013). Bioorthogonal chemistry: strategies and recent developments. *Chemical communications (Cambridge, England), 49*(94), 11007-11022.

Ravasco, J. M. J. M., Faustino, H., Trindade, A., & Gois, P. M. P. (2019). Bioconjugation with Maleimides: A Useful Tool for Chemical Biology. *Chemistry – A European Journal, 25*(1), 43-59.

Redman, J. M., Hill, E. M., AlDeghaither, D., & Weiner, L. M. (2015). Mechanisms of action of therapeutic antibodies for cancer. *Molecular immunology, 67*(2 Pt A), 28-45.

Reslan, L., Dalle, S., & Dumontet, C. (2009). Understanding and circumventing resistance to anticancer monoclonal antibodies. *mAbs, 1*(3), 222-229.

Riddell, S. R., & Greenberg, P. D. (1990). The use of anti-CD3 and anti-CD28 monoclonal antibodies to clone and expand human antigen-specific T cells. *Journal of Immunological Methods, 128*(2), 189-201.

Rohaan, M. W., van den Berg, J. H., Kvistborg, P., & Haanen, J. (2018). Adoptive transfer of tumor-infiltrating lymphocytes in melanoma: a viable treatment option. *J Immunother Cancer, 6*(1), 102.

Rosenberg, S. A., Restifo, N. P., Yang, J. C., Morgan, R. A., & Dudley, M. E. (2008). Adoptive cell transfer: a clinical path to effective cancer immunotherapy. [Review Article]. *Nature Reviews Cancer, 8*, 299.

Rosenberg, S. A., Spiess, P., & Lafreniere, R. (1986). A new approach to the adoptive immunotherapy of cancer with tumor-infiltrating lymphocytes. *Science, 233*(4770), 1318-1321.

Rosenberg, S. A., Yang, J. C., Sherry, R. M., Kammula, U. S., Hughes, M. S., Phan, G. Q., et al. (2011). Durable complete responses in heavily pretreated patients with metastatic melanoma using T-cell transfer immunotherapy. *Clin Cancer Res, 17*(13), 4550-4557.

Ross, P. L., & Wolfe, J. L. (2016). Physical and Chemical Stability of Antibody Drug Conjugates: Current Status. *J Pharm Sci, 105*(2), 391-397.

Rostovtsev, V. V., Green, L. G., Fokin, V. V., & Sharpless, K. B. (2002). A stepwise huisgen cycloaddition process: copper(I)-catalyzed regioselective "ligation" of azides and terminal alkynes. *Angew Chem Int Ed Engl, 41*(14), 2596-2599.

Rudiger, M., Wehland, J., & Weber, K. (1994). The carboxy-terminal peptide of detyrosinated alpha tubulin provides a minimal system to study the substrate specificity of tubulin-tyrosine ligase. *Eur J Biochem, 220*(2), 309-320.

Rudolph, M. G., Stanfield, R. L., & Wilson, I. A. (2006). HOW TCRS BIND MHCS, PEPTIDES, AND CORECEPTORS. *Annual Review of Immunology, 24*(1), 419-466.

Ryman, J. T., & Meibohm, B. (2017). Pharmacokinetics of Monoclonal Antibodies. *CPT: pharmacometrics & systems pharmacology, 6*(9), 576-588.

Sawyers, C. (2004). Targeted cancer therapy. *Nature, 432*(7015), 294-297.

Schachter, H. (2000). The joys of HexNAc. The synthesis and function of N-andO-glycan branches. [journal article]. *Glycoconjugate Journal, 17*(7), 465-483.

Schendel, D. J., & Frankenberger, B. (2013). Limitations for TCR gene therapy by MHC-restricted fratricide and TCR-mediated hematopoietic stem cell toxicity. *Oncoimmunology, 2*(1), e22410-e22410.

Schroeder, H. W., Jr., & Cavacini, L. (2010). Structure and function of immunoglobulins. *The Journal of allergy and clinical immunology, 125*(2 Suppl 2), S41-S52.

Schumacher, D., Hackenberger, C. P. R., Leonhardt, H., & Helma, J. (2016). Current Status: Site-Specific Antibody Drug Conjugates. *Journal of clinical immunology, 36 Suppl 1*, 100-107.

Schumacher, D., Helma, J., Mann, F. A., Pichler, G., Natale, F., Krause, E., et al. (2015). Versatile and Efficient Site-Specific Protein Functionalization by Tubulin Tyrosine Ligase. *Angew Chem Int Ed Engl, 54*(46), 13787-13791.

Schumacher, D., Lemke, O., Helma, J., Gerszonowicz, L., Waller, V., Stoschek, T., et al. (2017). Broad substrate tolerance of tubulin tyrosine ligase enables one-step site-specific enzymatic protein labeling. *Chem Sci, 8*(5), 3471-3478.

Schumacher, T. N. M., & Ploegh, H. L. (1994). Are MHC-bound peptides a nuisance for positive selection? *Immunity, 1*(9), 721-723.

Schürch, C. M. (2018). Therapeutic Antibodies for Myeloid Neoplasms—Current Developments and Future Directions. [Review]. *Frontiers in Oncology, 8*(152).

Scott, A. M., Wolchok, J. D., & Old, L. J. (2012). Antibody therapy of cancer. [Review Article]. *Nature Reviews Cancer, 12*, 278.

Sečkutė, J., & Devaraj, N. K. (2013). Expanding room for tetrazine ligations in the in vivo chemistry toolbox. *Current opinion in chemical biology, 17*(5), 761-767.

Senter, P. D., & Sievers, E. L. (2012). The discovery and development of brentuximab vedotin for use in relapsed Hodgkin lymphoma and systemic anaplastic large cell lymphoma. *Nat Biotechnol, 30*(7), 631-637.

Serwa, R., Wilkening, I., Del Signore, G., Mühlberg, M., Claußnitzer, I., Weise, C., et al. (2009). Chemoselective Staudinger-Phosphite Reaction of Azides for the Phosphorylation of Proteins. *Angewandte Chemie International Edition, 48*(44), 8234-8239.

Shen, B. Q., Xu, K., Liu, L., Raab, H., Bhakta, S., Kenrick, M., et al. (2012). Conjugation site modulates the in vivo stability and therapeutic activity of antibody-drug conjugates. *Nat Biotechnol, 30*(2), 184-189.

Shuptrine, C. W., Surana, R., & Weiner, L. M. (2012). Monoclonal antibodies for the treatment of cancer. *Seminars in cancer biology, 22*(1), 3-13.

Slavoff, S. A., Chen, I., Choi, Y. A., & Ting, A. Y. (2008). Expanding the substrate tolerance of biotin ligase through exploration of enzymes from diverse species. *J Am Chem Soc, 130*(4), 1160-1162.

Sotillo, R., Schvartzman, J. M., Socci, N. D., & Benezra, R. (2010). Mad2-induced chromosome instability leads to lung tumour relapse after oncogene withdrawal. *Nature, 464*(7287), 436-440.

Spirig, T., Weiner, E. M., & Clubb, R. T. (2011). Sortase enzymes in Gram-positive bacteria. *Molecular microbiology, 82*(5), 1044-1059.

Staudinger, H., & Meyer, J. (1919). Über neue organische Phosphorverbindungen III. Phosphinmethylenderivate und Phosphinimine. *Helvetica Chimica Acta, 2*(1), 635-646.

Stefan, N., Gebleux, R., Waldmeier, L., Hell, T., Escher, M., Wolter, F. I., et al. (2017). Highly Potent, Anthracycline-based Antibody-Drug Conjugates Generated by Enzymatic, Site-specific Conjugation. *Mol Cancer Ther, 16*(5), 879-892.

Stengl, A., Gerlach, M., Kasper, M.-A., Hackenberger, C. P. R., Leonhardt, H., Schumacher, D., et al. (2019). TuPPL: Tub-tag mediated C-terminal protein–protein-ligation using complementary click-chemistry handles. [10.1039/C9OB00508K]. *Organic & Biomolecular Chemistry, 17*(20), 4964-4969.

Stone, J. D., Chervin, A. S., & Kranz, D. M. (2009). T-cell receptor binding affinities and kinetics: impact on T-cell activity and specificity. *Immunology, 126*(2), 165-176.

Sun, M. M., Beam, K. S., Cerveny, C. G., Hamblett, K. J., Blackmore, R. S., Torgov, M. Y., et al. (2005). Reduction-alkylation strategies for the modification of specific monoclonal antibody disulfides. *Bioconjug Chem, 16*(5), 1282-1290.

Szijj, P. A., Bahou, C., & Chudasama, V. (2018a). Minireview: Addressing the retro-Michael instability of maleimide bioconjugates. *Drug Discovery Today: Technologies*.

Tobin, P. H., Richards, D. H., Callender, R. A., & Wilson, C. J. (2014). Protein engineering: a new frontier for biological therapeutics. *Current drug metabolism, 15*(7), 743-756.

Tsuchikama, K., & An, Z. (2018). Antibody-drug conjugates: recent advances in conjugation and linker chemistries. *Protein & Cell, 9*(1), 33-46.

Ulrich, S., Boturyn, D., Marra, A., Renaudet, O., & Dumy, P. (2014). Oxime Ligation: A Chemoselective Click-Type Reaction for Accessing Multifunctional Biomolecular Constructs. *Chemistry – A European Journal, 20*(1), 34-41.

Vallée, M. R. J., Majkut, P., Wilkening, I., Weise, C., Müller, G., & Hackenberger, C. P. R. (2011). Staudinger-Phosphonite Reactions for the Chemoselective Transformation of Azido-Containing Peptides and Proteins. *Organic Letters, 13*(20), 5440-5443.

van Berkel, S. S., van Eldijk, M. B., & van Hest, J. C. M. (2011). Staudinger Ligation as a Method for Bioconjugation. *Angewandte Chemie International Edition, 50*(38), 8806-8827.

VanBrunt, M. P., Shanebeck, K., Caldwell, Z., Johnson, J., Thompson, P., Martin, T., et al. (2015). Genetically Encoded Azide Containing Amino Acid in Mammalian Cells Enables Site-Specific Antibody–Drug Conjugates Using Click Cycloaddition Chemistry. *Bioconjugate Chemistry, 26*(11), 2249-2260.

Vega-Avila, E., & Pugsley, M. K. (2011). An overview of colorimetric assay methods used to assess survival or proliferation of mammalian cells. *Proc West Pharmacol Soc, 54*, 10-14.

Viganò, S., Utzschneider, D. T., Perreau, M., Pantaleo, G., Zehn, D., & Harari, A. (2012). Functional avidity: a measure to predict the efficacy of effector T cells? *Clinical & developmental immunology, 2012*, 153863-153863.

Wagner, I., & Musso, H. (1983). New Naturally Occurring Amino Acids. *Angewandte Chemie International Edition in English, 22*(11), 816-828.

Wang, K., Wei, G., & Liu, D. (2012). CD19: a biomarker for B cell development, lymphoma diagnosis and therapy. *Experimental hematology & oncology, 1*(1), 36-36.

Wang, L., Amphlett, G., Blattler, W. A., Lambert, J. M., & Zhang, W. (2005). Structural characterization of the maytansinoid-monoclonal antibody immunoconjugate, huN901-DM1, by mass spectrometry. *Protein Sci, 14*(9), 2436-2446.

Wang, L., Brock, A., Herberich, B., & Schultz, P. G. (2001). Expanding the genetic code of Escherichia coli. *Science, 292*(5516), 498-500.

Wang, X., Teng, F., Kong, L., & Yu, J. (2016). PD-L1 expression in human cancers and its association with clinical outcomes. *OncoTargets and therapy, 9*, 5023-5039.

Williamson, D. J., Fascione, M. A., Webb, M. E., & Turnbull, W. B. (2012). Efficient N-terminal labeling of proteins by use of sortase. *Angew Chem Int Ed Engl, 51*(37), 9377-9380.

Wucherpfennig, K. W., Gagnon, E., Call, M. J., Huseby, E. S., & Call, M. E. (2010). Structural biology of the T-cell receptor: insights into receptor assembly, ligand recognition, and initiation of signaling. *Cold Spring Harbor perspectives in biology, 2*(4), a005140-a005140.

Xenaki, K. T., Oliveira, S., & van Bergen En Henegouwen, P. M. P. (2017). Antibody or Antibody Fragments: Implications for Molecular Imaging and Targeted Therapy of Solid Tumors. *Frontiers in immunology, 8*, 1287-1287.

Xiao, H., Chatterjee, A., Choi, S. H., Bajjuri, K. M., Sinha, S. C., & Schultz, P. G. (2013). Genetic incorporation of multiple unnatural amino acids into proteins in mammalian cells. *Angew Chem Int Ed Engl, 52*(52), 14080-14083.

Yarchoan, M., Johnson, B. A., 3rd, Lutz, E. R., Laheru, D. A., & Jaffee, E. M. (2017). Targeting neoantigens to augment antitumour immunity. *Nat Rev Cancer, 17*(4), 209-222.

Ye, Q., Song, D. G., Poussin, M., Yamamoto, T., Best, A., Li, C., et al. (2014). CD137 accurately identifies and enriches for naturally occurring tumor-reactive T cells in tumor. *Clin Cancer Res, 20*(1), 44-55.

Young, C. L., Britton, Z. T., & Robinson, A. S. (2012). Recombinant protein expression and purification: a comprehensive review of affinity tags and microbial applications. *Biotechnol J, 7*(5), 620-634.

Yu, I., Garnham, C. P., & Roll-Mecak, A. (2015). Writing and Reading the Tubulin Code. *J Biol Chem*.

Zhang, S. Q., Parker, P., Ma, K. Y., He, C., Shi, Q., Cui, Z., et al. (2016). Direct measurement of T cell receptor affinity and sequence from naive antiviral T cells. *Sci Transl Med, 8*(341), 341ra377.

Zimmerman, E. S., Heibeck, T. H., Gill, A., Li, X., Murray, C. J., Madlansacay, M. R., et al. (2014). Production of Site-Specific Antibody–Drug Conjugates Using Optimized Non-Natural Amino Acids in a Cell-Free Expression System. *Bioconjugate Chemistry, 25*(2), 351-361.

7 Appendix

7.1 Abbreviations

ACT	Adoptive cell therapy
ADC	Antibody-drug conjugate
ADCC	Antibody dependent cellular cytotoxicity
ALL	Acute lymphocytic leukemia
APC	Antigen presenting cells
BCN	Bicyclononyne
BCR	B cell receptor
BiTE	Bispecific T cell engager
bsIgG	Bispecific IgG
CAR	chimeric antigen receptor
cCPP	cyclic cell penetrating peptide
CD	Cluster of differentiation
CDC	Complement dependent cytotoxicity
CH	Constant heavy (chain)
CL	Constant light (chain)
CuAAC	Copper(I)-catalyzed azide-alkyne cycloaddition
DAPI	4′,6-diamidino-2-phenylindole
DAR	Drug to antibody ratio
DARPin	designed ankyrin repeat protein
DBCO	Dibenzocyclooctyne
DIBAC	Aza-dibenzocyclooctyne
DMSO	Dimethyl sulfoxide
DNA	Deoxyribonucleic acid
EdU	5-ethynyl-2′-deoxyuridine
eGFP	Enhanced green fluorescent protein
EGFR	Epidermal growth factor receptor
ELISA	Enzyme-linked immunosorbent assay
EPL	Expressed Protein Ligtion
Fab	Fragment antigen binding
Fc	Fragment crystallizable
FcRn	neonatal Fc receptor
FDA	US food and drug administration
FGE	Formylglycine-generating enzyme
HCA	High-content analysis
HER2	Human epidermal growth factor receptor 2
HLA	Human leukocyte antigen
HMWS	High-molecular-weight species
IC50	Half maximal inhibitory concentration
IEDDA	Inverse electron-demand Diels-Alder reaction
IFNγ	Interferon γ
Ig	Immunoglobulin

IL	Interleukine
ITC	Isothermal titration calorimetry
k_{off} rate	Dissociation konstant
mAb	Monoclonal antibody
MHC	Major histocompatibility complex
MMAE	Monomethyl auristatin E
MMAF	Monomethyl auristatin F
MS	Mass spectrometry
NHS	*N*-hydroxysuccinimide
OCT	Cyclooctyne
PD-L1	Programmed cell death protein 1 ligand1
PEG	polyethylene glycol
pK_a	negative log of the acid dissociation constant
pMHC	Peptide major histocompatibility complex
RP-HPLC	Reverse-phase high-performance liquid chromatography
scFv	Single chain fragment variable
SpAAC	Strain-promoted azide-alkyne cycloaddition
SPhR	Staudinger-phosphonite reaction
SPR	Surface plasmon resonance
SrtA	Sortase A
TCEP	Tris(2-carboxyethyl)phosphine
THPTA	Tris(3-hydroxypropyltriazolylmethyl)amine
TIL	Tumor infiltrating lymphocyte
tRNA	Transfer ribonucleic acid
TTL	Tubulin tyrosine ligase
TuPPL	Tub-tag mediated C-terminal protein-protein-ligation
UAA	Unnatural amino acids
VC	valine-citrulline
VH	Variable heavy (chain)
VHH	VH of heavy chain only antibodies
VL	Variable light (chain)
β2m	β_2 microglobulin

7.2 DECLARATION OF CONTRIBUTION

A SIMPLE AND SENSITIVE HIGH-CONTENT ASSAY FOR THE CHARACTERIZATION OF ANTIPROLIFERATIVE THERAPEUTIC ANTIBODIES

This study was conceived by Heinrich Leonhardt, Jonas Helma and Andreas Stengl. Andreas Stengl performed all experiments and data analysis, wrote the manuscript and handled the submission process. David Hörl assisted in DNA content quantification and developed the script for DNA content analysis. Jonas Helma assisted in manuscript writing and manuscript submission. Jonas Helma and Heinrich Leonhardt and David Hörl proofread the manuscript.

TUPPL: TUB-TAG MEDIATED C-TERMINAL PROTEIN-PROTEIN-LIGATION USING COMPLEMENTARY CLICK-CHEMISTRY HANDLES

This study was conceived by Andreas Stengl, Heinrich Leonhardt, Jonas Helma and Dominik Schumacher. Andreas Stengl designed and performed experiments corresponding to protein production, functionalization, conjugation, analysis and binding assays. Marc Andre Kasper performed LC-MS experiments and corresponding data analysis. Marcus Gerlach performed peptide conjugation experiments, corresponding data analysis and provided graphs for the corresponding data (Figure 1B, 1C, S1 and S2). Andreas Stengl evaluated all remaining data and generated corresponding graphs and figures. The manuscript was written by Andreas Stengl with assistance of Dominik Schumacher and Jonas Helma. The manuscript was proofread by Dominik Schumacher, Jonas Helma, Markus Gerlach, Marc Andre Kasper, Heinrich Leonhardt and Christian Hackenberger.

CYSTEINE-SELECTIVE PHOSPHONAMIDATE ELECTROPHILES FOR MODULAR PROTEIN BIOCONJUGATIONS

Christian Hackenberger conceived this study. Andreas Stengl generated HEK293F pools stably expressing trastuzumab, expressed and purified trastuzumab, designed and performed cellular imaging experiments with AFCs and generated corresponding figure 4B. Andreas Stengl assisted in manuscript writing and proofreading.

_____	_____
Andreas Stengl	Prof. Dr. Heinrich Leonhardt

ETHYNYLPHOSPHONAMIDATES FOR THE RAPID AND CYSTEINE SELECTIVE GENERATION OF EFFICACIOUS ANTIBODY-DRUG-CONJUGATES

Christian Hackenberger designed and conceived this study. Andreas Stengl expressed and purified trastuzumab, performed all cell-based proliferation assays and cytotoxicity assays including trastuzumab, conceived and performed fluorescence imaging experiments visualizing tubulin disorder. Andreas Stengl analyzed data and generated figures 1c, 1d, S2 and S3 and assisted in manuscript writing and proofreading.

_____	_____
Andreas Stengl	Prof. Dr. Heinrich Leonhardt

FLEXAMERS: A DOUBLE-TAG FOR UNIVERSAL GENERATION OF VERSATILE PMHC MULTIMERS

This study was conceived by Manuel Effenberger, Andreas Stengl, Heinrich Leonhardt and Dirk Busch. Manuel Effenberger performed recombinant pMHC production, multimer generation, reversible and irreversible T cell staining and k_{off}-rate measurements. Andreas Stengl performed FLEXamer functionalization, recombinant production of TTL, SrtA catalyzed labeling reactions, SDS PAGE analysis and determination of conjugation efficacy. Andreas Stengl analyzed conjugation data and generated corresponding figures 2, 6A, 6B, S3A and schematics depicted in figures 1, 2A, 3A, 4A, 5A and S1A. Manuel Effenberger, Andreas Stengl and Kilian Schober wrote the manuscript and jointly handled the submission and revision process. Dominik Schumacher, Jonas Helma, Heinrich Leonhardt and Dirk Busch assisted in manuscript revision and proofreading.

_____	_____
Manuel Effenberger	Andreas Stengl
_____	_____
Dr. med. Kilian Schober	Prof. Dr. Heinrich Leonhardt